C 345(04)
I - 33

Proceedings of VII ICFA Beam Dynamics Workshop on Beam-Beam Issues for Multibunch, High Luminosity Circular Colliders

Dubna 95



JOINT INSTITUTE FOR NUCLEAR RESEARCH

Proceedings of VII ICFA Beam Dynamics Workshop on *Beam-Beam Issues for Multibunch, High Luminosity Circular Colliders*

Dubna, 18 - 20 May 1995

Edited by
P. Beloshitsky and E. Perelstein

Dubna 1996

International Advisory Committee

A. Ando
V. Balbekov
K. Hirata
A. Hofmann
C. S. Hsue
J. L. Laclare
A. Lebedev
S. Y. Lee
L. Palumbo
C. Pellegrini
E. Perelstein
D. Pestrikov
R. Siemann
F. Willeke
C. Zhang

Program Committee

B. Chirikov
N. Dikansky
J. Le Duff
K. Hirata
J. Jowett
E. Keil
K. Oide
D. Pestrikov
A. Piwinski
D. Rice
P. Zenkevich

Local Organizing Committee

A. Sissakian (Chairman)
D. Pestrikov
P. Beloshitsky (scientific secretary)
E. Perelstein (Deputy Chairman)
A. Romanov
V. Novikova (secretary)

© Объединенный институт ядерных исследований, Дубна, 1996

Contents

Preface

Plenary Session

Beam-Beam Interaction at a Crossing Angle and its Analysis at DESY 9
A. Piwinski

Beam Lifetime and Beam-Beam Tails in LEP 22
H. Burkhardt

Crossing Angle Issues in KEKB 29
K. Hirata

Parasitic Collisions in PEP-II 36
M. Furman

Crossing Angles at CESR, Experiments and Experience 48
A. Temnykh and J. Welch

Novosibirsk Tau-Charm Factory Design Study 55
N. Dikansky, V. Parchomchuk, A. Skrinsky and V. Yakimenko

Working Group I: Beam-Beam Instability with Crossing Angle

Crossing Angle Collision and Lifetime: Simulation, Analysis, Measurements and More Simulations 63
T. Chen

Synchrobetatron Resonances in Long Bunches Due to Horisontal Crossing 77
D. V. Pestrikov

Summary of Working Group I 91
T. Chen

Working group II: Multibunch Head-on Beam-Beam Effects

Lifetime and Tail Simulations for Beam-Beam Effects in PEP-II B Factory 99
D. N. Shatilov and A. A. Zholents

Beam-beam Simulations for KEKB 102
K. Ohmi

Beam-Beam Observations at Large Amplitudes and Lifetime Determination 111
D. Shatilov

Comparison of Beam-Beam Simulations 123
M. Furman, A. Zholents, T. Chen and D. Shatilov

Decoherence of a Gaussian Beam due to Beam-Beam Interaction 143
G. V. Stupakov, V. V. Parkhomchuk, V. D. Shiltsev

Coupling Correction for the Beam-Beam Effects Optimization 151
D. V. Parkhomchuk

Summary of Working Group II 155
V. I. Balbekov

Working Group III: Multibunch Beam-Beam Manipulations

The Program of the Beam-Beam Effects Study on the VEPP-4M 159
G. M. Tumaikin

Synchro-Betatron Coupling in Crab Cavities 164
Y. Alexahin

Invariants for Nonlinear Accelerator Optics and Round Colliding Beams 167
V. V. Danilov and E. A. Perevedentsev

Magnetic Structure of the Novosibirsk Tau-Charm Factory 183
V. Yakimenko

Beamstrahlung Dynamic Transformation During Beam-Beam Interaction 192
Arutunian S. G. and Mailian M. R.

List of participants 198

Preface

The Workshop on "Beam-Beam Issues for Multibunch, High Luminosity Circular Colliders" was held at International Conference Hall of JINR, Dubna, from 18 to 20 May 1995. It was organized by the Joint Institute for Nuclear Research and Beam Dynamics Panel of the International Committee on Future Accelerators.

The goal of the Workshop was to discuss the current understanding of the limitations due to the beam-beam effects on the performance of multibunch, high luminosity circular colliders.

The Workshop started with plenary sessions, and continued with three working group sessions on the following topics: beam-beam instability with crossing angle; multibunch head-on beam-beam effect; multibunch beam-beam manipulations. The proceedings are organized in the same four chapters.

We should like to thank JINR for support, Russian Government and Russian Fundamental Investigation Foundation for sponcoring former Soviet Union participants.

P. Beloshitsky and E. Perelstein



Plenary Session

BEAM-BEAM INTERACTION AT A CROSSING ANGLE AND ITS ANALYSIS AT DESY

A.PIWINSKI
Deutsches Elektronen-Synchrotron DESY
22603 Hamburg, Germany
E-Mail: h01pwn@dsyibm.desy.de

ABSTRACT

The mechanism of the excitation of synchro-betatron resonances by the beam-beam interaction with a crossing angle is described. Experimental results from DORIS I and computer simulations for HERA are shown. A method for adjusting the collision of the two beams is discussed.

1. Introduction

DORIS I is a double ring in which the electrons and positrons collided at two interaction points with a vertical crossing angle. When the first collisions of the two beams were obtained the lifetime of many of the 480 bunches in each beam was very small. The bunch currents had, after some minutes, a statistical density distribution displaying no systematic structure. First investigations showed a strong dependence of the bunch density distribution on the synchrotron frequency and on the vertical betatron frequency but no dependence on the horizontal betatron frequency. This was the first indication that the vertical crossing angle was the cause for the reduction of lifetime.

A detailed analysis of the beam-beam interaction with a crossing angle revealed a strong coupling of the betatron and synchrotron oscillations due to the crossing angle and a computer simulation showed many synchro-betatron resonances or satellite resonances which are given by

$$kQ_x + \ell Q_y + mQ_s = n \tag{1}$$

where k, ℓ, m, and n are integers and Q_x, Q_y, and Q_s are the betatron and synchrotron frequencies in units of the revolution frequency. Measurements with a single bunch in one beam confirmed the simulations by showing sharp particle losses exactly at the predicted frequencies.

The reason for the statistical behavior of the losses came from an rf quadrupole and from a decoupling transmitter which gave to different bunches different betatron and synchrotron frequencies. These tools were necessary in order to suppress multi-bunch instabilities since a feedback system was not yet developed at that time. Due to the frequency spread there were always several bunches on a resonance, and since the mean betatron frequencies of the two beams were also different no structure could be seen.

In order to get a reasonable lifetime DORIS I was operated with smaller currents which yielded an average beam-beam tune shift of only 0.01 instead of the expected 0.025. The luminosity was, therefore, smaller by a factor of 6.25, however, compared with single bunch beams and head-on collision the luminosity was still higher by a factor of 480/6.25=76.8 (see Fig.1).

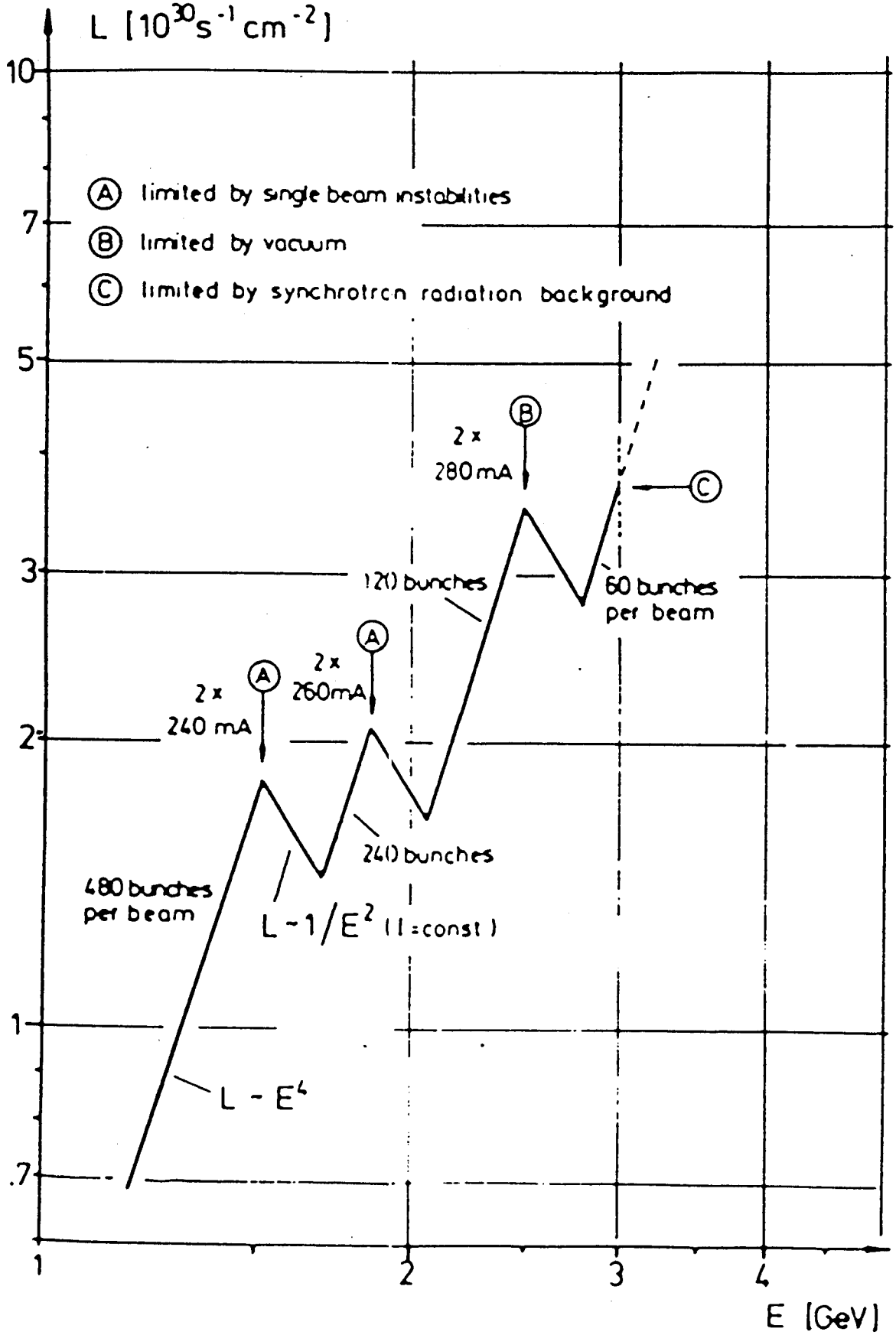


Fig. 1 Maximum luminosity in DORIS I as a function of the energy.

These synchro-betatron resonances were examined also during the design of HERA[5]. Computer simulations have shown that many strong synchro-betatron resonances would be excited since the proton bunch length was longer than the electron bunch length by a factor of three, and the crossing angle was abandoned.

2. Investigations for DORIS I

2.1. General Description

If a particle has a distance s from the center of its own bunch but no transverse displacement it will pass the center of the opposing bunch at a distance of $s \tan\phi \approx s\phi$ where the total crossing angle is 2ϕ. The particle therefore gets a transverse kick, and this means a coupling from the synchrotron oscillation to the betatron oscillation, since the kick, i.e. the change of the betatron angle, depends on the longitudinal synchrotron coordinate s. If the particle has also a transverse displacement x the kick is given by[1]

$$\delta x' = f(x + s\phi). \tag{2}$$

The function f describes the space charge forces. It is antisymmetric and, for small arguments, a linear function. The synchrotron oscillation, on the other hand, is influenced by the betatron oscillation. The change of the momentum is, in the case of a horizontal crossing angle, always horizontal. This can be seen by transforming the two bunches into the reference system where they collide head-on. A decomposition of the momentum change gives

$$\delta p_s = \phi\, \delta p_x \tag{3}$$

and the change of the relative energy is

$$\frac{\delta E}{E} \approx \frac{\delta p}{p} \approx \frac{\delta p_s}{p} = \phi \frac{\delta p_x}{p} = \phi\, \delta x' \tag{4}$$

or

$$\frac{\delta E}{E} = \phi f(x + \phi s). \tag{5}$$

The complete coupling is now described by Eqs.(2) and (5). For small oscillation amplitudes the function f may be linearized and one obtains a linear coupling with

$$f(x + \phi s) = -\frac{4\pi\xi_x}{\beta_x^*}(x + \phi s) \tag{6}$$

and

$$\xi_x = \frac{r_e N_b \beta_x^*}{2\pi\gamma\sigma_{xef}(\sigma_{xef} + \sigma_y)} \tag{7}$$

$$\sigma_{xef} = \sqrt{\sigma_x^2 + \phi^2 \sigma_s^2} \tag{8}$$

r_e = electron radius, N_b = number of particles per bunch, β_x^* = amplitude function at the interaction point, γ = particle energy divided by its rest energy, σ_s, σ_x, σ_y = standard deviations for longitudinal , horizontal and vertical bunch dimensions, respectively.

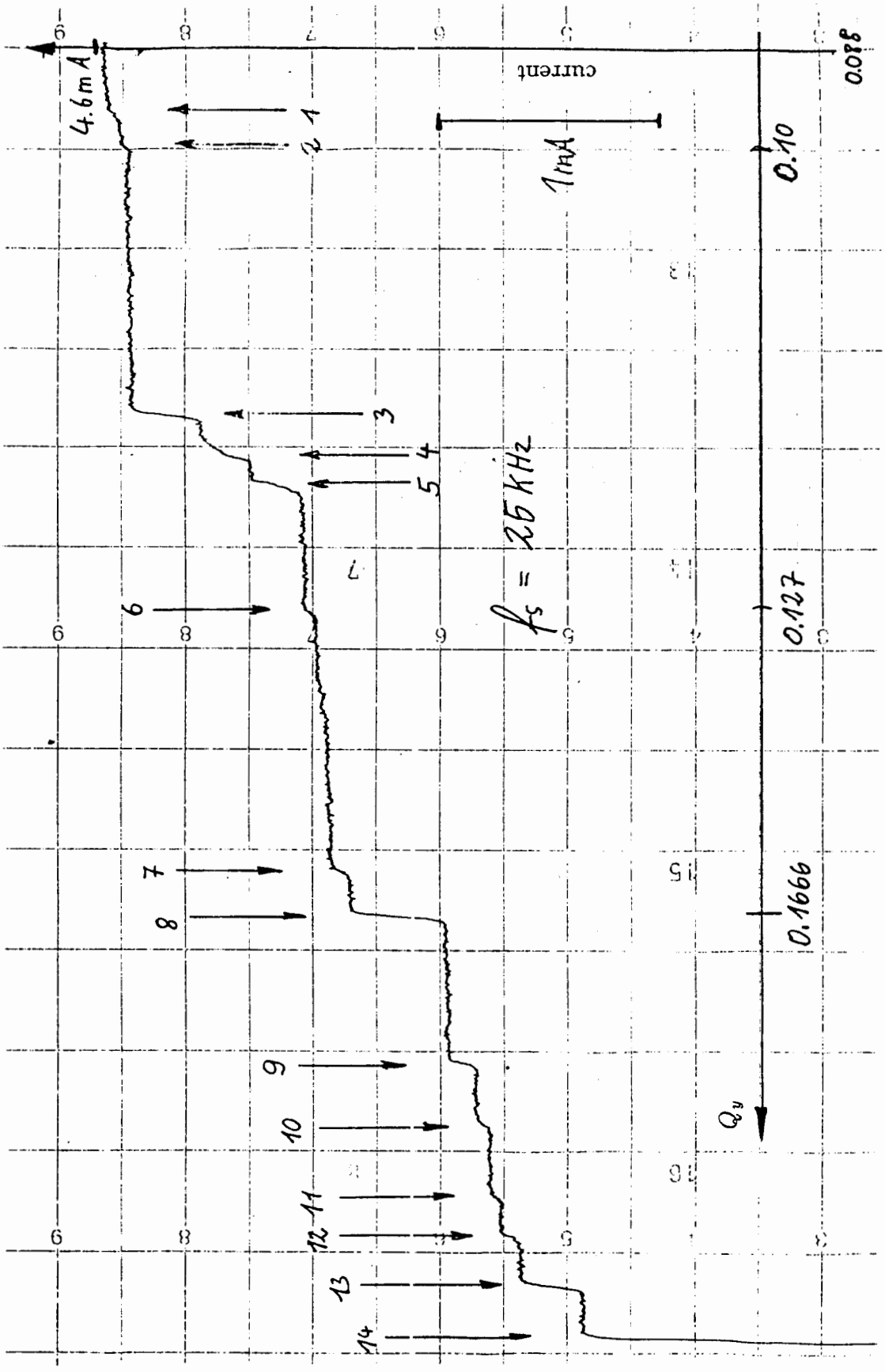


Fig. 2 Variation of the beam current with the betatron frequency.

In case of linear coupling one can apply the matrix formalism and obtains for the phases $\mu_{1,2}$ of the eigenvalues[1,2]

$$\mu_1 = \mu_x + 2\pi\xi \pm 2\pi\xi\phi\sqrt{\frac{-\alpha_M C}{\beta_x^* \sin\mu_x}} \tag{9}$$

$$\mu_2 = \mu_s - 2\pi\xi\phi^2\frac{\alpha_M C}{\mu_s\beta_x^*} \pm 2\pi\xi\phi\sqrt{\frac{-\alpha_M C}{\beta_x^* \sin\mu_x}} \tag{10}$$

where α_M is the momentum factor, C is the circumference, and $\mu_{x,s} = 2\pi Q_{x,s}$. Eqs.(9) and (10) show that an instability occurs on a difference resonance ($\sin\mu_x > 0$, $n < Q_x < n+1/2$, $Q_s < 1/2$).

The nonlinear satellite resonances, which occur for $|k|, |m| > 1$ (Eq.(1)), can be investigated with help of approximation methods[1]. Only one result is given here. One can derive an invariant of motion which is determined by

$$\hat{x}^2 + \frac{k}{m}\frac{\alpha_M C\beta_x}{2\pi Q_s}\left(\frac{\hat{\Delta E}}{E}\right)^2 = \text{const.} \tag{11}$$

where $\hat{x}$ and $\hat{\Delta E}$ are the oscillation amplitudes, and k and m are given by Eq.(1). For most cases $\hat{x}^2$ is smaller than the second term in Eq.(11), and the change of the betatron amplitude is larger than the change of the synchrotron amplitude.

Since m can be positive or negative, the betatron and synchrotron amplitudes can increase or decrease at the same time or they can exchange their oscillation energy periodically. So an instability occurs again for a difference resonance, whereas in the case of a coupling resonance of horizontal and vertical betatron oscillations the difference resonance is stable and the sum resonance is unstable. The reason for this different behavior is the assumption that the particle energy is above transition energy. Below transition energy one has to replace the momentum compaction factor α_M by $(\alpha_M\gamma^2 - 1)/(\gamma^2 - 1)$. So below transition energy ($\alpha_M\gamma^2 < 1$) the satellite resonances show a behavior similar to that of the coupling resonances of horizontal and vertical betatron oscillations.

In case of a horizontal crossing angle only those satellites can be excited for which the relation

$$k + m = \text{even}$$

is satisfied. This follows from the antisymmetric distribution of the space charge forces. It holds, of course, only if the centers of the two bunches collide. In case of an off-set also odd resonances will be excited. Many resonances are suppressed if the interaction points are equidistant. If one takes into account that the crossing angles can have equal signs or alternating signs one gets the conditions for the excitation of satellites[1]

$$\frac{n}{N_i} = \text{integer (equal signs)}$$

$$\frac{2n}{N_i} + m = \text{even (alternating signs)}$$

where N_i is the number of interaction points. If, however, the phase advances between the interaction points are different, e.g. due to machine errors, more resonances can be excited.

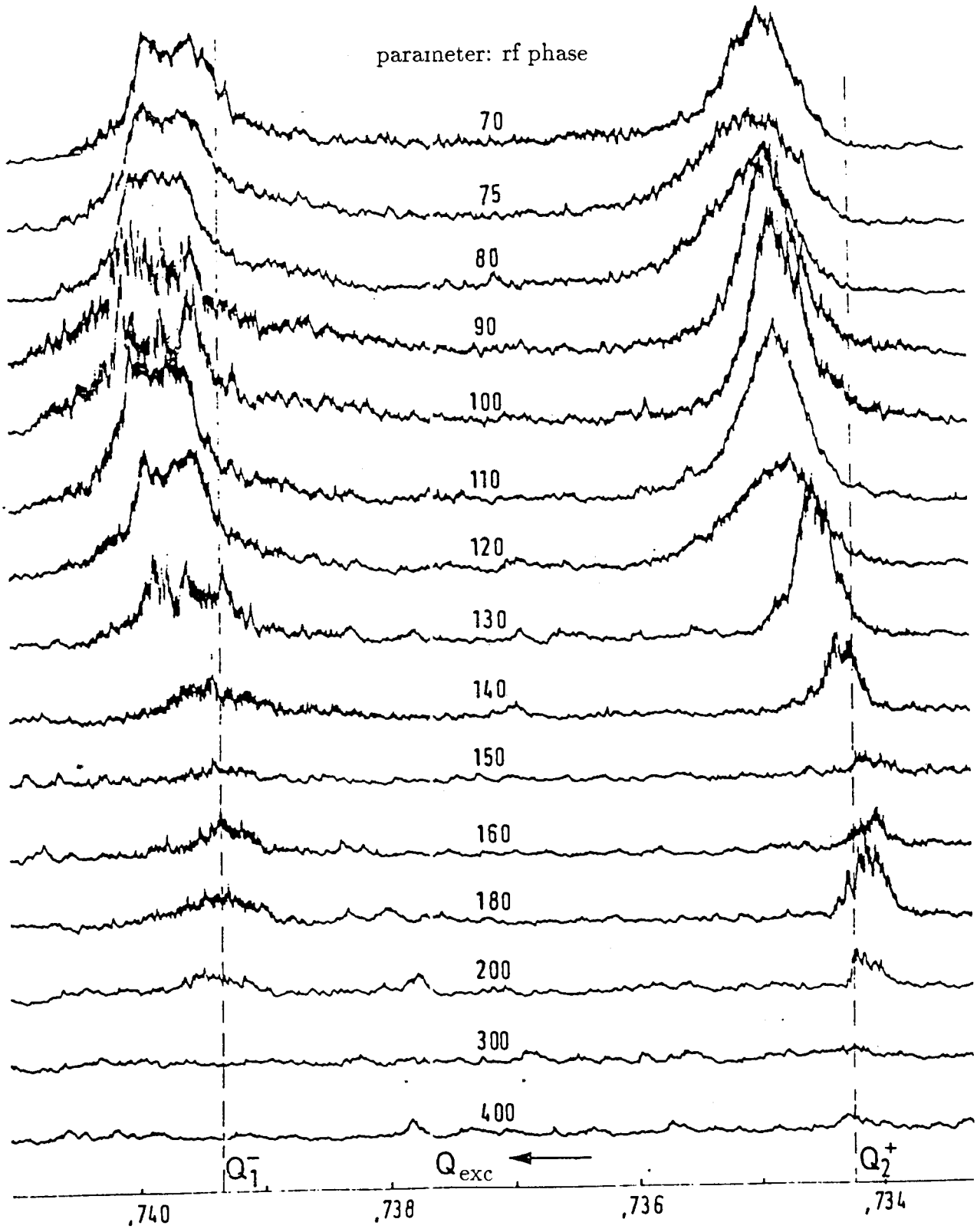


Fig. 3 Coherent signal of the positron beam as a function of the excitation frequency.

The synchro-betatron resonances due to the beam-beam interaction at a crossing angle can be avoided by the so-called crab crossing where the bunches are tilted before and behind the interaction point so that they collide head-on[3]. The tilt angle is obtained by transversely deflecting cavities[3] or by the accelerating cavities with a large dispersion[4]. In both cases the necessary voltages and number of cavities are very large and the impedances of the ring increase strongly. This scheme can be applied, therefore, only with low energy storage rings.

2.2. Measurements

To get an idea of the strength of the satellites due to the beam-beam interaction with a crossing angle the rise times of the amplitudes for the storage ring DORIS I with a vertical crossing angle are given. The parameters are[1]: $2\phi = 24$ mrad, $\xi_y = 0.01$, $\alpha_M = 0.018$, $C = 288$ m, $\beta_y^* = 1$ m, $Q_s = 0.034$, $f_o = 1.04$ MHz. With these parameters one gets a rise time for the vertical betatron oscillation of 0.3 msec.

Many measurements were done with DORIS I with a weak positron bunch colliding with a strong electron bunch. The vertical betatron frequency of the positrons was varied continuously by a computer whereas the synchrotron frequency was kept constant. Simultaneously the current of the positron bunches was plotted. An example of such a measurement is shown,Fig.2,for one interaction point. The sharp losses yield exactly the frequencies of the satellite resonances. Because of the very small width of the resonances and because of the speed of the variation, the only resonances which could be observed were those which gave a lifetime of less than 15 min. In several measurements with one interaction point the following 25 vertical resonances were seen:

$$
\begin{aligned}
&6 + 3Q_s,\ 6 + 4Q_s,\\
&49/8,\ (49 + Q_s)/8,\ (49 - 2Q_s)/8,\\
&43/7,\ (43 \pm Q_s)/7,\ (43 - 2Q_s)/7,\\
&37/6,\ (37 - Q_s)/6,\ (37 - 2Q_s)/6,\\
&31/5,\ (31 \pm Q_s)/5,\ (31 - 2Q_s)/5,\ (31 \pm 3Q_s)/5,\ (31 \pm 4Q_s)/5,\\
&25/4,\ (25 - Q_s)/4,\ (25 - 2Q_s)/4,\\
&28 - 3Q_x,\ Q_x - 1 - Q_s
\end{aligned}
$$

The width of the satellite resonances was measured for several cases. It is only about 0.0005. This small width is caused by the strong nonlinear tune shift of the beam-beam interaction. If the oscillation amplitudes increase the particles come out of resonance and the amplitude growth comes to an end. The frequency variation with amplitude is small only for large amplitudes and hence the amplitude can increase further.

The currents in DORIS I were limited by these satellite resonances. An additional reason for this limitation were multi-bunch instabilities which were suppressed with help of an rf quadrupole and a decoupling transmitter. The rf quadrupole gave to different bunches different betatron frequencies with a spread of $\Delta Q_y = \pm 0.005$ and the decoupling transmitter produced a spread in synchrotron frequencies of $\Delta Q_s = \pm 0.006$. Thus with these operating conditions there were always some bunches on a resonance.

2.3. Finding the beam-beam collision

Since the orbits in the two rings were completely independent the beams did not collide automatically and orbit bumps must be varied in two planes in order to find the

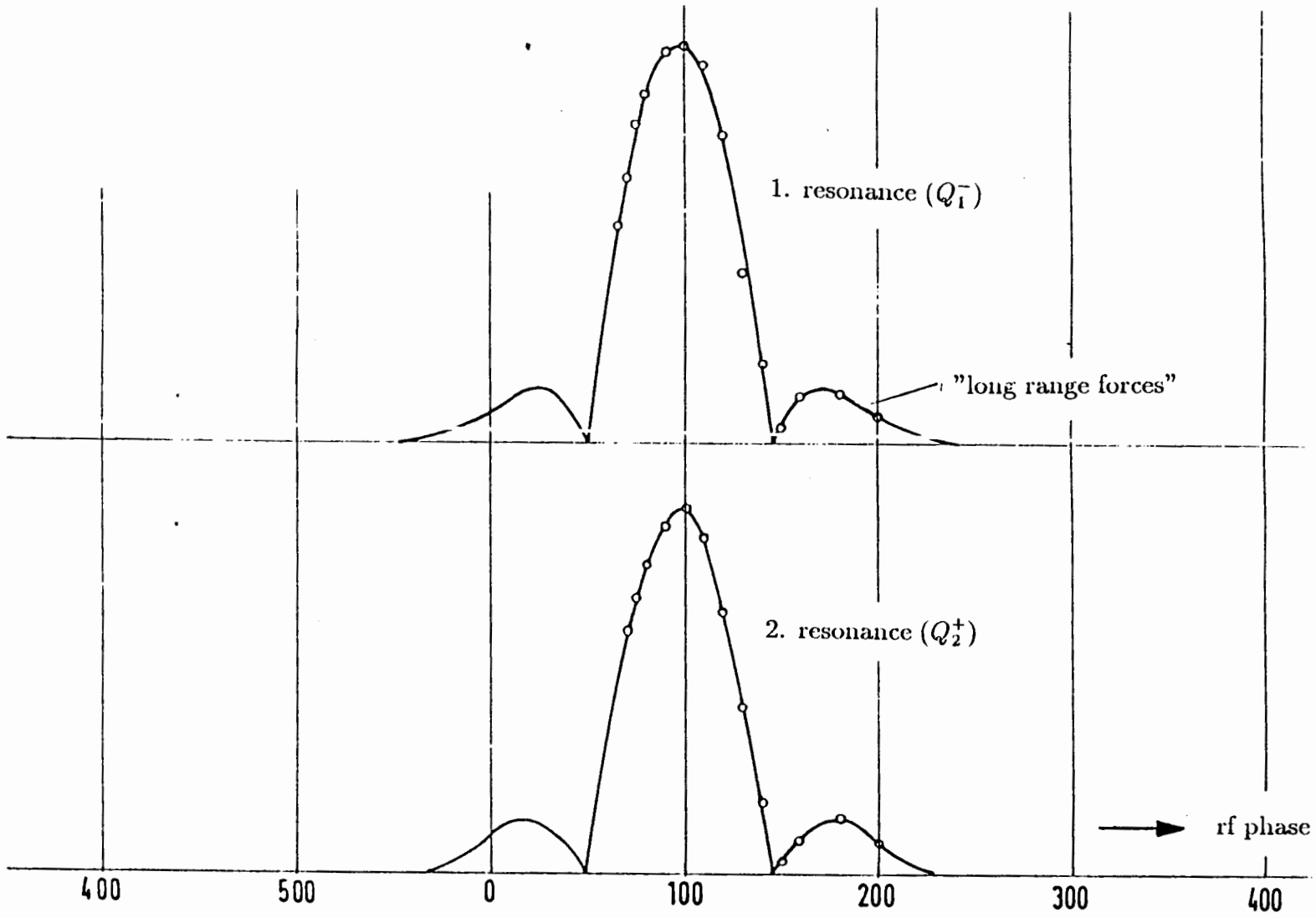


Fig. 4 Coherent signal of the positron beam as a function of the distance between the two beams (rf phase)

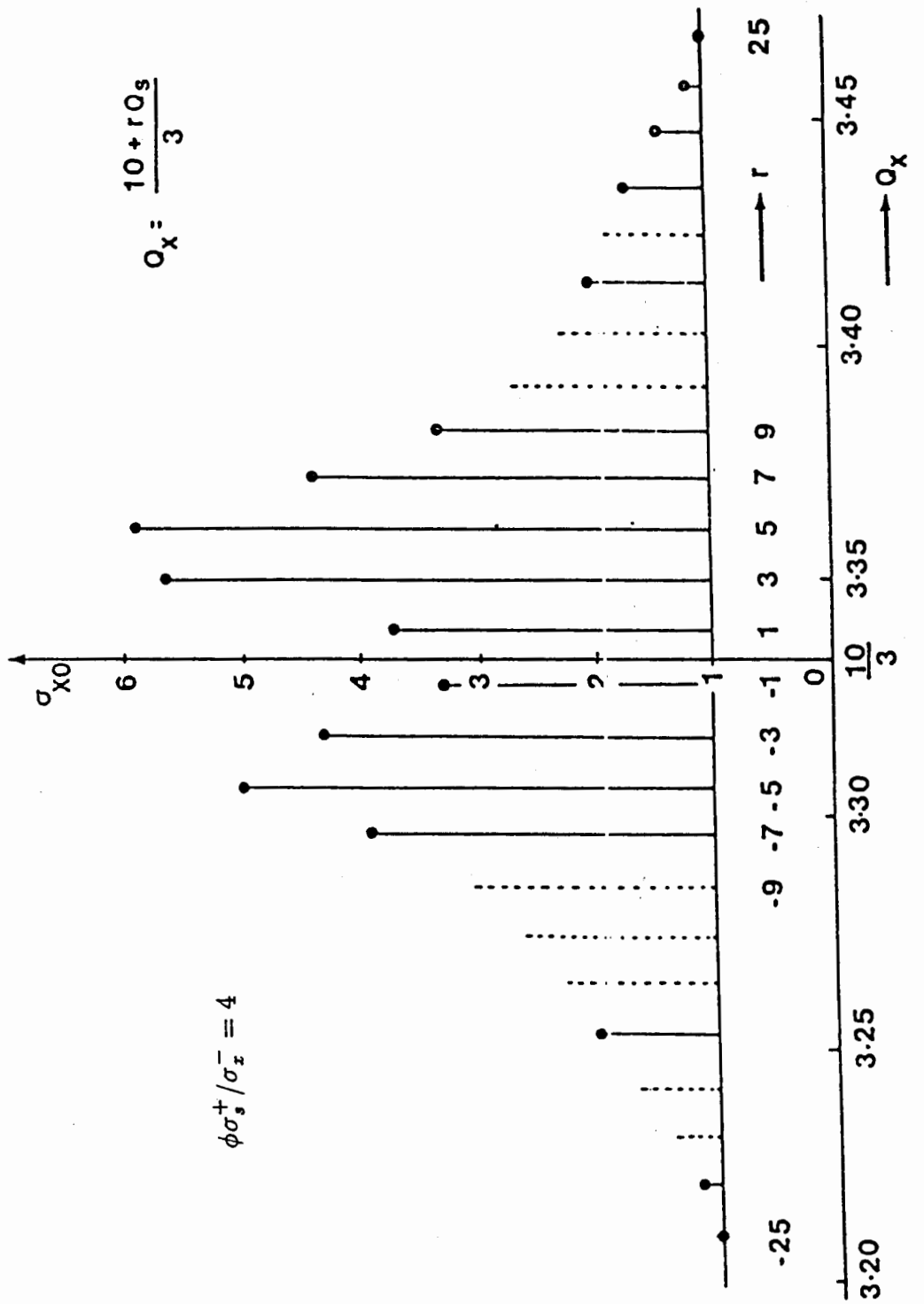


Fig. 5 Maximum amplitudes on all satellites of the resonance $Q_x = 10/3$
(—— simulated, - - - estimated).

collision and optimize it. Once collision has been achieved, it was lost mostly after a change of the optics or the energy or, especially, after a shut down of the accelerator. The fastest method for finding the collision made use of the space charge forces of the two beams[6]. With this method one beam is excited, usually on both resonance frequencies of the two beams, and the response is observed in the other beam. This method is useful both for finding collision and for optimizing the luminosity.

The response is proportional to the inverse of the difference of the fractional tunes of the two rings provided it is large as compared to the tune shift and it is proportional to the derivative of the beam-beam forces with respect to the distance of the beams. For almost equal tunes in the two rings the coupling of the two beams due to the long range forces is very strong. It covers a region of ± 10 transverse standard deviations whereas the luminosity measurement was useful only within a region of ± 2 standard deviations since for larger distances of the two beams the counting rate became too small and the measuring time became too long. Thus this method was particularly effective in case of large distances.

Fig.3 shows a plot of the measured coherent amplitudes of one beam as a function of the frequency with which the other beam was excited. The coherent amplitudes increase on both vertical frequencies of the two beams where the two frequencies had a large distance in this special case. One can see the shift of the frequencies due to the space charge forces which is given by[6]

$$Q_{res1,2} = \left(Q_1 + Q_2 + \Delta Q_1 + \Delta Q_2 \pm \sqrt{(Q_1 - Q_2 + \Delta Q_1 - \Delta Q_2)^2 + 4\Delta Q_1 \Delta Q_2}\right)/2 \quad (12)$$

where Q_1 and Q_2 are the undisturbed vertical betatron frequencies of the two beams and ΔQ_1 and ΔQ_2 are the incoherent tune shifts for arbitrary distances between the two beams given by the derivative of the space charge forces.

Fig.4 shows the measured coherent amplitudes on the two frequencies of the two beams. They vary exactly as the absolute value of the derivative of the space charge forces with respect to the distance between the beams. The distance was changed in this case by the rf phase which has the same effect as a vertical orbit bump.

This method was also used successfully with HERA[7] where the collision of electrons and protons was adjusted. Although the proton oscillations are not damped and the excitation must be very weak a precise adjustment could be made.

3. HERA

In the first proposal for the e-p storage ring HERA a horizontal crossing angle was foreseen since it has some advantages over head-on collision, e.g. less synchrotron radiation hits the detectors and the optics of the two rings are completely independent. It was assumed that with a smaller space charge parameter (ξ=0.0006 instead of 0.01 as in DORIS I) and without spread in betatron and synchrotron frequencies a good working point for the protons could be found. Computer simulations, however, have shown that in this case even more satellite resonances would be excited[5] and the crossing angle was abandoned.

The simulations have shown satellites of nonlinear resonances up to the order 11. Fig.5 shows all satellites of the resonance $Q_x = 10/3$. Only odd resonances are excited. This follows from the antisymmetric distribution of the space charge forces.

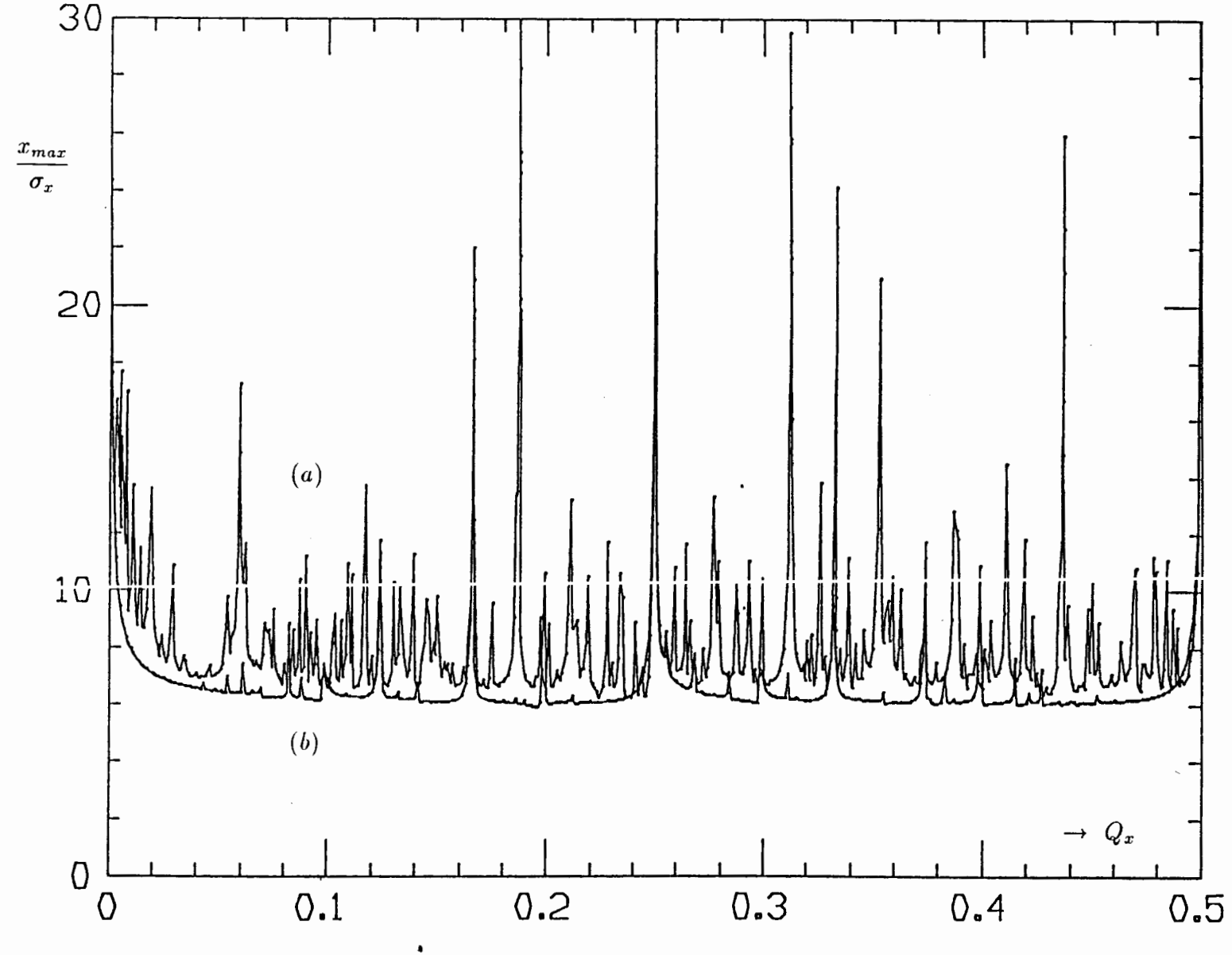


Fig. 6 Maximum horizontal amplitudes vs tune with a horizontal crossing angle $2\phi = 15$ mrad ($\phi\,\sigma_s/\sigma_x = 0.4$) (a), with head-on (b).

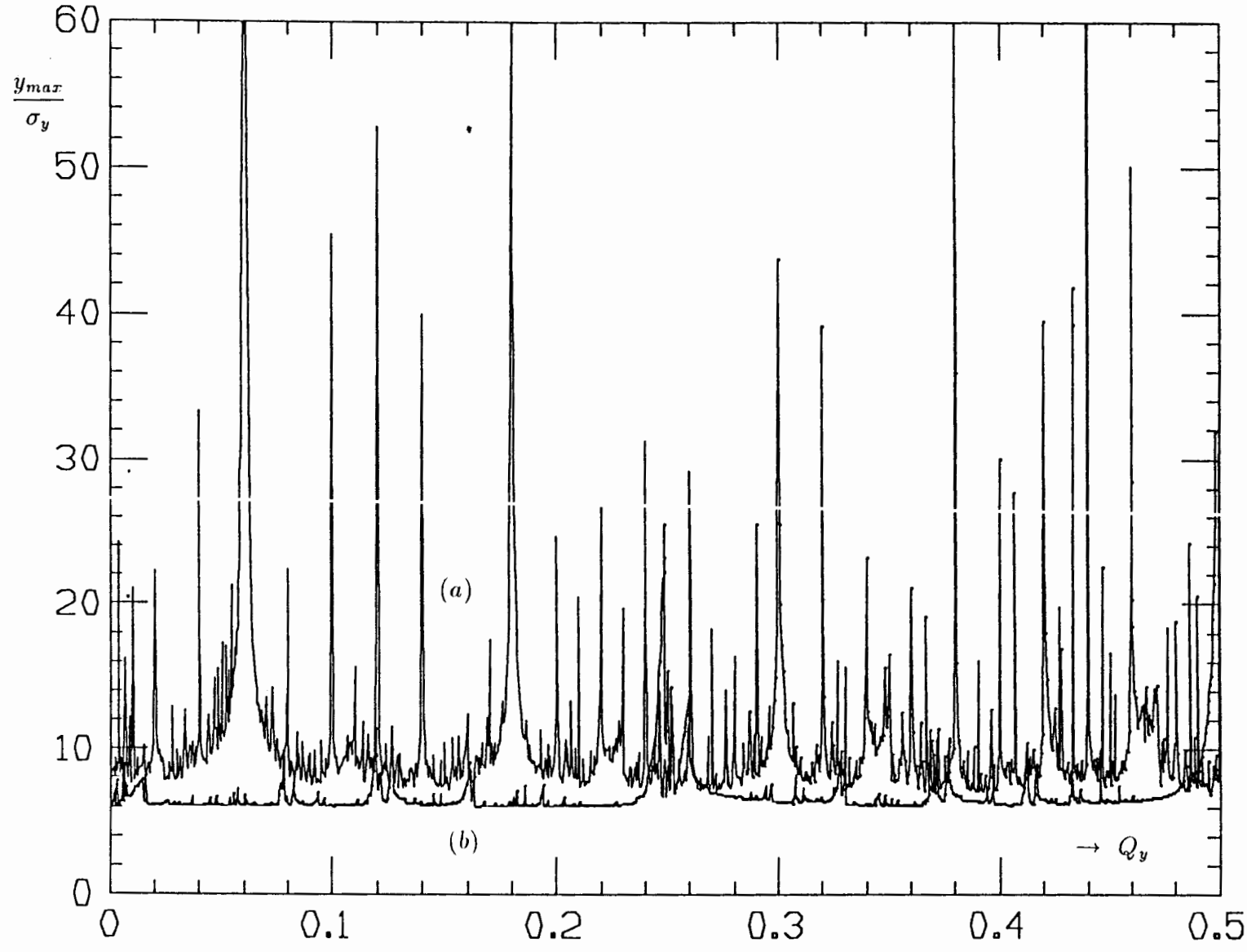


Fig. 7 Maximum vertical amplitudes vs tune with a vertical crossing angle $2\phi = 15$ mrad ($\phi\sigma_s/\sigma_x = 10.$) (a), with head-on (b).

One reason for the larger number of satellite resonances was the fact that the proton bunch length was much larger than the electron bunch length, and the normalized crossing angle for the protons $\phi\sigma_s^+/\sigma_x^-$ was 4 in HERA whereas the normalized crossing angle for DORIS I was only 0.5. This means that the synchrotron motion of the protons covers more nonlinearities and more satellite resonances can be excited. Another reason is that even weak satellites with a rise time of several hours become dangerous since there is no damping for protons.

The planned crossing angle for HERA was horizontal since a vertical crossing angle gives, for the same absolute crossing angle ϕ, a larger normalized crossing angle $\phi\sigma_{lon}/\sigma_{tr}$. A comparison of satellite resonances due to a horizontal and a vertical crossing angle[8] is shown in Figs.6 and 7.

4. Conclusions

The experiments with DORIS I as well as the simulations have shown that the synchro-betatron resonances excited by the beam-beam interaction with a crossing angle reduce mainly the lifetime and do not affect seriously the beam size or the specific luminosity. Four parameters are important for the reduction of the lifetime:

1) the normalized crossing angle $\phi\sigma_{lon}/\sigma_{tr}$,
2) the beam-beam space charge parameter ξ,
3) the synchrotron frequency Q_s,
4) the physical or dynamical aperture of the ring.

In principle each of the four parameters can be chosen such that the resonances are rendered harmless even if the other three parameters are given arbitrarily. If, for example, the normalized crossing angle is smaller than 0.1 it will not excite many satellites with large amplitudes. If the synchrotron frequency is smaller than 0.001 the satellites are so close to the betatron resonances that they will not significantly reduce the free space in the tune diagram[9], and if the acceptance is larger than 30 σ the amplitudes will not reach the aperture. But also with a combination of weaker conditions for the four parameters an operation with a crossing angle should be possible.

5. References

1. A. Piwinski, 1977 Particle Accel. Conf., IEEE Trans. V. NS-24, No.3, (1977), p.1408.
2. A. Piwinski, 11th Intern. Conf. on High-Energy Accel., Geneva, (1980), p.638.
3. K. Oide, K. Yokoya, SLAC-PUB-4832 (1989).
4. G. Jackson, AIP Conference Proceedings 214(1990)
5. A. Piwinski, 1985 Particle Accel. Conf., Vancouver, (1985).
6. A. Piwinski, DESY H2-75/03 (1975).
7. S. Herb, F. Zimmermann, 15th Intern. Conf. on High Energy Accelerators, Hamburg, Germany(1992), p.227.
8. A. Piwinski, SLAC-PUB-5430 (1991).
9. W. Chou, A. Piwinski, SSCL-Preprint-119(1992).

Beam Lifetime and Beam-Beam Tails in LEP

H. Burkhardt*
CERN, SL Division, CH-1211 Geneva 23, Switzerland

1. Introduction

LEP is currently running in its 6th year at Z-energies with beam energies of about 45.6 GeV. Single beam emittances can be rather small. About ε_x = 12 nm in the horizontal plane and still 2 orders of magnitude less in the vertical plane. Single beam lifetimes are about 40-50 hours and mainly limited by Compton scattering with black body radiation.
In collisions, beam sizes increase significantly in both planes as result of the beam-beam interaction. Lifetimes are reduced to about 17 hours due to "loss" of particles in e^+e^- collisions. Beam-beam tuneshift parameters in excess of 0.04 have been reached routinely in operation [1]. Significant beam-beam tails are observed for high beam-beam tuneshifts and bunch currents. They limit the maximum current that can safely be collided [2].

2. Standard Operation

LEP is filled at 20 GeV beam energy via a sequence of accelerators (the dedicated LIL and EPA and the PS and SPS as pre-accelerators). Currents of about 350 μA per bunch corresponding to $2 \cdot 10^{11}$ particles are accumulated in a couple of minutes. LEP was operated 1993 and 1994 with 8+8 bunches in the horizontal Pretzel scheme[3]. The number of bunches can be doubled this year using bunch trains with vertical separation.
Ramping the beam energy E_b from 20 to 45.6 GeV beam energy takes 6.5 minutes. Beams are then squeezed vertically to β_y^* = 5 cm in one minute. The horizontal β_x^* is kept constant at 2.5 m. Pre-collision tunes in LEP are set to $Q_x = 90.3$ and $Q_y = 76.2$.
For flat beams ($\varepsilon_x \gg \varepsilon_y$) with n = $2 \cdot 10^{11}$ particles, a Lorentzfactor $\gamma = E_b/m_e = 89237$, the horizontal beam-beam tuneshift becomes (r_e is the classical electron radius):

$$\xi_x = \frac{r_e\, n}{2\pi\, \gamma\, \varepsilon_x} \approx \frac{1\text{ nm}}{\varepsilon_x} \tag{1}$$

The horizontal single beam emittance is increased from ε_x = 12 to 36 nm using a wiggler in a region of horizontal dispersion (the "emittance wiggler") to bring beams safely into collision. This assures that ξ_x cannot exceed the value given by equation(1) (or a value of 0.028 for 350 μA per bunch) and proved to be very effective to avoid flip-flop and excessive beam-beam tails with background and life-time problems.

*email: hbu@cernvm.cern.ch

3. Beam Lifetimes, example of LEP fill 2420

Fig. 1 illustrates the evolution of luminosity and currents in a recent LEP coast. About 2.6 mA per beam or 320 μA per bunch were brought into collision. The positron current was about 7 % higher than the electron current. The ratio luminosity to beam current (L/I) is directly proportional to the

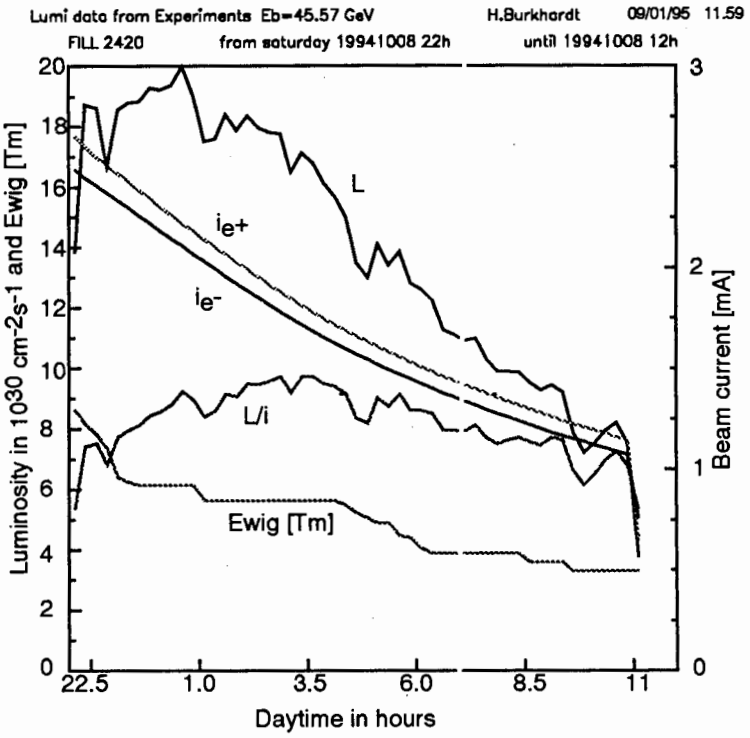


Figure 1: Evolution of Luminosity and Currents in Fill 2420. The setting of the emittance wiggler (Ewig) is also shown.

vertical beam-beam tune shift parameter ξ_y and tends to be about constant during coasts. In this fill, ξ_y quickly exceeded values of 0.04 with peak values up to 0.047 after about five hours in coast. Fig. 2 compares the vertical beam-beam tune shift parameter ξ_y, calculated from the measured luminosity current ratio, with the beam-beam lifetimes of the e^+ and e^- beams. The beam-beam lifetime τ_{bb} is obtained as difference of the total measured lifetime τ and single beam lifetime τ_s according to:

$$\frac{1}{\tau_{bb}} = \frac{1}{\tau} - \frac{1}{\tau_s}$$

The 1994 data for single and separated beams is consistent with a constant value of $\tau_s = 45$ hours. In [4] it was shown that the expected beam-beam lifetime τ_{bb} follows ξ_y according to:

$$\tau_{bb} = \frac{2 r_e m_e}{n_{cross}\, f\, \sigma} \frac{\beta_y^*}{E_b\, \xi_y} \approx 1 \text{ hour}/\xi_y$$

$\sigma \approx 0.21$ barn is the total e^+e^- cross-section leading to the loss of a beam particle. It is dominated by beam-beam Bremsstrahlung, or more precisely, since we are dealing with e^+e^- collisions, by radiative Bhabha scattering. The full kinematics of the process and the introduction of a cutoff parameter corresponding to the mean half-distance between the particles in the bunch is discussed in [5]. About the same result is obtained by introducing a cutoff corresponding to the beam height as advocated in [6].

The proportionality between ξ_y and beam-beam lifetime is well visible in fig. 2. Some additional losses

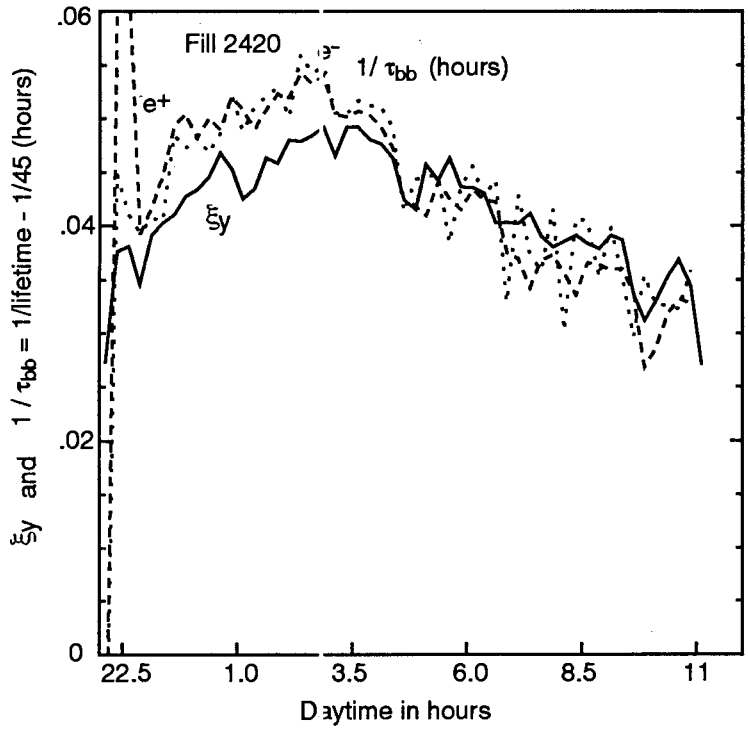


Figure 2: The vertical beam-beam tuneshift parameter ξ_y (solid line) and the inverse e^+ (dashed line) and e^- (dotted line) beam-beam lifetimes in 1/hours for the same fill.

are seen in the first hours of the fill and in particular during times of very high vertical beam-beam tuneshifts. The additional losses reached about 1 % per hour (100 hours lifetime from extra losses). Still, the total lifetime stayed well above 10 hours. This can be seen in Fig. 3 which shows the same data again but this time directly as total measured and calculated lifetime in hours.
Attempts to collide higher currents or less favorable conditions like significant differences in currents of colliding bunches resulted in severe background or lifetime problems. A systematic study of the luminosity and beam current data of LEP coasts gave the following results

- Lifetimes for low currents are well explained by collision processes
- Observation of lifetimes below 10 hours imply significant extra losses
- Low lifetimes are often connected with background bursts seen by the experiments
- For similar running conditions, the probability for lifetime problems increases rapidly with current.

Operational experience has shown that the threshold for lifetime problems can be increased through

- a careful choice of the tune working point
- emittance control, - increasing the horizontal emittance using a wiggler
- increasing aperture, - using wider collimator settings

We believe that the lifetime and background problems are connected to losses by scraping into transverse beam-beam tails. It is difficult to localize losses and to optimize parameters for smooth running conditions based on studies of beam-current data. A much higher sensitivity can be achieved with loss monitors [7]. Scintillators have been installed in LEP at the aperture limiting collimators [8]. Recently,

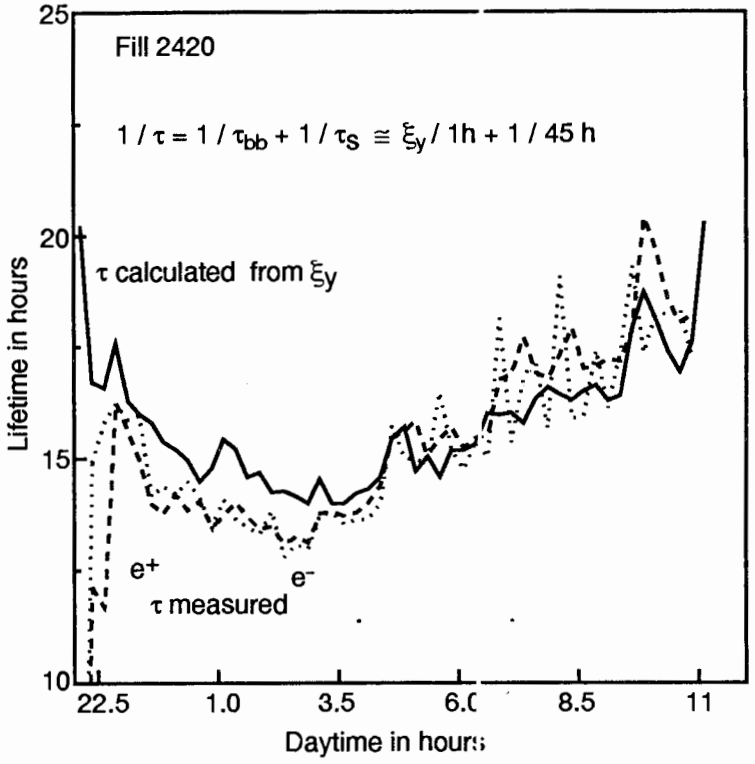


Figure 3: Total lifetime as obtained from fixed single beam lifetime and beam-beam lifetime via ξ_y (solid line) and measured e^+ (dashed line) and e^- (dotted line) lifetimes.

many more loss monitors using pin-diodes based on a design for HERA [9] were installed close to most collimators in LEP. Several measurements using loss monitors have been performed in recent machine development sessions and are being analyzed [10], [11]. First preliminary results will be discussed in the following chapter.

4. Beam-Beam Tails

Figures 4 and 5 show tail distributions as measured in two machine development sessions:

1) Fill 2364 on 4-9-94, 4x4 bunches, about 350μA per bunch, tails measured using pin-diode loss monitors
e^+, e^- emittances were ε_x = 40 nm and ε_y = 3.6 nm,
beam-beam tuneshift parameters ξ_x = 0.025 and ξ_y = 0.042 .
Results are shown as solid lines for different settings of chromaticity (Q' between +5 and +10).
In the vertical plane tails were also measured with separated beams.

2) Fill 2724 on 10-6-95, 4x4 bunches, about 250μA per bunch, losses measured with scintillators
beams colliding, using '95 optics with vertical separation on either side of the interaction regions for bunch trains.
Rather unequal e^+, e^- beam sizes, about 60 % higher e^- emittances in both planes.
e^- beam parameters were ε_x = 44 nm and ε_y = 4 nm,
with beam-beam tuneshifts of ξ_x = 0.025 and ξ_y = 0.035 .
Measurements were done for one machine setting with Q'=10 in both planes.
The results are shown as broken lines

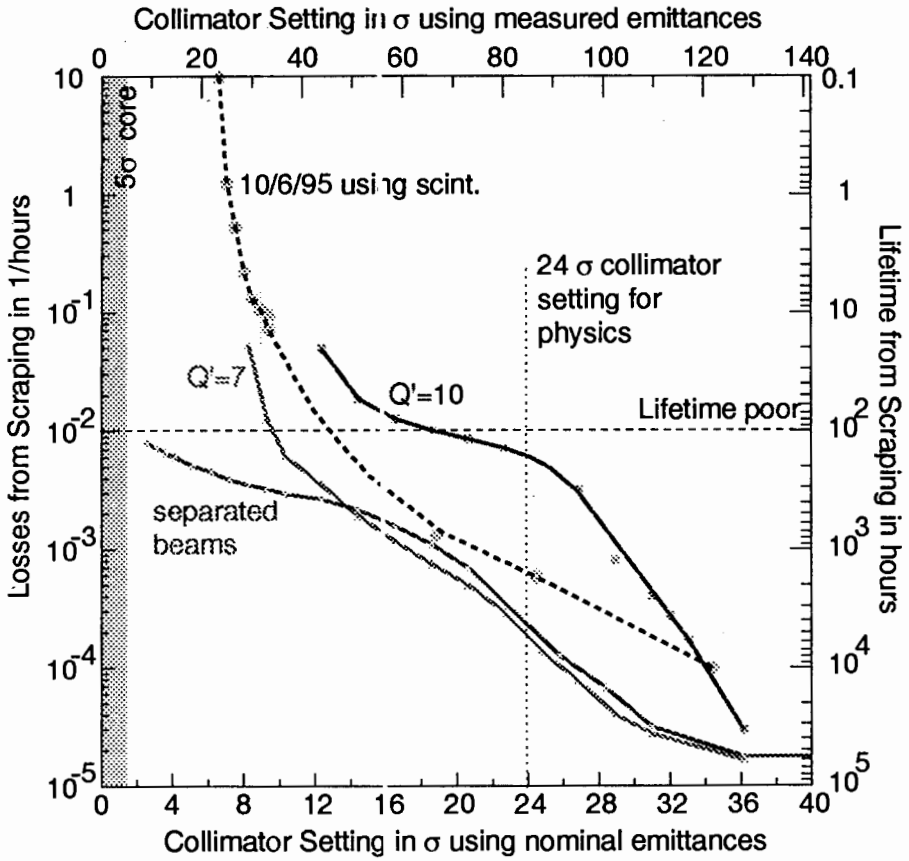


Figure 4: Measured beam tails in the vertical plane.

Measurements were performed by moving one jaw of a collimator closer to the beam in steps. Beam current and beam size measurements were recorded for each collimator setting. The collimators were moved closer until significant lifetime reductions were observed. Lifetimes calculated from beam currents for these points were used to calibrate the loss monitors. This allows to give loss rates directly in terms of equivalent lifetimes from scraping. The uncertainty in the absolute calibration is estimated to be about 30 %. There is some additional systematic error from noise and saturation for very high and low loss rates:

The pin-diode monitors are nearly noise-free but give only counts and saturate therefore at one hit per bunch passage. Measurements have been linearized using Poisson statistics.

The scintillators use pulse height information and did not reach saturation. Due to noise, these monitors are not sensitive to losses below 10^{-4}/hour.

The two different types of loss monitors are therefore rather complementary.

At the end of the second machine development scraping in the vertical plane was continued down to very low electron lifetimes in the order of minutes.

We distinguish between nominal and measured emittances. The nominal emittances are 45 nm for the horizontal and 4.5 nm for the vertical plane. Nominal emittances are very useful to compare collimator settings for various optics and positions around the ring. The values of 45 and 4.5 nm have been used in LEP for the last couple of years and still reflect quite well the maximum beam sizes observed in operation.

The collimator settings in figures 4, 5 are given in units of σ of nominal beam sizes. In addition, a second x-scale is shown on top of the figures using the measured beam sizes (measured beam sizes of both experiments were equal within errors of about 10 %). The expected gaussian core is illustrated

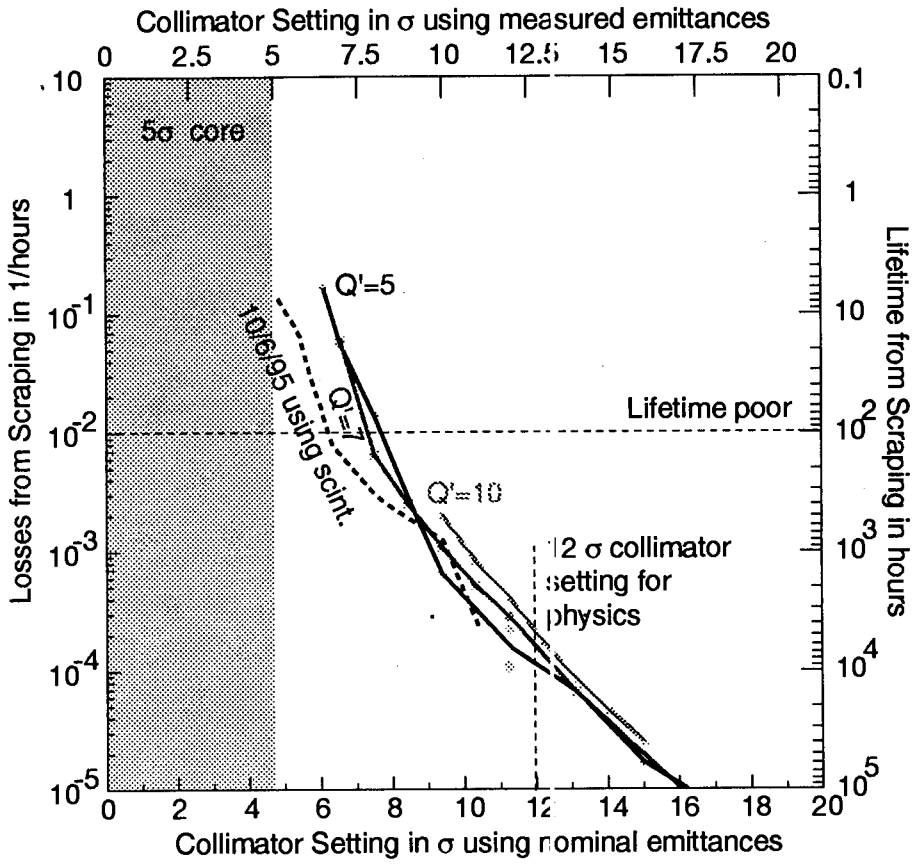


Figure 5: Measured beam tails in the horizontal plane.

as shaded area to 5 σ using the measured emittances.
At this stage of measurements and analysis we found indications for:

- Non-gaussian transverse tails in both planes. Far tails and losses corresponding to lifetimes of order 10^3 hours were also recorded without colliding beams and might originate in processes like scattering on beam-gas or photons from black-body radiation
- Very substantial non-gaussian beams are present for colliding beams in the vertical plane. High chromaticities increase vertical tails.

5. Summary

Lifetimes for single beams, separated beams and low-current colliding beams in LEP are well explained by known physics collision processes

- Compton scattering on black-body radiation photons
- Beam-Gas scattering
- Beam-Beam Bremsstrahlung

These collision processes result mainly in off-energy particles. If the energy loss exceeds the stable bucket height (about 1 % for LEP1) these particles will be lost, typically by hitting an aperture limit in a dispersion region.

Extra losses are seen for colliding beams and higher currents and have limited the maximum useful bunch currents at LEP1. They are attributed due to transverse tails generated by the beam-beam effect. Emittance blow up is observed for colliding beams in LEP in both planes. A wiggler is used to artificially increase the horizontal beam sizes and to avoid flip-flop and excessive tails. Very substantial tails are present for colliding beams in the vertical plane. More measurements and a detailed analysis including comparison with beam-beam simulation [12] are planned for the near future.

References

[1] R.Bailey et al.; *Operational procedures to obtain high beam-beam tune shifts in LEP operation*, CERN-SL-95-49 OP and proceedings of PAC conference, Dallas 1-5 may 1995.

[2] H.Burkhardt; *What is the maximum current we can collide at 45 GeV ?*, Proc. of the 5th LEP Perf. Workshop, Ed. J.Poole, CERN SL/95-08, pages 131-134

[3] R.Bailey et al.; *LEP Operation in 1993 with the Pretzel Scheme*, Proc. 4th Europ.Part.Acc.Conf. EPAC London 1994, Eds. V.Suller and Ch.Petit-Jean-Genaz, Vol I page 439-441

[4] H.Burkhardt, R.Kleiss; *Beam Lifetimes in LEP*, Proc. 4th Europ.Part.Acc.Conf. EPAC London 1994, Eds. V.Suller and Ch.Petit-Jean-Genaz, Vol II page 1353-1355

[5] R.Kleiss, H.Burkhardt; *BBBREM: Monte Carlo Simulation of Radiative Bhabha Scattering in the very forward direction.* Comp.Phys.Commun.81:372-380,1994.

[6] G.L.Kotkin, V.G.Serbo, A.Schiller; *Processes with Large Impact Parameters at Colliding Beams.* Int.J.Mod.Phys. A7 (1992) 4707-4745

[7] S.Zholents; Presentation 78, 2nd workshop on LEP Performance, Ed. J.Poole, CERN SL/92-29

[8] K. Cornelis et al.; *Commissioning of a Scintillator at the Aperture Collimators for the Study of Beam Tails*, SL-MD Note 60, October 1992.

[9] W.Bialowons, F.Ridoutt, K.Wittenburg; *Electron Beam Loss Monitors for HERA*, Proc. 4th Europ.Part.Acc.Conf. EPAC London 1994, Eds. V.Suller and Ch.Petit-Jean-Genaz, Vol II page 1628-1630

[10] H.Burkhardt, K.Cornelis, J.J.Gras, I.Reichel; *Scrapers and Tails*, SL-MD Note 175, June 1995

[11] I.Reichel; University of Aachen/Germany and CERN, *work for Ph.D. thesis on transverse beam profiles in LEP*

[12] T.Chen, J.Irwin, R.Siemann; *Simulation of the Beam-Beam Lifetime for LEP*, Proc. 4th Europ.Part.Acc.Conf EPAC London 1994, Eds. V.Suller and Ch.Petit-Jean-Genaz, Vol II page 1356-1358

Crossing Angle Issues in KEKB

HIRATA Kohji
(hirata@kekvax.kek.jp)
KEK, National Laboratory for High Energy Physics
Oho, Tsukuba, Ibaraki 305 Japan

KEKB uses a rather large crossing angle. The beam-beam effects have been studied by means of a fairly accurate mapping. Some simulation results (luminosity and beam halo) are shown, which have convinced us the feasibility of such a scheme.

1. Introduction

The KEKB[1] at KEK is an asymmetric, double-ring electron-positron collider. To achieve the highest possible luminosity, we will use the finite crossing angle (half angle $\phi = 11$ mrad), because it allows us to use all the buckets. It seems widely believed, however, that the crossing angle is a quick-tempered goddess: she may destroy the whole project using the violent "synchro-betatron" resonances and nobody can calm her. They say that such a disaster has happened in DORIS[2]. The beam-beam issues for KEKB are not only the large crossing angle (the normalized crossing angle $\Phi \simeq 1/2$) but also the long bunch ($\sigma_s \simeq \beta_y$) effects (so-called hourglass[3]effects) are involved.

I believe that the beam-beam interaction with a large crossing angle and/or a long bunch has not yet been studied in detail enough to treat the KEKB parameters. Several authors have studied it either theoretically or by simulation. They, however, have introduced some rather crude approximation and simplification. For example, the standard treatment of Piwinski[2] might have been good enough for short bunches but it is not trivial to extend his method to long bunches. Nowadays, on the other hand, the single particle tracking is being performed with a great accuracy; thick sextupoles, for example, if necessary[4]. The beam-beam interaction is not more complicated than the thick sextupole with nonlinear edge. From this point of view, we have proposed a new mapping[5] for (almost) head-on collisions which I believe is the most accurate 6D symplectic mapping we have and which I believe is applicable to KEKB parameters. To apply it to the collision with an angle, all one should do is just to introduce the Lorentz boost[6] before the collision and its inverse transformation after the collision. The bunch length effect is treated by the longitudinal slicing[7] in the boosted frame.

In this paper, we do not discuss the detail of the tracking program[5, 6, 8]. The basic idea, however, may be read off from Fig.1. We show how we have arrived at the present working point and how we have confirmed it.

2. Geometrical Considerations

Before going into details, it seems useful to consider some geometrical (not dynamical) effects of the crossing angle and the bunch length.

It seems useful to define the geometrical luminosity L_g and effective beam-beam parameter ξ in the boosted frame. Including the hourglass and the beam tilt effects due to the Lorentz boost, but excluding the dynamical effects, we define R_L (luminosity reduction factor) and $R_\xi^{x,y}$

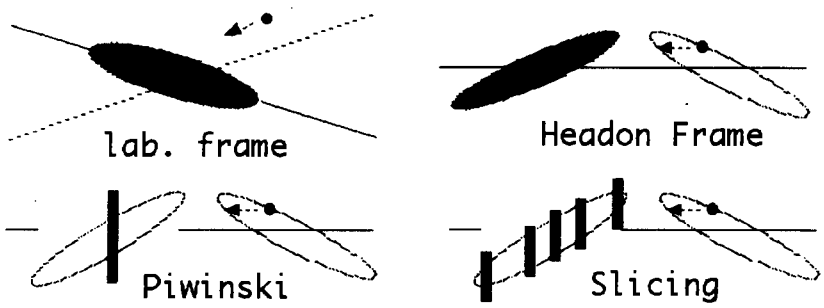


Figure 1: Collision with an angle can be seen as a head-on collision with tilted beams when seen from the boosted heading frame. We perform a Lorentz transformation such that the barycenters of both bunches collide head-on. In the head-on frame, the collision can be thought of as successive collisions with many slices.

(beam-beam reduction factor) as follows:

$$R_L = \frac{L_g}{L_0} = \sqrt{\frac{2}{\pi}} a e^b K_0(b), \tag{1}$$

$$a = \frac{\beta_y^*}{\sqrt{2}\sigma_z^*}, \qquad b = a^2 \left[1 + \left(\frac{\sigma_z^*}{\sigma_x^*}\tan\phi\right)^2\right].$$

When $\phi = 0$, this expression agrees with that by Furman[3].

$$R_\xi^{x,y}(z) = \xi_{x,y}/\eta_{x,y} \tag{2}$$
$$= \int dz^\dagger \rho(z^\dagger) \frac{\beta_{x,y}(S)}{\beta_{x,y}^*} F_{x,y}(z^\dagger \tan\phi, \sigma_x^*(S), \sigma_y^*(S)),$$

$$S = (z - z^\dagger)/2.$$

where L_0 and η are the luminosity and the beam-beam parameter without hourglass nor tilt effects,

$$L_0 = \frac{N^2 f}{4\pi\sigma_x\sigma_y}, \qquad \eta_{x,y} = \frac{N r_e}{2\pi\gamma} \frac{\beta_{x.y}}{\sigma_{x,y}(\sigma_x + \sigma_y)}$$

where N is the number of particles in the bunch, f the revolution frequency, σ's are the beam sizes at $s = 0$; K_0 is a Bessel function and $F(x, \sigma_x, \sigma_y)$s are Montague's reduction factor[9] of ξ for an off center particle, which falls down with ϕ quite rapidly.

The R_L is shown in Fig.2 (left) as a function of ϕ and β_y/σ_z. The R_L and R_ξ are shown in Fig.2 (right) as functions of ϕ for parameters a little more extreme than those of KEKB. For small ϕ, R_ξ is even larger than 1 due to the hourglass effect which makes the beam-beam interaction more serious. This decreases rapidly for larger ϕ. At the same time, R_L also decreases but less rapidly. If we assume that the seriousness of the beam-beam effect is characterized by ξ, we can vaguely understand that the crossing angle might have a merit rather than demerit: for the same value of ξ, the L_g is larger.

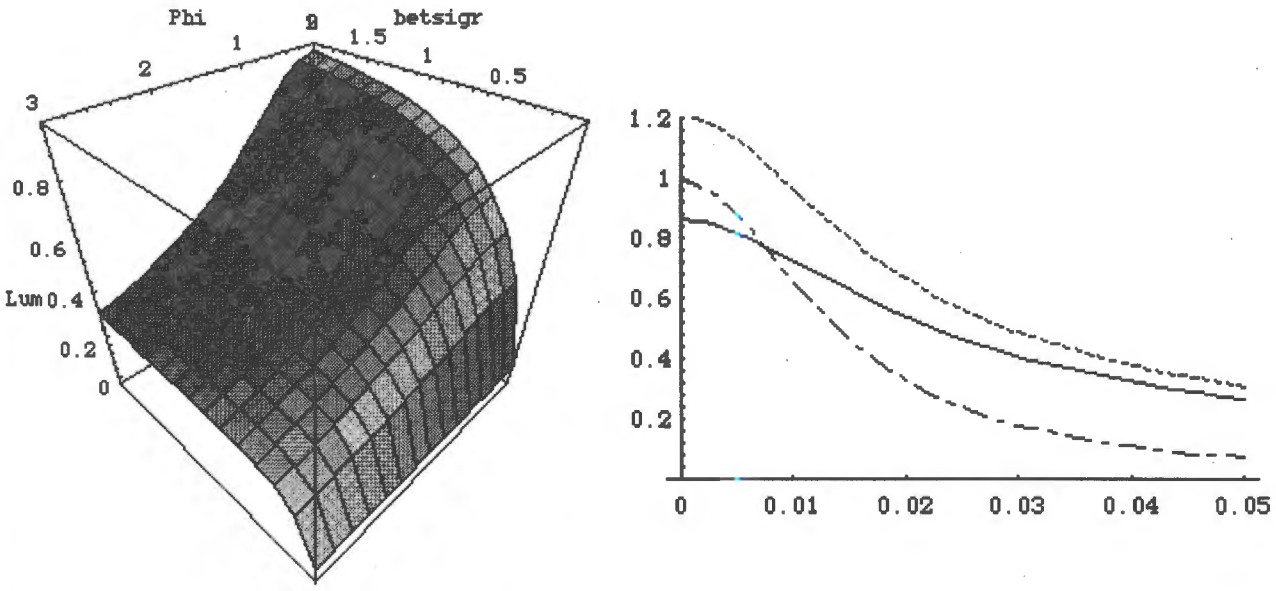


Figure 2: Left: The geometrical luminosity reduction factor R_L as a function of $\Phi \equiv \phi\sigma_z/\sigma_x$ and β_y/σ_z. Right: The (geometrical) luminosity reduction factor R_L (solid), and tune shift reduction factors R_ξ^y (dotted) and R_ξ^x (dot-dash), as functions of ϕ (rad), for the case $\beta_y = \sigma_z$. R_ξ's are plotted for a particle at the center ($z = 0$).

3. "Optimization" of the Parameters

Since there are too many parameters to determine and there are many constraints for them, one cannot survey all the possible parameters in detail. Here, we show how we have gotten a sort of the "optimizing" parameters. There can be other better sets of parameters.

First, we have certain constraints from lattice and instability considerations. The former gives possible range for the horizontal and vertical emittances ($\varepsilon_{x,y}$) and the betatron functions ($\beta_{x,y}$) at the interaction point (IP). The latter gives the number of particles in a bunch (N).

Under these constraints, we have looked for an optimal operation point as follows:

1. from several preliminary simulation results, it was known that ν_s should be small because of the synchro-betatron resonance reason. Also, β_y was set as small as possible from lattice point of view.

2. the crossing angle ϕ should be large to avoid the use of the separation bending magnets[1, 8]. We chose 10 mrad.

3. for reasonable values of ϵ_x, by using Eq.(1), we find ϵ_y which gives the geometrical luminosity L_g $1.16\times10^{34}\mathrm{cm}^{-2}\mathrm{s}^{-1}$.

4. for each set of (ϵ_x, ϵ_y) thus obtained, by the weak-strong simulation with linear lattice without errors, we surveyed all the tune plane ($0 < \nu_x < 1$, $0 < \nu_y < 1$) roughly and find the largest possible value of the luminosity L.

5. by comparing these L for each set of (ϵ_x, ϵ_y), we choose the optimum set of (ϵ_x, ϵ_y). We arrive at the "optimum" parameters as shown in Tab.1.

6. for this optimum set, we perform more detailed tune survey and find the optimum set of tunes (ν_x, ν_y). The values should be consistent with the dynamic aperture and coupling-control considerations including the error effects. This part will be discussed in the next section.

7. confirm this operation point by various ways:

   (a) including the nonlinear lattice first without and later with the lattice errors. This is not discussed here. See Ref[1].

   (b) perform a simplified strong-strong simulation with nonlinear lattice. This is not discussed here. See Ref[1].

   (c) perform a weak-strong simulation to confirm the operation point from the beam-tail point of view. This part will be discussed in section 5.

(ϵ_x, ϵ_y)	$(1.74\times10^{-8}, 3.44\times10^{-10})$ m	ϕ	10 mrad
(β_x, β_y)	(0.33, 0.008) m	η_y	0.057
σ_z	4mm	ξ	(0.04,0.052)
σ_ϵ	8.8×10^{-4}	ν_s	0.017

Table 1: "Optimum" parameters. In actual KEKB design, ϕ is 11mrad. By historical reasoning, we keep using 10 mrad.

4. Luminosity

We have performed a detailed tune scan for the parameters obtained above assuming the linear lattice without errors. We track 50 particles for more than 10 damping times. The number of longitudinal slices is 5. We evaluate the luminosity after 3 damping times. The results are shown in Fig.3.

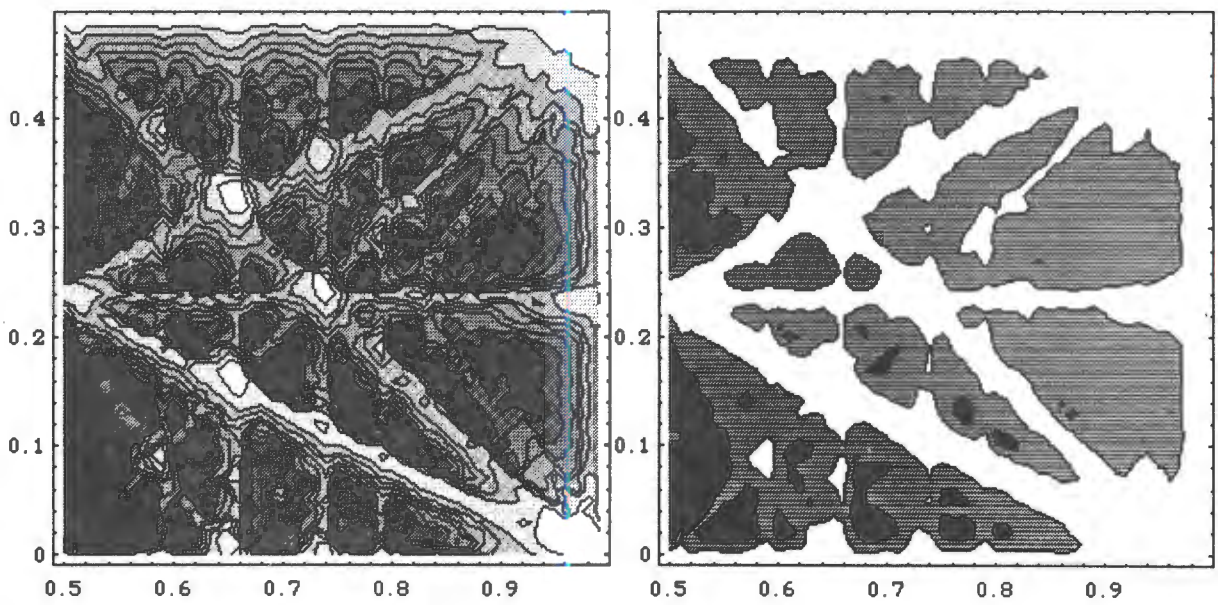


Figure 3: Luminosity evaluated as a function of (ν_x, ν_y). The left and the right are the same but with different steps in contour lines. In the right, the most dense part corresponds to the luminosity more than the design value ($L_d \equiv 1\times10^{34}\mathrm{cm}^{-2}\mathrm{s}^{-1}$). The next dense part corresponds to between $L_d/2$ to L_d.These graphs are composed of 50×50 data points.

From this result along with optics considerations, we have decided the operation point as

$$\text{Fractional Part of } (\nu_x, \nu_y) = (0.52, 0.08).$$

Note that in evaluating the luminosity, we did not assume the Gaussian distribution of the weak-bunches. Instead, we have evaluated the integral for the luminosity using all the particle data (for 50 particles and for all turns) assuming the Gaussian distribution of the strong bunch in the same manner as the Monte Carlo method. If we have assumed the Gaussian distribution, we would have obtained a little less luminosity. The luminosity was evaluated in the boosted frame.

After identifying the operation point, we have surveyed tunes around the operation point quite densely in order not to miss the possible bad points. From these results, we concluded that our "optimal" parameters will provide enough region in the tune space for the operation.

If we apply the same optimization process to the case without the crossing angle, we get larger region for $L > L_d$. It implies that if the crab cavities work appropriately, the operation will be easier or safer. But even without the crab cavities, the region is large enough.

5. Beam-Beam Tail

The beam-beam interaction is believed to be one of the major sources of the beam-halo, which affects the detector backgrounds and shortens the lifetime. I believe that there is no quick and reliable way of evaluating the tail of electron beams. Eventually, we should perform a brute force (long term) tracking. Still, however, just for getting some insights, it seems useful to evaluate the maximum amplitudes $A_{x,y}$. In the same job, which made Fig.3, we recorded the maximum (in all 50 particles and all turns) values of the horizontal and vertical amplitudes: if $A_{x,y}$ is large, it might imply large tail formation. The results are shown in Fig.4. We can see resonance structures clearly. Our operation point is outside the dangerous region.

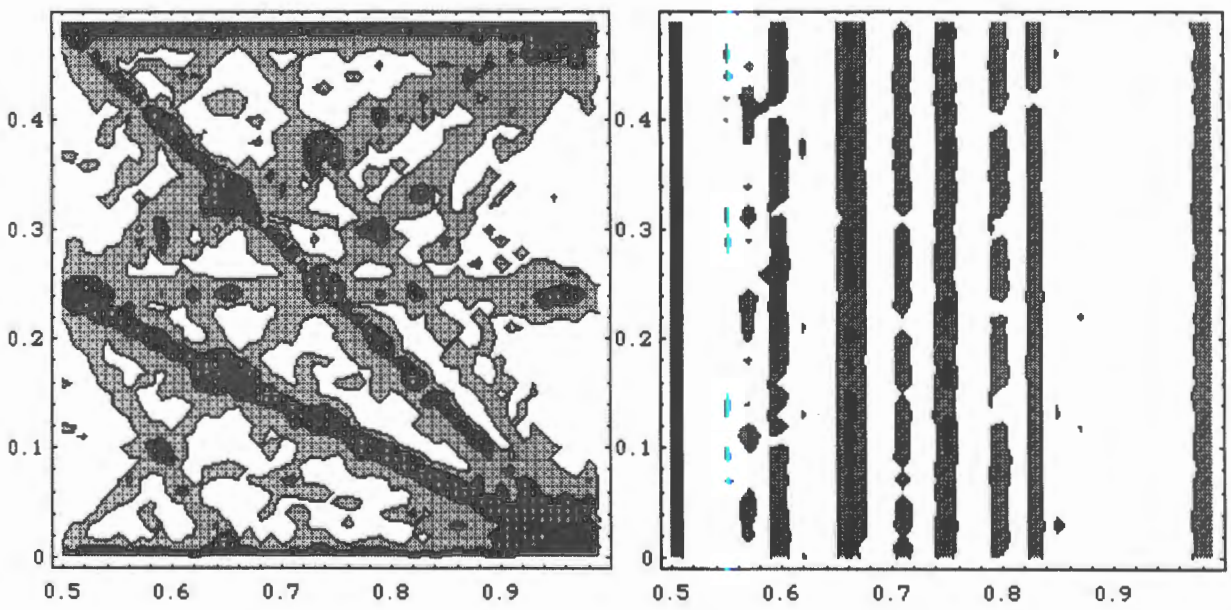


Figure 4: The maximum amplitudes $A_{x,y}$ as functions of tunes. The left is the A_y (contours are 30, 20, 10 σ_y) and the right A_x (contours are 15, 10, 5 σ_x).

Now, note that the maximum amplitude argument given above is only plausible. We cannot replace the long term tracking by it. In order to conclude that our operation point works from

the tail point of view, we have performed a long term tracking using 50 super particles for 10^8 turns. This corresponds to 1000 seconds for each particle. If we assume the Ergodicity, this corresponds to 4 hours for a single particle. The result is shown in Fig.5.

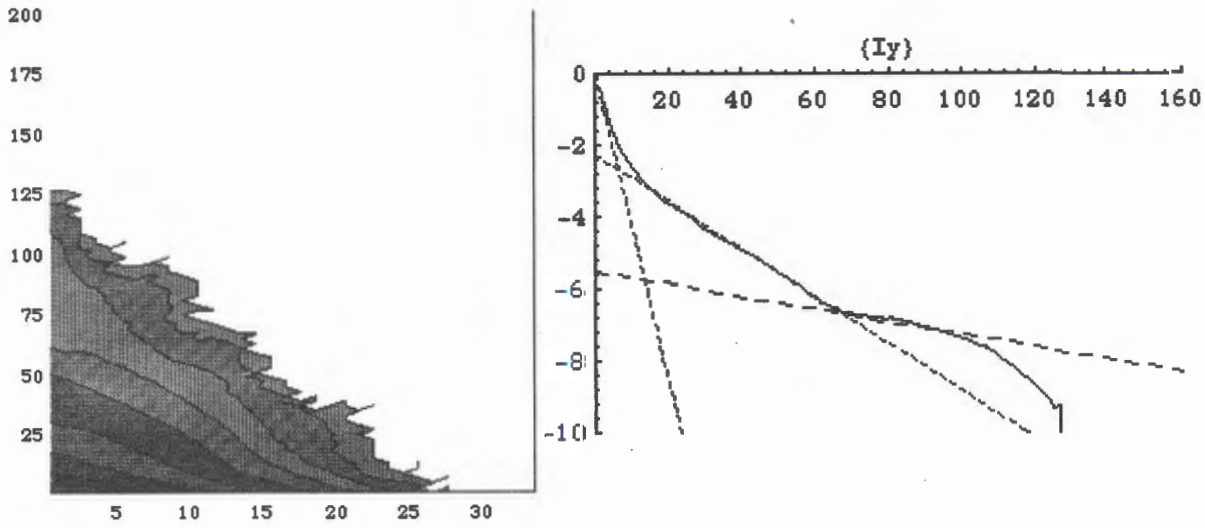


Figure 5: The long term average of the distribution for the ideal linear lattice. Left is the distribution in the action apace (contours are for every 1/10) and the right is its projection on the vertical action: $\log_{10}(\rho(I_y))$. The dashed lines are fitting curves in Eq.(3). The normalization is 1 for both graphs.

Non-gaussian tails in the particle distribution is seen. In this case the function $\rho(I_y)$ can be fitted with a sum of

$$\rho(I_y) \quad \sim \quad e^{-I_y} + 5.2 \times 10^{-3} e^{-0.15 I_y} + 3 \times 10^{-6} e^{-0.04 I_y}. \tag{3}$$

This seems to be safe enough for the detector background.

It was also observed that in the dangerous region with respect to the maximum amplitudes, the long-term tracking also shows a large tail. Thus, as an empirical law, it might be said that the maximum amplitudes are good indicators of the tail. As stressed before, however, anything cannot replace the long term tracking. (In other words, if results of the maximum amplitude arguments and the long term tracking contradict, one should believe the latter). Finally, it is interesting to see how the result depends on the number of slices. We have performed a tracking using 21 slices. The result is shown in Fig.6. It is remarkable that the vertical tail is suppressed. Thus, the tail estimated using 5 slices above (Fig.5) was an overestimate.

6. Discussion

We have shown how we have found the present operation point and how we have confirmed it. **All the arguments depend only** on the accuracy of the beam-beam mapping. I want to stress that our mapping contains all the known effects and more. If there is a contradiction between the present mapping and some previous one, we should believe the present one. *Simpler mapping cannot predict more than the more accurate one.* Of course, the possible bugs in the code should be always suspected. To find such bugs, K. Ohmi has written down the mappings newly based on the same theories and has compared the both numerically. He has also confirmed the symplecticity of the mapping using his DA package. From these comparisons, we are almost certain that there in no error in the programming.

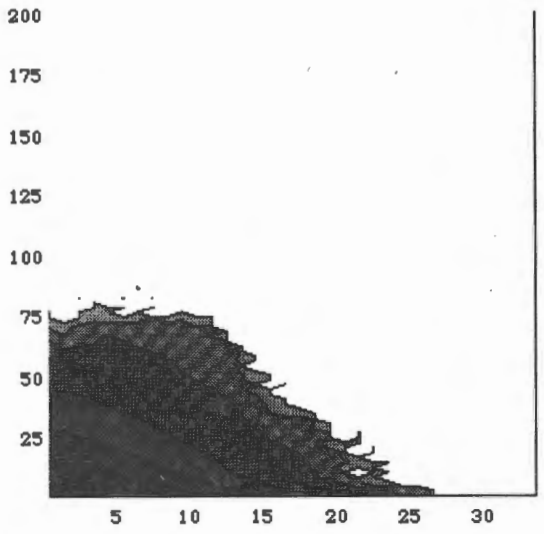


Figure 6: The same as the previous figure (left) but by using 21 slices.

The author thanks K. Ohmi for his collaboration mentioned above. N. Toge is acknowledged for his effort in time-consuming simulation. He also thanks K. Oide for discussion on the Lorentz transformations and the "optimization".

References

[1] *KEKB B-Factory Design Report*, KEK Report 95-7 (1995).

[2] A. Piwinski, DESY Report DESY 77/18 (1977).

[3] G. E. Fischer, SLAC report SPEAR-154 (1972). SPEAR Storage Ring Group, IEEE Trans. Nucl. Sci. **NS-20**, 3, 838 (1973). M. Furman, Proc. 1991 IEEE Particle Accelerator Conference p.422 (1991).

[4] E. Forest, M.F. Reusch, D. Bruhwiler and A. Amiry, Part. Accel., **45**, 65 (1994).

[5] K. Hirata, H. Moshammer and F. Ruggiero, Part. Accel. **40**, 205 (1993).

[6] K. Hirata, Phys. Rev. Lett.**74** 2228 (1995).

[7] Krishnagopal and Sieman, Phys. Rev. **D41**, 2312 (1990).

[8] N. Toge and K. Hirata, *Study on Beam-Beam Interactions for KEKB*, KEK Preprint 94-160 (1994).

[9] B. W. Montague, CERN report CERN/ISR-GS/75-36 (1975).

PARASITIC COLLISIONS IN PEP-II†

MIGUEL A. FURMAN

Accelerator and Fusion Research Division
B Factory Project
Lawrence Berkeley National Laboratory
Berkeley, CA 94720, USA

Abstract

The PEP-II collider design calls for large numbers of closely-spaced bunches and head-on collisions. These two features, taken together, imply that there are parasitic collisions in the neighborhood of the interaction point. Since the bunch populations of the beams are not uniform due to the ion-clearing gaps, the bunches at the head or tail of the train ("pacman bunches") experience different effects from those away from the edges ("typical bunches"). In this article we summarize the effects arising from the parasitic collisions on luminosity, tune shifts and closed orbit distortion both for typical bunches and for pacman bunches.

1. Introduction

The SLAC/LBNL/LLNL B Factory [1] is an asymmetric e^+-e^- collider with a design luminosity of 3×10^{33} cm^{-2} s^{-1} whose primary purpose is the detailed study of the B meson system. The energy asymmetry is intended to enhance the detection efficiency of certain decay modes that are of particular interest for the study of CP violation. The value chosen for the luminosity will lead to a productive program of studies of the B meson. The low-energy beam (LEB) is positrons, with an energy of 3.1 GeV, while the high-energy ring (HEB) is electrons, with an energy of 9 GeV. The center-of-mass energy is 10.6 GeV, corresponding to the $\Upsilon(4S)$ resonance. The machine is being built in the PEP tunnel and uses the SLAC linac as its injector. Construction started in 1993 and will be completed in 1998.

The two rings intersect at only one interaction point (IP). Although the interaction region (IR) design allows for the possibility of crossing with a finite angle, in the current design the beams collide head-on and are magnetically separated in the horizontal plane. This separation scheme entails parasitic collisions (PCs) near the IP whose effects on the beam-beam dynamics have been studied quite extensively [1,2]. The design also calls for an ion-clearing gap equivalent to ~5% of the total beam length. The gaps in the two beams have the same length and are positioned such that head bunch in one beam collides at the IP with the head bunch of the other beam (the two beams have the same bunch spacing and overall length).

In this article we summarize effects arising from the PCs from the perspective of the beam-beam interaction. Anticipating our conclusion, we can state that the PEP-II IR design solves or avoids all issues that were initially identified as potential difficulties.

2. IR Parameters

The IR is such that a typical bunch experiences four PCs on either side of the IP, for a total of 9 collisions. In contrast, pacman bunches experience only a subset of these. For example, the first bunch and the last bunch in the train experience only 5 (the main collision at the IP plus 4 PCs on

† Invited talk presented at the Seventh Advanced ICFA Workshop on Beam Dynamics, JINR, Dubna, Russia, 18–20 May, 1995. Work supported by the Director, Office of Energy Research, Office of High Energy and Nuclear Physics, High Energy Division, of the U.S. Department of Energy under Contract no. DE-AC03-76SF00098.

one side only). Figure 1 shows a plan sketch of the IR with typical bunches in collision; for the nominal bunch spacing of 1.26 m, the PCs occur every 0.63 m.

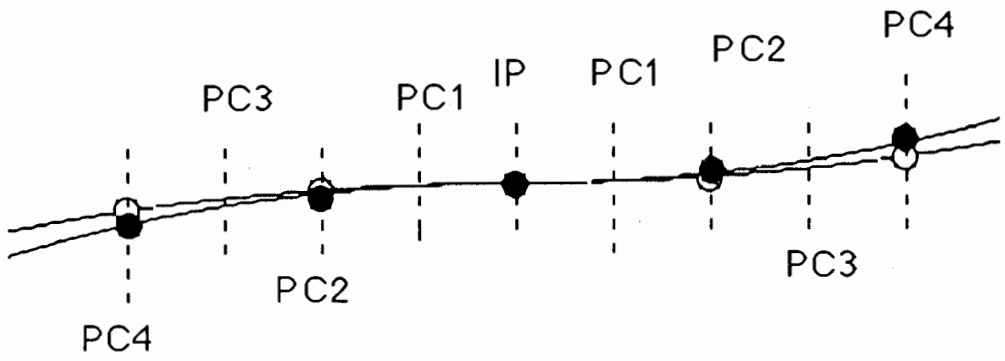


Fig. 1 Plan sketch of the IR showing the parasitic collisions.

It turns out that the first PC (labelled PC1 in Fig. 1) is much stronger than the others. For this reason we neglect PCs #2, 3 and 4 in some of our calculations. At the PC1 location, the center-to-center beam separation is d=3.5 mm, corresponding to $11.8\sigma_{0x+}$. Table 1 shows a selection of parameters including those of PC1 (the IR optics is symmetrical about the IP in this region).

Table 1: Nominal PEP-II parameters (CDR, June 1993)

	LEB (e^+)		HEB (e^-)	
$\mathcal{L}_0$ [cm^{-2} s^{-1}]	3×10^{33}			
N	5.63×10^{10}		2.57×10^{10}	
ε_{0x} [nm-rad]	61.3		45.9	
ε_{0y} [nm-rad]	2.45		1.84	
σ_z [cm]	1.0		1.0	
s_B [m]	1.26		1.26	
	IP	1st PC	IP	1st PC
β_x [m]	0.375	1.43	0.500	1.29
β_y [m]	0.015	26.46	0.020	19.85
α_x	0	−1.68	0	−1.26
α_y	0	−41.99	0	−31.49
σ_{0x} [μm]	151.6	296.3	151.6	243.8
σ_{0y} [μm]	6.063	254.6	6.063	191.0
d [mm]	0	3.5	0	3.5
d/σ_{0x}	0	11.8	0	14.3
ξ_{0x}	0.03	−0.000224	0.03	−0.000152
ξ_{0y}	0.03	+0.004133	0.03	+0.002326

In this table the subscript "0" attached to the luminosity ($\mathcal{L}$), rms beam sizes (σ's), emittances (ε's) and beam-beam parameters (ξ's) is meant to emphasize that these are nominal quantities, *i.e.*,

neglecting the effects from the beam-beam collisions. As it will be explained below, simulations show that the actual vertical beam sizes are a bit larger than nominal when the beams are in collision.

3. Beam Footprint and Long-Range Tune Shift Parameter

3.1. Footprints with and without PCs

If one neglects the effects from the PCs altogether, the beam footprint has a characteristic "necktie" shape that extends to the right and above the working point by about 0.03, corresponding to the value of the beam-beam parameters. Figure 2 shows such a footprint, obtained by computing the actual tunes of a single particle that is launched with various horizontal and vertical amplitudes.

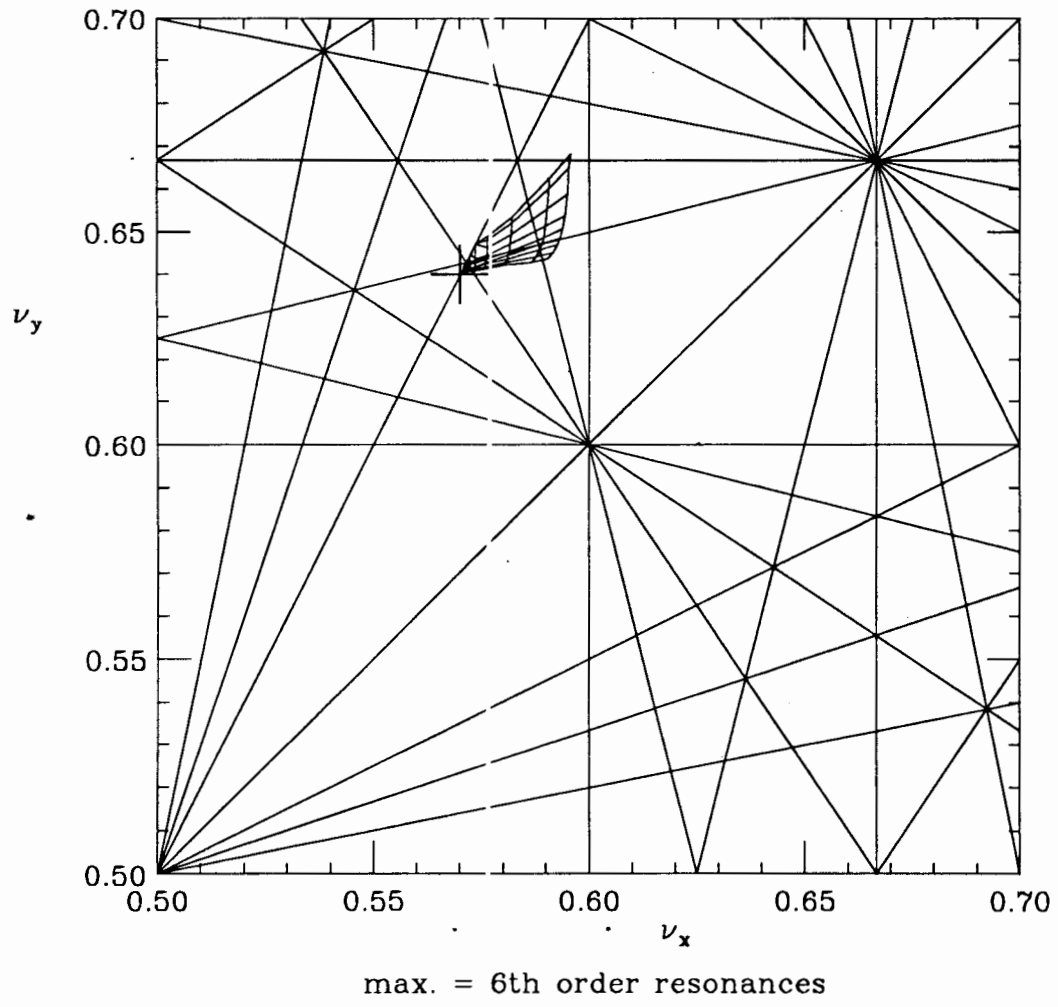


Fig. 2 Footprint of the LEB in the absence of PCs for a working point (0.57,0.64) (cross) obtained from particles launched at 0, 1, 2, 3, 4, 5, 6, 8 and $10\sigma_0$. Resonance lines up to a maximum of sixth order are shown.

In this plot the particle at the center of the bunch is at the top right corner of the footprint. The beam-beam kick it receives is characterized by the beam-beam parameter at the IP. For a positron, the vertical parameter is

$$\xi_{0y+} = \frac{r_e N_- \beta_{y+}}{2\pi\gamma_+\sigma_{0y-}(\sigma_{0x-} + \sigma_{0y-})} \tag{1}$$

where r_e is the classical electron radius and γ is the usual relativistic factor. The expression for the horizontal parameter is obtained by exchanging x $\leftrightarrow$ y, and those for an electron by exchanging + $\leftrightarrow$ −. By design, all four ξ_0's have the numerical value 0.03, as listed in Table 1. In Fig. 2, the tune of the central positron is shifted approximately by 0.03 in both planes (it is not exactly 0.03 on account of the so-called "dynamical effect" [5], as discussed below).

The large-amplitude particles experience a weaker beam-beam interaction and hence they tend to be at the lower left corner of the necktie, close to the lattice working point.

If one now adds the effect of the two PC1's, the footprint is substantially changed. Figure 3 shows the corresponding results, obtained under identical conditions as in Fig. 2, except that the PC1's have been included.

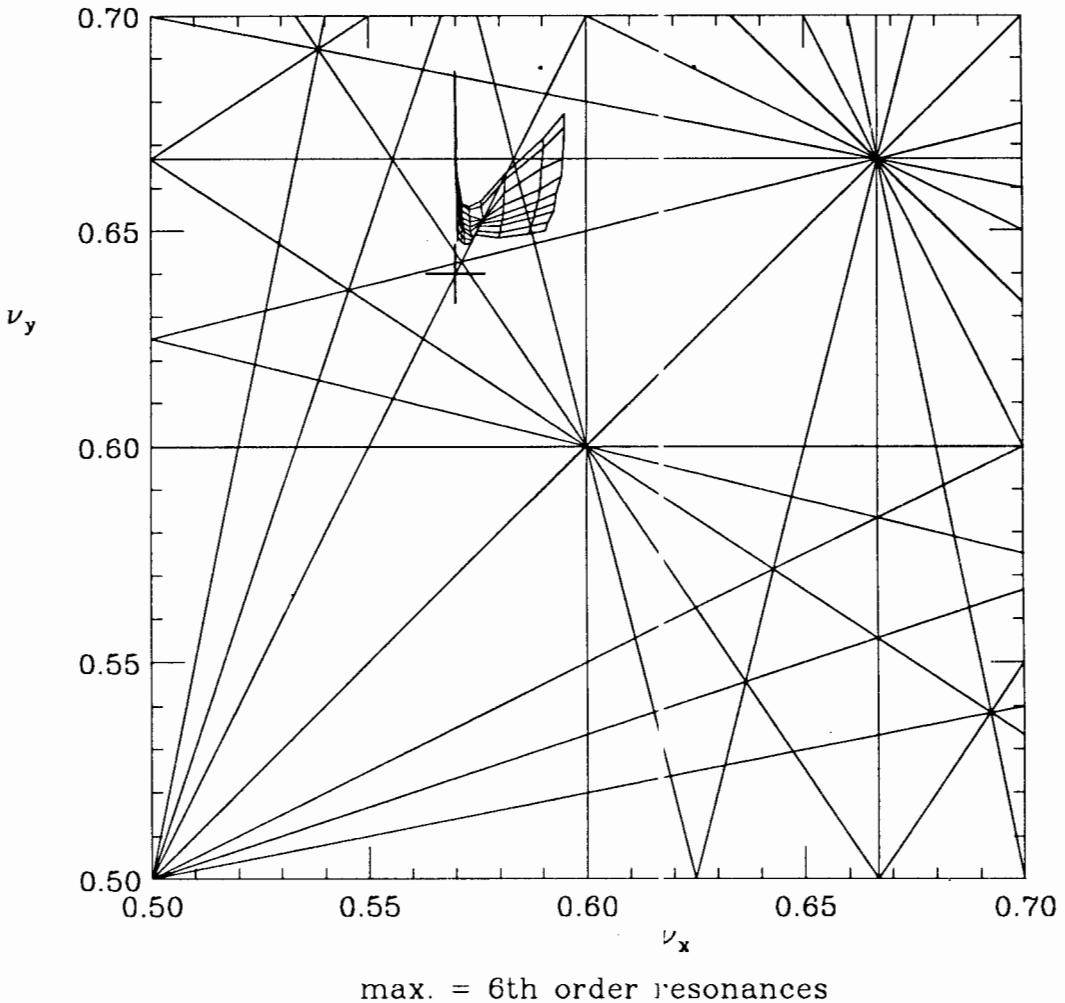


Fig. 3 Footprint of the LEB including the effect of the PCIs. The conditions are exactly the same as those in Fig. 2 except for the addition of the PCs.

One can see from this that the PCs have two distinct effects: (1) the tunes of the particle at the bunch center are shifted relative to the IP-only case; and (2) the tunes of the particles at large

horizontal amplitude (those that typically get close to the center of the opposing bunch at the PC location) are shifted vertically by a substantial amount.

In the calculation of the tune footprint we have neglected all lattice nonlinearities. This approximation is only justified for particles close to the beam center, where the nonlinear effects from the lattice are weak compared to those arising from the beam-beam collision. One should therefore be cautious when interpreting these footprints at large amplitudes in this approximation.

3.2. The long-range beam-beam parameter.

The beam-beam parameters for the central particle induced by the PCs (usually referred to as the "long-range beam-beam parameters") can be computed in perturbation theory in the usual fashion. The result for a positron is

$$\xi_{x+}^{PC} = -\frac{r_e N_- \beta_{x+}^{PC}}{2\pi d^2}, \qquad \xi_{y+}^{PC} = +\frac{r_e N_- \beta_{y+}^{PC}}{2\pi d^2} \tag{2}$$

with corresponding expressions for an electron, obtained from the above by replacing $+ \leftrightarrow -$. The numerical values for the case of PEP-II are listed in Table 1.

It should be noted that the vertical and horizontal long-range beam-beam parameters are of opposite signs. If the beams were to cross in the vertical plane, the signs would be reversed relative to those in Eq. (2). It is easy to see that Maxwell's equations imply in a very straightforward manner that the signs should always be opposite: consider a positron with coordinates (x,y) close to the center of its own bunch center as it experiences a parasitic collision with an electron bunch, as sketched in Fig. 4.

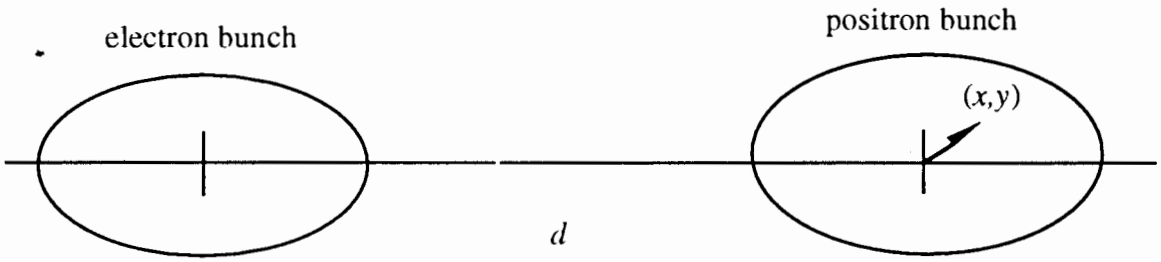


Fig. 4 Sketch of a parasitic collision in which the bunch centers are separated by a distance d. The positron, with coordinates (x,y), is very close to its own bunch center.

The ξ-parameters are, in general, defined by

$$\Delta x' = -4\pi \xi_{x+}^{PC} \frac{x}{\beta_{x+}^{PC}}, \qquad \Delta y' = -4\pi \xi_{y+}^{PC} \frac{y}{\beta_{y+}^{PC}} \tag{3}$$

where $\Delta x'$ and $\Delta y'$ are the angular deflections suffered by the positron in the collision. These deflections are given by

$$(\Delta x', \Delta y') = -\frac{r_e N_-}{\gamma_+} \mathbf{E}(x,y) \tag{4}$$

where $\mathbf{E}(x,y)$ is the electric field per unit charge produced by the electron beam. This electric field satisfies the equation

$$\nabla \cdot \mathbf{E}(x,y) = 4\pi \frac{\rho_-(x,y)}{Q_-} = 0 \tag{5}$$

where $Q_- = N_- e$ is the charge of the electron bunch. The right side is 0 because the beams are well separated ($d \gg \sigma_x, \sigma_y$) and hence there is a vanishingly small electron charge density at the location of the positron. Thus by combining Eqs. (3–5) we obtain

$$\frac{\xi_{x+}^{PC}}{\beta_{x+}^{PC}} + \frac{\xi_{y+}^{PC}}{\beta_{y+}^{PC}} = 0 \tag{6}$$

which immediately implies that the ξ's have opposite signs. Obviously, the expressions in Eq. (2) satisfy Eq. (6), but Eq. (6) is more generally valid because it holds regardless of the orientation of the beam separation as long as $d \gg \sigma_x, \sigma_y$.

4. Closed-Orbit Distortion Due to the PCs

As a result of the PCs there is a net attractive force between the beams that distorts their closed orbits [3]. There are two main manifestations of this closed-orbit distortion: an induced horizontal crossing angle, and a horizontal displacement of the pacman bunches at the IP. These effects depend on the horizontal tune of both beams. If the beams were uniformly populated, the crossing angle would be the same for all bunches. However, the existence of the ion-clearing gap implies that pacman bunches experience crossing angles different from typical bunches, and collide off-center due to the imbalance of the net forces to the right and to the left of the IP. Typical bunches experience only a crossing angle without orbit separation. Because the orbit distortion is a periodic function of the horizontal tune with period 1, only the fractional part of the tune matters. Since the tunes of the beams can, in principle, be chosen independently of each other, these closed orbit effects can be largely compensated if necessary. For the purposes of the calculation in this section, *we take into account all the PCs*, not just the first one.

4.1. Induced crossing angle at the IP

Figure 5 shows the orbit slopes at a point immediately upstream (seen from the perspective of the LEB) of the IP, and the full crossing angle, $\phi \equiv X'_+ - X'_-$ (the crossing angle curve assumes the same fractional tune for both beams). It should be noted that the crossing angle is quite small: for a fractional tune of 0.64, a value that has been used in many simulation studies [1,2], the crossing angle is 34 μrad, which is much smaller than $\sigma_x/\sigma_z = 15.6 \times 10^{-3}$. Even for a fractional tune as high as 0.9, the crossing angle is only 0.13 mrad. Therefore the effect on the beam-beam dynamics from this crossing angle is expected to be negligible [4].

The corresponding results for the first pacman bunch (*i.e.*, the bunch at the head or at the tail of the train) show that the magnitude of the effect is about half of that for typical bunches. The simple explanation for this is that the first pacman bunch suffers only half of the PCs, and hence its orbit distortion is roughly half of that for a typical bunch.

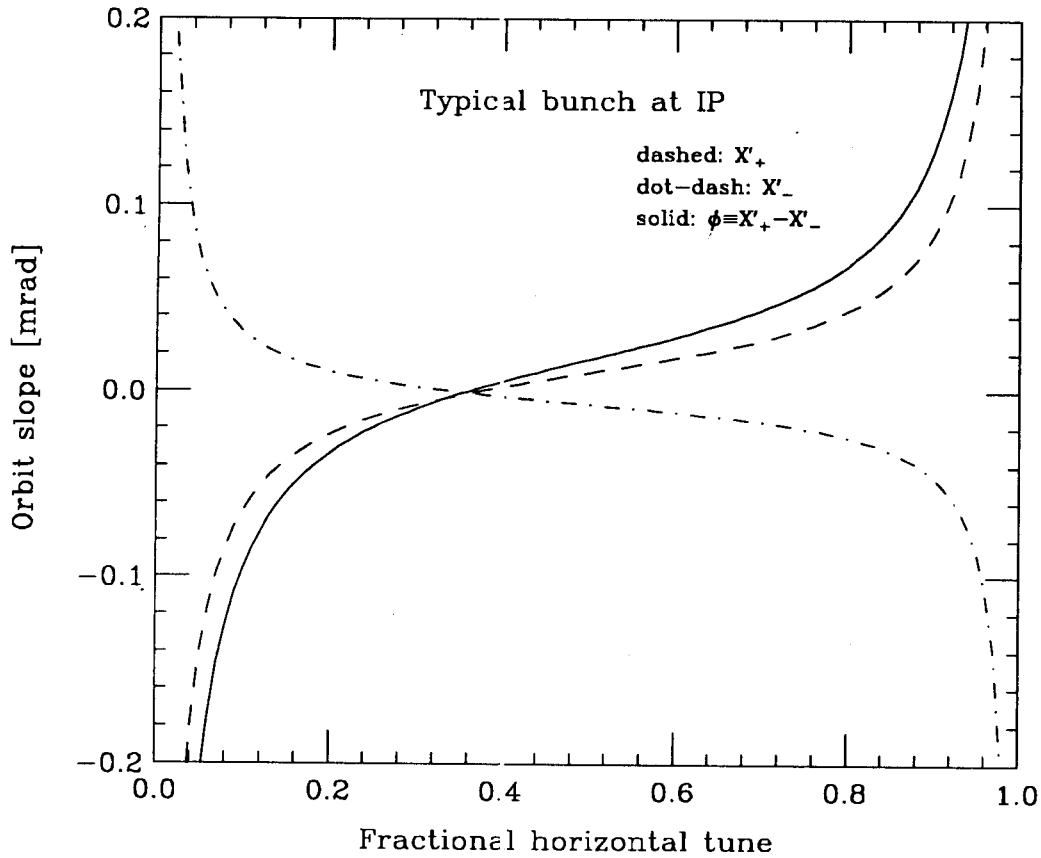


***Fig. 5** Horizontal orbit slopes and full crossing angle of typical bunches. The crossing angle is computed assuming the same fractional tunes in both beams.*

4.2. Induced orbit separation for pacman bunches at the IP

Figure 6 shows the absolute and relative displacements of the orbits of the first pacman bunch at the IP. It should be noted that, for most values of the fractional tune, both bunches are displaced to the *same side* of the nominal orbit (X_+ and X_- are of the same sign). This makes physical sense: there is a net imbalance of the forces from the PCs such that the head bunches of *both* beams are pulled to the same side. The magnitude of the displacement of the first pacman bunch from its nominal orbit is $\lesssim 10$ μm for most values of the tune. More interestingly, the displacement of one bunch *relative to the other*, which is what matters for the beam-beam dynamics, is even smaller, $\Delta X < 2$ μm. These numbers are small compared to the rms bunch width of 152 μm and therefore the effects from these displacements are not expected to be important.

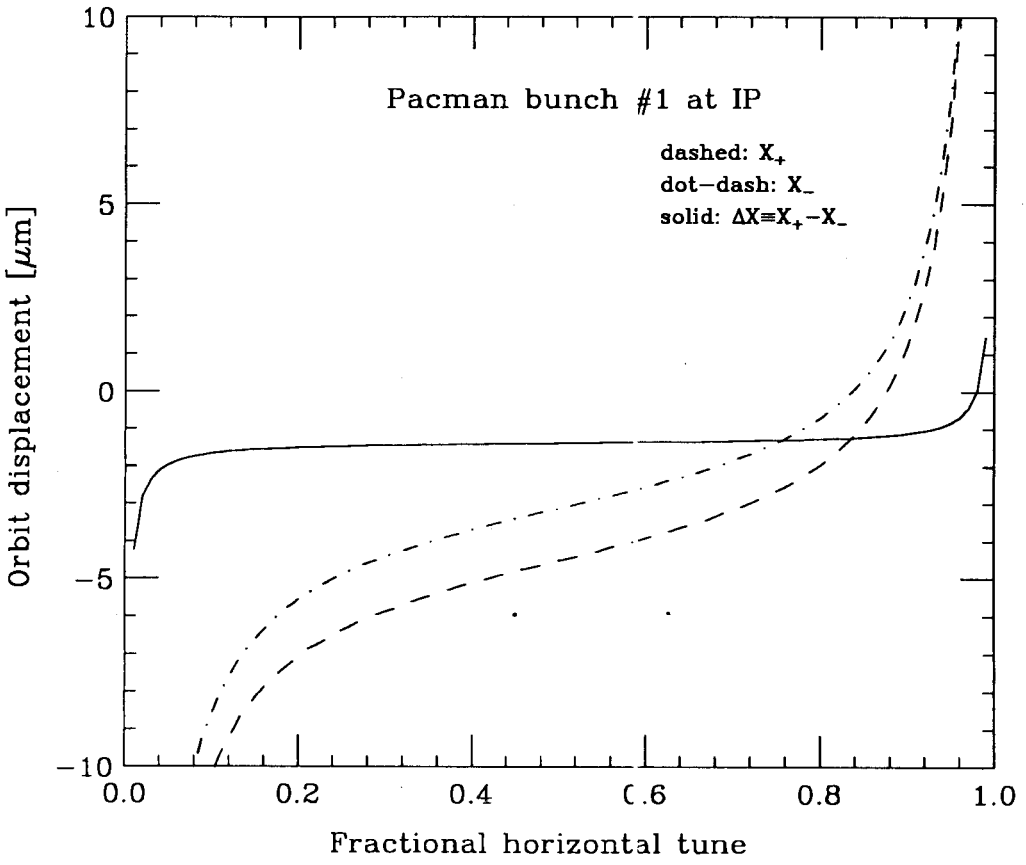


Fig. 6 Orbit distortions of the head pacman bunches at the IP. The change in orbit separation ΔX is computed assuming that the two beams have the same fractional tune.

5. Dynamical Effects for Typical and for Pacman Bunches

As mentioned above, the tune shift is not equal to the beam-beam parameter on account of the so-called dynamical effect: the tune shift is a function of the tune as well as the beam-beam parameter. By representing the beam-beam collisions as thin-lens kicks located at the IP and the PCs, one can compute the dynamical effects in standard linear approximation for the particles near the bunch center. The actual, or dynamical, beta function experienced by these particles is computed in a similar fashion [5]. This linear analysis of the beam-beam interaction exhibits constraints that are absolutely necessary, although far from sufficient, for acceptable luminosity performance. As in the previous section, here we *take into account all PCs*.

Figure 7 shows the tune shifts for a typical bunch as a function of the lattice (or "bare") tune. In this case, the curves repeat with a periodicity of half a unit in tune. If the PCs were neglected, all four curves would coincide (they would be very close to the solid line, corresponding to the horizontal tune shift of the LEB).

One can see that the tune shifts have a nontrivial dependence on the tune. In particular, stopbands appear just below the half-integer and the integer. The stopband width can be calculated in first order in terms of the beam-beam parameters with the result

$$\delta\nu = 2\xi_0 + 4\sum_{n\geq 1}\xi_n \cos 2\phi_n + O(\xi^2) \qquad (7)$$

where ξ_0 is here the beam-beam parameter at the IP, the summation is over the beam-beam parameters of the PCs to one side of the IP only, and the ϕ_n's are the betatron phases of the PCs (this formula is valid only for left-right symmetric optics). It is interesting to note that the PCs tend to make the *vertical stopbands narrower* than in the IP-only case. This can be seen from Eq. (7) by taking into account only the first PC (which is a good approximation) as follows: there are no intervening focusing elements between the IP and PC1, and the vertical β-function at the IP (1.5 or 2 cm) is small compared to the distance to the PC1 location (0.63 cm); therefore the phase ϕ_1 is close to $\pi/2$, hence $\cos 2\phi_1 \approx -1$. Now since, according to Eq. (3), $\xi_1 > 0$, we conclude that $\delta\nu$ is smaller than what it would be in the absence of PC1. This can be seen in Fig. 7, which shows that the right edges of the vertical stopbands are shifted downward from the half-integer relative to the IP-only case.

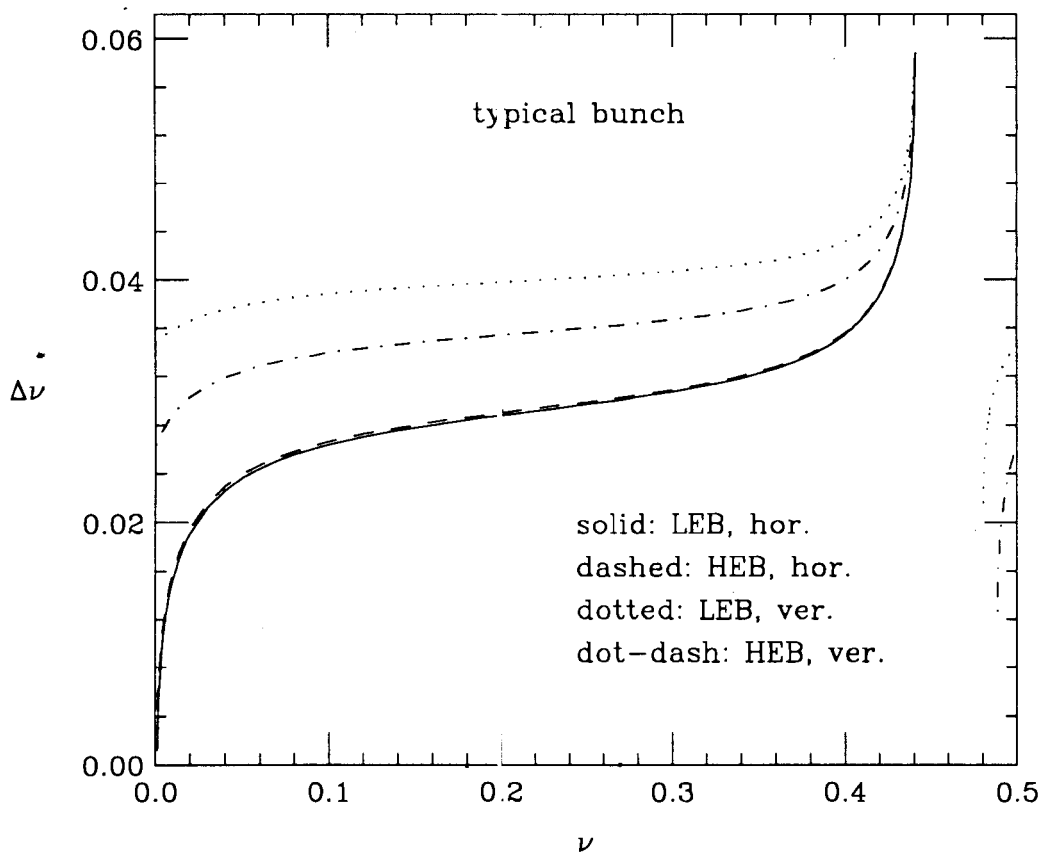


Fig. 7 The beam-beam tune shift for a typical bunch as a function of the corresponding tune for nominal PEP-II parameters. The figure is periodic in ν with a period of 0.5. If the PCs were neglected, all four curves would coincide.

For most values of the tune, the vertical tune shifts are larger than the horizontal on account of the fact that the vertical long-range beam-beam parameters are positive and larger in absolute value than the horizontal counterparts (Eq. (3) and Table 1). However, the tune shifts become relatively

small just above the integer (and half-integer), which suggests that these values of the tune are desirable choices as a working point (actually, the vertical tune shifts are even smaller just *below* the half-integer, as discussed above; however, it's probably dangerous to choose a working point in this region!).

The corresponding results for the pacman bunches are qualitatively similar, except that the effects on the tune shifts are smaller in magnitude. The reason is the same as for the closed-orbit distortion: the pacman bunches experience fewer collisions which results in smaller tune shifts.

6. The Pacman Tune Spread and a Possible Compensation Method

The difference in beam-beam tune shifts between the pacman and typical bunches is the "pacman tune spread." This spread implies that a working point that may be appropriate for typical bunches might not be good for the pacman bunches and vice versa. It may be desirable, therefore, to cancel this spread.

We consider a positron at the bunch center and take only PC1 into account. Neglecting the dynamical beta function effect, the vertical pacman tune spread is given by the difference between a typical bunch and the first pacman bunch,

$$\Delta\nu_{y+} \approx \xi_{0y+}^{PC1} \tag{8}$$

with a corresponding expression for the other beam. This vertical tune spread can be compensated simultaneously in both beams in first order approximation by tailoring the bunch currents [6]. The results of the compensation method are shown schematically in Fig. 8, which sketches the currents in all bunches of both beams. The first and last bunches of the train have a current slightly higher than the typical bunches, while the second and next-to-last bunches have slightly lower current. The rule of thumb is that the extra current in the first and last bunch of the HEB necessary to compensate the vertical LEB tune spread is given by

$$\frac{\Delta N_-}{N_-} \approx \frac{\xi_{y+}^{PC1}}{\xi_{y+}^{IP}} \approx 0.14 \tag{9}$$

while the second and next-to-last bunches must have currents *lower* than nominal by $0.14^2=0.02$. A similar analysis applies to the other beam, obtained by replacing $+ \leftrightarrow -$ in the above.

The differences in sign and magnitude between the vertical and horizontal beam-beam parameters at the PCs, however, make it impossible to compensate vertical and horizontal tune spreads simultaneously. In fact, a generic feature of the method is the trade-off between the vertical tune spread and the horizontal: if the vertical tune spread is compensated, the horizontal tune spread becomes roughly equal to the uncompensated vertical tune spread, which is typically larger than the nominal value of the horizontal spread. However, the horizontal beam dynamics is much more tolerant than the vertical, so horizontal tune spreads of this magnitude should not cause any problems, and the method therefore implies a net advantage. We believe that this beneficial trade-off is a generic feature of flat beams, such as in the case of PEP-II. By the same token, this technique seems unlikely to be applicable to round beams, such as those encountered in multibunch proton colliders. Tailoring $N_\pm$ of the first and last bunches to the level required by this method is well within the capabilities of the PEP-II injection system. Tailoring $N_\pm$ of the second and next-to last bunches to the level required is more difficult, but probably much less important.

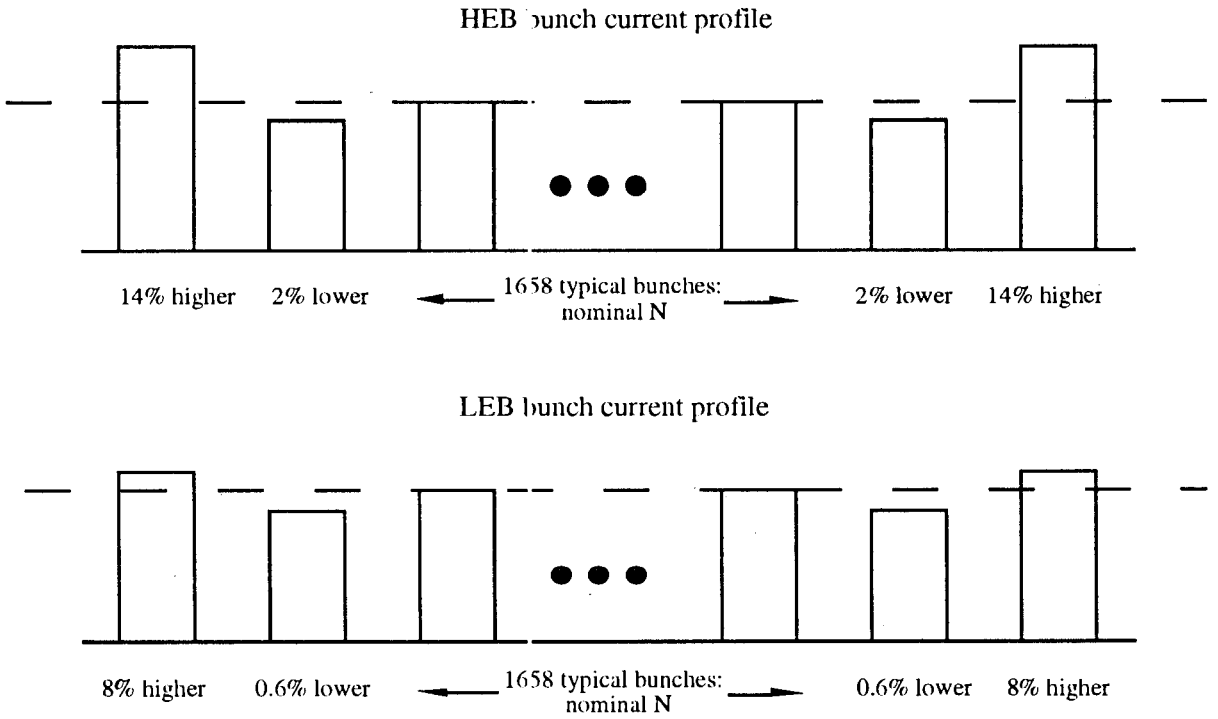


Fig. 8 The number of particles per bunch (N) necessary to compensate the vertical tune spreads in both beams. The first and last pacman bunches in the HEB and LEB have bunch currents 14% and 8% higher, respectively, than the nominal value, indicated by the dashed lines.

7. Beam Blowup Due to the PCs

The PCs also cause blowup of the beam core. Figure 9 shows the results of a "strong-strong" simulation with the code TRS [7] in which we plot the relative beam blowup as a function of the beam separation at PC1 normalized to the local beam size of the LEB (the other PCs are neglected). In this case the beams were represented by 1024 particles and the tracking was carried out for five damping times (approximately 27000 turns) for each value of the beam separation. All parameters were fixed except for the beam separation at PC1 (the nominal design value is listed in Table 1).

It can be seen that there is substantial vertical beam blowup when the separation falls below $6\sigma_{0x+}$ or so. For the nominal separation of $11.8\sigma_{0x+}$ there is some 10-15% blowup relative to the nominal value. This blowup has the effect of reducing the nominal value of the luminosity, but this reduction can be easily compensated by a small increase in the bunch current. As the separation decreases, the onset of substantial beam blowup happens sufficiently below the nominal value of the separation that we can say that the design is quite safe, since it is not "close to an edge".

8. Conclusions

We have summarized some of the beam dynamics effects in PEP-II arising from the PCs. Other issues, such as dynamics during injection and beam lifetime are discussed in the CDR [1]. In general, all studies to date show that there are no unusual problems relative to those that arise in symmetric colliders and that the PEP-II IR design is conservative from the perspective of the beam-beam interaction. Thus the head-on collision scheme is comfortable and it allows room for upgrading if necessary.

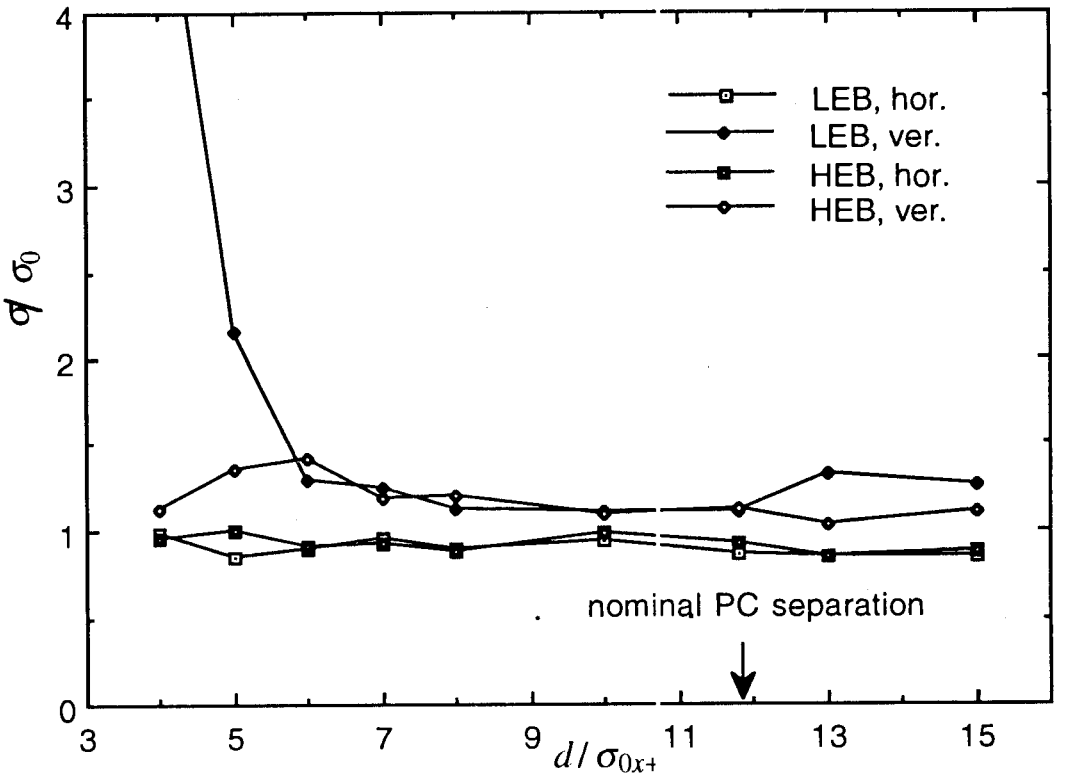


Fig. 9 Beam blowup as a function of the beam separation at the first PC (strong-strong simulation with TRS). The working point is: LEB: (0.580, 0.622); HEB: (0.580, 0.625).

9. Acknowledgments

I am grateful to Sasha Zholents for many discussions and for kindly presenting this talk at the Workshop in my stead. I am grateful to M. Zisman for comments.

References

[1] "PEP-II: An Asymmetric B Factory Conceptual Design Report," June 1993, LBL-PUB-5379/SLAC-418/CALT-68-1869/UCRL-ID-114055/UC-IIRPA-93-01.

[2] M. A. Furman and J. R. Eden, "Beam-Beam Effects for the PEP-II B Factory," Proc. Part. Accel. Conf., Washington, DC, May 17–20, 1993, p. 3485 and references therein.

[3] M. A. Furman, "Closed Orbit Distortion from Parasitic Collisions in PEP-II," Proc. European Particle Accelerator Conference, London, England, June 27 - July 1, 1994, p. 1147.

[4] Proc. Sixth Advanced ICFA Beam Dynamics Workshop, Funchal (island of Madeira), Portugal, October 24–30, 1993.

[5] M. A. Furman, "Beam-Beam Tune Shift and Dynamical Beta Function in PEP-II," Proc. European Particle Accelerator Conference, London, England, June 27 - July 1, 1994, p. 1145.

[6] M. A. Furman, "Compensation of the Pacman Tune Spread by Tailoring the Beam Current," LBL-36471/PEP-II AP Note 95.07, April 25, 1995; to be published in the Proc. 1995 Particle Accelerator Conf., Dallas, TX, May 1-6, 1995.

[7] J. L. Tennyson, undocumented code TRS, 1989.

Crossing Angles at CESR, Experiments and Experience

Alexander B. Temnykh *and James J. Welch
Cornell University, Ithaca, NY 14853, USA †

Operational Experience

The highest priority of modern colliding beam storage rings to produce the maximum of number particle collisions. The rate of these collisions is proportional to luminosity and may be written in the following way:

$$L = 2.17\,(1+r)\,E_{beam}\frac{\xi_v}{\beta_v^*}I_{beam}$$

Where L is the luminosity in units $10^{32}cm^{-2}s^{-1}s^{-1}$, r is the beam aspect ratio at the collision point, E_{beam} the beam energy in GeV, ξ_v the beam-beam tune shift parameter, β_v^* the beta function at collision point and I_{beam} is the average single beam current in amperes.

Our strategy for increasing L is described in reference [1]; here we will reiterate the main points. Provided the single bunch current can be kept at a reasonable high value so that a good tune shift parameter can be obtained, we are attempting to:

- increase the number of bunches.
- reduce β_v^* and the bunch length

These two tactics are relatively independent.

The historical view of β_v^* variation and variation of number of bunches per beam since start of operation in 1977 and up to now is shown on figure 1 One can see two steps of β_v^* reduction in 1981 and in 1986. These are explained in reference [2]. Now (1995) β_v^* is 1.8 cm, which is approximately equal to bunch length.

In 1981 after electrostatic separators were installed, CESR started operation in multibunch mode. From 1982 to 1988 CESR ran with 3 bunches per beam. The number of bunches in this period was limited by an RF problem. In 1988, after the problem was solved, the number of bunches was increased to 7 per beam. Further increases in the number bunches did not occur until a configuration of bunch trains with a crossing angle was implemented in 1994.

The main idea of the bunch train is illustrated on figure 2. An angle between the two beams at the main interaction point translates to good beam separation in a short distance. This allows a dramatic reduction in the distance between bunches and therefore an increase in total number of bunches. Note that crossing angle or space between bunches must be big enough to provide suitable reduction

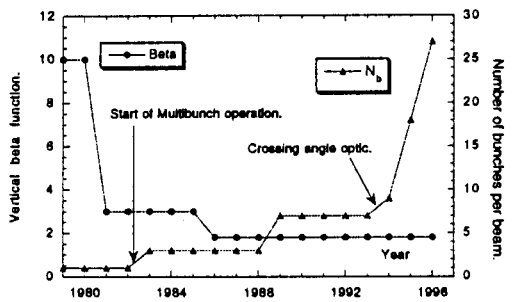


Figure 1: Evolution of β_v^* and the number of bunches per beam at CESR

of beam-beam interaction at the crossing point nearest to the IP. Closely spaced bunches are grouped in trains to maintain good separation in the arcs using the ordinary pretzel scheme for 7 bunches.

One can see three critical issues involved in bunch trains and crossing angles.

- The beam-beam interaction is modified by the crossing angle.
- The long-range beam-beam interactions are increased.
- The separation pretzel exists everywhere.

After two years of intensive experimentation and modifications to CESR we have analyzed these issues and overcome their limitations. It was shown that ±2.5 milliradian crossing angle in horizontal plane does not significantly affect the beam-beam tune shift parameter. Analysis of long-range beam-beam interaction experiments allowed us choose criteria for adequate beam separation, which was incorporated into optic design, and reduced the required physical separation so that only a 2.3 mr crossing angle is needed. Nonlinearities in the magnets, particularly the wiggler magnets which previously were not in the pretzel, were much more severe. After wigglers were converted to an even number of poles and adjusted there effect on the pretzeled beam was greatly reduced. The field quality of a number of other magnets was also improved.

Prior to the beginning of the crossing angle machine studies or best performance in 1990 was:

$$\hat{L} \;=\; 1.5 \times 10^{32}\ cm^{-2}s^{-1} \qquad (1)$$

*On leave from BINP, Novosibirsk

†Work supported by the National Science Foundation

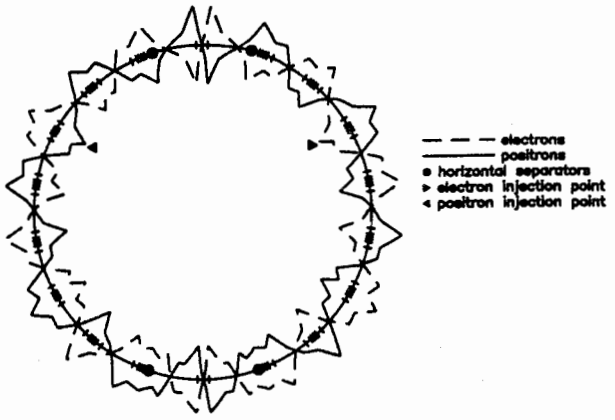


Figure 2: Crossing angle scheme at CESR

$$\xi_v = 0.030 \quad (2)$$

$$\hat{I} = 85\ mA/beam \quad (3)$$

At the beginning of 1994, CESR started HEP operation with a crossing angle lattice. In the beginning it was without trains and had 9 bunches per beam. Later after new digital broad band feedback was developed it came smoothly to operation with 18 bunches per beam grouped in 9 trains. Now we have regular operation under this condition with best performance to date as of February 1995 of:

$$\hat{L} = 3.3 \times 10^{32}\ cm^{-2}s^{-1} \quad (4)$$

$$\xi_v = 0.035 \quad (5)$$

$$\hat{I} = 160\ mA/beam \quad (6)$$

During machine study periods we have had successful operation with 9 trains 3 and even 5 bunches per train. We expect that in 1996 we will reach 300 mA/beam and a peak luminosity of $6.0 \times 10^{32}\ cm^{-2}s^{-1}$.

Beam-Beam Performance with a Crossing Angle

The main problem of beam-beam interaction with crossing angle in IP is the following. Let 2θ be a crossing angle. A particle without transfers displacement but with distance S from bunch center will cross the opposite bunch with coordinate θS and will get transverse kick. This kick is proportional opposite bunch density and has nonlinear dependence on S. It gives mechanism for coupling between synchrotron and betatron motion, which introduces synchro-betatron resonances with strength proportional to opposite bunch intensity.

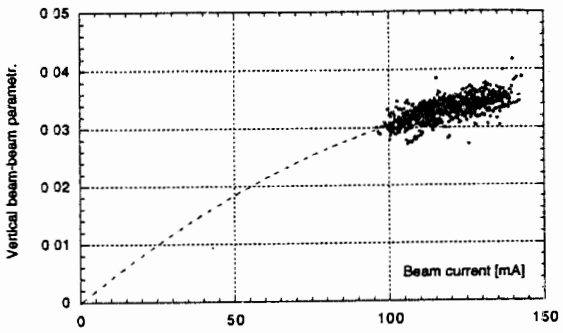


Figure 3: Beam-beam tune shift parameter versus current.

CESR is operating now with ±2.3 milliradian crossing angle at IP. The beam-beam tune shift parameter calculated from luminosity during HEP running 11th April 1995 is shown in figure 3 as function of current per bunch. One can see that the maximum is about 0.036. This good beam-beam performance was arrived at after a several steps. One was a modification of the permanent magnet wigglers [5]. It significantly reduced wigglers nonlinear components. Another step was to turn off several elements with strong nonlinear components of magnetic field. After cleaning up the magnetic lattice the working point was shifted very close to the half integer: Qh=10.52 and Qv=9.63 — a region where there are no principal low order beam-beam resonances. Finally very careful beta function correction and the machine tuning resulted in the beam-beam tune shift parameter reported above.

The CESR guide field, as it was mentioned before, includes two 2.5 meter long permanent magnet wigglers for production of intense X-ray beams. The wiggler gap may be varied by remote control. In closed position the peak wiggler's field is 1.2 T. During electron injection the wigglers are opened which lowers the field to about 0.4 T. Just before the beams are collided the wigglers are again closed. Data shown in figure 3 were collected when both wigglers are closed. During machine studies it was found that for both wigglers opened beam-beam tune shift parameter reaches 0.04, *independent of crossing angle for angles less than 2 milliradians*. Thus the nonlinearities of the guide field have so far been more important to the obtainable tune shift parameter than the synchrobetatron coupling introduced by the crossing angle and beam-beam interaction.

Long range Beam-Beam Interaction

One of the most serious problems of multibunch operation is the long range beam-beam interaction at crossings points. The answer to the question of how big the separa-

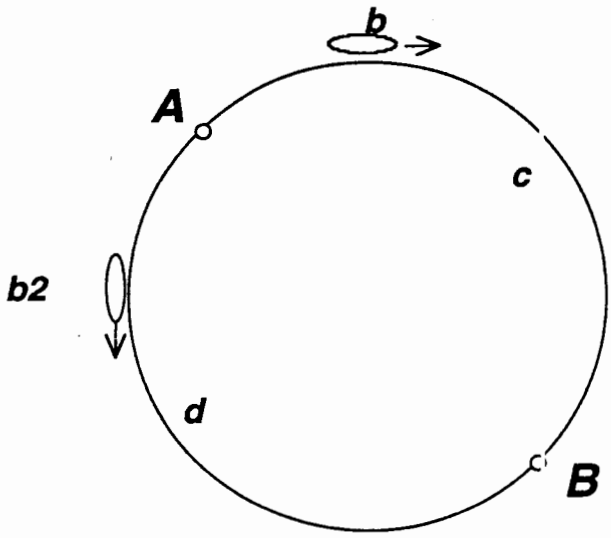


Figure 4: Electrons in bunch b_1 interact with positions in bunch b_2 at positions **A** and **B**. The phase advance along arc c may be different from the phase advance along arc d.

tion should be at each crossing to provide beam stability determines many of the collider's features. This motivated us to carry out an intensive experimental studies. The results of these studies are grouped in two sections. The first one based on [6] describes a linear model of the long range beam-beam interaction and measurements of tune shifts due to parasitic crossings. The second section discuses separation criteria necessary for good lifetime, (see also [7]).

Linear Model of the long range beam-beam interaction

Let us assume the separation distances at the crossing points are large compared with the beam sizes. Then the linear approximation of the beam-beam kick angle does not contain significant terms coupling vertical and horizontal motion. Likewise, we assume the linear transport between crossing points does not include coupling and therefore develop only a one dimensional model.

Consider the simplest case of one bunch per beam and refer to figure 4. The electron and positron bunches should interact with each other only at two points **A** and **B** located at the opposite sides of the storage ring. If these points are not on a symmetry axis of the lattice, the betatron phase advance from **A** to **B** on side c would not in general be equal to the phase advance on side d. This kind of asymmetry leads to some unexpected behavior of coherent modes.

Let us form the vector (X_1, X_1', X_2, X_2'), where $X_{1,(2)}$ and $X'_{1,(2)}$ are the horizontal coordinates and associated angles of bunch $b_{1,(2)}$, appropriately normalized by the horizontal beta function. The matrix that transports both bunches simultaneously (in opposite directions) through the magnetic structure from **A** to **B** is,

$$M_{A,B} = \begin{pmatrix} \cos\mu_c & \sin\mu_c & 0 & 0 \\ -\sin\mu_c & \cos\mu_c & 0 & 0 \\ 0 & 0 & \cos\mu_d & \sin\mu_d \\ 0 & 0 & -\sin\mu_d & \cos\mu_d \end{pmatrix} \quad (7)$$

where μ_c and μ_d are the absolute values of phase advance from **A** to **B** along side c and d accordingly. For simplicity we have assumed that magnitude of horizontal beta function is equal to one and its derivative is equal to zero at both points **A** and **B**.

To get the matrix describing the long range beam-beam interaction consider the kick angle produced by the electromagnetic field of b_2 on b_1. If distance between centers of bunches is much larger than the bunch size, then the change of angle will be $\delta X_1' = 2N_2 r_0/\gamma d$, where N_2 is the number of particles in bunch 2, r_0 the classical electron radius, γ, the Lorentz factor, and d is the distance between bunch centers. Note that d is composed of a closed orbit separation, d_0, and $X_{1,2}$ which are the displacements of bunches $b_{1,2}$ relative to the closed orbit, i.e., $d = d_0 + X_1 - X_2$. Assuming $|X_{1,2}| \ll d_0$ we can rewrite formula for angle change as:

$$\delta X_1' = \frac{2N_2 r_0}{\gamma d_0} - \frac{2N_2 r_0}{\gamma d_0^2}(X_1 - X_2) \quad (8)$$

Here the first term is a dipole kick, which gives a very small orbit distortion that does not depend on X_1 or X_2. The second term is proportional to bunch displacements. It is like a gradient error and couples the motion of the two beams to produce coherent motion. In what follows, we will ignore the first term and only take into account the gradient term. Conceptually this means we must include the effects of the dipole error as a distortion of the closed orbit. In practice, the distortion of the closed orbit is too small to matter.

The long range beam-beam interaction matrix from just before the kick to just after kick will be

$$M_{int} = \begin{pmatrix} 1 & 0 & 0 & 0 \\ 4\pi\delta\nu_1 & 1 & -4\pi\delta\nu_1 & 0 \\ 0 & 0 & 1 & 0 \\ -4\pi\delta\nu_2 & 0 & 4\pi\delta\nu_2 & 1 \end{pmatrix} \quad (9)$$

where $\delta\nu_{1,2} = N_{2,1} r_0 \beta / 2\pi\gamma d^2$ is the tune shift for a single crossing point and $N_{2,1}$ is the number of particles in bunch 2,1. To get a single turn matrix M_{tot} we must make a matrix multiplication:

$$M_{tot} = M_{int} M_{B,A} M_{int} M_{A,B} \quad (10)$$

where $M_{B,A}$ describes the bunch motion from **B** to **A**. Eigenvalues and eigenvectors of M_{tot} characterize the coherent modes.

In figure 5 we present results of numerical calculation of beam-beam coherent modes as described above. We can

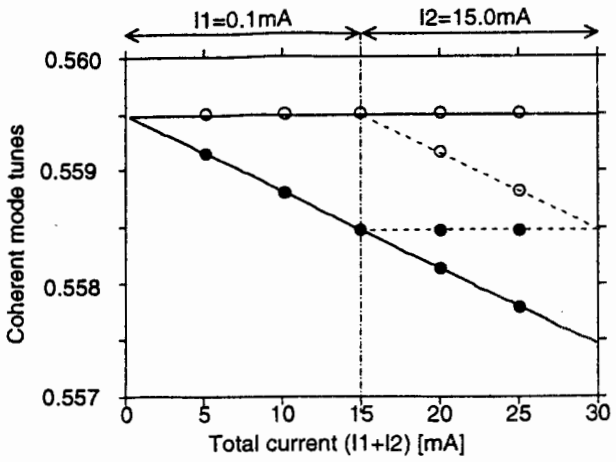


Figure 5: Calculated mode tunes. Open and solid circles refer to the two different modes. Here the effects of asymmetries in the phase advance are evident. Dashed and continuous lines are for the cases of $|\mu_c - \mu_d| = \pi$ or 0. The calculation was done for $\gamma = 10^4$, $d = 29$ mm, $\beta = 40$ m, $N_b = 1.6 \times 10^{11} \times I\ [mA]$.

see that at low total current, where one bunch is very weak, the tune of the higher frequency mode doesn't depend on bunch intensity, but the lower tune goes down with increasing bunch current. The resulting tune split is proportional to bunch intensity. This picture has a simple interpretation. The unaffected tune belongs to the strong bunch, while the decreasing tune is associated with the motion of the weak bunch. The fact that the tune is decreasing means there is a defocussing effect by large bunch. The tune shift or tune split, both are the same in this case, is the sum of the tune shifts calculated for each of the single crossing points, i.e., $2\delta\nu_1$. An asymmetry in phase advance between c and d does not matter.

A different situation arises in the case where both bunches have significant intensity. Here the asymmetry in phase advance $\mu_{as} = |\mu_c - \mu_d|$ plays an important role. In figure 5 we see that if the phase advance is zero, i.e., $(\mu_{as} = 0)$, the dependence of mode tunes resembles that of the strong-weak case. The tune shift of the lower mode is proportional to sum of bunch intensities and tune split equals to sum of tune shifts at both crossing points. However, if $\mu_{as} = \pi/2$, the higher tune goes down with increasing bunch intensities, while the lower tune remains constant. At the point where the bunch intensities become equal one to another, both coherent beam-beam modes have the same tune shift, which is equal one half the tune split in the $\mu_{as} = 0$ case. Moreover *the tune split equals zero in spite of beam-beam interaction.*

To get a more realistic model which can be compared with experimental data, the beam-wall coherent tune shift and multiple bunches must be taken into account. The beam-wall coherent tune shift should be introduced as an extra phase advance $\delta\mu_{b-w}$ for each bunch. The magnitude of $\delta\mu_{b-w}$ is proportional to bunch intensity and is taken from single beam measurements. To describe a configuration with k bunches per beam, the eigenvalues of matrices of order $2k$ must be evaluated.

Measurements of the long range tune shift

Machine studies were carried out at CESR to measure the long range tune shifts under different conditions as a function of beam current. The choice of bunches and the pretzel configuration insured that there were no head-on collisions at the normal interaction points. Betatron tune shifts were measured on a spectrum analyzer connected to beam pickup electrodes. For an accurate measurement of the frequency it was necessary to artificially spread the tunes of the two beam enough that the peaks would not overlap. This was done by varying sextupole strengths in the region of separated orbits. The betatron resonance widths were about 1 kHz wide which is larger than many of the tune shifts. Signal averaging and careful attention to the frequency measurement were paid – not always successfully – resulting in a variance of the frequency shift measurements of order 0.1 kHz. The optics used were the same as those used during normal operation of CESR.

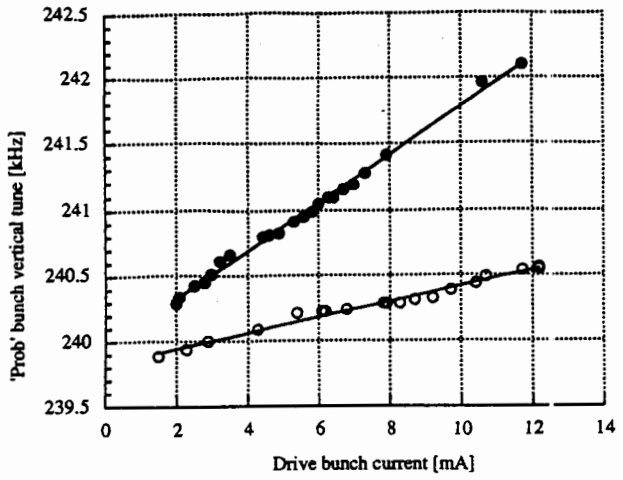
One of the measurements consisted of one bunch of positrons circulating against one bunch of electrons. The electron bunch was used as a 'probe' beam. Its betatron tunes were measured and its current held constant at 2 mA/bunch while the positron bunch current was reduced from 2 mA to 2 mA. One of the nicer features of this technique is that there is no confusion introduced by frequency shifts due to impedance as the measured beam is held at constant current. Data was taken at two different pretzel amplitudes.

The results are presented on figure 6 and given in the table 1 in comparison with theoretical calculation:

In conclusion one can say the use of tune splits of coherent beam-beam modes to test parasitic interaction points, analogous to the use of $\pi - mode$ and $\sigma - mode$ for head-on collisions may lead to confusing results. Under certain conditions the tune split may be reduced, moreover it may be zero in spite of a strong beam-beam interaction. The best way to study the tune shifts due to the long range beam-beam interaction is to use one bunch per beam and measure the dependence of the coherent tunes on the intensity of one of the bunches keeping the intensity of the other bunch fixed and quite small. Only in this case can you be sure that the tune shift of smallest bunch will be equal to sum of tune shifts for the single interaction points.

Separation Criteria

We have conducted fairly extensive experiments at CESR to measure the minimum separation possible for adequate beam lifetime using a variety of different lattices, crossing points, beam currents, and energies. In all cases we found that if the opposing beam current is large enough, we can



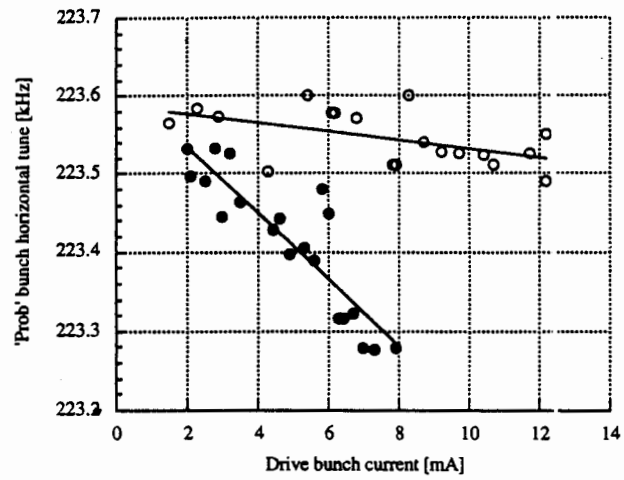


Figure 6: Vertical and horizontal tunes of the 'probe' bunch versus drive bunch current.Open circles refer to the 800 [c.u.] pretsel. Solid ones are for 1200 [c.u.] pretsel.

Bunch		$\nu_x \left[\frac{Hz}{mA}\right]$		$\nu_y \left[\frac{Hz}{mA}\right]$		pretsel
e^+	e^-	data	theory	data	theory	
1	5	-6 ± 2	-16.4	60 ± 2	66.3	1200
1	5	-42 ± 5	-36.9	183 ± 3	149	800

Table 1: Predicted versus measured long range beam-beam tune shifts.

adequately fit the minimum separation to a function proportional to the square root of the opposing beam current. However, if the opposing beam current is instead quite small, reasonable lifetime may be obtained with no separation at all. Tracking simulations give similar results. We also found that the minimum required separation depends significantly on the beta functions at the crossing points. A number of phenomenological models/criteria have been evaluated against the experimental data, see [7]. Some of them used have been used to design optics and are discussed here.

Experiments

The basic technique used to study the long range interaction was to fill selected noncolliding bunches and reduce the separation at the crossing points until a poor ($\approx$ 50 minutes) lifetime was observed. The value of the separation obtained represents the minimum necessary (but not sufficient) for acceptable lifetime. Almost always, a small $\approx$ 10% increase in the separation above the measured minimum was sufficient to obtain very long lifetimes.

In most tests, only one bunch from each beam was filled. In these cases the effects of the long range beam-beam interactions at *two* crossing points are combined. In general, the separation distances, beam sizes, beta functions, etc., were different at the two crossing points, though often the effects from one crossing point dominated. In other tests, one bunch was filled against two or three noncolliding bunches in the opposite beam. For each test, only the overall separation amplitude was adjusted so the individual separation distances at the different crossing points were changed proportionally.

Four completely different lattices were used for the experiments, with varying beta functions, tunes, sextupole distributions, emittances and in the case of optics D of table 2, slightly different energy. We tested several crossing points by filling different combinations of bunches. Note the rather broad range of maximum tune shift parameters (0.00082 to 0.00357) and a rather narrower range of B parameters (0.089 to 0.146).

For each configuration, the minimum separation was measured over a range of opposing beam currents. An example of the current dependence of the minimum required separation is given in figure 7. A best fit curve, assuming the minimum separation is proportional to the square root of the current, is superposed on the plot. This choice of fitting does a somewhat better job than a simple linear fitting when applied to all the data, though in this case the difference is small. It does not fit well if the current is reduced to the point where it is possible to obtain head-on collisions, but such currents are generally less than the design currents.

Set	Optics	$\delta\nu_{max}$	$B \times 10$
1	A	2.44×10^{-3}	1.46 ± 0.07
2	A	1.76×10^{-3}	1.34 ± 0.05
3	B	1.00×10^{-3}	0.89 ± 0.17
4	C	0.86×10^{-3}	0.93 ± 0.01
5	C	1.12×10^{-3}	0.93 ± 0.09
6	C	1.30×10^{-3}	0.98 ± 0.04
7	C	0.82×10^{-3}	1.00 ± 0.06
8	D	1.43×10^{-3}	1.41 ± 0.29
9	C	3.57×10^{-3}	1.33 ± 0.03
10	C	2.11×10^{-3}	1.30 ± 0.32
11	C	1.86×10^{-3}	1.40 ± 0.24
12	C	3.57×10^{-3}	1.05 ± 0.04

Table 2: Various set of crossing points for four different lattices experimentally yield a range of maximum long range tune shift parameters and B parameters at the minimum limiting pretzel amplitude. B parameter definition see below.

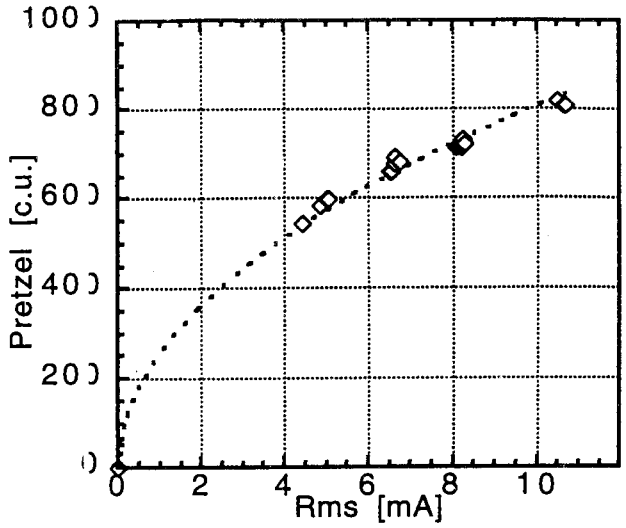


Figure ": The minimum separation amplitude obtained for different opposing beam currents is plotted. 1000 units of separation corresponds roughly to a typical maximum separation of ±10 mm. In this case one bunch in each beam is colliding at two points with optical properties defined in table 2 row 1.

Phenomenology

In the previous section it was mentioned that square root fitting of minimum separation as function of current does a good job for all experimental data sets if current is big enough. This fact motivated us to check out the separation criteria based on assumption that long range tune shift per crossing point is fundamental limit. Column 3 in table 2 named $\delta\nu_{max}$ shows the maximum long range tune shift among parasitic crossings calculated from square root fitting for various data sets.

In some cases the maximum of residual tune shift is in vertical direction and some times it is in horizontal plane. It depends on ration between β_v and β_h and probably η. By itself, with this criterion can expect large uncertainty in the prediction of required separation for good lifetime.

The experimental results of another approach are in column 4 of table 2. Using the B parameter described below, we have a much more reliable predictor of the required separation.

The definition of B is motivated by the following observations:

- Minimum separation is roughly proportional square root of current. So expect combinations like I_b/d^2.
- Primitive tracking shows that instabilities are happening in vertical direction. This motivated us put β_v into parameter in combination with current as $I_b\beta_v$.
- The criterion should contain beam size σ_x because for bigger σ_x and a given separation more particles pass close to opposite beam making situation worse.
- The resulting interaction caused instability must incorporate interactions from each parasitic crossing in an effectively incoherent way. So, we can assume that criteria should have construction like $\sqrt{\sum_i^{N_{cp}}(I_b\ldots)_i^2}$. Where N_{cp} is number of crossing points and I_b is current per bunch.

All above assumptions collected together give us criterion in form:

$$B = I_b\sqrt{\sum_i^{N_{cp}}(\frac{\beta_v\sigma_x^2}{d^2})_i^2} \qquad (11)$$

Table 2 shows the value of B for 12 data sets for different kind of optics, where various $\beta_{x,y}$ and η function and for different number of parasitic crossings were used. Numerical value of B were calculated for $\beta_{h,v}$ in m, σ_x and d in mm, bunch current in mA. One can see that the spread of B parameter value among experimental data sets, $B = (1.17 \pm 0.22) \times 10^{-1}$, is much smaller than it is for $\delta\nu_{max}$, $\delta\nu_{max} = (1.82 \pm 0.96) \times 10^{-3}$.

Really three criteria relating to long range beam-beam interaction were included in process of crossing angle optic design [9]. The first was that separation between opposite beam orbit at crossing points should be bigger than $10\sigma_x$. The second request was that residual long range tune shift due to interaction in each crossing should be less than 1.0×10^{-3}. The last criterion was to minimize B. The substantial difference between the two first constraints and the last criteria is that only the B parameter criteria has a direct dependence on the number of parasitic crossings.

Note that B parameter is not dimensionless and it is not clear its physical interpretation. In addition we do not

know any data from other facilities to check out how it works on them.

Conclusions

In conclusion let us say that CESR has been running quite successfully for over a year with crossing angles. This has resulting in a new record luminosity. The experience gained in implementing crossing angles has shown that so far the pretsel effects are more important than the beam-beam synchrobetatron coupling introduced. Finally, numerous experiments studying the effects of the long range beam-beam interaction have given us sufficient understanding to be able to design lattice where the effects are minimised.

Acknowledgments

Much of the work reported in this paper, especially the beam-beam performance with a crossing angle was done by D. Rubin. He also was responsible for overall optics design and led the machine studies effort which resulted in the successful implementation of crossing angles. We would also like to acknowledge the rest of the CESR operations group for their support.

References

[1] David Rice for CESR Operations Group. *CESR Luminosity Upgrades and Experiments*, -In proc. PAC 93, p.1978.

[2] David Rice for CESR Operations Group. *High Luminosity Operation of the Cornell Electron storage Ring*, -In proc. PAC 89, p.444.

[3] R.E. Meller *Proposal for CESR Mini-B*, CESR Operation Note CON 90-17 (1990).

[4] A. Piwinski, 1977 Particle Accelerator Conference., IEEE Trans. on Nuclear Science, NS-24, No.3, 1408 (1977).

[5] D. Frachon, I. Vasserman, J Welch and A. Temnykh *Magnetic Measurements of the West Wiggler in CESR*, CBN 93 - 7, Cornell 1993.

[6] A. B. Temnykh and J. J. Welch, *Some Aspects of the Long Range Beam-Beam Interaction in Storage Ring*, - In: Proc of PAC 93, Washington, D.C., May 17-20, (1993), CBN 92-13, Nov. 1992.

[7] A. B. Temnykh, J. J. Welch and D. H. Rice, *The Long Range Beam-Beam Interaction at CESR - Experiments, Simulation and Phenomenology*, - In: Proc of PAC 93, Washington, D.C., May 17-20, (1993)

[8] D. Rice, *et. al. Symmetric Beam-Beam Experience* CBN 92-10 Cornell U., proc. SLAC B Factory Workshop, April 1992

[9] D. Rubin, *et. al. CESR Upgrade* , - In: Proc of PAC 95, Dallas, May 1-5, (1995)

Novosibirsk Tau-Charm Factory Design Study

N. Dikansky, V. Parchomchuk, A.N.Skrinsky, V. Yakimenko,
Budker Institute of Nuclear Physics, Novosibirsk, 630090, Russia

Abstract

A method of colliding beams is developed to study the fundamental properties of matter in two directions. The first direction is aimed at achieving higher energies allowing the discovery of new particles and fields The goal of the second one is the study of more delicate fundamental properties of quarks and fields by increasing luminosity in crudely studied energy ranges. The study of CP violation is the most famous example. To study the CP violation in the region of B-quarks, the project of a B-factory as an asymmetrical electron-positron collider with a beam energy of 7/4 GeV and luminosity up to $10^{34} cm^{-2} s^{-1}$ was developed at BINP. During the development of this project, it became clear that the Institute's economical situation, which grew worse in the period of 1990-1993, did not allow us to carry out this project in a reasonable time. Besides, Japan (KEK) and USA (SLAC) began to build the B-factories. Therefore, it is hardly probable to obtain any new results on the third B-factory. On the other hand, a beam energy region of 0.7-2.5 GeV, which still is very interesting, is not studied completely. The interest in this field of research is due to a great body of information obtained on a LEAR facility which is utilized to study proton-antiproton annihilation approximately in this energy region. Studying the cross-section of birth of observed resonances in electron-positron annihilation noticeably increases the value and reliability of their interpretation. In 1993, as a result of discussions, the International Program Committee on High-Energy Physics of the Ministry of Science recommended to reorientate the Novosibirsk project VEPP-5 into a Tau-Charm-factory with high luminosity [1].

1. Parameters of Colliding Beams and Interaction Points

The beam parameters for the Tau-Charm-factory should satisfy the requirements for obtaining a maximum high luminosity of $1.0 10^{34} cm^{-2} s^{-1}$. In addition to the maximum luminosity regime, it is planned to obtain the beam parameters required for the so-called monochromatization of colliding beams and polarized colliding ones. To work in these regimes, the beam emittance control systems are needed. Thus, to obtain monochromatic colliding beams, it is necessary that the main contribution to the vertical size be made by energy spread at the interaction point and the vertical betatron size be substantially less. To control and preserve polarization, rather long solenoids with a longitudinal magnetic field are required. It is undoubtedly impossible to provide simultaneously all these regimes; so, regime-to-regime transition will be made by replacing magnetic elements in straight

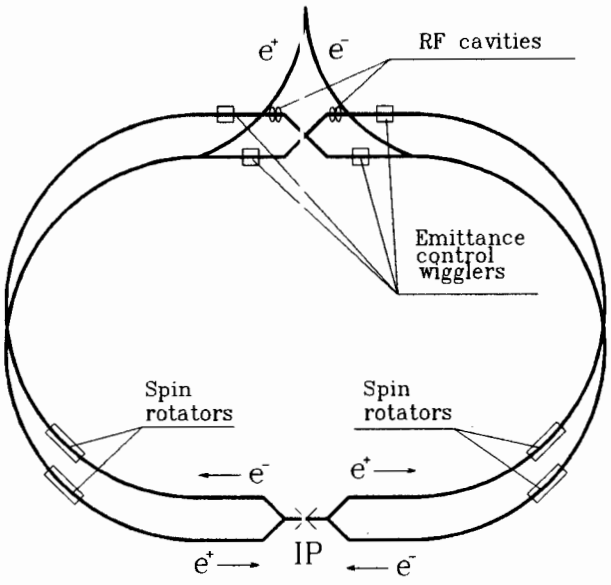


Figure 1: Schematic layout

sections. In this case, the contribution of half-rings into emittances should be as small as possible. The maximum luminosity of the facility is determined by the expression

$$L_{max} = \frac{cN_{max}\gamma\xi_{max}}{r_e D_{min}\sigma_l}, \tag{1}$$

where N_{max} is the maximum number of particles in a bunch; D_{min} is the interbunch distance, ξ_{max} is the parameters of beam interaction; r_e is the classical electron radius; $\gamma = E/mc^2$, and σ_l is the bunch length (sigma). Assuming that a RF system is used at a 700 MHz frequency and the interbunch distance is multiple to the RF wave length, we can present the beam parameters for the maximum luminosity in Table 1.

It is necessary full reconstruction of the experimental stright section to obtain ultra monochromatic colliding beams $\sigma_M \approx 6$ keV. The strong quadrupoles and weak dipoles should be used for beam separation and control of the vertical dispertion function at interection point. The length of such section estimated more than 30 m.

The Tau-Charm-factory is located in a tunnel with a $3x3m^2$ cross-section, whose floor and ceiling are 163 and 166 m above the sea level, respectively. The underground room consists of two half-rings, 89.58 m in radius, and strait section length 100 m, which connect the half-rings. In this case, the length of an ideal orbit is 773.036 m, corresponding to 1805 lengths of the RF wave. With such a geometry, each 19th separatriss contains a particle bunch; in all, the ring has 95 bunches. To install the injection equipment and magnetic systems of emittance control, the technical gap is increased up to $3x5m^2$. The gap should be widened to the side of injection channels so that to have 1.5 m to the inner

Energy (GeV)	2.0
Number of particles in bunch	2.010^{11}
Interbunch distance (m)	8.14
Beta-function at IP (cm)	1
The value of ξ_{max}	0.1
Beam radius $\sigma(\mu m)$	33
Beam emittance $\epsilon_x = \epsilon_y(cm)$	10^{-5}
Beam current (A)	1.12
Circumference (m)	773.036
Radius of ring (m)	89.63
Straite section length (m)	100
Luminosity $(cm^{-2}s^{-1})$	1.010^{34}

Table 1: Parameters of the TAU-Charm beams

Number of particles in bunch	1.510^{11}
Interbunch distance (m)	16.28
Beta-function at IP (cm) β_x/β_y	20 / 2
The value of ξ_{max}/ξ_D	0.05 / 0.01
Beam emittance ϵ_x/ϵ_y (cm)	10^{-5} / 10^{-9}
Beam current (A)	0.4
Energy resolution σ_M (keV)	6
Luminosity $(cm^{-2}s^{-1})$	5.010^{31}

Table 2: Parameters of the TAU-Charm beams for monochromatic coliding

wall and 3.5 m to the external one. The nearest-to-the-surface point of the tunnel is at a 10 m depth; the nearest-within-reach point is the bottom of a technological line, which is 168.6 m above the sea level, corresponding to a ground thickness of 2.6 m above the ceiling of the Tau-Charm-factory tunnel. At present, the tunnel, 200 m long, beginning from the injection complex to a shaft, where the injection channel of the Tau-Charm-factory begins, has been built. In the nearest future, we shall begin to build the channels distributing the electron and positron bunches into an injection gap. The factory is built by the firm "Gornyak" at a pace depending mainly on the financial possibilities. Keeping the pace, we shall need about 5 years to build the underground part.

2. Element of Magnetic System Periodicity

The Tau-Charm-factory magnetic system consists of two storage rings located over each other and intercrossing at the interaction point. To provide collisions of longitudinally polarized beams, spin rotators are supposed to be installed in the half-rings. As an example of the specific magnetic system, we present a simple system which consists of a dipole magnet, 1.5 m long, with a field of 1024 G and quadrupole lenses, each has a 0.4 m length, whose parameters are given in detail in Table 2. In the energy monochromatization regime, the beams remain round, with a dispersion radius of 33 micrometers; the

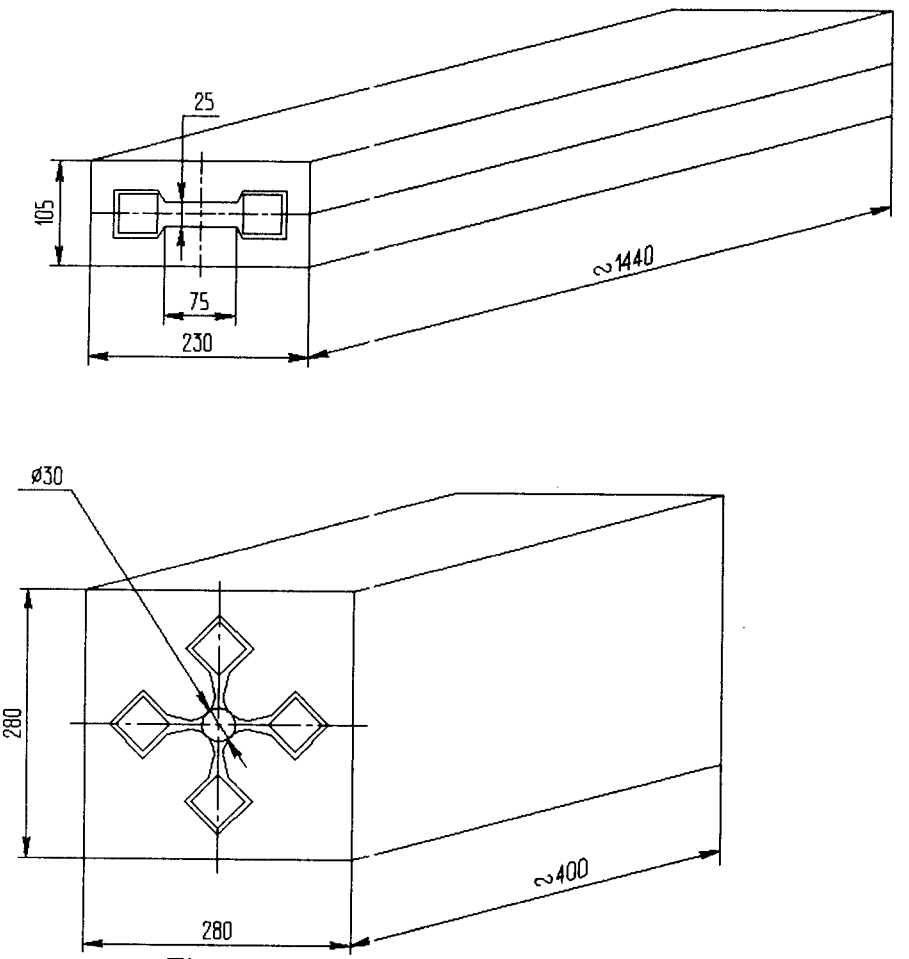


Figure 2: Magnet elements of periodicity cell

value of a vertical energy dispersion is chosen according to the spread. In this case, the value of monochromatization is determined by the ratio of the vertical betatron size and the vertical energy one.

3. Emittance Control Section

To control emittance, it is necessary to use special magnetic system sections where the magnetic field can be changed. A well-known element used for this purpose is the Wiggler-magnet which allows us to noticeably increase the energy loss for radiation. As a rule, the ψ-function is small in the wiggler-magnet. As a result, introducing strong decay, the magnet does not give a considerable increase in the emittance. Let us consider a special magnet design which gives a strong dispersion and the introducing of which will significantly increase the emittance. The equation for the ψ-function has the form

$$\frac{d^2\psi}{ds^2} + G\psi = K. \tag{2}$$

In a smoothed approximation, in the case where the frequency is assumed to be constant along the magnetic gap and the dipole magnetic field to be modulated by the resonance

	Length (cm)	Field (kG)	Gradient (kG/cm)
Quad	40		1.0631
Gap	30		
Dipole	150	1.042	
Gap	30		
Quad	40		-1.0631
Gap	30		
Dipole	150	1.042	
Gap	30		

Table 3: Parameters of the magnet elements

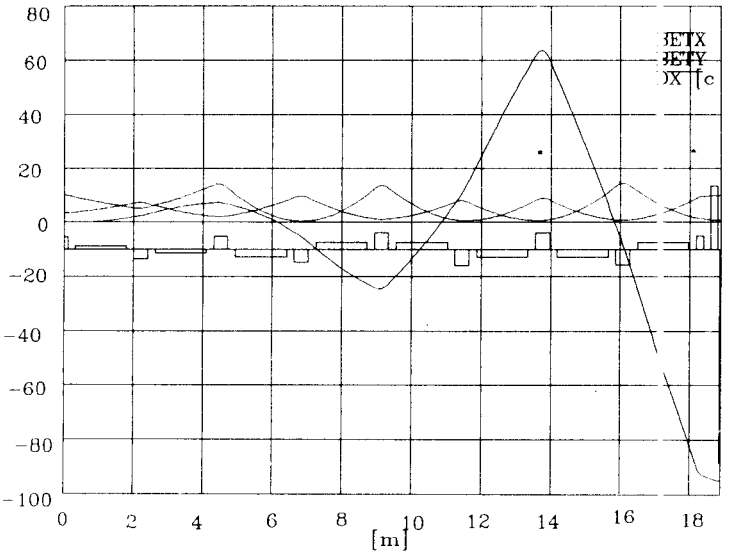


Figure 3: Insertion of the ψ-function control

frequency, the amplitude of the ψ-function beats increases linearly. To obtain the necessary emittance under these conditions, the length of such a section should be several tens meters. At the point where ψ is maximum, the Wiggler-magnet controlling the emittance value in the given direction is placed. For two rings, the electron and positron ones, we need four Wiggler-magnets to independently tune the beam emittances.

4. Interaction Point

The most interesting possibility of obtaining the maximum luminosity is the setting up of the interaction point with a small β-function using a strong longitudinal field (9.6 T and 2.18 m long). Possessing symmetrical focusing in both directions, such a system satisfies the idea of operation with round beams and can allow us to obtain the parameters for a space charge $\xi_{max} > 0.1$. The main problem in setting up the interaction point is a necessity of electrostatic beam separation. The total length of separation plates with a field of 100 kV/cm is 2 m. They are located at the point where the β-function value is high, presenting the difficulties in providing the coherent beam stability. A steady

obtaining of a powerful electrical field under the conditions of synchrotron irradiation of the separation plates is also a rather serious problem.

5. Conclusion

The construction of the Tau-Charm-factory under the existing economic conditions in Russia is not a simple problem. However, the successful completion of this project will allow us to enter the third thousand years with an interesting machine which the world scientific community needs to acquire fundamental knowledge.

References

[1] Dikansky N.S., at al. *Status of the VEPP-5 Complex*, Proc. of EPAC94, London, 1994, p.482

Working Group I
Beam-Beam Instability with Crossing Angle

Crossing Angle Collision and Lifetime: Simulations, Analysis, Measurements and More Simulations*

TONG CHEN

Stanford Linear Accelerator Center, Stanford University, Stanford, CA 94309

I. INTRODUCTION

To achieve the high luminosity required by heavy quark factories, multibunch operation is almost the only choice. The key to gain luminosity in multibunch operation is to reduce the bunch spacing. Therefore, colliding beams with a crossing angle become the favorite interaction region scheme.

The introduction of a crossing angle in e^+e^- colliders causes non-linear coupling between horizontal motion and longitudinal motion. This is illustrated in Figure 1. The beam-beam kick occurs when the particle passes the center of the opposing bunch. The strength of the kick, $\Delta r' = F(r)$, is a nonlinear function of the distance, r, between the particle and the center of the opposite bunch. In head-on collisions, r is the transverse displacement, and the kick is in the transverse plane, so that the process is nonlinear but not influenced by the longitudinal motion. In collisions with a crossing angle, however, r is a function of longitudinal displacement, s, and the crossing angle, F, as well as transverse displacement. The distance r between the test particle and the bunch center can be written:

$$r = x + \tan\Phi \cdot s \,. \tag{1}$$

*Work supported in part by Department of Energy contract DE-AC03-76SF0051.

Presented at ICFA Workshop on Beam-Beam Issues for Multibunch, High Luminosity Circular Colliders, Dubna, Russia, May 18-20, 1995

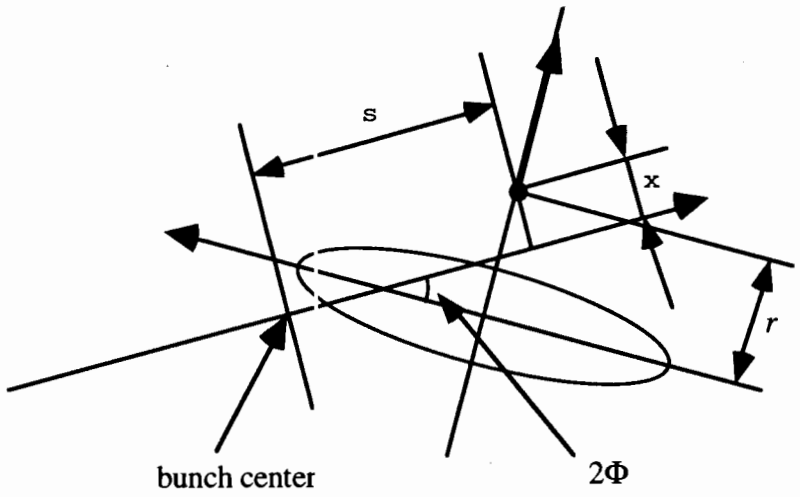


Figure 1. Kick in crossing angle collision

The kick is a function of both transverse and longitudinal positions and, as a result, nonlinear synchrobetatron coupling is generated by the crossing angle collision.

Previous experience on crossing angle collision indicate that the major problem is having bad lifetime. Following discussion will concentrate on this issue.

II. PRELIMINARY SIMULATIONS

A simple simulation program similar to Piwinski's work [1] was written to study the crossing angle collision problem. The simulation program adopts a weak-strong beam-beam interaction model, and consists of only a single beam-beam kick and a linear map for the ring. The beam-beam kick incorporates the crossing angle collision. Three-dimensional motion is simulated. Particles are launched in six dimensional phase space with 6σ amplitudes, which are the typical large amplitude particle that may affect lifetime. For convenience of studying resonances, the program scans the horizontal fractional tune from 0 to 1. The maximum amplitude of all particles ever reached during the 1000-turn tracking is recorded as a function of horizontal tune.

The simulation was performed based on CESR B design. The half crossing angle Φ is 10 mrad. The beam sizes σ_x and σ_s, are taken as 0.36 mm and 1 cm, respectively. The normalized crossing angle, defined as $(\sigma_s/\sigma_x)\Phi$, is 0.278. Results of a simulation with Φ=10 mrad crossing angle are shown in Figure 2. Some one-dimensional resonances, such as Q_x = 1/2, 1/4 and 1/6, already exist in head-on collision. They are not introduced by the crossing angle. Besides these resonances, many synchrobetatron resonances appeared. The strongest new resonances are identified as $5\,Q_x \pm Q_s$ = integer resonances. The coupling resonance $Q_x \pm Q_s$ = integer can also be seen in this picture.

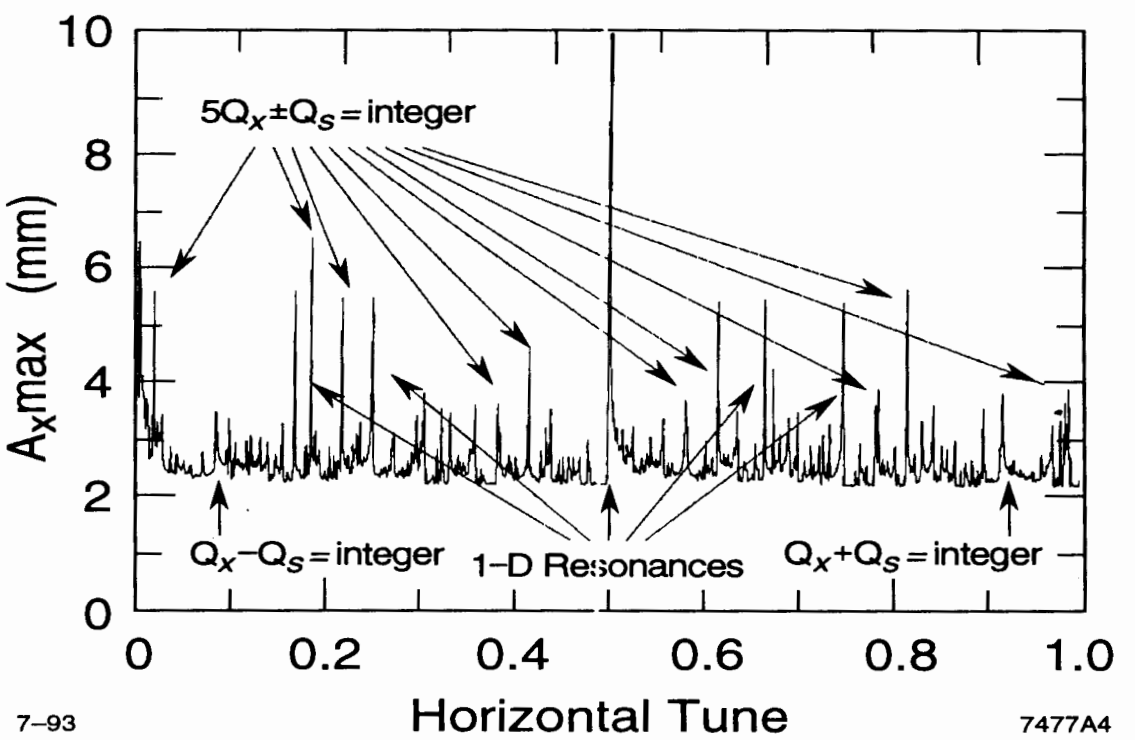


Figure 2. Maximum horizontal amplitude versus tune for crossing angle collision (Q_S = 0.081).

III. ANALYSIS

The simulation result of the previous section, makes us question why the particular resonance family, $5Q_x \pm Q_s$ = integer, is excited. To answer this question, a resonance analysis method is introduced here. The analysis is good for a linear storage ring with a single nonlinear thin element [2], which is a reasonable approach to the beam-beam interaction problem. This method is developed to employ the Fourier Transform to expand the nonlinear force, and relates the Fourier expansion components to certain resonances.

In the crossing angle problem, we are interested in the horizontal (x) and longitudinal (s) motion. Two dimensional difference equations are used to describe the motion. If we sit at one point of a linear ring observing a particle, its motion can be described by:

$$x_{t+1} - 2x_t \cos\mu_x + x_{t-1} = 0 , \tag{2}$$

$$s_{t+1} - 2s_t \cos\mu_s + s_{t-1} = 0 , \tag{3}$$

where t stands for turn number and μ_x and μ_s are the whole-turn phase advances of the oscillations. It is straight forward to find their solutions:

$$x_t = A_x \cos(\mu_x t) , \tag{4}$$

$$s_t = A_s \cos(\mu_s t) . \tag{5}$$

With the crossing angle collision, the difference equations become:

$$x_{t+1} - 2\cos\mu_x\, x_t + x_{t-1} = -\beta_x \sin\mu_x\, F(x_t + \tan\Phi \cdot s_t)\cos^2\Phi , \tag{6}$$

$$s_{t+1} - 2\cos\mu_s\, s_t + s_{t-1} = \beta_s \sin\mu_s\, F(x_t + \tan\Phi \cdot s_t)\sin\Phi\cos\Phi . \tag{7}$$

where F is the horizontal beam-beam kick that can be approximated by a Dawson's integral [3]:

$$F(r) = F_d\left(\frac{r}{\sqrt{2}\ \sigma_x}\right), \tag{8}$$

and

$$F_d(y) = e^{-y^2}\int_0^y e^{t^2}\ dt\ , \tag{9}$$

where σ_x is the horizontal beam size and β_s can be defined in a way analogous to the transverse motion[4]. In the difference Eqs. (6) and (7), the kick modulation of the arrival time is neglected. This is because:

(1) The β_x at the interaction point (IP) is much larger than the bunch length. The β_x change in the bunch length range is negligible.

(2) If the kick $(\Delta x')$ is transferred back to the IP through drift space, it remains the same. For small crossing angle Φ, the nonlinear kick in the longitudinal plane is very weak. In addition, the longitudinal emittance is much larger than the horizontal emittance, which means s is much larger than x. Therefore, the longitudinal nonlinear kick is negligible. Thus, the above equations are simplified:

$$x_{t+1} - 2\cos\mu_x x_t + x_{t-1} = -\beta_x \sin\mu_x F(x_t + \tan\Phi s_t)\cos^2\Phi\ ,5 \tag{10}$$

$$s_{t+1} - 2\cos\mu_s s_t + s_{t-1} = 0\ . \tag{11}$$

Equation (11) has the same solution as Eq. (5). As the first step approximation, substitute Eq. (4) into the right-hand side of Eq. (10). Particles at large amplitude were used to evaluate the resonances, because previous studies have shown that crossing angles would mostly affect the large-amplitude particles [1]. The 6σ amplitude is chosen because it is the typical amplitude for

large amplitude particles, which we are concentrating on, and changes near this amplitude do not change the qualitative conclusion. Taking $A_x=6\sigma_x$ and $A_s=6\sigma_s$, the Dawson's integral becomes:

$$F_d\left(\frac{6}{\sqrt{2}}\ \frac{\sigma_x\cos\mu_x t\ +\ \sigma_s\tan\Phi\cos\mu_s t}{\sigma_x}\right). \tag{12}$$

From Eq. (12), we notice that the coupling term is actually proportional to $(A_s/s_x)\tan\Phi$, rather than $\tan\Phi$. Since $A_s\sim\sigma_s$, the coupling generally scales as $(s_s/s_x)\tan\Phi$. This is called the normalized crossing angle.

Expanding the nonlinear kick in a two-dimensional Fourier Series, the right-hand side of Eq. (10) can be written:

$$\text{RHS} = \frac{1}{2}\sum_{m,n} c_{m,n}\cos(m\mu_x + n\mu_s)t\ +\ d_{m,n}\cos(m\mu_x - n\mu_s)t\ . \tag{13}$$

Similarly, a solution is expected in the form:

$$x_t = \frac{1}{2}\sum_{m,n} a_{m,n}\cos(m\mu_x + n\mu_s)t\ +\ b_{m,n}\cos(m\mu_x - n\mu_s)t\ . \tag{14}$$

Substituting the above equations into Eq. (10), it is easy to find the resonance driving relations:

$$a_{m,n} = \frac{c_{m,n}}{2\sin\frac{1}{2}[(m+1)\ \mu_x\ +\ n\mu_s]\ \sin\frac{1}{2}[(m-1)\ \mu_x + n\mu_s]} \tag{15}$$

$$b_{m,n} = \frac{d_{m,n}}{2\sin\frac{1}{2}[(m+1)\ \mu_x\ -\ n\mu_s]\ \sin\frac{1}{2}[(m-1)\ \mu_x - n\mu_s]}\ . \tag{16}$$

Near resonances $(m\pm1)\ Q_x\pm nQ_s$ = integer, the denominator is small. Then, $(a,b)_{m,n}$ has strong response to $(c,d)_{m,n}$. We can therefore say that $c_{m,n}$ and $d_{m,n}$ drive these resonances.

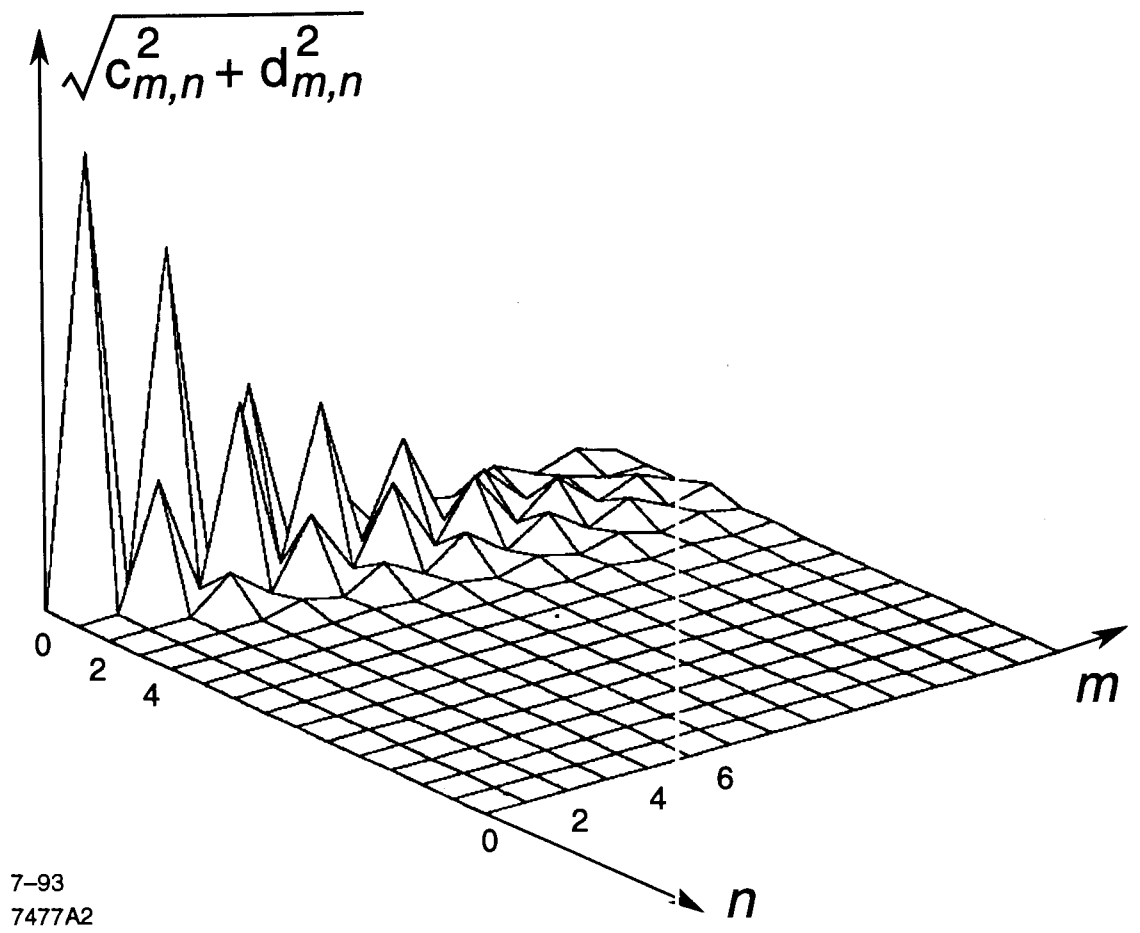


Figure 3. The power spectrum of the crossing angle beam-beam kick.

Figure 3 shows the power spectrum of the Dawson's integral, Eq. (12), created by two-dimensional FFT. The power spectrum $\sqrt{c_{m,n}^2 + d_{m,n}^2}$ gives the resonance driving strength. The phase of the driving terms are not important. Due to the symmetry of the function, the terms with $m+n$ = even vanish. In the calculation, the parameters are the same as for the simulation.

From Figure 3, we can easily see that, besides the 1-dimensional resonance driving terms ($n = 0$), the strongest coupling resonance ($n \neq 0$) driving terms are those with m =4, n =1 and $m = 6$, $n = 1$. According to the previous analysis, these two terms will drive $3Q_x \pm Q_s$ = integer, $5Q_x \pm Q_s$ = integer and $5Q_x \pm Q_s$ = integer, $7Q_x \pm Q_s$ = integer resonances, respectively. It is natural to conclude that the $5Q_x \pm Q_s$ = integer resonances are the strongest coupling resonances, since they are driven by both of the two largest driving terms. This conclusion is consistent with

the simulation result. Notice that the spectrum in Figure 3 is a function of the normalized crossing angle. This conclusion applies for only the small normalized crossing angle.

IV. MEASUREMENTS

The experiment is designed to observe the $5Q_x+Q_s$ resonance associated with crossing angle collision, which is predicted by the theory in the previous section and by simulations. The theory shows that the $5Q_x \pm Q_s$ resonances are driven for large amplitude particles, and simulation shows these particles are sent to even larger amplitudes, which can result in losing those particles. One should therefore expect to see a bad lifetime near those resonances.

The experiment is based on the setup of the CESR crossing angle experiment [5]. CESR has been running with multibunch mode (seven bunches of e^- on seven bunches of e^+). The key point of making multibunch mode possible is to separate bunches around the ring, except at the IP where the detector is located. In CESR, four electrostatic separators were used to separate electron and positron orbits at parasitic crossing points. As shown in Figure 4, the orbits (thin lines) were separated at thirteen would-be collision points, but were merged between the two south (lower) separators, including the IP where the collision takes place. The crossing-angle lattice is essentially a modified version of the normal-operation lattice. The experiment was performed with one bunch on one bunch. A certain amount of antisymmetric voltage was applied to the south separators, which creates antisymmetric orbits about the IP. This is displayed in Figure 5 as the thick lines. It is easy to see from the picture that the beams will collide at the IP with an angle. The half crossing angle can go up to about ±2.5 mrad. The crossing angle is limited by the physical aperture at the interaction region quadrupoles, where the closed orbit is moved to 8.6 σ from vacuum chamber.

The procedure of the experiment is similar to the simulation: scan the horizontal tune while the beams collide at an angle, and measure the decay rate (time derivative of the beam current). The weak-strong scenario is reproduced via collisions of a 2 mA beam of electrons and a 10 mA beam of positrons. The tune scan is carried out near the $5Q_x+Q_s = 43$ (for $Q_S = 0.064$,

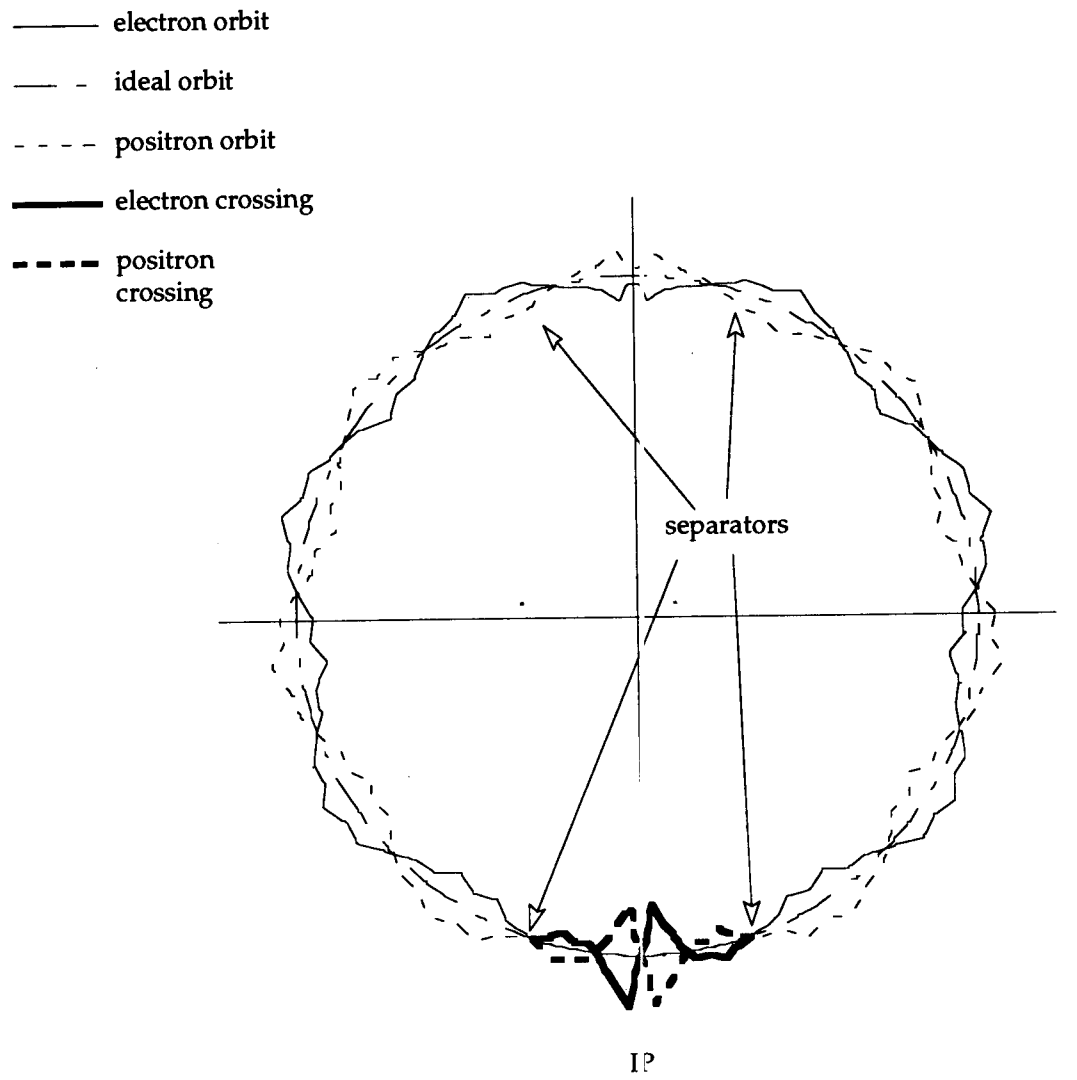


Figure 4. Diagram of the orbits for the crossing angle experiment

Q_x = 8.587) resonance. This resonance is chosen because the crossing angle lattice working point is close to the resonance (nominal horizontal tune Q_x = 8.57). It is easy to move the tune to the vicinity of the resonance. In addition, simulation shows that this resonance is in a "clean" area; *i.e.*, there are no other strong resonances near by.

The experiment consists of two measurements. The first measurement is of the $5Q_x + Q_s$ resonance with and without crossing angle. The synchrotron tune was Q_S = 0.0628.

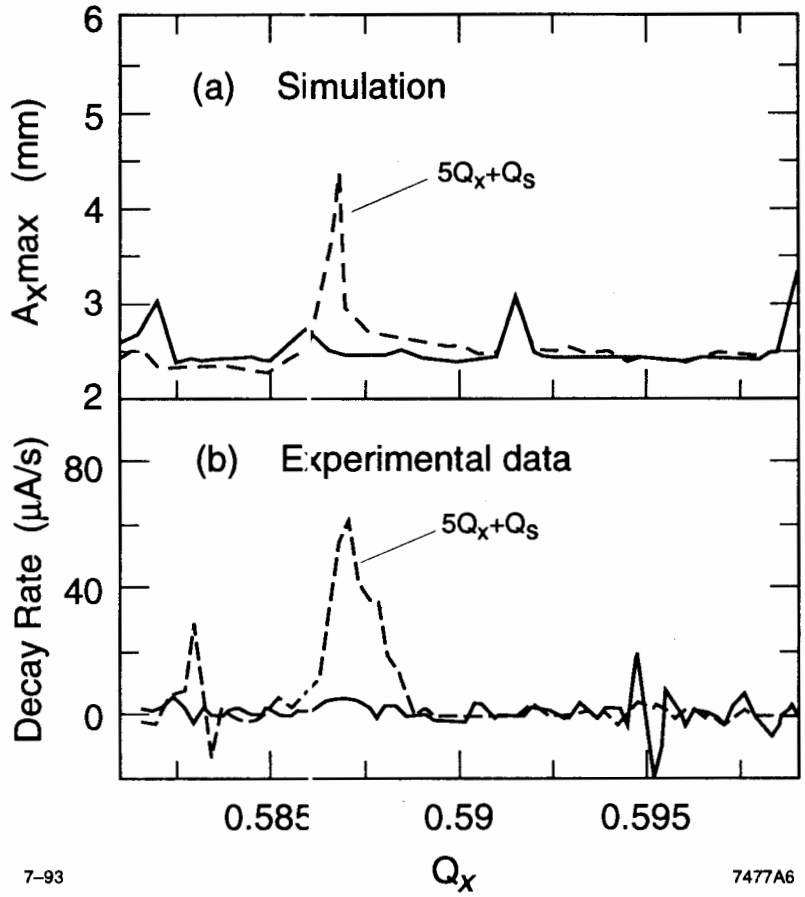


Figure 5. (a) Simulation result, maximum amplitude versus horizontal tune. (b) Experimental data, decay rate as a function of horizontal tune. Solid lines are the head-on collision data, and dashed lines are the crossing angle data.

For comparison, Figure 5 gives both the simulation and experimental results. Figure 5(a) shows the simulation results for head-on collisions (solid line) and crossing angle collisions (dashed line). The plot gives the maximum horizontal amplitude as a function of horizontal tune. It shows that the $5Q_x+Q_s$ resonance appears only when the beams collide at an angle. Figure 5(b) plots the measured results. The data is from two separate measurements: one with the crossing angle turned on (dashed line), and the other one with the angle turned off (solid line). Both measurements employ strong-weak collisions; *i.e.*, 10 mA positron on 2 mA electron. The weak beam (electron) is driven by the resonance, suffering bad lifetime (or large decay rate).

The decay rate is obtained by digitally differentiating the electron current versus time (as the result of differentiation, some jitters in the current measurement creates bi-polar spikes, which result in unrealistic negative decay rates). The predicted resonance at Q_x = 0.587 appears in the data plotted in Figure 5.The second measurement is the resonance ($5Q_x+Q_s$) strength as a function of crossing angle. The crossing angle was set to different values and a one-dimensional tune scan was performed to measure the decay rate as a function of tune at each angle. The angle is controlled by the antisymmetric voltage applied to the south separators. Figure 6 gives the measured results. Test runs have indicated that the resonance is not measurable for half crossing angle smaller than 1.4 mrad. Hence, detailed measurements took place at larger half crossing angles, up to 2.4 mrad. The picture shows a clear ridge of the decay rate at the $5Q_x+Q_s$ resonance, growing as the crossing angle increases.

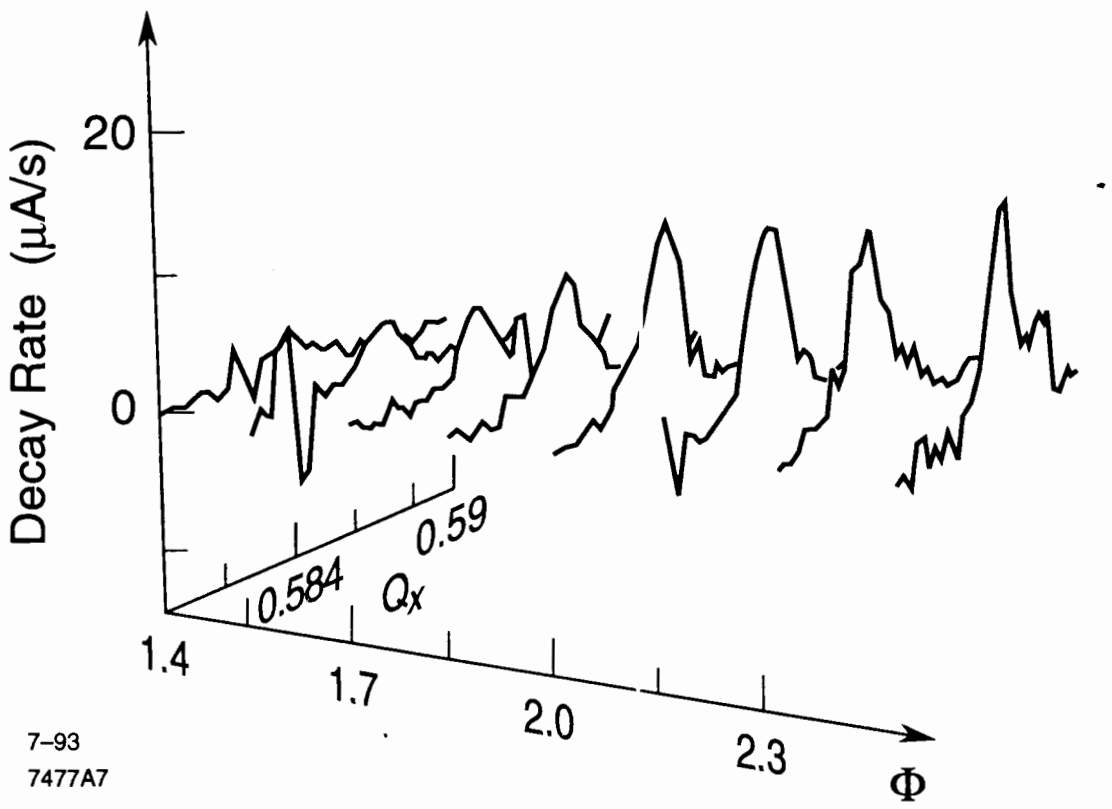


Figure 6. Tune scans versus different crossing angles.

V. LIFETIME SIMULATIONS

The simulation described in Section II tracks only 1000 particles for 1000 turns, which is far from enough to provide lifetime information. To simulate the lifetime, extremely long CPU time is required. A new technique was proposed by J. Irwin to do the simulation with dramatically reduced CPU time [6]. With this method, we can investigate the development of beam-beam tails and calculate lifetime [7].

Using the new program, the simulation is repeated. In a manner similar to that used in the experiments, tune scan and angle scan are simulated separately. The simulation gives the lifetime as a function of horizontal and vertical apertures. In the crossing angle case, horizontal tail excited by the $5Q_x \pm Q_s$ resonance dominates the lifetime. Figure 7 plotted the simulated lifetime at the horizontal aperture of 8.5 σ. The measurement data, converted from that of Figure 5(b), is shown in the same plot.

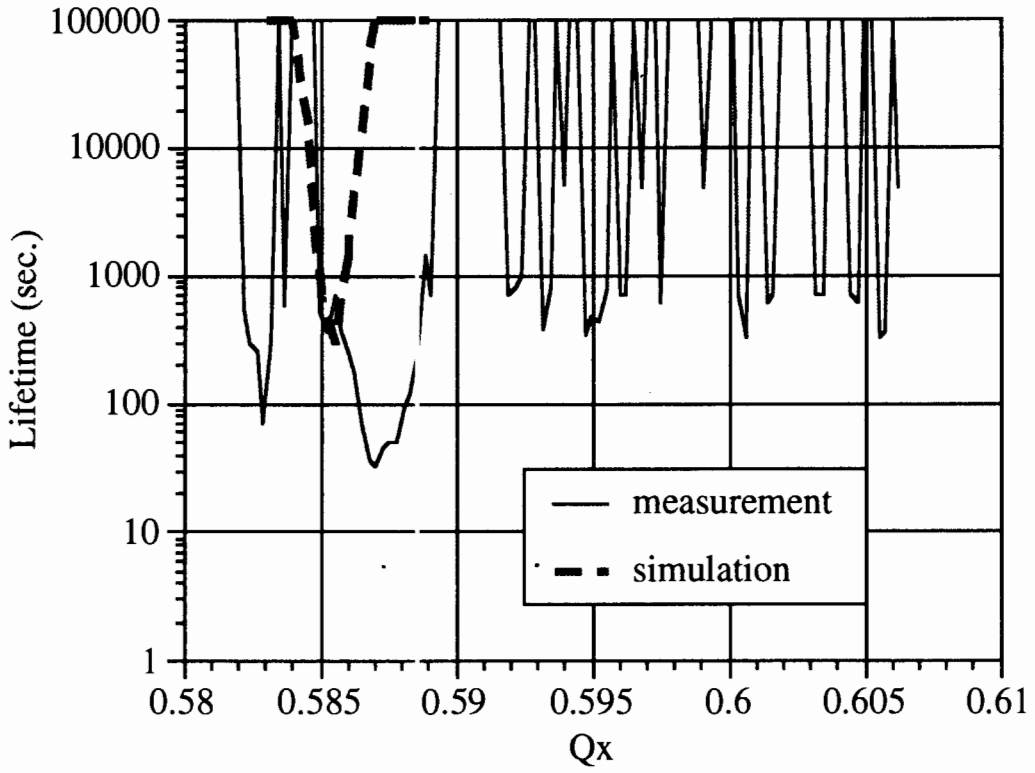


Figure 7. The lifetime versus tune near $5Q_x+Q_s$ resonance. Simulation and measurement results are compared.

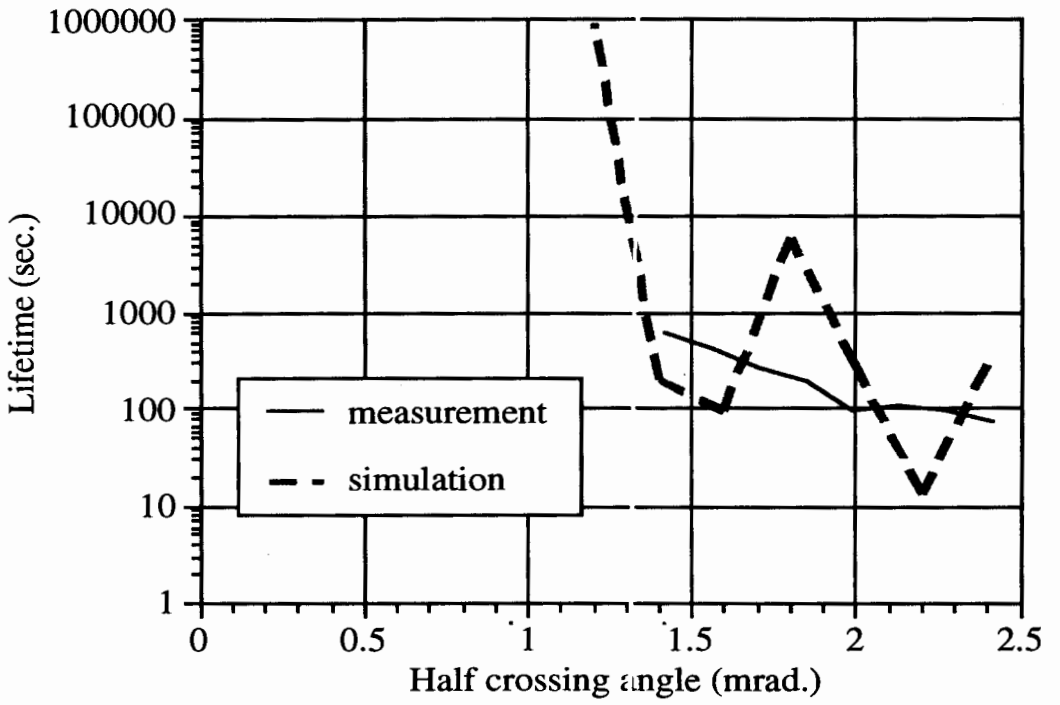


Figure 8. Lifetime versus half crossing angle. Simulation and measurement.

The angle scan simulation was done at $Q_x = 0.5855$. The half crossing angle was scanned from 1.2 mrad to 2.4 mrad. The lifetime at 8.5 σ_x is shown in Figure 8. The minimum lifetime at various angles from the data in Figure 6 is also plotted for comparison.

VI. REMARKS

This is a preliminary attempt in an ongoing effort to compare simulated lifetime with measurements. In the tune scan data, the minimum lifetime at the resonance is missing by a factor of 10. For the angle scan data, simulated results fluctuate strongly—however, the measured results vary from time-to-time, as well.

Many uncertainties may affect the simulation results. The aperture that determines the lifetime is not well known, and it is a sensitive parameter. The most important factor, I believe, are the lattice errors. Studies have shown that lattice errors, including nonlinearities, solenoid coupling, misalignment, chromaticities, etc., can dramatically change the tail distribution, as well

as lifetime. For CESR, these are not negligible. However, there is not enough information on those errors to put in the simulation.

VII. ACKNOWLEDGMENT

The author thanks M. Tigner, D. Rubin, D. Rice, D. Sagan, and the CESR operating group who were involved in the crossing angle studies, especially in making measurements on CESR. The author also thanks R. H. Siemann and J. Irwin for working together on the beam-beam lifetime simulations.

VIII. REFERENCES

[1] A. Piwinski, "Simulations of Crab Crossing in Storage Rings," SLAC–PUB–5430 (1991).

[2] S. Peggs and R. Talman, "Nonlinear Problems in Accelerator Physics," *Ann. Rev. Nucl. Part. Sci.* **36**, 287 (1986).

[3] S. Peggs, PhD thesis, Cornell Universit, 1981.

[4] T. Chen, PhD thesis, Cornell University, 1993.

[5] D. Rubin et al., "Beam-Beam Interaction with a Horizontal Crossing Angle," *Nuclear Instruments and Methods in Physics Research* **A330**, 12, (1993); and CLNS 92/1183.

[6] J. Irwin, *Proc. 3rd Advanced ICFA Beam Dynamics Workshop,* Novosibirsk, USSR, 123 (1989); and SLAC–PUB–5743 (1992).

[7] T. Chen, J. Irwin, and R. Siemann, Phys. Rev. **E49**, No. 3, 2323 (1994).

Synchrobetatron Beam-Beam Resonances in Long Bunches Due to Horizontal Crossing

D.V. Pestrikov
Budker Institute for Nuclear Physics
630090 Novosibirsk, Russian Federation
pestrikov@inp.nsk.su

1. Introduction

The goal luminosities of the future electron-positron factories must reach huge values ($10^{33} \div 10^{34}$ $1/\mathrm{cm}^2\mathrm{s}$). As is known, the luminosity of a collider generally can be increased rising the collision frequency, or/and simultaneously reducing the β-function at the interaction point (β_z^*) and the lengths of colliding bunches (σ_s). In large colliders the collision frequency is increased using the multi-bunch beams. In order to avoid, or to suppress effects from parasitic collisions it is reasonable to use the schemes, where in the interaction region the orbits of colliding bunches cross each-other at some angle (2ϕ, see in Fig.1). The performance of schemes with the crossing in the vertical plane is limited by resonances between vertical and synchrotron oscillations of particles [1]. Since usually colliding bunches have very small vertical size the limitation, found in [1], seems to be very severe to use the schemes with vertical crossings in the high-luminosity collider projects. For this reason, the designs of the future B-factories mainly focus on the schemes with the crab- or conventional crossing in the horizontal plane (see, for instance, [2, 3]). Since the crab-crossing is a very new technique, the schemes with a conventional crossing in the horizontal plane are presently considered as a number one for practical applications.

Present understanding of the beam-beam instability in colliding schemes with small β-function and σ_s cannot be reduced to several simple recipes and generally, demands an additional study. From one side, due to large phase advance of betatron oscillations along the interaction region (the so-called phase-averaging effect [4]) this can strongly suppress the beam-beam resonances [4, 5, 6]. From the other, an increase in the angular spread of bunches due to the decrease in β_z^* results in the spontaneous crossings of the counter-moving bunch with angles ($\phi_{eff} \sim a_z/\beta_z^*$) and in corresponding excitation of synchrobetatron resonances. The study of the common effect of the phase averaging and of the crossing angle was only started in Refs.[7] and [8].

In this paper we calculate the strengths of the synchrobetatron beam-beam resonances with the excitation of vertical betatron oscillations and tune shifts for long bunches, crossing each-other in the horizontal plane. These resonances occur due to a nonlinear

dependence of the beam-beam deflecting force on the transverse offsets of a particle. In a collider with flat bunches, like B-factory, relevant instability of the vertical betatron oscillations can limit the acceptable value of the crossing angle. In colliders with round bunches, these resonances can result in additional limitations to those, which were found in [9], on the position of the working point in the tune space. We assume the weak-strong

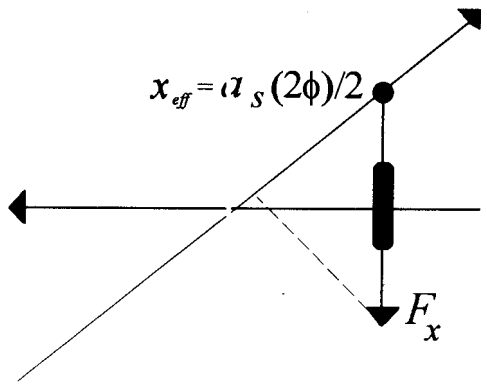


Figure 1: Collision scheme.

beam approximation, zero dispersion function in the interaction region and neglect the lattice chromatic effects.

2. Strengths of Resonances

The oscillations of particles in the interaction region will be described by the following equations:

$$
\begin{gathered}
z = \sqrt{J_z\beta_z(s)}\cos(\psi_z + \alpha_z(s)), \quad x = \sqrt{J_x\beta_x(s)}\cos(\psi_x + \alpha_x(s)), \\
s = R_0\theta = ct + R_0\varphi, \quad R_0\varphi = a_s\cos\psi_s, \quad \Delta p = -\frac{p_0\nu_s}{\eta}\varphi_s\sin\psi_s, \\
R_0(p_z/p) = dz/d\theta = z', \quad R_0(p_x/p) = x', \quad \Delta p = p - p_0, \\
\psi_z' = \nu_z, \quad \frac{d}{ds}(\psi_z + \alpha_z) = \frac{1}{\beta_z}, \quad \psi_x' = \nu_x, \quad \frac{d}{ds}(\psi_x + \alpha_x) = \frac{1}{\beta_x} \quad \psi_s' = \nu_s, \\
I_{z,x} = \frac{pJ_{z,x}}{2} \qquad I_s = \frac{p\nu_s a_s^2}{2R_0|\eta|} = \frac{pJ_s}{2}.
\end{gathered}
\tag{1}
$$

Here, $\Pi = 2\pi R_0$ is the perimeter of the closed orbit, $\eta = (1/\gamma^2) - \alpha$, α is the momentum compaction factor, and $p_0 \simeq \gamma Mc$ is the momentum of the synchronous particle. Equations of motion of the test particle from the weak beam are generated by the Hamiltonian:

$$
H(J, \psi, \theta) = \nu_x J_x + \nu_z J_z + \nu_s J_s - V_{bb}(J, \psi, \theta), \tag{2}
$$

where the term V_{bb} describes the perturbations due to the beam-beam interaction. For the sake of simplicity we assume that the distribution over transverse coordinates in the strong bunch $\rho(\mathbf{r}_\perp)$ is a Gaussian

$$\rho(\mathbf{r}_\perp) = \frac{N}{2\pi\sigma_x\sigma_z}\exp\left(-\frac{(x+\phi s)^2}{2\sigma_x^2} - \frac{z^2}{2\sigma_z^2}\right). \tag{3}$$

Then, if $\lambda(s)$ is a linear density in the strong bunch, for ultrarelativistic $\gamma \gg 1$ electron and positron bunches colliding at the angle 2ϕ (see in Fig.1) we can write V_{bb} in the following form

$$V_{bb} = \frac{4Ne^2R_0}{pc}\lambda(s+ct)\int\frac{d^2k}{\pi k^2}\exp\left\{i[k_x(x+2\phi s)+k_z z] - \frac{k_x^2\sigma_x^2+k_z^2\sigma_z^2}{2}\right\}. \tag{4}$$

This equation describes the perturbation of the weak bunch as a sequence of the periodic and very short kicks (during $\Delta t \simeq \sigma_s/c$, where σ_s is a bunch length). Since without other perturbations equations of motion read

$$J'_\alpha = \frac{\partial V_{bb}}{\partial\psi_\alpha}, \quad \psi'_\alpha = \nu_\alpha - \frac{\partial V_{bb}}{\partial J_\alpha}, \quad \alpha = x, z, s, \tag{5}$$

the amplitudes ($\sqrt{J_\alpha}$) and phases (ψ_α) of oscillations get systematic variations when the tunes (ν_x, ν_z and ν_s) approach the resonant values

$$m_x\nu_x + m_z\nu_z + m_s\nu_s = n. \tag{6}$$

The strengths of these resonances are estimated by the values of the amplitudes of the Fourier-expansion of V_{bb} in phases and azimuth

$$V_{bb} = \sum_{m,n} V_{m,n}\exp(i[m_x\psi_x + m_z\psi_z + m_s\psi_s - n\theta]), \quad m \equiv \{m_x, m_z, m_s\}. \tag{7}$$

Using an expansion

$$\exp[ika\cos\psi] = \sum_{m=-\infty}^{\infty} i^m J_m(ka)e^{im\psi},$$

and Eq.(4) we rewrite V_{mn} in the following form

$$V_{m,n} = \frac{2Ne^2}{\pi pc}\int_0^{2\pi}\frac{d\psi_s}{2\pi}e^{-im_s\psi_s}\int_{-\infty}^{\infty} ds\lambda(2s - a_s\cos\psi_s)\int\frac{d^2k}{\pi k^2}J_{m_x}(k_x\sqrt{J_x\beta_x(s)})\times$$
$$J_{m_z}(k_z\sqrt{J_z\beta_z(s)})\exp\left\{-\frac{k_x^2\sigma_x^2+k_z^2\sigma_z^2}{2} - ik_x2\phi s + im_z\psi_z(s) + im_x\psi_x(s)\right\}, \tag{8}$$

where $d\psi_{x,z}(s)/ds = 1/\beta_{x,z}(s)$. Generally, an analysis of particle motion with such perturbations is embarrassed by very complicated dependences of amplitudes V_{mn} on the amplitudes of particles oscillations. To simplify this analysis we consider a special case, when colliding bunches are very flat so that

$$\sigma_x \gg \sigma_z, \quad \beta_x^* \gg \beta_z^*,$$

and when their closed orbits intersect each other in the horizontal plane at small angle ϕ. Taking into account that near the interaction point the betatron functions vary according to

$$\beta_x(s) = \beta_x^* + \frac{s^2}{\beta_x^*}, \quad \beta_z(s) = \beta_z^* + \frac{s^2}{\beta_z^*},$$

and

$$\psi_x(s) = \arctan(s/\beta_x^*), \quad \psi_x(s) = \arctan(s/\beta_x^*).$$

we find that in the region $\beta_x^* \gg \beta_z^*$ the harmonics $V_{m,n}$ can be calculated neglecting the variations of β_x and ψ_x along the interaction region. Then, for a resonance $m_z\nu_z + m_s\nu_s = n$ we obtain (for the sake of simplicity we take $J_x = 0$)

$$V_{m,n} \simeq \frac{2Ne^2}{\pi pc} \int \frac{d^2k}{\pi k^2} \int_0^{2\pi} \frac{d\psi_s}{2\pi} e^{-im_s\psi_s} \int_{-\infty}^{\infty} ds\lambda(2s - R_0\varphi)\times$$
$$J_{m_z}(k_z\sqrt{J_z\beta_z(s)}) \exp\left\{-\frac{k_x^2\sigma_x^2 + k_z^2\sigma_z^2}{2} - ik_x 2\phi s + im_z\psi_z(s)\right\}. \tag{9}$$

In the region $\sigma_z \ll a_z \ll \sigma_x$ due to a fast convergency of the integral over k_x, we can neglect in Eq(9) the variation of $1/k^2$ with k_x. Remaining integration over k_x yields

$$\int_{-\infty}^{\infty} dk_x \exp\left\{-\frac{k_x^2\sigma_x^2}{2} - ik_x 2\phi s\right\} = \frac{\sqrt{2\pi}}{\sigma_x} \exp\left\{-\frac{2\phi^2 s^2}{\sigma_x^2}\right\} \tag{10}$$

Substituting this expression in Eq.(9), we obtain

$$V_{n,n} = Y_m^f V_{m,n}^{(0)}. \tag{11}$$

Here, (see in [10] and in Appendix A for more detail)

$$V_{m,n}^{(0)} = 2\xi_z\epsilon_z\sqrt{\frac{2}{\pi}} \int_{-\infty}^{\infty} \frac{dv}{v^2} J_{m_z}(2v\sqrt{\chi_z}) e^{-v^2/2}, \quad \chi_z = \frac{J_z}{4\epsilon_z},$$
$$= \begin{cases} \dfrac{2\xi_z\epsilon_z k e^{-\chi_z}}{k^2 - 1/4}\left(I_k(\chi_z) + \dfrac{\chi_z}{k+1/2}[I_k(\chi_z) + I_{k+1}(\chi_z)]\right), & m_z = 2k\ , \\ 0, & m_z = 2k+1\ , \end{cases} \tag{12}$$

is the strength of the resonance calcu ated for the synchronous particle due to head-on collisions with a strong bunch of a zero length, ξ is the so-called beam-beam parameter

$$\xi_z = \frac{Ne^2\beta_z^*}{2\pi pc\sigma_x\sigma_z}, \tag{13}$$

and

$$Y_m^f = 2\int_0^{2\pi} \frac{d\psi_s}{2\pi} e^{-im_s\psi_s} \int_{-\infty}^{\infty} ds\lambda(2s - R_0\varphi) \exp\left\{-\frac{2\phi^2 s^2}{\sigma_x^2} + im_z\psi_z(s)\right\} \sqrt{\frac{\beta_z(s)}{\beta_z^*}} \tag{14}$$

is the so-called resonance suppression factor [4, 5, 6]. For a Gaussian linear density in the strong bunch we can rewrite Eq.(14) in the form

$$Y_m^f = \sqrt{2/\pi}\int_0^{2\pi}\frac{d\psi_s}{2\pi}e^{-im_s\psi_s}\int_{-\infty}^{\infty}du\exp\left(-2\left[u-\frac{a_s\cos\psi_s}{2\sigma_s}\right]^2 - \frac{2\phi^2\sigma_s^2u^2}{\sigma_x^2}+im_z\psi_z(\zeta u)\right)\sqrt{1+\zeta^2u^2},\quad \zeta=\sigma_s/\beta_z^*. \tag{15}$$

Note, that this expression only by a factor $\exp(-2\phi^2\sigma_s^2u^2/\sigma_x^2)$ in the integrand differs from similar expressions, calculated for head-on collisions of long bunches (see, for instance, in Ref.[6]). As against the case of short bunch, Y^f in Eq.(15) generally differs from zero for both even and odd m_s. It means that the interaction with a long bunch is accompanied by excitation of additional family of synchrobetatron resonances with $m_s = 2k+1$. Some impression concerning effects of the bunch length and of the crossing angle

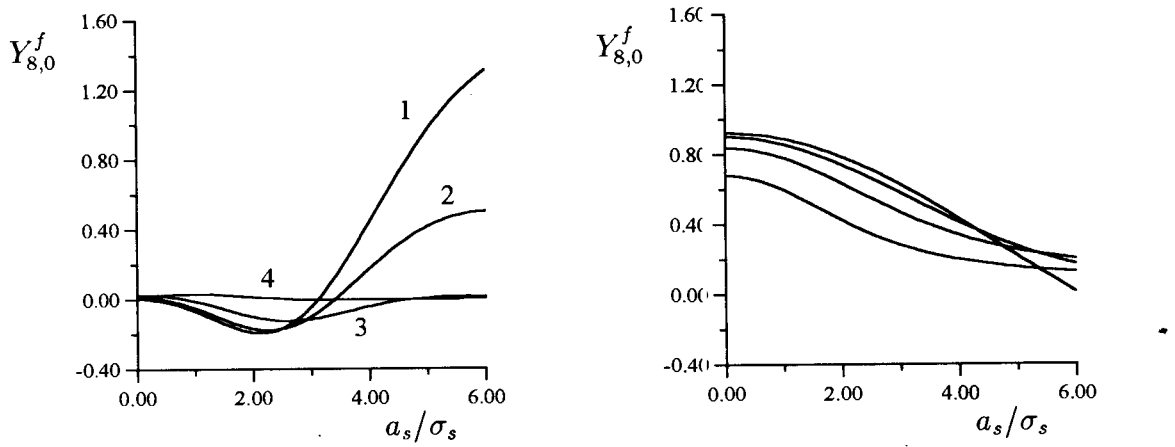


Figure 2: Dependence of Y_m^f on amplitude of synchrotron oscillations; $\sigma_x/\sigma_s = 0.01$, $m_z = 8$, $m_s = 0$. Left picture - $\sigma_s = \beta$, 1: $\phi = 0.0$, 2: $\phi = 0.0025$, 3: $\phi = 0.005$, 4: $\phi = 0.01$. Right picture - $\sigma_s = 0.1\beta$, from top to bottom (at $a_s = 0$) $\phi = 0.0$, 0.0025, 0.005, 0.01.

on the strength of betatron resonances (as an example we take the resonance $\nu_z = 1/8$) gives Fig.2. Like in the case of head-on collisions, comparable values of σ_s and β_z^* result in the significant suppression of betatron resonances at small amplitudes of synchrotron oscillations ($a_s \leq \sigma_s$; bunch core). Left picture in Fig.2 indicates, however, that with an increase in the crossing angle the width of the suppression region in a_s increases. As seen from Fig.3, such a behavior of Y_m^f is common for both betatron and synchrobetatron resonances. Conversely, right picture in Fig.2 shows a very little effect of the crossing angle on the strength of betatron resonances, if strong bunch is short. A comparison of Figs.3 and refyfsb2 shows that strengths of next synchrobetatron resonances is not necessarily smaller. This fact is not very surprising since for short bunches ($\sigma_s \to 0$) there are no odd synchrobetatron resonances at all.

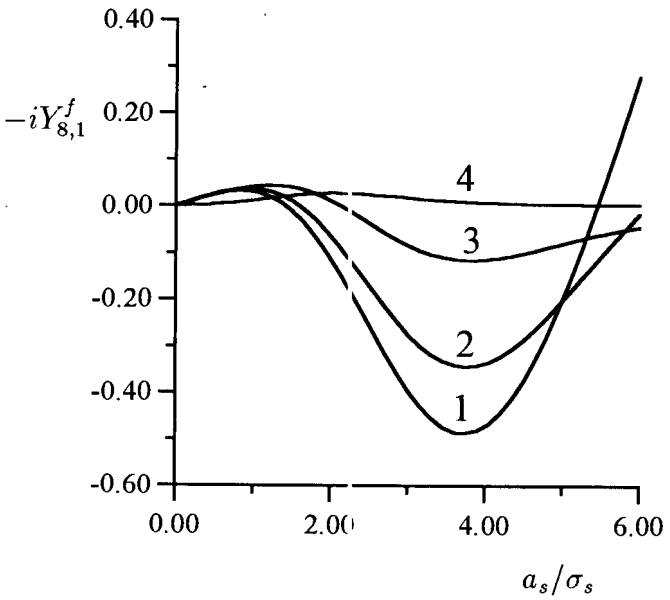


Figure 3: Dependence of Y^f_m on amp itude of synchrotron oscillations; $\sigma_s = \beta$, $\sigma_x/\sigma_s = 0.01$, $m_z = 8$, $m_s = 1$, 1: $\phi = 0.0$, 2: $\phi = 0.0025$, 3: $\phi = 0.005$, 4: $\phi = 0.01$.

3. Tune Shifts

Apart from the excitation of nonlinear resonances, specified by Eq.(6), the collisions of bunches result in the tune shifts of particle oscillations, which are determined by the average value of V_{bb}

$$\Delta\nu_\alpha = -\frac{\partial V_{0,0}}{\partial J_\alpha}, \quad \alpha = x, z, s, \tag{16}$$

Due to nonlinear dependence of the bunch fields on the particle coordinates, these tune shifts ($\Delta\nu_\alpha$) generally depend on the amplitudes of oscillations. For this reason, the resonant condition in Eq.(6) generally holds for definite combinations of amplitudes and therefore, determines some surface in the space of variables J_x, J_z and J_s. For our example we have to calculate $\Delta\nu_z(J_z, J_s)$ and $\Delta\nu_s(J_z, J_s)$. That can be done directly, using Eqs(16) and (9). For the tune shift of vertical oscillations we write

$$\Delta\nu_z(J_z, J_s) = \frac{2Ne^2}{\pi p c} \int \frac{d^2k}{\pi k^2} \int_0^{2\pi} \frac{d\psi_s}{2\pi} \int_{-\infty}^{\infty} ds\lambda(2s - R_0\varphi)\times$$

$$\frac{k_z\sqrt{\beta_z(s)}}{2\sqrt{J_z}} J_1(k_z\sqrt{J_z\beta_z(s)}) \exp\left\{-\frac{k_x^2\sigma_x^2 + k_z^2\sigma_z^2}{2} - ik_x 2\phi s\right\}. \tag{17}$$

Assuming $\beta^*_x \gg \beta^*_z$, we again neglect in this expression the variation of β_x along the interaction region, as well as the variation of $1/k^2$ with k_x. Then, for a Gaussian linear

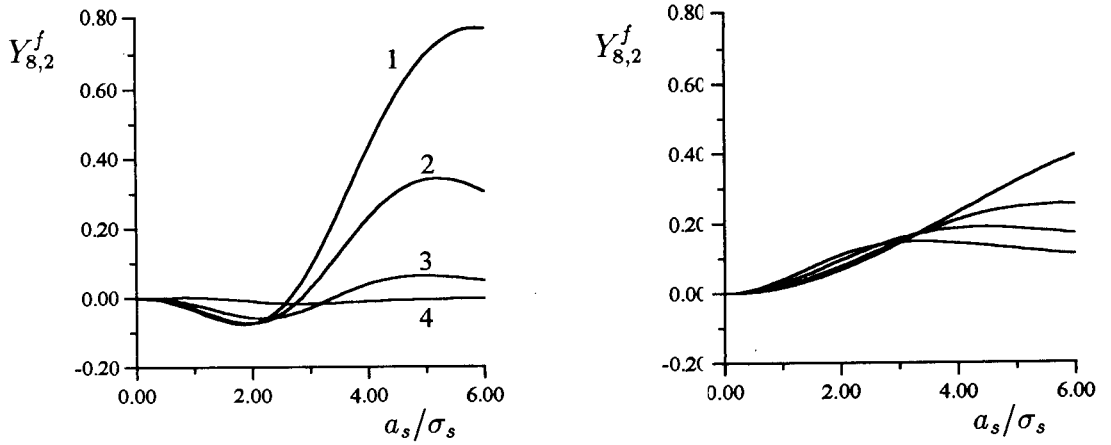


Figure 4: Dependence of Y^f_m on amplitude of synchrotron oscillations; $\sigma_x/\sigma_s = 0.01$, $m_z = 8$, $m_s = 2$. Left picture - $\sigma_s = \beta$, 1: $\phi = 0\,0$, 2: $\phi = 0.0025$, 3: $\phi = 0.005$, 4: $\phi = 0.01$. Right picture - $\sigma_s = 0.1\beta$, from top to bottom (at $a_s = 6\sigma_s$) $\phi = 0.0$, 0.0025, 0.005, 0.01.

density simple transformations result in [1]

$$\Delta\nu_z(J_z, J_s) = \xi_z e^{-\chi_z}[I_0(\chi_z) + I_1(\chi_z)]Y^f_0(a_s, \zeta), \quad \chi_z = J_z/(4\epsilon_z),$$

$$Y^f_0 = \sqrt{\frac{2}{\pi}}\int_0^{2\pi}\frac{d\psi_s}{2\pi}\int_{-\infty}^{\infty} du \exp\left(-2\left[u - \frac{a_s\cos\psi_s}{2\sigma_s}\right|^2 - \frac{2\phi^2\sigma_s^2u^2}{\sigma_x^2}\right)\sqrt{1+\zeta^2u^2}. \tag{18}$$

Here, $I_m(x)$ is the Bessel function of an imaginary argument. The factor Y^f_0 describes dependences of the vertical beam-beam tune shift ($\Delta\nu_z$) on the amplitude of synchrotron oscillations, on the crossing angle and on the bunch length. As seen from Fig.5 with an increase in the crossing angle the dependence of $\Delta\nu_z$ on a_s varies from rising (for head-on collisions) to decreasing (at $\phi \geq 0.003$). One also can mention that in the region $\phi \simeq 0.003$ (and for aspect ratio $\sigma_z/\sigma_x = 0.01$) this dependence becomes very weak. The variation in resonant lines for betatron resonances ($\Delta\nu_z(a_z, a_s) = -\varepsilon_{mn}$, $\varepsilon_{mn} = \nu_z - (n/m)$) with an increase in the crossing angle is shown in Figs.6. If the beam cooling does not destroy the resonances, a damping of synchrotron oscillations will result in the drifting of particles along these resonant lines. Then, from Fig.6(a) we can conclude that for head-on collisions particles can reach the bunch core region only in the vicinity of the lower border of the resonant stopband, while at the upper border ($|\varepsilon_{mn}| \ll \xi_z$) most resonant lines end outside

[1] From Eq.(12) we find that the resonant contribution to $\Delta\nu_z$:

$$(\Delta\nu_z)_m = -\frac{\xi_z k e^{-\chi_z}}{k^2 - 1/4}\left[I_k(\chi_z)\left(1 + \frac{k+1}{k+1/2} + \frac{k}{\chi_z}\right) - \frac{I_{k+1}(\chi_z)}{2k+1}\right]\cos(m\psi_m), \quad m = 2k,$$

where $\psi_m = \psi_z - \theta(n/m)$ is the so-called slow phase, is small for higher order resonances.

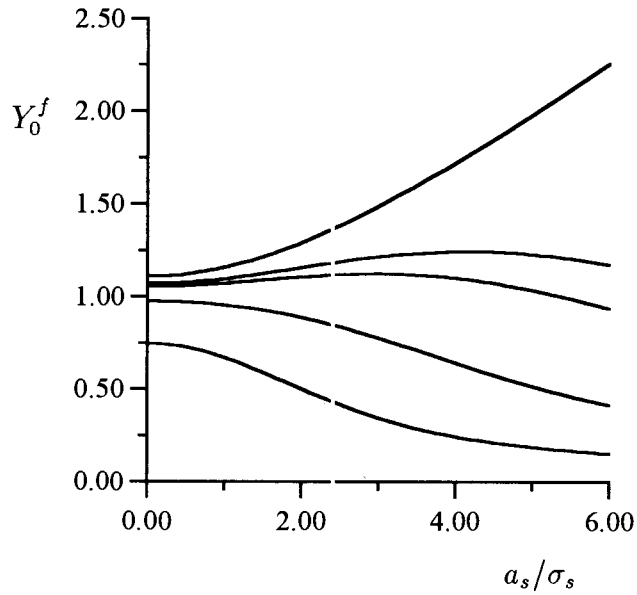


Figure 5: Dependence of Y_0^f on amplitude of synchrotron oscillations; $\sigma_s = \beta$, $\sigma_x/\sigma_s = 0.01$, from top to bottom: $\phi = 0, 0.0025, 0.003, 0.005, 0.01$.

the bunch core. For high crossing angles (Fig.6(b)) the resonant lines have non-positive slopes, which will result in the blowup of vertical oscillations due to longitudinal cooling (see, for instance, in Ref.[11]).

The tune shift of synchrotron oscillations can be calculated similarly. Using Eq.(16) we write

$$\Delta\nu_s = -\frac{\eta R_0}{2\nu_s a_s}\frac{\partial V_{0,0}}{\partial a_s}. \tag{19}$$

Since a_s enters in this expression via the function $\lambda(2s - a_s\cos\psi_s)$, we can use

$$\frac{\partial\lambda}{\partial a_s} = -\frac{\cos\psi_s}{2}\frac{\partial\lambda}{\partial s}.$$

Then, after integration in Eq.(19) over s by parts, we rewrite this equation in the form

$$\Delta\nu_s = -\frac{\eta R_0}{2\nu_s a_s}\frac{Ne^2}{\pi pc}\int\frac{d^2k}{\pi k^2}\int_0^{2\pi}\frac{d\psi_s}{2\pi}\cos\psi_s\int_{-\infty}^{\infty}ds\lambda(2s - a_s\cos\psi_s)$$
$$\times\frac{d}{ds}\left\{J_0(k_z\sqrt{J_z\beta_z})\exp\left(-\frac{k_x^2\sigma_x^2}{2} - \frac{k_z^2\sigma_z^2}{2}\left(1 + \frac{s^2}{\beta_z^{*2}}\right) - 2ik_x\phi s\right)\right\}. \tag{20}$$

The calculation of the derivative over s in the integrand results in an expression

$$\Delta\nu_s = \Delta_1 + \Delta_2 + \Delta_3, \tag{21}$$

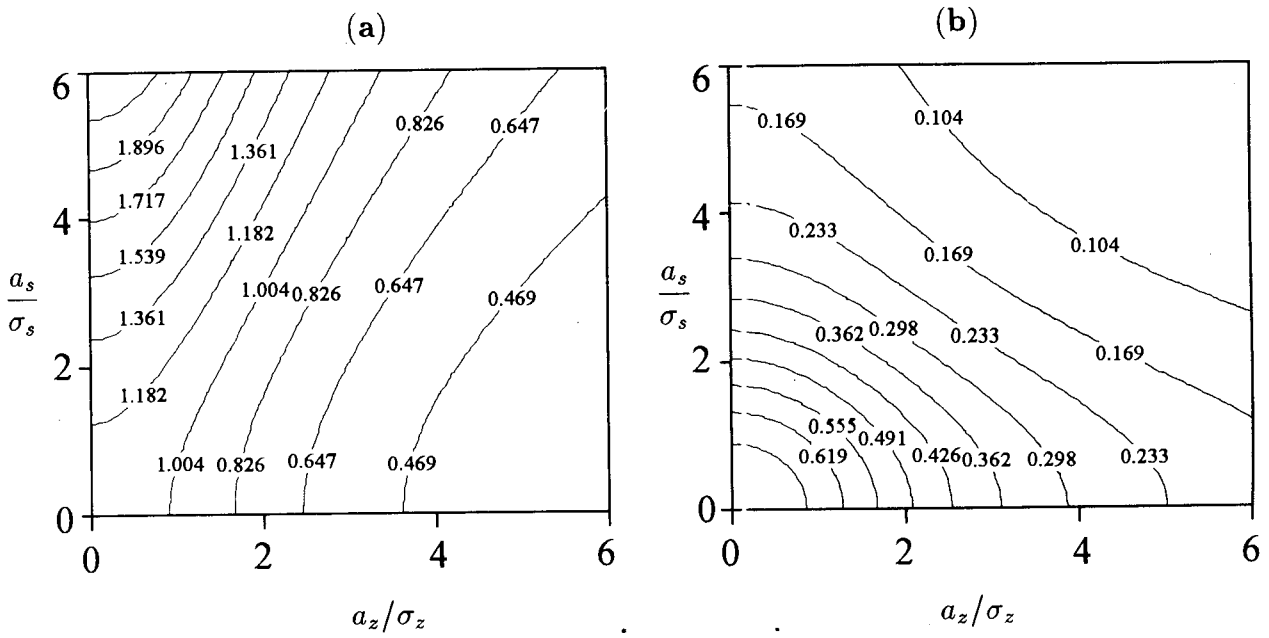


Figure 6: Resonant lines for the vertical betatron oscillations; **a**: $\phi = 0$, **b**: $\phi = 0.01$. The numbers near contour lines give the ratio ε_{mn}/ξ_z, $\sigma_z = \beta$, $\sigma_x/\sigma_s = 0.01$.

where

$$\Delta_1 = \frac{\eta R_0}{2\nu_s a_s}\frac{Ne^2}{\pi pc}\frac{\sigma_z^2}{\beta_z^{*2}}\int_0^{2\pi}\frac{d\psi_s}{2\pi}\cos\psi_s\int_{-\infty}^{\infty}dss\lambda(2s - a_s\cos\psi_s)$$
$$\times\int\frac{d^2kk_z^2}{\pi k^2}J_0(k_z\sqrt{J_z\beta_z})\exp\left(-\frac{k_x^2\sigma_x^2}{2} - \frac{k_z^2\sigma_z^2}{2}\left(1+\frac{s^2}{\beta_z^{*2}}\right) - 2ik_x\phi s\right), \tag{22}$$

$$\Delta_2 = \frac{\eta R_0}{2\nu_s a_s}\frac{Ne^2}{\pi pc}\int_0^{2\pi}\frac{d\psi_s}{2\pi}\cos\psi_s\int_{-\infty}^{\infty}ds\lambda(2s - a_s\cos\psi_s)$$
$$\times\int\frac{d^2k2i\phi k_x}{\pi k^2}J_0(k_z\sqrt{J_z\beta_z})\exp\left(-\frac{k_x^2\sigma_x^2}{2} - \frac{k_z^2\sigma_z^2}{2}\left(1+\frac{s^2}{\beta_z^{*2}}\right) - 2ik_x\phi s\right), \tag{23}$$

and

$$\Delta_3 = \frac{\eta R_0}{2\nu_s a_s}\frac{Ne^2}{\pi pc}\frac{\sqrt{J_z}}{\beta_z^{*3/2}}\int_0^{2\pi}\frac{d\psi_s}{2\pi}\cos\psi_s\int_{-\infty}^{\infty}\frac{dss}{\sqrt{1+(s/\beta_z^*)^2}}\lambda(2s - a_s\cos\psi_s)$$
$$\times\int\frac{d^2kk_z}{\pi k^2}J_1(k_z\sqrt{J_z\beta_z})\exp\left(-\frac{k_x^2\sigma_x^2}{2} - \frac{k_z^2\sigma_z^2}{2}\left(1+\frac{s^2}{\beta_z^{*2}}\right) - 2ik_x\phi s\right). \tag{24}$$

For the case of very flat bunches ($r = \sigma_z/\sigma_x \ll 1$) these very complicated expressions can be essentially simplified. Let us briefly discuss, for example, the calculation of Δ_1. We note that, if the aspect ratio r of the bunch is very small, and since the main contribution to integral over k_x in Eq.(22) gives the region $|k_x|\sigma_x \leq 1$, we may neglect in this expression

the dependence of $1/k^2$ on k_x. Then, the integration over k_x results in

$$\frac{\sqrt{2\pi}}{\sigma_x}\exp\left(-2\frac{\phi^2 s^2}{\sigma_x^2}\right).$$

Remaining integral over k_z can be transformed to the form

$$\frac{\sqrt{2\pi}}{\pi\sigma_x\sigma_z}\frac{1}{\sqrt{1+s^2/\beta_z^{*2}}}\int_{-\infty}^{\infty}dkJ_0\left(k\sqrt{\frac{J_z}{\epsilon_z}}\right)e^{-k^2/2}=\frac{2}{\sigma_x\sigma_z}e^{-\chi_z}I_0(\chi_z),$$

while the substitution of this expression and of a Gaussian linear density in Eq.(22) yields

$$\Delta_1=\frac{\eta R_0}{\nu_s}\frac{\xi_z\epsilon_z}{4\beta_z^{*2}}e^{-\chi_z}I_0(\chi_z)F_1$$

$$F_1=\frac{8\sigma_s}{a_s\sqrt{2\pi}}\int_0^{2\pi}\frac{d\psi_s}{2\pi}\cos\psi_s\int_{-\infty}^{\infty}\frac{du\,u}{\sqrt{1+\zeta^2u^2}}\exp\left[-2\left(u-\frac{a_s\cos\psi_s}{2\sigma_s}\right)^2-2\frac{\phi^2\sigma_s^2}{\sigma_x^2}u^2\right]. \tag{25}$$

This expression can be simplified for synchrotron oscillations with small amplitudes ($a_s \ll \sigma_s$), when the leading contribution to Δ_1 reads

$$\Delta_1=\frac{\eta R_0}{\nu_s}\frac{\xi_z\epsilon_z}{\beta_z^{*2}}e^{-\chi_z}I_0(\chi_z)\frac{e^{\chi_x/\zeta^2}[K_1(\chi_x/\zeta^2)-K_0(\chi_x/\zeta^2)]}{\sqrt{2\pi}\zeta^3} \tag{26}$$

$$\chi_x=\Sigma_x^2/\sigma_x^2,\quad \Sigma_x^2=\sigma_x^2+\phi^2\sigma_s^2.$$

For a short strong bunch ($\zeta \ll 1$) using

$$e^z[K_1(z)-K_0(z)]\approx\frac{\sqrt{\pi}}{(2z)^{3/2}},\quad |z|\gg 1$$

we obtain form Eq.(26)

$$\Delta_1=\frac{\eta R_0}{\nu_s}\frac{\xi_z\epsilon_z}{4\beta_z^{*2}}\left(\frac{\sigma_x}{\Sigma_x}\right)^3,\quad \chi_z\ll 1,\quad a_s\ll\sigma_s,\quad \zeta\ll 1. \tag{27}$$

Similar calculations result in the following expression for Δ_3

$$\Delta_3=\frac{\eta R_0}{\nu_s}\frac{\xi_z\epsilon_z}{4\beta_z^{*2}}(\chi_z/2)e^{-\chi_z}[I_0(\chi_z)+I_1(\chi_z)]F_1,\quad a_z=\sqrt{J_z\beta_z^*}\ll\sigma_x. \tag{28}$$

Note, that in contrast to Eq.(25) the contribution from Δ_3 to $\Delta\nu_s$ increases $\propto\sqrt{\chi_z}$ for large amplitudes of betatron oscillations until $a_z \ll \sigma_x$. This term describes an effect of the crossings of the strong bunch at the angles due to betatron oscillations of a particle, when $\phi_{eff}\sim\sqrt{J_z/\beta_z^*}$. Since in the region $a_z \ll \sigma_x$ the transverse electric field of the bunch can be estimated like $E_\perp \simeq Ne\lambda/\sigma_x$, such crossings produce a longitudinal kick

$$\delta(\Delta p)\sim\sqrt{\frac{J_z}{\beta_z^*}}E_\perp,$$

which results in the contribution to the longitudinal tune shift increasing proportional to a_z.

The term Δ_2 in Eq.(21) directly describes an effect of the crossing at the angle (ϕ) on the tune shift of synchrotron oscillations. As seen from Eq.(23), in the region, where $r \ll 1$ and $a_z \ll \sigma_x$, this term can be calculated taking in the integrand $\sigma_z = 0$. Then, for a Gaussian linear density in the strong bunch the leading term of the expansion of Δ_2 in powers of a_z/σ_x reads

$$\Delta_2 \simeq 4\phi \frac{\eta R_0 \xi_z \sigma_z}{\beta_z^* \nu_s a_s} \int_0^{2\pi} \frac{d\psi_s}{2\pi} \cos\psi_s \int_{-\infty}^{\infty} \frac{du}{\sqrt{2\pi}} \exp\left[-2\left(u - \frac{a_s \cos\psi_s}{2\sigma_s}\right)^2\right] \times \int_0^{\infty} dk \sin\left(2ku\frac{\phi\sigma_s}{\sigma_x}\right) e^{-k^2/4}, \quad a_z \ll \sigma_x. \tag{29}$$

Direct calculation of integrals in this expression (see in Appendix B) results in

$$\Delta_2 \simeq \frac{\eta R_0}{\nu_s} \frac{Ne^2}{\pi p c a_s^2} \left[1 - \exp\left(-\frac{\phi^2 a_s^2}{2\Sigma_x^2}\right)\right], \quad \Sigma_x^2 = \sigma_x^2 + \phi^2 \sigma_s^2. \tag{30}$$

For oscillations with small amplitudes ($a_s \ll \sigma_s$) Eq.(30) yields

$$\Delta_2 \simeq \frac{\eta R_0}{\nu_s} \frac{\xi_z \epsilon_z}{4\beta_z^{*2}} 4 \frac{\sigma_x^2}{\Sigma_x^2} \frac{r\phi^2}{\theta_z^2}, \tag{31}$$

where $\theta_z = \sqrt{\epsilon_z/\beta_z^*}$ is the vertical rms angular divergency in the strong bunch. A comparison of Eqs(30) and (27) shows that the contribution from Δ_2 will dominate, if $\theta_z \ll \sqrt{r}\phi$. If, for example, $\sigma_x = 100\mu$m, $r = 0.01$, $\sigma_s = \beta_z^* = 1$ cm, which is typical for B-factory projects, we find that $\theta_z = 10^{-4}$ and that Δ_2 will exceed Δ_1 and Δ_3, if the crossing angle exceeds $\phi = 10^{-3}$.

4. Discussion

Collisions of flat bunches at the angle in the horizontal plane is accompanied by the excitation of both horizontal and vertical synchrobetatron resonances and, generally, may result in the blowup of the vertical beam size. These synchrobetatron resonances can be especially important for the tail particles of the bunch ($\phi a_s > \Sigma_x$). An accumulation of particles in the buckets of vertical oscillations near these resonances can saturate the luminosity of the collider, if the perturbation due to horizontal synchrobetatron resonances is small. If the perturbation due to horizontal synchrobetatron resonances is strong, such an accumulation will result in the decrease of the luminosity.

The dependence of the transverse beam-beam tune shifts on the amplitude of synchrotron oscillations and on the crossing angle generally vary the geometry of one-dimensional betatron resonances in the space of amplitudes of oscillations. No phase-convection is predicted for head-on collisions. However, near the upper side of the resonant stopbands the

damping of synchrotron oscillations may result in the storing of particles in the betatron tail region. For high crossing angles similar blowup in vertical direction happens due to the phase-convection effect. Such a variation in the geometry of resonant lines means that there is some optimum crossing angle, when the vertical tune shift does not depends on the amplitude of synchrotron oscillations, and when the damping of synchrotron oscillations has a little effect on the dynamics near betatron resonances.

The beam-beam tune shift of the synchrotron oscillations generally is contributed by the bunch waist, by the betatron angular spread in the weak bunch and by the crossing angle itself. The contributions from the bunch waist (Δ_1) and from the betatron angular spread decrease as the crossing angle increases. The contribution due to crossing angle collisions (Δ_2) saturates, when the crossing angle increases. For typical parameters of the future B-factories this contribution may dominate starting from very small crossing angles. However, until $a_x, a_z \ll \sigma_x\ \Delta_2$ does not depend on amplitudes of betatron oscillations. This tune shift (Δ_2) is proportional to the bunch current. For this reason, its effect must be analyzed together with perturbations due to longitudinal bunch wake fields.

The common effect of the phase-averaging and of the crossing at the angle substantially decreases the strengths of the vertical synchrobetatron resonances for flat colliding bunches. The reason is that the drop of the resonance strength due to crossing angle collisions compensates its increase due to mismatching between the beam-beam kick and the reaction of the betatron oscillations, which is specific for collisions of flat bunches.

A. Calculation of $V_{mn}^{(0)}$

The integral in Eq.(12) can be calculated expanding the Bessel function $J_{2k}(2v\sqrt{\chi})$ in the power series [10]

$$J_{2k}(2v\sqrt{\chi}) = (v^2\chi)^k \sum_{m=0}^{\infty} \frac{(-v^2\chi)^m}{m!(m+k)!}, \tag{A.1}$$

which results in

$$\int_0^{\infty} \frac{dve^{-v^2/2}}{v^2} J_{2k}(2v\sqrt{\chi}) = \frac{\Gamma(k-1/2)2^k}{\sqrt{2}\Gamma(2k+1)} \chi^k e^{2\chi} F(k+3/2, 2k+1, 2\chi), \tag{A.2}$$

where $F(\alpha, \gamma, z)$ is the confluent hypergeometric function. Using the identities [10]

$$F(\alpha+1, \gamma, z) = \left(1 + \frac{z}{\alpha}\frac{d}{dz}\right) F(\alpha, \gamma, z), \quad F(k+1/2, 2k+1, 2\chi) = \frac{2^k k!}{\chi^k} e^{\chi} I_k(\chi)$$

and

$$\frac{2^{2k-1}\Gamma(k+1/2)\Gamma(k)}{\Gamma(2k)} = \sqrt{\pi},$$

we obtain

$$\int_0^{\infty} \frac{dve^{-v^2/2}}{v^2} J_{2k}(2v\sqrt{\chi}) = \frac{k\sqrt{\pi/2}e^{-\chi}}{k^2 - 1/4} \left(I_k(\chi) + \frac{\chi[I_k(\chi) + I_{k+1}(\chi)]}{k+1/2} \right). \tag{A.3}$$

B. Calculation of integrals for Δ_2

Let us calculate the integrals in Eq.(29). After obvicus substitution

$$u - \frac{a_s \cos\psi_s}{2\sigma_s} \to u$$

we rewrite the integrals over u and k in the form

$$\begin{aligned}
&\int_{-\infty}^{\infty} \frac{du}{\sqrt{2\pi}} e^{-2u^2} \int_0^{\infty} dk \sin\left(2ku\frac{\phi\sigma_s}{\sigma_x} + k\frac{\phi a_s}{\sigma_x}\cos\psi_s\right) e^{-k^2/2} \\
&= \int_0^{\infty} dk e^{-k^2/2} \sin\left(k\frac{\phi a_s}{\sigma_x}\cos\psi_s\right) \int_{-\infty}^{\infty} \frac{du}{\sqrt{2\pi}} e^{-2u^2} \cos\left(2ku\frac{\phi\sigma_s}{\sigma_x}\right) \\
&= \frac{1}{2}\int_0^{\infty} dk \exp\left(-\frac{k^2}{2}\frac{\Sigma_x^2}{\sigma_x^2}\right) \sin\left(k\frac{\phi a_s}{\sigma_x}\cos\psi_s\right).
\end{aligned}$$

Now, using

$$\int_0^{2\pi} \frac{d\psi}{2\pi} \cos\psi \sin(z\cos\psi) = J_1(z),$$

we obtain

$$\begin{aligned}
\Delta_2 &\simeq 2\frac{\eta R_0 \xi_z \sigma_z}{\beta_z^* \nu_s}\frac{\sigma_x}{a_s^2}\int_0^{\infty} dz J_1(z) \exp\left(-\frac{z^2}{2}\frac{\Sigma_x^2}{\phi^2 a_s^2}\right) \\
&\simeq 2\frac{\eta R_0 \xi_z \sigma_z}{\beta_z^* \nu_s}\frac{\sigma_x}{a_s^2}\left[1 - \frac{\Sigma_x^2}{\phi^2 a_s^2}\int_0^{\infty} dz J_0(z) \exp\left(-\frac{z^2}{2}\frac{\Sigma_x^2}{\phi^2 a_s^2}\right)\right] \\
&\simeq 2\frac{\eta R_0 \xi_z \sigma_z}{\beta_z^* \nu_s}\frac{\sigma_x}{a_s^2}\left[1 - \exp\left(-\frac{\phi^2 a_s^2}{2\Sigma_x^2}\right)\right].
\end{aligned}$$

References

[1] A. Piwinski. IEEE Trans on Nucl. Sci. **NS-24**, 1408, 1977.

[2] An Asymmetric B-Factory Based on PEP. Conceptual Design Report. LBL PUB-5303, SLAC-372, CALT-68-1715, UCRL-ID-106426, UC-HRPA-91-01, 1991.

[3] Accelerator Design of the KEK B-factory. Ed by S. Kurokawa, K. Satoh and E. Kikutani. KEK Report 90-24, 1991.

[4] S. Krishnagopal, R. Siemann. Phys.Rev. D **41**, 2312, 1990.

[5] N.S. Dikansky, P.M. Ivanov, D.V. Pestrikov, E.A. Simonov. In Procedings of the USA National Particle Accelerators Conference, San-Francisco May 1991, v.1, p. 523, 1991.

[6] N.S. Dikansky, D.V. Pestrikov NIM, A 344, 286, 1994; Phase Averaging of the Beam-Beam Instability. KEK Preprint 93-7, 1993.

[7] D. Sagan, R. Siemann and S. Krishnagopal. In Proc of the 2nd European Particle Accelerator Conference, v. 2, p. 1649. Edittions Frontieres, 1990.

[8] D.V. Pestrikov. NIM, A 336, 427, 1993.

[9] W. Chou, A. Piwinski. In Proc. of the Conf. on B Factories, The State of the Art in Accelerators, Detectors and Physics. SLAC, 1992, p. 134.

[10] I.S. Gradsteyn, I.M. Ryzhik. Table of Integrals, Series and Products. Academic Press, New York, 1965.

[11] A. Gerasimov. Physica **D 41**, 89, 1990.

Summary of Working Group I—Beam-Beam Instability with Crossing Angle

T. Chen†

Stanford Linear Accelerator Center, Stanford University,

Stanford, CA 94309

Working Group Members

K. Hirata	KEK	L. Palumbo	INFN
V. Parkhomchuk	BINP	D. Pestrikov	BINP
A. Piwinski	DESY	D. Shatilov	BINP
J. Welch	Cornell	P. Zenkevich	ITEP

INTRODUCTION

The luminosity of circular colliders is given by

$$L = \xi \frac{I_T}{e} \frac{\gamma}{r_e \beta_y^*},$$

where e=1.6×10^{-19}C and r_e=2.82×10^{-15}m are constants. The parameter ξ is the beam-beam tune shift parameter. It is limited by the beam-beam dynamics to ~0.05. The parameter γ is the beam energy, which is determined by the physics to be studied by the collider. The parameter β_y^* is the vertical β-function at the interaction point (IP). It has to be comparable to the bunch length in order to avoid losing luminosity due to a geometrical factor increasing the overlap area. Therefore, the only possible parameter left for increasing luminosity is the total current I_T. We can write I_T=$N_b I_b$, where I_b is the current per bunch. It is limited by the single bunch instabilities. To increase I_T., the best one can do is to increase the number of bunches in the ring N_b.

In order to meet the high luminosity requirement of heavy quark factories, modern high-luminosity circular colliders take the approach of multibunch operation. The electrons and positrons are stored in two separate rings and brought together at a single interaction point. The key to achieving high luminosity in these machines is reducing the space between bunches. This makes the crossing angle collision scheme very favorable.

† Work supported by Department of Energy contracts DE-AC03-76SF00515

However, a crossing angle introduces synchro-betatron coupling. In a head-on collision, particles receive a transverse kick, $F(x)$, from the counter beam. This kick depends on the transverse coordinates. When a crossing angle, $\pm\Phi$, in x plane is introduced, the transverse kick becomes $F(x + \tan\Phi \cdot s)\cos^2\Phi$, where s is the longitudinal position, and a longitudinal kick is associated. Obviously, the crossing relates transverse motion with the longitudinal motion.

To compare machines with different parameters, the crossing angle should be scaled as

$$\phi = \frac{\sigma_s}{\sigma_x}\tan\Phi \approx \frac{\sigma_s}{\sigma_x}\Phi.$$

ϕ is called the normalized crossing angle. In most analysis and simulations, crossing angles appear in this form.

By now, two electron-positron colliders have operated with a crossing angle: DORIS I and CESR. Their experience is the most useful information on this issue.

HORIZONTAL CROSSING ANGLE VERSUS VERTICAL CROSSING ANGLE

A conclusion that was well agreed to is that a crossing angle in the horizontal plane is better than the one in vertical plane. The major reason leading to this conclusion, I believe, is the fact that DORIS I, which used a vertical crossing angle of ± 12 mrad, had bad performance and eventually gave up, while CESR, which adopted a horizontal crossing angle ± 2 mrad, has been performing very well. However, this is not completely convincing because CESR has a much smaller crossing angle than DORIS I.

To look into this problem, one can compare the normalized crossing angles in horizontal and vertical planes. The denominator in the normalized crossing angle definition is the transverse beam size corresponding to the crossing direction. Assuming the physical crossing angle and the bunch length are the same, the smaller the transverse beam size, the larger the normalized crossing angle is, and hence the stronger synchrobetatron coupling. In the newly designed high luminosity colliders, most of them have a flat beam at the collision point. Therefore, the normalized vertical crossing angle would be considerably larger than a horizontal one. This should be the primary reason for choosing a horizontal crossing angle.

Another view on this problem is the orders of emittances. Due to radiation noise, the longitudinal emittance is usually two magnitudes larger than horizontal emittance, and the horizontal emittance is about two orders of magnitudes larger than vertical emittance. So, the effect of coupling between longitudinal and vertical will be much more sensitive than the effect of longitudinal-horizontal coupling.

LIFETIME PROBLEM DUE TO CROSSING ANGLE

The best known consequence of a crossing angle is that it leads to a bad lifetime. Early experience of DORIS I was that the lifetime went bad even with a small beam-beam tune shift parameter, even before it saturated. Both simulation and observation show that the bad lifetime is correlated with longitudinal-vertical resonances induced by the vertical crossing angle[1].

The same problem happened in crossing angle operation at CESR. Simulations and analysis predicted that certain groups of synchrobetatron resonances are to be excited because of the crossing angle, causing a lifetime problem. This was confirm by experiment[2].

It is worth mentioning that the resonance family excited by the crossing angle depends on the normalized crossing angle ϕ. With larger ϕ, higher order sidebands tend to be excited. Simple simulations and analysis can provide reasonably good qualitative prediction of this. More sophisticated simulations can calculate the lifetime due to the crossing angle, but quantitative agreement is poor[3].

More analysis shows that a horizontal crossing angle may help in suppressing vertical synchrobetatron resonances excited by the bunch length effect[4]. Whether this will help the machine performance depends on the aperture that limits the lifetime.

PEAK LUMINOSITY PERFORMANCE WITH CROSSING ANGLE

The question here is: what is the maximum beam-beam tune shift parameter that can be achieved with a crossing angle?

DORIS I's experience is discouraging. The beam-beam tune shift achieved was between 0.005~0.01, far below what can be reached with head-on collisions. CESR made a change on this issue. CESR runs constantly with a beam-beam tune shift of more than 0.04[5,6].

Again, it is hard to draw conclusion from these experiences. DORIS I had a normalized crossing angle of 0.5, while CESR has 0.09. In addition, CESR is equipped with feedback system, etc., that DORIS I did not have.

From the underlying physics point of view, the small amplitude particles, or the beam core, should suffer from synchrobetatron coupling due to the crossing angle too. Because different amplitude particles experience quite different nonlinear forces the sensitivities to various resonances are very different. As the result, there could be another family of resonances, different from the ones that limit the lifetime, that makes the luminosity performance bad.

Simulations have been carried out to study the luminosity performance of KEKB[7]. Tune scan shows reasonably large "workable" area.

EXPERIMENTAL INVESTIGATION

Since the beam-beam simulations have not been able to provide quantitative agreement with observation and adequate prediction of performance, an experimental investigation is well justified. There are two goals in doing experiments: checking the credibility and predictability of simulations and testing the machine performance under certain conditions.

Before a large crossing angle collider is built, a way to perform tests on a existing machine is proposed. A finite dispersion η^* at the IP functions essentially as a crossing angle. The beam-beam kick with η^* can be written as $F(x+\eta^*\delta)$. Compared with crossing angle kick $F(x + \tan\Phi \cdot s)$, one can see the major difference is in the longitudinal phase (s replaced by δ). This will only make a difference at resonances $Q_X \pm Q_S$. Therefore, a crossing angle can be emulated by a η^* which is chosen to have the equivalent normalized crossing angle: $\frac{\sigma_\delta}{\sigma_x}\eta^* = \frac{\sigma_s}{\sigma_x}\Phi$.

In principle, it is not difficult to generate a η^* in many existing e^+e^- colliders, such as VEPP-2M, CESR, BEPC, *etc.* The working group would like to call for an experimental study of a collider with dispersion at the collision point. It will be extremely helpful in new machine design, learning operating collider under new conditions which may speed up commissioning process, and understanding beam-beam physics.

REMARKS

Based on the discussion, the working group concluded that the crossing angle collision introduces new resonances that limited the choice of working points. Therefore, to live with a crossing angle, the most critical issue is finding a good working point in the tune space that provides the required performance. Experience has proved that a good working point can be found with a normalized crossing angle up to 0.09.

The underlying physics behind crossing angle collision is the introduction of synchrobetatron coupling. As the results, two families of resonances are introduced to the tune plane. One family of resonances causes bad lifetime, which has been studied and observed. The other family may limit peak luminosity performance. The composition of the families and the strength of the resonances vary with the normalized crossing angle. Experimental investigation is strongly recommended for larger normalized crossing angle.

REFERENCES

[1] A. Piwinski, IEEE Trans on Nucl Sci **NS-24**, 1408 (1977)

[2] T. Chen, Phys Rev **E49**, 2251 (1994).

[3] T. Chen, this proceeding.

[4] D. Pestrikov, this proceeding.

[5] D. Rubin, *et al*, Nucl Inst Meth **A330**, 12 (1993).

[6] J. Welch, this proceeding.

[7] K. Hirata, this proceeding.

Working group II
Multibunch Head-on Beam-Beam Effects

LIFETIME AND TAIL SIMULATIONS FOR BEAM-BEAM EFFECTS IN PEP-II B FACTORY*

D. N. Shatilov[a] and A. A. Zholents[b]
[a] Budker Institute of Nuclear Physics, 630090 Novosibirsk 90, Russia
[b] Center for Beam Physics, Accelerator and Fusion Research Division, Lawrence Berkeley Laboratory, University of California, Berkeley, CA 94720

Abstract

A fast tracking technique for doing beam tail simulations has been applied to a study of beam-beam effects in the SLAC/LBL/LLNL PEP-II B Factory. In particular, the dependence of beam lifetime and particle density distribution due to vacuum pressure, damping times, machine nonlinearity and parasitic crossings has been analyzed. Effects of accidental orbit separation and dispersion function at the interaction point (IP) have also been considered.

I. BEAM PARAMETERS AND MODEL

Beam and machine parameters for PEP-II B factory are described elsewhere [1]. For the sake of completeness, we reproduce in the Table I all parameters we need for a discussion of beam-beam effects. Our notation for most of the parameters has a standard and obvious meaning. Only a few definitions need explanation. In the PEP-II B factory, electron and positron bunches collide head-on at the IP. After the IP, beam orbits are magnetically separated in the horizontal plane. However, before entering its own vacuum pipe, each electron bunch and each positron bunch experiences four more interactions with other bunches of the opposite beam. We refer to these interactions as parasitic crossings (PC's). A parameter d_{sep} defines orbit separation at the first PC. Orbit separation at the remaining PCs is much larger and, consequently, the effect of beam-beam interactions at these PC is negligible. We will ignore them in our model and will consider only the first parasitic crossing on either side of the IP. Parameters $\Delta\nu_x$ and $\Delta\nu_y$ define horizontal and vertical betatron phase advance, in units of the betatron tune, from the main IP to the first PC.

A goal of our study was understanding the mechanisms leading to a beam lifetime limitation in electron-positron colliders. According to experimental observations [2], these mechanisms are fairly insensitive to particle density distribution in the beam core. Thus, a weak-strong model of beam-beam effects seems adequate to our task.

All our simulations were carried out with the beam-beam program LIFETRAC [3]. This program allows the following physics to be included in the simulation:

1. Beam-beam kick.
2. One turn, six-dimensional linear map.
3. Chromaticity up to the third order:

$$\nu_x = \nu_{0x} + C_x\delta + C_{xx}\delta^2 + C_{xxx}\delta^3$$

$$\nu_y = \nu_{0y} + C_y\delta + C_{yy}\delta^2 + C_{yyy}\delta^3.$$

Here $\delta = \Delta p/p$ and $C_x, C_{xx}, C_{xxx}, C_y, C_{yy}, C_{yyy}$ are parameters of chromaticity.

4. Machine nonlinearity in the form of an amplitude-dependent betatron tune:

$$\nu_x = \nu_{0x} + \varepsilon_x a_{xx} A_x^2 + \varepsilon_y a_{xy} A_y^2$$
$$\nu_y = \nu_{0y} + \varepsilon_x a_{xy} A_x^2 + \varepsilon_y a_{yy} A_y^2.$$

Here A_x and A_y are normalized amplitudes and a_{xx} a_{xy} and a_{yy} are coefficients.

5. Elastic scattering on nuclei of the residual gas.
6. Parasitic crossings.
7. Dispersion functions at the IP and at the PC.
8. Slicing of a bunch with an arbitrary number of slices (typically, we use 5 pancake-like slices).
9. Orbit separation at the IP.

Table I
Beam parameters

	weak beam (e^+)	strong beam (e^-)
E [GeV]	3.1	9.0 [a]
ν_{0x}, ν_{0y}	34.57, 35.64	34.57, 35.64 [a]
ν_s	0.037	0.052 [a]
ξ_{0x}, ξ_{0y}	0.03, 0.03	0.03, 0.03 [a]
$\tau_{x,y}$ [turns]	7200, 7200	5014, 5014 [a]
τ_z [turns]	3600	2507 [a]
$\sigma_{\Delta p/p}$	0.80×10^{-3}	0.62×10^{-3} [a]
σ_z [cm]	1.0	1.0
ε_x [m×rad]	6.4×10^{-8}	4.8×10^{-8} [a]
ε_y [m×rad]	1.9×10^{-9}	1.4×10^{-9} [a]
	Main crossing	
$\beta^*_{x,y}$ [m]	0.50, 0.015	0.667, 0.02
$D^*_{x,y}$ [m]	0, 0	0, 0 [a]
$\sigma^*_{0x}, \sigma^*_{0y}$ [μm]	177, 5.3 [a]	177, 5.3
	Parasitic crossing	
d_{sep} [mm]	3.5	
σ_x, σ_y [μm]	284, 223 [a]	243,167
$\Delta\nu_x$, $\Delta\nu_y$	0.143, 0.246	0.117, 0.245 [a]

[a] These parameters do not enter the weak-strong simulation

II. SIMULATION TECHNIQUE

The fast tracking technique developed in LIFETRAC [3] emerged from a concept proposed earlier in [4] and realized

*Work supported by DOE under Contract DE-AC03-76SF00098 and by Budker INP of the Russian Academy of Science.

later in [5]. It allows a determination of beam lifetime on a level of 10 hours with a statistical confidence of a few percent by tracking only about 10^7 particle-turns. Along with the lifetime, this technique is able to provide information on the particle density distribution in the beam tails.

The idea of the algorithm is based on the presence of a random component (such as quantum fluctuation noise) in the particle motion [4]. It turns out that a particle's trajectory in phase space depends only on current coordinates and momenta (and noise). A history of the particle's motion is irrelevant for its future trajectory. After accumulating rich statistics of a particle's motion in a certain region of phase space, one can ignore the exact knowledge of a particle trajectory in this region and replace it by statistical information. This information could contain particle coordinates and momenta recorded at the moment when the particle leaves the region. Then, each time the particle's trajectory goes inside that region, one can interrupt tracking and begin a new trajectory from one of the prerecorded points. By this technique, we force actual tracking to go on only in a region with poor statistics rather than tediously tracking in a region with well-defined statistics.

This algorithm was recently checked against 'brute-force' calculations performed with the program TRS [6] and we found excellent agreement in the results [7]. It is worth mentioning that the 'brute-force' calculations took 818 minutes of CPU time on a Cray-2S, while LIFETRAC reached the same accuracy in the tail distribution in 55 minutes of CPU time on a VAX-6610.

III. RESULTS

A result of the simulation of beam-beam effects in PEP-II for the nominal conditions without PC's is presented in Figure 1a. This plot (and other similar plots) shows particle distribution contours in amplitude space. The first contour corresponds to a particle density a factor $\sqrt{e}$ below the peak and all the following contours correspond to successive reduction with a factor of e. Amplitudes A_x, A_y are normalized amplitudes, i.e. $A_x = 1$ corresponds to a physical amplitude of $1\sigma_{0x}$ and $A_y = 1$ corresponds to a physical amplitude of $1\sigma_{0y}$.

The particle density distribution is obviously perturbed by nonlinear resonances $\ell\nu_x + m\nu_y + n\nu_s = k$. The identified resonances are shown by arrows. On top of each arrow we draw numbers, which correspond to the ℓ, m, n resonance identification. Particularly strong is the resonance $14\nu_x = k$. It is partly overlapped with some other resonances, which we were not able to identify.

For the lifetime determination we assumed a limiting aperture of $A_x = 10$ and $A_y = 25$. With that aperture we were not able to determine the lifetime, because it was very long. We interrupted calculations when the lifetime exceeded 8 years. We also did not find any blow-up of the beam core.

A. *Parasitic Crossings*

Adding PC's did not affect beam lifetime. It was still very long to be determined. But PC's did affect the beam

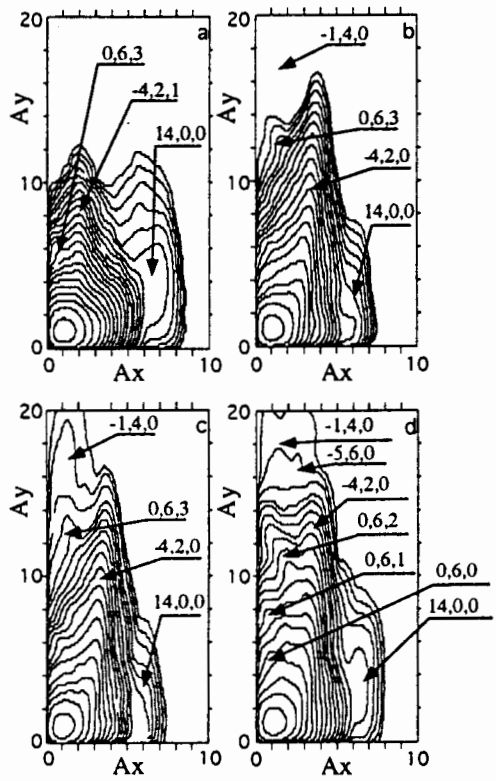


Figure. 1. Particle distribution contours: a) nominal case without parasitic crossings; b) the same as a) plus PC; c) the same as b) plus elastic scattering; d) the same as c), but with $\xi_{0x} = \xi_{0y} = 0.05$ and $a_{xx} = -200$ m^{-1}.

core (we found a 26% increase in the vertical beam size) and particle density distribution (see Figure 1b). The main factors giving rise to the effect of the PC's are strong resonances: $6\nu_y + 3\nu_s = k$ and $-4\nu_x + 2\nu_y = k$. At the same time, we found that resonances $-4\nu_x + 2\nu_y + \nu_s = k$ and $14\nu_x = k$ became weaker. This resonance restructuring is a result of a new beam footprint in tune space in the case with PC's.

B. *Vacuum*

Aside from beam-beam effects, the leading mechanism defining the beam lifetime in PEP-II on a level of 23 hours is elastic scattering on nuclei of the residual gas [1]. Since the beam-beam lifetime defined above is much larger, one might think that the beam-beam interaction will have no noticeable effect on the beam lifetime, but this is not right. The interference of beam-beam effects and elastic scattering could be significant. Imagine that the beam-beam interaction creates some resonance islands in phase space close to the aperture limit. Then, particles scattered inside these islands from the beam core, could be trapped there. As a result, the growing population of particles in the tails will decrease beam lifetime. This is exactly what we found when we included elastic scattering [3] in our sim-

ulation for PEP-II. The lifetime dropped from 22.9 hours (vacuum lifetime) to 16.7 hours. We attribute this to the elastic scattering into the resonance $-\nu_x + 4\nu_y = k$, which perturbs the particle density distribution at large vertical amplitudes (compare Figure 1c with Figure 1b).

C. Damping Time

We compared beam-beam effects for two damping times. First we used a damping time of 5400 turns as it is in [1]; second we took a damping time of 7200 turns, as proposed in [8]. In Figure 2, we show the dependence of the lifetime versus beam-beam parameters for our two cases. The difference between two cases is less than the statistical error expected in the calculations.

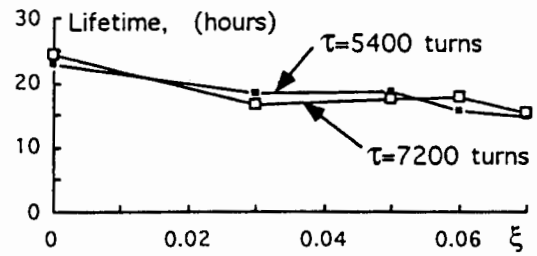


Figure. 2. Beam lifetime versus $\xi = \xi_{0x} = \xi_{0y}$ for two damping times. Arrows indicate damping time.

D. Machine Imperfections

In order to be more sensitive to the beam-beam effects, we did all the rest of our simulations with $\xi_{0x} = \xi_{0y} = 0.05$.

Chromaticity. We did not find any significant effect of chromaticity when we varied C_{xx}, C_{yy} in the range of ± 500 and C_{xxx}, C_{yyy} in the range of $\pm 10^4$, which are larger values than we anticipate for the machine.

Tune shifts with amplitude. In our notation, typical dependence of betatron tunes from amplitudes for PEP-II corresponds to a_{xx}=a_{yy}~-200m^{-1} and a_{xy}~-1000m^{-1} [9]. Simulations with these coefficients gave qualitatively similar results to those with zero nonlinearity. By adjusting a_{xx} with a_{yy}=a_{xy}=0 we could slightly increase the strength of the resonance $14\nu_x = k$ at a_{xx}=-200m^{-1} or significantly reduce it at a_{xx}=400m^{-1} (compare Figure 1d and Figure 3a), but both the beam lifetime and the beam core remained fairly insensitive to this change. For the rest of the simulations we used a_{xx}=-200m^{-1}.

Orbit separation at the IP. Table II contain all results. One can see that only the vertical beam size was sensitive to the orbit separation Δx, Δy.

Dispersion at the IP. Simulations with non-zero horizontal and vertical dispersions at the IP showed that the lifetime began to drop below 10 hours when $D_x^* \geq 4$ cm or $D_y^* \geq 0.5$ cm. An example with $D_y^* = 0.53$ cm is shown in the Figure 3b. Moreover, we found that a dispersion $D_x^* = 2.2$ cm already reduced the lifetime below 10 hours when combined with an accidental orbit separation of $\Delta x/\sigma_{0x}^* = 0.4$.

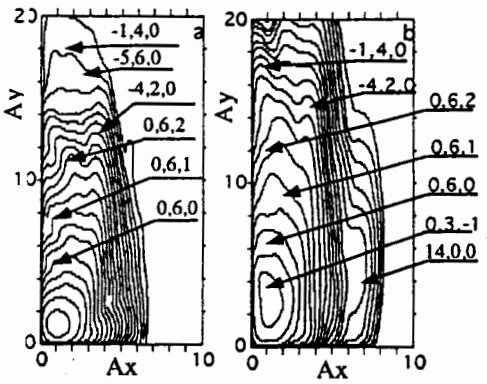


Figure. 3. Particle distribution contours: a) the same as Figure 1d, but with a_{xx}=400 m^{-1}; b) the same as Figure 1d plus $D_y^* = 0.53$ cm.

Table II
Orbit separation

$\Delta x/\sigma_{0x}^*$	$\Delta y/\sigma_{0y}^*$	$\sqrt{x^2}/\sigma_{0x}^*$	$\sqrt{y^2}/\sigma_{0y}^*$	Lifetime,[h]
0	0	1.10	1.46	18.9
0.2	0	1.07	1.71	18.4
0.4	0	1.12	1.93	18.4
0	0.2	1.07	1.99	19.9
0	0.4	1.07	2.57	18.6

IV. Conclusion

Our study demonstrated that beam-beam effects should not affect the performance of the PEP-II B factory if $\xi_{0x} = \xi_{0y} = 0.03$. We did not find significant reduction in the beam lifetime even for larger beam-beam parameter, but we did see in many occasions a large increase in the vertical beam size.

Acknowledgment. We are grateful to M. Furman and M. Zisman for many useful discussions.

References

[1] PEP-II Design Report, SLAC-Report-418, 1993.
[2] A. Temnykh, Third Advance ICFA Beam Dynamics Workshop, INP, Novosibirsk, 1989, p.5.
[3] D.Shatilov, Preprint BINP 92-79, Novosibirsk, 1992, (in russian), unpublished.
[4] J. Irwin, ref.2, p.123.
[5] T. Chen et al., Phys. Rev. E49, 1994, p.2323.
[6] J. Tennyson, unpublished code 'TRS', 1989.
[7] M. Furman et al., CBP Note-59 (1995).
[8] J. Heim et al., Wiggler Insertion of the PEP-II B Factory LER, these proceedings.
[9] E. Forest et al., EPAC 1994, London, 1994, p.1033.

Beam-Beam Simulations for KEKB

Kazuhito OHMI

KEK, National Laboratory for High Energy Physics
Oho, Tsukuba, Ibaraki 305, Japan

Email address: ohmi@kekvax.kek.jp

1. Introduction

KEKB is a asymmetric two ring collider of electrons (8GeV) and positrons (3.5GeV). The two rings are called a high energy ring (HER) and a low energy ring (LER), respectively. Each beam collides to the other with a half crossing angle of 11mrad. Our goal is to get a luminosity $10^{34}cm^{-2}s^{-1}$ on the conditions of asymmetric collision of e^+e^- with the finite crossing angle. The parameter set of KEKB which is important for beam-beam effect is summarized in Table 1.

To study the beam-beam effect, some studies have been carried out with computer simulation. In this paper, we discuss problems for core distributions of beams. A weak strong simulation with linearized lattice has beer performed to choose our working point as shown in ref.[1]. A luminosity 1.24×10^{34} was obtained from the simulation. Here we investigated with following methods. First is a perturbative approach with the differential algebra. Second is weak strong simulation including lattice nonlinearity. Third is quasi-strong-strong simulation. Tail issues are treated in ref.[1].

2. Beam-beam map

Beam-beam map of the weak-strong model with crossing angle is discussed. Since the basic formalism is presented in ref.[2], some trivial extensions concerning beam envelope matrix and closed orbit of the strong beam are presented here. The shape of the strong beam is assumed to be gaussian distribution in 6-dimensional phase space $\boldsymbol{X} = (X, P_x, Y, P_y, Z, \Delta)$, thus it is characterized by $21 + 6$ parameters:

$$< X_i X_j > \qquad i,j = 1,6 \tag{1}$$

$$< X_i > \qquad i = 1,6. \tag{2}$$

Treatment of the crossing angle is presented in ref.[3]. The weak and strong beams are transformed into head-on frame with a Lorentz boost[4]. Here it is enough that the strong beam is transformed by a linear part of the Lorentz boost because it is approximated as gaussian:

$$\begin{aligned} < \boldsymbol{X}^* > &= T < \boldsymbol{X} > \\ < \boldsymbol{X}^* \boldsymbol{X}^{*t} > &= T < \boldsymbol{X}\boldsymbol{X}^t > T^t \end{aligned} \tag{3}$$

Table 1: KEKB parameters

Beam energy	3.5GeV (e^+) and 8GeV (e^-)
Horizontal emittance (ε_x)	$1.8 \times 10^{-8} m$
Vertical emittance (ε_y)	$3.6 \times 10^{-10} m$
Bunch length (σ_z)	4 mm
β_x at the collision point	0.33 m
β_y	0.008 m
Tune ($\nu_x/\nu_y/\nu_s$)	0.52/0.08/0.017
Energy damping decrement of LER (T_0/τ_e)	2.5×10^{-4}
Energy damping decrement of HER (T_0/τ_e)	5.9×10^{-4}
Half crossing angle	11 mrad
Number of electron in a bunch (N_-)	1.4×10^{10}
Number of positron in a bunch (N_+)	3.3×10^{10}

where

$$T = \begin{pmatrix} 1 & 0 & 0 & 0 & \tan\phi & 0 \\ 0 & 1/\cos\phi & 0 & 0 & 0 & 0 \\ 0 & 0 & 1 & 0 & 0 & 0 \\ 0 & 0 & 0 & 1/\cos\phi & 0 & 0 \\ 0 & 0 & 0 & 0 & 1/\cos\phi & 0 \\ 0 & -\tan\phi & 0 & 0 & 0 & 1 \end{pmatrix}. \tag{4}$$

On the other hand, the weak beam is transformed with the exact Lorentz transformation. Now $s^* = 0$ is the collision point on the head-on frame. The beam distribution at $s^* = 0$ is characterized by Eq.(3) and is expressed as

$$\psi^*(\boldsymbol{X}^*, s^* = 0) = \frac{1}{(2\pi)^3\sqrt{det\Sigma^*}} \exp\left(-\frac{1}{2}\Sigma^{*-1}_{ij}(X^*_i - < X^*_i >)(X^*_j - < X^*_j >)\right). \tag{5}$$

To integrate the weak beam motion, the strong beam envelope is cut into slices. To simplify the notations, we remove the suffix $*$ hereafter. Four dimensional beam envelope of each slice is expressed as

$$\begin{aligned} < X_\mu X_\nu >_z &= \frac{\int X_\mu X_\nu \psi(\boldsymbol{X}, Z) dX dP_x dY dP_y d\Delta}{\int \psi(\boldsymbol{X}, Z) dX dP_x dY dP_y d\Delta} = \Sigma_{4,\mu\nu}(Z) \\ < X_\mu >_z &= \frac{\int X_\mu \psi(\boldsymbol{X}, Z) dX dP_x dY dP_y d\Delta}{\int \psi(\boldsymbol{X}, Z) dX dP_x dY dP_y d\Delta} \qquad \mu, \nu = 1, 2, 3, 4\,. \end{aligned} \tag{6}$$

Now the synchro-beam mapping[2] is available for the collision between weak beam and strong sliced beam. Each slice collides with the weak beam at collision points,

$$s_{col}(z(0)) = (z(0) - Z_n(0))/2\,. \tag{7}$$

The strong beam sliced is transformed to the interaction points of each slice.

$$\Sigma_4(Z_n, s_{col}) = M(s_{col}, 0)\Sigma_4(Z_n, 0)M^t(s_{col}, 0), \tag{8}$$

where if the collision point is in drift space,

$$M(s) = \begin{pmatrix} 1 & s & 0 & 0 \\ 0 & 1 & 0 & 0 \\ 0 & 0 & 1 & s \\ 0 & 0 & 0 & 1 \end{pmatrix}.$$

The beam envelope matrix includes information on beam deformation: $< X(Z_n, s_{col})Y(Z_n, s_{col}) >$, $< X(Z_n.s_{col})P_y(Z_n, s_{col}) >$ etc.. To make easy the collision map, we resolve $X - Y$ tilt of the envelope. The coordinate system is rotated by following R matrix such as $< XY >= 0$,

$$R = \begin{pmatrix} I_2 \cos\theta & I_2 \sin\theta \\ -I_2 \sin\theta & I_2 \cos\theta \end{pmatrix} \tag{9}$$

$$\theta = -\frac{1}{2} tan^{-1}\left(\frac{2 < XY >}{< XX > - < YY >}\right).$$

The weak beam is transformed by the same manner. Now we use the synchro-beam mapping in Ref.[2] on the beam-beam interactions. The beam-beam map was implemented to a differential algebra code[5] and SAD[6].

3. Study using a perturbation theory

A perturbative approach using the differential algebra has been tried to study the characteristics of the beam-beam interactions. We consider a virtual machine with a linearlized lattice and the beam-beam interaction discussed above. A Taylor map was obtained with the differential algebra technique[7],

$$\mathcal{M} = a_0 + a_{1,i}x_i + a_{2,ij}x_i x_j + a_{3,ijk}x_i x_j x_k + ... \tag{10}$$

The Taylor map was parametrized into linear and nonlinear parts as

$$\mathcal{M} = \mathcal{R}e^{:f:}, \tag{11}$$

where

$$f = b_{3,ijk}x_i x_j x_k + b_{4,ijkl}x_i x_j x_k x_l + ... \tag{12}$$

Here the canonical variables are normalized by beta function. Now we take the resonance base as

$$\begin{aligned} h_{x+} &= \frac{x + ip_x}{\sqrt{2}} = \sqrt{J_x}e^{i\phi_x} \\ h_{x-} &= \frac{x - ip_x}{\sqrt{2}} = \sqrt{J_x}e^{-i\phi_x} \quad et.al. \end{aligned} \tag{13}$$

By substituting Eq.(13) into Eq.(12), we obtain the Taylor expansion of $g(h_{x+}, h_{x-}, ...)$.

$$f(\boldsymbol{x}) = g(\boldsymbol{h}) = \sum_{\boldsymbol{m}} c_{\boldsymbol{m}} \left(\prod_{a=1}^{6} h_a^{m_a}\right), \tag{14}$$

where the vector $\boldsymbol{m}$ characterize orders of h, that is, $m_a, a = 1, 6$ is the degrees of $h_{+.x}, h_{-,x}, h_{+,y}, ...$, respectively. The coefficient $c_{\boldsymbol{m}}$ shows a strengths of a resonance,

$$\sum_{b=1}^{3}(m_{2b} - m_{2b+1})\nu_b = integer, \tag{15}$$

where b's are related to x, y, z.

Fig.1 shows coefficients of $\boldsymbol{m} = (1,0,0,2,0,0)$ and $(1,0,0,2,1,0)$, that is, they are those of $h_{+,x}h_{-,y}^2$ and $h_{+,x}h_{-,y}^2 h_{+,z}$. These are resonance amplitudes of $\nu_x - 2\nu_y = n$ and $\nu_x - 2\nu_y + \nu_s = n$, respectively. These figures show the resonance amplitude grows up with larger crossing angle.

The amplitude of $\boldsymbol{m} = (1,0,0,2,1,0)$ represents the strength of synchrotron side band of $\boldsymbol{m} = (1,0,0,2,0,0)$. To compare two figures, a factor of $\sqrt{\varepsilon_z} = 1.74 \times 10^{-3}$ should be multiplied by values of later one. The amplitude is about 0.4 times of that of the fundamental. The amplitude of $\boldsymbol{m} = (1,0,0,2,0,1)$ was the same strength as that of $\boldsymbol{m} = (1,0,0,2,1,0)$. Thus the side band resonance will not be important.

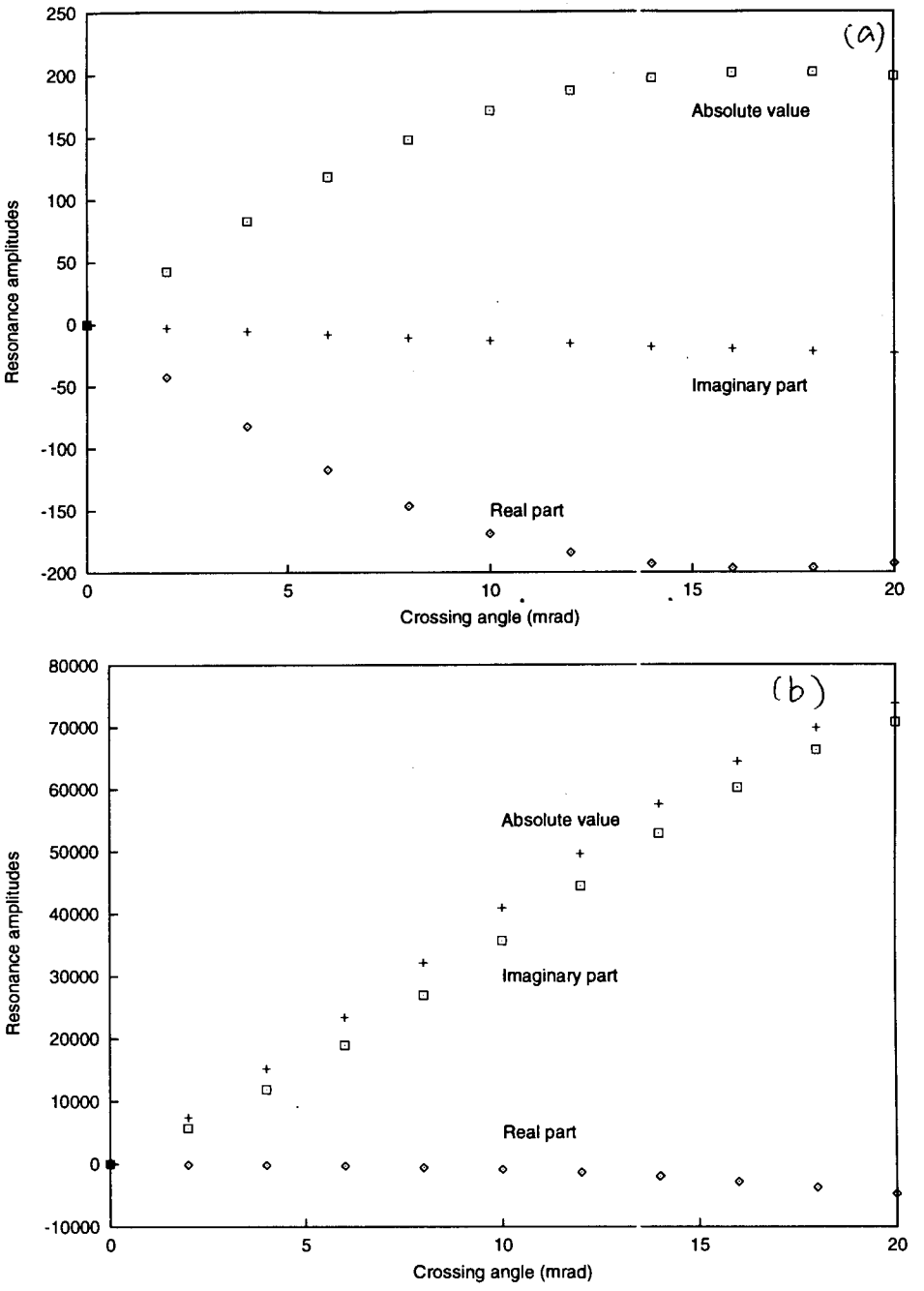


Figure 1: Resonance amplitudes of (a)m=(1,0,0,2,0,0) and (b)(1,0,0,2,1,0).

Table 2: Errors

Type of element	BPM	B	Q	S	Steering
Horizontal shift (μm)	75	0	100	100	0
Vertical shift(μm)	75	100	100	100	0
x-y rotation (mrad)	0	0.1	0.1	0.1	0.1
strength error	0	10^{-4}	10^{-3}	10^{-3}	0

4. Beam-beam simulation including lattice

We have got a favorable luminosity in the beam-beam simulation with the linearized lattice[1]. However if we consider the actual lattice with nonlinearity, we may face a luminosity reduction. For example, anomalous emittance growth[8] which comes from lattice and beam-beam nonlinearities may blowup the beam size. We have performed a simulation with SAD[6] in which the beam-beam map was implemented. SAD is a general purpose code for accelerator designs. Its tracking module includes all of lattice nonlinearities which we should consider. The tracking module also includes the synchrotron radiation damping and fluctuation. An equilibrium beam envelope and luminosity are obtained by carrying out multi-turn tracking exceeding radiation damping time.

Here we consider the positron beam as weak beam. Perhaps it is anticipated the positron beam is blown up hardly, because it has longer damping time than the electron beam. A lattice shown in Ref.[9] is used. We have designed the lattice such that vertical emittance was 2% of horizontal one. We consider errors of beam position monitors and magnets which are shown in Table 2. The errors were generated with random numbers. A closed orbit distortion was caused by the errors. It was corrected by an orbit correction module[10] in SAD. We should consider the vertical beam size rather than vertical emittance. Twenty trials were performed with different random seeds. The vertical beam sizes distribute between $0.5\mu m$ to $3\mu m$. The design value is $1.7\mu m$.

The tracking was performed with 50 macro-particles and 90000 turns ($> 10 \times \tau_x$). The strong beam is cut into 5 slices. Luminosity was integrated after 30000-th turn ($4 \times \tau_x$).

Fig.2 shows the luminosities for various seeds. The average and standard deviation of the luminosities were $(1.44 \pm 0.27) \times 10^{34}$. They showed the luminosity reduction was not serious.

The correlation between vertical beam sizes and luminosities is shown in Fig.3. They have clear correlation. It means that the luminosity is expected to be $\sim 1.2 \times 10^{34}$ if we achieve the design vertical beam size.

5. Quasi-strong-strong simulation

We would go to strong-strong simulation for next step. However the strong-strong simulation requires much computer power. If it is not enough, a statistical error by a poor number of particle often excites unphysical coherent oscillation. Thus before the step, we tried a quasi-strong-strong simulation presented here.

First we consider e^+ and e^- beams are weak and strong ones, respectively. 500 macro-particles, which are weak e^+ beam, are allocated. They collide with strong e^- beam, and are tracked 500 turns. Beam position and envelope are averaged for all turn. Coordinates of the weak e^+ beam are stored when the first tracking is finished. Next the roles of both beam are exchanged. Now the e^+ beam is replaced by a strong beam which has the position and

envelope obtained by the first step. The same number of macro-particles, which are e^- beam now, collide with the strong e^+ beam. By repeating these procedure, equilibrium beam position and envelope are obtained. We can study beam deformations by dynamic twiss effects in this method. A typical example is dynamic beta effect. Nonlinear effect which deforms the beam distribution can be investigated. However this method is quite insensitive for rapid motions like coherent motions, because position and envelope are averaged in the 500 turns to get a gain of statistics.

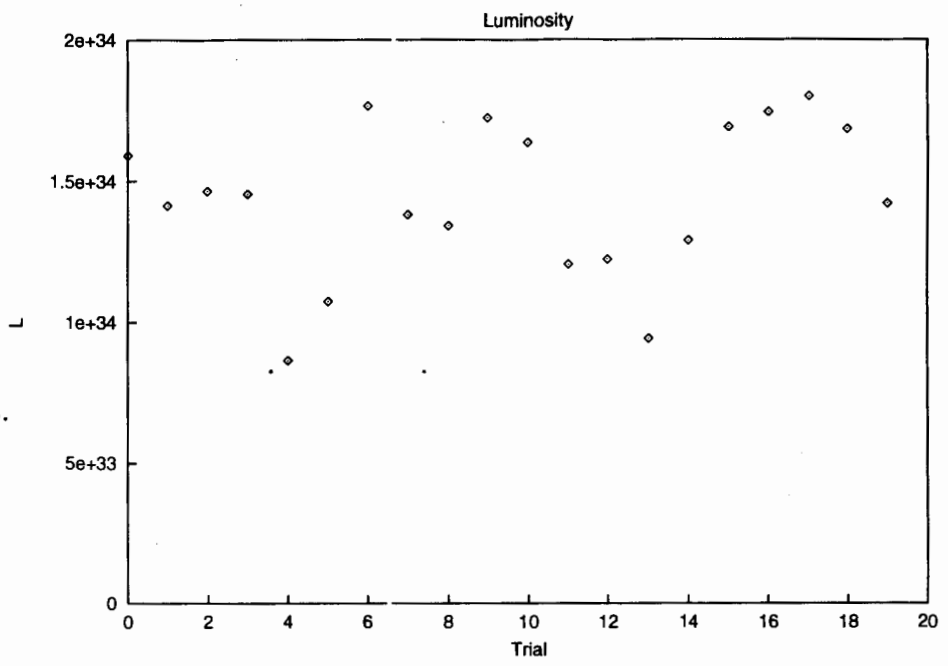


Figure 2: Luminosities for different random seeds. Our goal is 10^{34}.

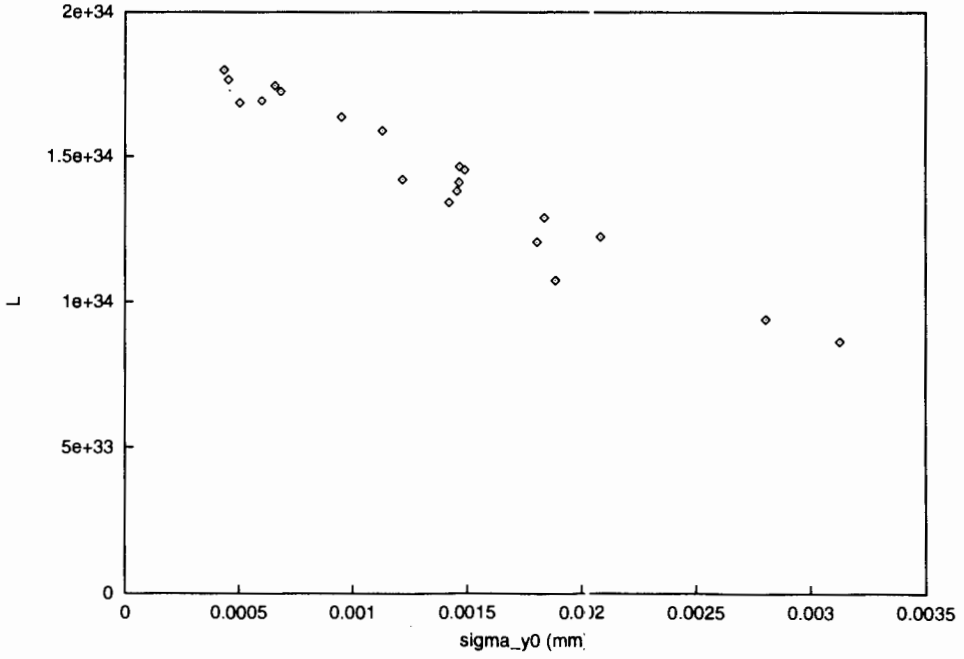


Figure 3: Correlation between vertical beam sizes and luminosities. The design value of vertical beam size (σ_y) is $1.66 \times 10^{-6} m$.

Fig.4 shows the luminosity every 500 turns. The lattice is linearized one. It shows that the luminosity was enhanced rather than reduced. It comes from the dynamic beta effect. Fig.5 shows the horizontal beam size as function of revolutions. It shows $\sigma_x = 6.2 \times 10^{-5} m$, while the design value is $7.6 \times 10^{-5} m$.

Next we consider vertical beam size. In KEKB, e^+ beam (LER) has longer damping time than e^- beam. We consider a possibility that both rings have the same damping time by using damping wigglers in the LER. Fig.6 shows the vertical beam sizes of both the cases in every 500 turns. Beam blow-up was observed only in the positron beam in asymmetric damping time, while was not in symmetric damping time. However concerning the luminosity, there is little difference between the two results. This means that the positron beam does not blow up in core, but in tail.

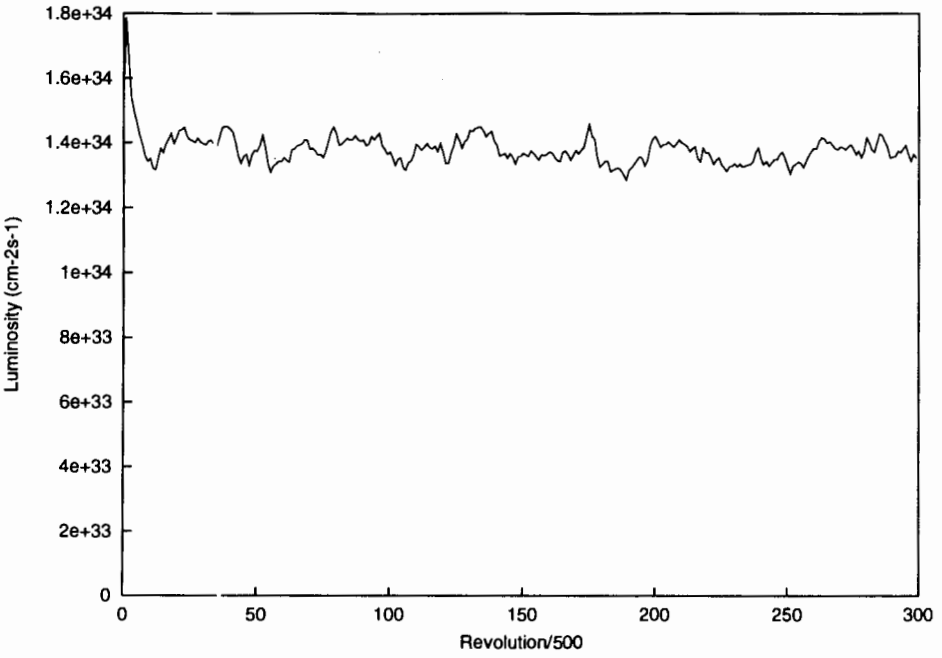


Figure 4: luminosity obtained by quasi-strong-strong simulation.

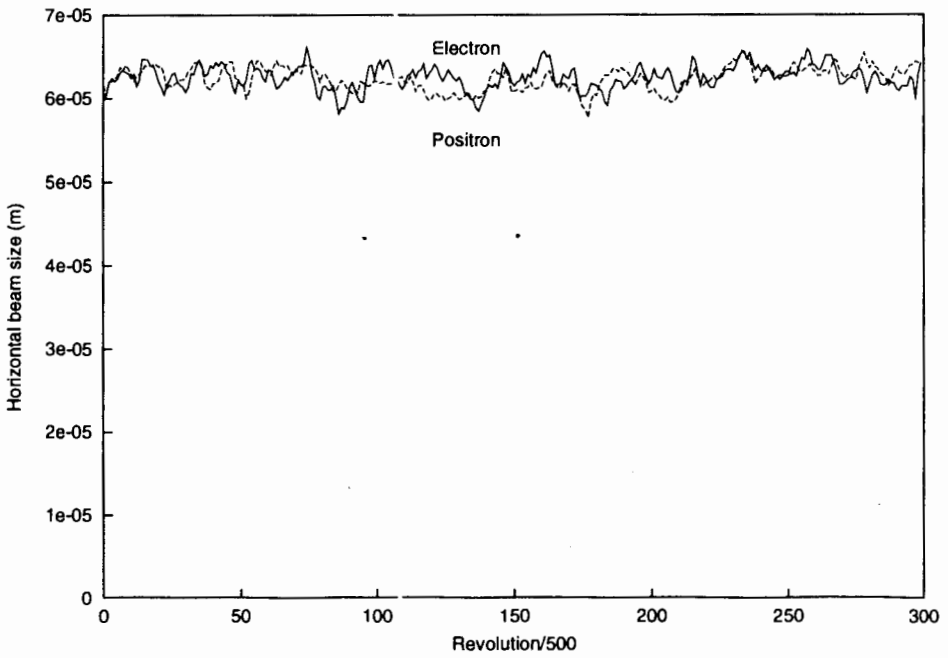


Figure 5: Horizontal size of electron and positron beam

6. Summary

Some simulations were performed to investigate the luminosity of KEKB. Concerning the core distribution, we could not find negative signs to get the design luminosity. These simulations show the luminosity exceeds our goal $10^{34} cm^{-2} s^{-1}$, if beam sizes of both the rings are achieved to be the design values. We need to study the beam-beam effect further. A strong-strong simulation is a major subject to study the core problem.

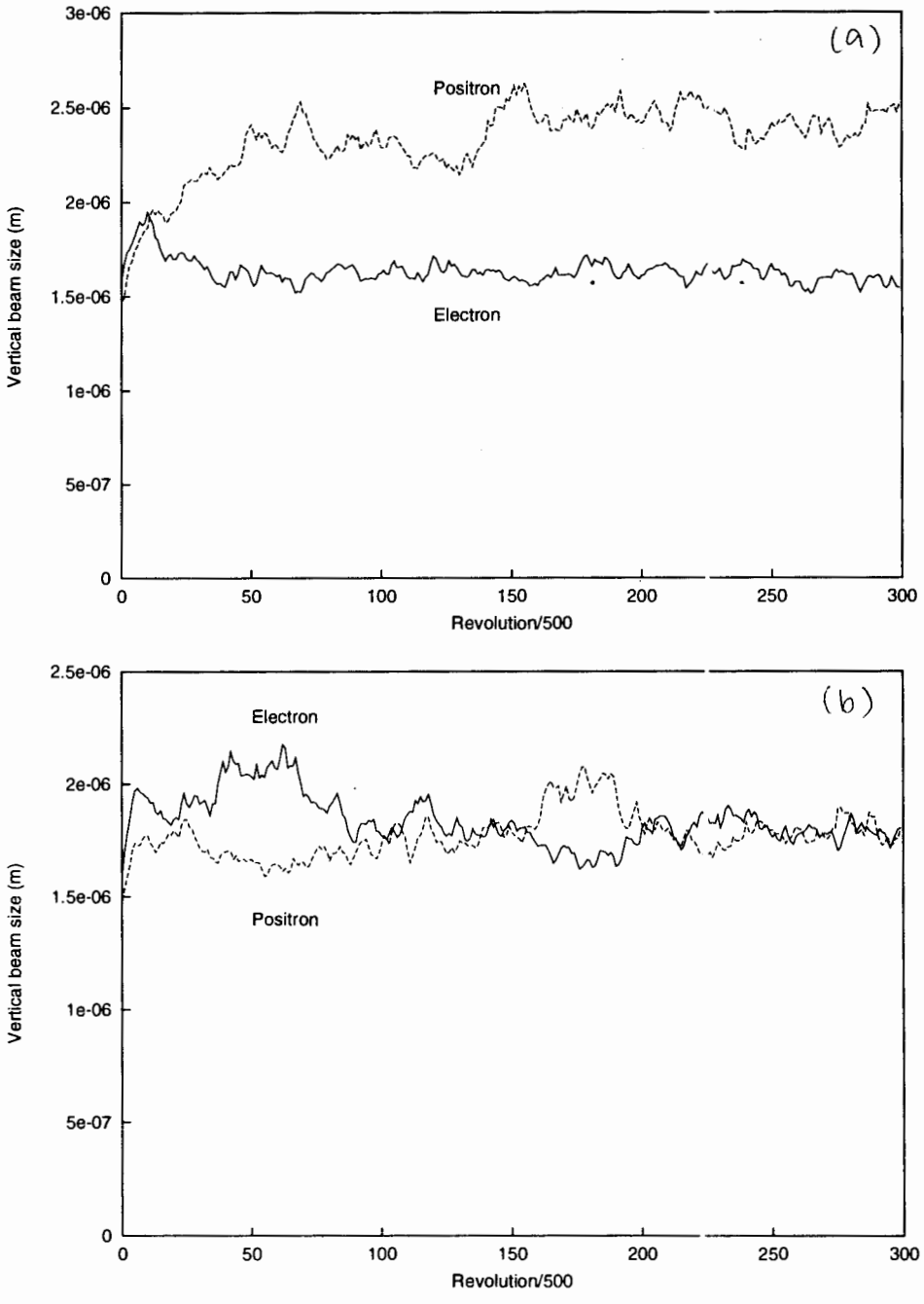


Figure 6: Vertical size of electron and positron beam. (a) is for the case when both beam have the equal damping time. (b) is when positron beam has a damping time longer by factor 2 than electron beam.

References

[1] K.Hirata, in this proceedings.

[2] K.Hirata, H.Moshammer and F.Ruggiero, Particle Accelerator,40, 205 (1993).

[3] K.Hirata, Phys.Rev.Lett.74, 2228 (1995).

[4] J.Augustin, Orsay, 36-69 (1969).
K.Oide, private communication (1990).

[5] K.Ohmi, This code has been developed by the author (1994).

[6] Strategic Acelerator Desgin Code (SAD) is a beam transport and simulation software, which is developed at KEK. See, K.Oide, Nucl. Instr. Meth., A176, 427 (1989).

[7] M.Beltz, SSC-166 (1988).

[8] K.Oide and H.Koiso, Phys. Rev. E49, 4474 (1994).

[9] H.Koiso and K.Oide, Talk presented at 1995 Particle Accelerator Conference, Dallas, U.S.A. (1995).

[10] M.Kikuchi, private comunications (1994).

BEAM-BEAM SIMULATIONS AT LARGE AMPLITUDES AND LIFETIME DETERMINATION

Dmitry Shatilov
Budker Institute of Nuclear Physics (BINP), 630090 Novosibirsk, Russia
E-mail: Shatilov@inp.nsk.su

I. INTRODUCTION

We study incoherent beam-beam effects. Strong nonlinearity of the interaction leads to resonances and stochasticity, so that the behavior of the particles in the phase space becomes very complicated for analytical estimations. This is the reason for a wide employment of computer simulation for studying the beam-beam effects.

The perturbations of the equilibrium distribution can be conventionally divided into two parts: the perturbations at small amplitudes (core region) and the ones at large amplitudes (tails). The first cause an emittance growth, the second result in the lifetime decrease. Both effects restrict the beam current and, therefore, the luminosity, but the connection between them is rather weak. This means that one can have a strong beam size growth with a very good lifetime and vice versa, a bad lifetime with almost an unperturbed core region. The lifetime determination is the most difficult problem here, because a huge CPU time is required to correctly determine the distribution in the tails. Besides, almost all the CPU time is spent for improving core distribution. Such situation motivates the search for possibility of "CPU redistribution" for large amplitudes. Naturally, the question of accuracy arises since the tracking algorithm is changed artificially. Maintaining accuracy is the main problem we shall discuss below.

The base idea of the technique described below has been proposed in 1989 by J. Irwin[1]. It was developed later by T. Chen, J. Irwin and R. Siemann[9]. In INP this concept was developed independently by the author. Actually, this paper is a simple translation of the preprint INP 92-79 (in russian[7]). It should be noticed, that justification and realization of Chen et al's and the author's methods are rather different, although recently carried out comparison indicated good agreement between both of them and the brute force technique.

The method was developed for the "weak-strong" case, but this limitation is not so important and after a simple modification it can be used for the "strong-strong" case as well.

II. DESCRIPTION OF THE METHOD

There are different ways to simulate the equilibrium distribution of the beam particles. The first one, the ensemble of N independent particles is considered. If the simulation time is much greater than the damping time the initial positions of these particles do not matter. Otherwise, they will influence the results and one has to care about correct initialization. Another way is watching for a single particle only. If the simulation time here is chosen N times greater than in the first case, both of them become equivalent, but there is no the initialization problem in the last one. For future discussion it does not matter which way is used, but for definiteness we consider a single particle for a long time (hundreds of damping times).

Besides coordinates and momenta, we use normalized amplitudes and phases as well:

$$x_\beta = \sqrt{\beta_x} A_x \cos\varphi_x \qquad x'_\beta = \frac{\sigma_{\beta x}}{\beta_x} A_x (\sin\varphi_x + \alpha_x \cos\varphi_x) \quad (1)$$

$$z_\beta = \sqrt{\beta_z} A_z \cos\varphi_z \qquad z'_\beta = \frac{\sigma_{\beta z}}{\beta_z} A_z (\sin\varphi_z + \alpha_z \cos\varphi_z) \quad (2)$$

$$s = \sigma_l A_s \cos\varphi_s \qquad \frac{\Delta E}{E_0} = \frac{\sigma_E}{E_0} A_s \sin\varphi_s \quad (3)$$

Here all the parameters (σ, β, α) are related to an unperturbed beam. During simulation, the particle moves along a very complicated trajectory within a 6-dimensional phase space. The equilibrium distribution and the density of the flows in this space are the most complete information one can extract, but not all of it is of equal importance. The distribution in the space of amplitudes is much more important because the amplitudes are "slow" variables. The amplitudes define the nonlinear tune shifts and, therefore, the falling within a resonance. The distribution in the space of phases is not so informative since the phases are "quick" variables, but this distribution is also important for the motion within resonances. As far as the flows are concerned, the most important one is the flow to the aperture (which is defined as the limit values of the amplitudes). This flow, not the distribution in the tails, defines the lifetime, though there is a connection between these two.

For the sake of simplicity, let us consider the two-dimensional case (four-dimensional phase space). The three-dimensional case will be discussed separately in section IV. We observe the test particle and locate its position in the plane of amplitudes at certain moments each turn (at the Interaction Point), so its motion looks like "jumps" from point to point. These jumps are produced by damping, noise and kicks from the opposite beam. The lattice nonlinearity, if any, also makes a contribution.

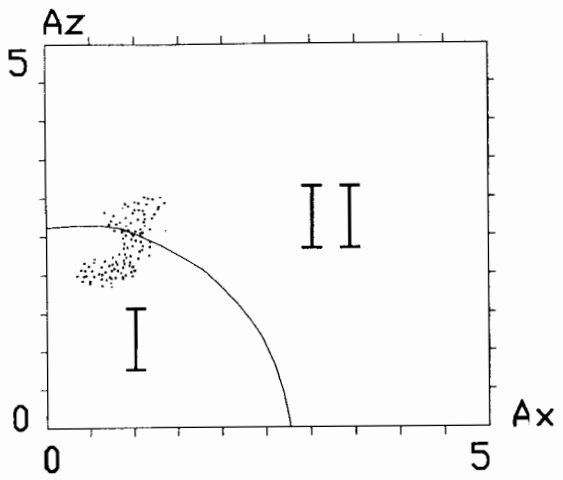


Figure. 1. A plane of amplitudes is split into internal (I) and external (II) regions. A small piece of the particle's trajectory is shown by points.

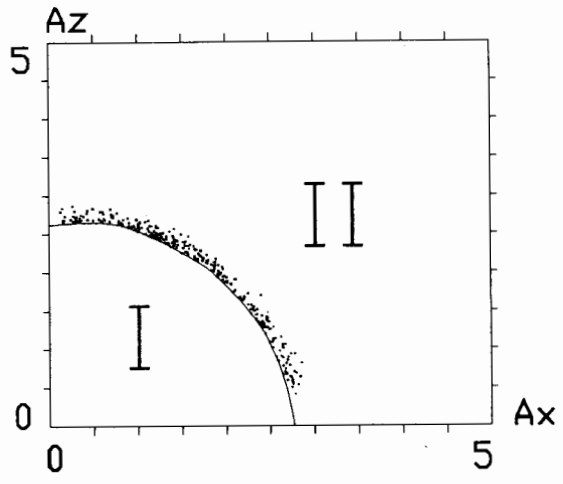


Figure. 2. The outflights are shown by points, which form a specific halo above a boundary. In future these points will be used as the positions for restarts.

Now we draw a special line, or boundary, to split the amplitude plane into two parts: *internal* (I) and *external* (II) (see Fig. 1). During the first step of the new algorithm we record all particle's coordinates and momenta each time it leaves the internal region for the external one (at once after crossing the boundary). These points (we call them *outflights*) form an original halo above the boundary (see Fig. 2). After some time, we get enough statistics of such outflights to proceed to the next step. Let us imagine that the internal region becomes a "black box" (or *hidden* region), so that we cannot watch a particle within it. In this case, the particle's trajectory looks like a large number of completely independent pieces, which starts from the points of outflights and ends when the particle falls into the hidden region. During the second step, we put the test particle to one of the outflight points immediately when it leaves for the hidden region. Such a procedure is called *restart*. The points for the restarts are chosen from the complete outflights statistics by using a random number generator.

It should be noted that this algorithm violates the course of events with time. This means that the observer is able to distinguish a real trajectory from our simulation. The reason is as follows: when the particle falls into the hidden region, it spends some time near the boundary and there is a high probability of crossing the boundary many times in close proximity to this place. In other words, the outflights are usually made by local groups, before the particle goes away from the boundary. This means that there is a correlation between the location of outflights and the time, when they take place. But this correlation vanishes since we use a random number generator to choose the points for restarts. Luckily, such rearrangement of events in time has no influence on the motion characteristics: we obtain quite correct distribution and flows in the phase space during the second step. The reason is that the process under consideration is a Markovian process (without memory). The particle's behavior does not depend on its history, and since we reproduce the probability of falling into a certain cell of the phase space when the particle leaves the hidden region, we must obtain the correct density and flows within this space.

Now it is easy to understand how to proceed to large amplitudes. After completion of the first step the regions change their meaning: the internal region becomes hidden, and the next boundary is drawn to split the "old" external region into internal and external ones (see Fig. 3). During the second step the position of the particle is checked each turn. As soon as it leaves for the hidden (I) region, a restart is produced. In case it moves from the internal region (II) to the external one (III), all its coordinates and momenta are registered to accumulate the statistics of outflights across the second boundary. Later on, we call the boundary between the hidden and internal regions as R-boundary (boundary for restarts); the boundary between the internal and external regions we call C-boundary (boundary for crossings). For the third step, the regions I and II are joined to form the new hidden region (so the C-boundary becomes the R-boundary), and the third boundary (it is the C-boundary for the third step) is drawn to split region III into the internal and external regions (their numbers are III and IV, respectively), and so on. The reduction of CPU time can be calculated as a ratio between the number of restarts and the number of corresponding outflights. Usually this value is about 5–10 for each step.

Approximately in this form this technique has been already suggested by J. Irwin[1]. He used simple circular arcs as boundaries and the radius of the arc was chosen so that particles spent 90% of the CPU time in the internal region and 10% in the external one.

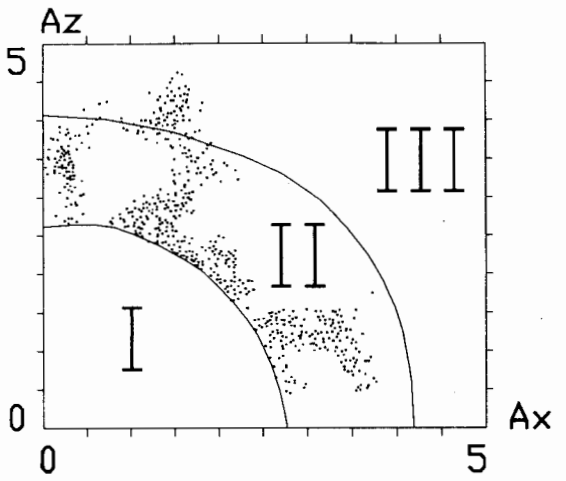


Figure. 3. The particle's trajectory during the second step, consisting of a large number independent pieces. I — hidden, II — internal, III — external regions.

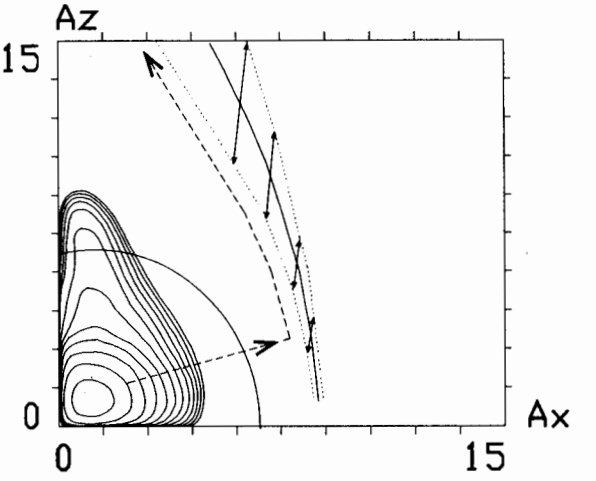


Figure. 4. An example of location of the boundary which leads to a loss of accuracy. The most probable way of a particle going to the aperture is shown by dashed line.

This solution is very attractive due to its simplicity and can give good result, but sometimes loss of accuracy is possible in the case where the lifetime is calculated. Maintaining accuracy is the main problem here. The difficulties result from our wish to develop a universal method which must work correctly for systems with very different (practically arbitrary) "phase space portraits".

Rigorously speaking, the only source of errors is the incorrect (insufficient) statistics of outflights from the hidden region. However, the accuracy of the results depends on many factors: simulation time, damping times, shape and location of boundaries within the amplitude plane. It is easy to guess that there is direct connection between the accuracy and the decrease in the CPU time this method provides. The accuracy can be increased at the expense of efficiency, for example, by increasing the simulation time for each step and decreasing the distance between the boundaries. The aim is to achieve an optimal compromise here: to get high efficiency with good enough guaranteed accuracy.

The amplitude of noise measured in units of normalized amplitude is defined by the damping time according to the formula:

$$\delta_A = 2\sqrt{\alpha}. \qquad (4)$$

Here α is the damping decrement and δ_A is the r.m.s. of amplitude change due to noise after a single turn. Without loss of generality, we can assume a Gaussian distribution for kicks caused by the noise. The damping time (in units of revolution time) is defined as $1/\alpha$ and this is a natural time scale of the system. The damping times are different for different degrees of freedom, but all of them are of the same order of magnitude. The largest one is denoted by τ and the simulation time for each step, measured in units of τ, is denoted by T (we assume it to be approximately the same from step to step).

Now let us consider the example shown in Fig. 4 to understand the influence of the shape and location of the boundaries. Here we can see two strong resonances disturbing substantially the equilibrium distribution. The first one is located at small amplitudes (it is shown as the disturbance of lines of equal density). The second one (shown as resonance line and resonance vectors) plays a main role in the process of losing particles at the aperture. The dashed line shows the Most Probable Way of a particle going to the Aperture (MPWA): first of all it moves to the second resonance (due to the noise only), is captured in it, and then moves to the high amplitudes along the resonance by streaming[2]. The first resonance leads to a very strong change in the density (several orders of magnitude) along the boundary which is chosen as a circular arc. As a result, since the simulation time is finite, all the outflights across this boundary are concentrated at the place where the boundary crosses the first resonance. This means that there are no outflights in the region where the MPWA is located. So, we lose this path for all following steps and the error in the lifetime determination can reach several orders of magnitude! By increasing the simulation time, we can get few outflights in the direction we need, but the insufficient statistics of such events leads to incorrect probability for this process and the accuracy of lifetime determination will not be good enough.

What is the optimal shape of the boundary? On the face of it, the main condition is the equal linear density of the outflights along the boundary. Indeed, a large number of outflights under this condition prevents from the above situations. Nevertheless, this choice has some essential disadvantages. First of all, it does not perfectly correspond to our goal of moving to large amplitudes because there is a possibility of forming spacious areas at small amplitudes with very weak flows out from the core. As a result, the line of

equal linear density of the outflights can have such a form that these areas will be located in the external region for several steps in spite of the high density of equilibrium distribution within them. Such a situation leads to the essential decrease in the efficiency of the method. After that it is not so easy to build such a boundary since each particle's jump within the amplitude plane can be an outflight or not, depending on the location of the boundary which we do not know a priori.

The other approach turns out to be more successful. Instead of the line of equal linear density of the outflights, we use the line of equal distribution density (or level line) as a boundary. To get this distribution, we should divide the plane of amplitudes into small rectangular cells (it is convenient to use cells of size δ_A). During the simulation we will account (individually for each step) how many times a test particle falls within each cell. After completion of the step, we will have an array of such numbers (N_p), which describe the equilibrium distribution outside the hidden region. The dispersion of N_p along the C-boundary must be sufficiently small since the boundary was chosen as a level line. The mean value of N_p on the C-boundary is marked by a tilde. It can be affirmed that the main condition, we must satisfy to get good statistics and solve our problems, is

$$\widetilde{N}_p \geq \overline{N} \gg 1, \qquad (5)$$

where $\overline{N}$ is the constant (to be defined below), while $\widetilde{N}_p$ can vary from step to step. Indeed, on the one hand, this condition guarantees the representation of all the details of the "phase space portrait" since these details cannot be greater than δ_A. In other words, this is a criterion of statistical reliability of the obtained level lines. On the other hand, for the next step we will get a high value of N_p along all the border of the hidden region (or R-boundary). This means that we reproduce correctly the probability of any particle's "journey" which begins inside the hidden region and crosses the area with the high "density" $\widetilde{N}_p$. It is worth of noting two important details: $\widetilde{N}_p$ keeps approximately the same value from step to step and the simulation time T, necessary to satisfy condition $\widetilde{N}_p \geq \overline{N}$, does not depend on the damping time τ for the two-dimensional case.

Let us consider now Fig. 5, in which the situation similar to Fig. 4 is shown. Here the dotted lines show the flows of phase convection, which result in almost all the outflights located at a certain place in spite of the boundary (bold) is a level line. The MPWA is connected with capture in the second resonance and streaming along it, as well as in Fig. 4. As is seen, the short way from the core to this resonance is improbable. Nevertheless, even if there is a "channel" crossing the boundary at the place where no outflights have been obtained, during the next step we reproduce the probability of getting to this channel correctly since

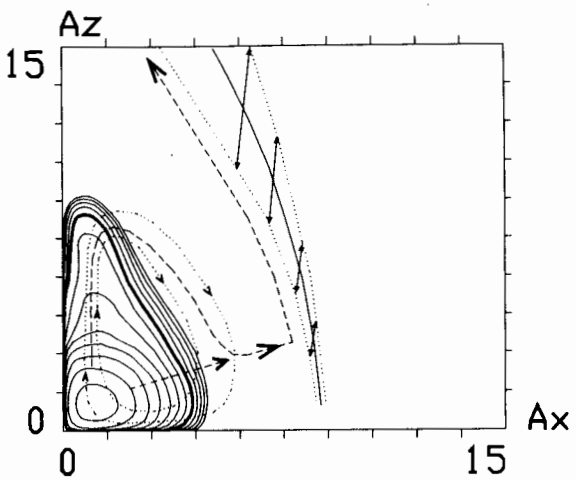


Figure. 5. The boundary (bold) coincides with a level line. Nevertheless, almost all the outflights are concentrated at a certain place due to the convective flows (dotted). The short dashed line shows a possible (but improbable) channel of going away. Since this channel crosses the area with high value of N_p, we correctly reproduce the probability of getting to it.

the value of N_p around the hidden region is sufficiently high (at least several times greater than $\overline{N}$).

It is convenient to measure the distance between the boundaries through the logarithm of density change. Indeed, any boundary can be defined by a single value, i.e., the number of the corresponding level. Let us introduce for each step an individual reference system of levels Q_i in which they are read from the border of hidden region. So, the level $Q_i = 0$ corresponds to the R-boundary for the i-th step, the level $Q_i = k$ corresponds to the density $\exp(k)$ times less than the density at the level $Q_i = 0$, and so on. In these terms, the distance between the neighboring boundaries j and $(j+1)$ (i.e. R- and C-boundaries for the $(j+1)$-th step) is just a value of Q_j at the boundary $(j+1)$. In future these distances are assumed to be equal to the same constant q for all the steps. Now we have to understand what the values q and the simulation time for each step T must be. We should keep in mind the following:

- The condition $\widetilde{N}_p \geq \overline{N}$ must be satisfied, otherwise we will get a wrong distribution. This means that with the distance between boundaries q, the value of T must also increase exponentially.
- The value of N_p obtained in time T at the level q depends on the shape of equilibrium distribution, so we cannot know it a priori.
- We need a lot of the outflights. If the boundaries are chosen correctly, as it was described above, the accuracy of the lifetime is determined by the statistics of the outflights. We can estimate it as $\sqrt{C_g/C}$, where C is the number of outflights and C_g is the mean number of outflights within a group (as a rule the outflights occur by local groups, which we can consider as the particular events).

- Deviations of the boundary from the true level line, if they are not so large (the true density data disagreement by a factor of 2–3 along the boundary), have practically no influence on the accuracy since we keep high value of N_p along the boundary. To calculate the lifetime accuracy, we need to take into account only the statistics of the outflights.

To estimate the optimal distance between the boundaries, the same time $T = T_0$ is assumed to be necessary for each step to achieve the number of particles per cell $N_p = \overline{N}$ at the level $Q_i = 0$ (just above the border of the hidden region). In this case, the full simulation time to move to m levels is as follows:

$$t = \frac{m}{q} T_0 \exp(q). \tag{6}$$

Here m/q is the number of steps and $T_0 \exp(q) = T$ is the simulation time for each step to achieve $N_p = \overline{N}$ at the level $Q_i = q$. We have to set $q = 1$ to minimize the time t. This means that the density falls down by a factor of e between the boundaries. Pay attention to that in this case we optimize q without taking into consideration the accuracy of the lifetime, which is defined through the statistics of the outflights. Fixing the final accuracy of the lifetime, we get the other expression for q. Indeed, on each step we have a statistical error of the outflights $\sqrt{C_g/C} \ll 1$. Since we follow the rules of building boundaries, the accuracy of the lifetime can be estimated as $(m/q)\sqrt{C_g/C}$. Here we assume (for estimation only) the equal number of the outflights across each boundary if $\widetilde{N}_p$ keeps the same value from step to step. So, the simulation time T is proportional to the square of the number of steps and for the full time we get

$$t \sim \frac{\exp(q)}{q^3}. \tag{7}$$

In this case, the minimum is achieved at $q = 3$.

To estimate the value of T_0, let us consider an unperturbed beam. The equilibrium distribution density (including the phase volume) is represented by the equation

$$\rho(A_x, A_z) = A_x A_z \exp(-\frac{A_x^2 + A_z^2}{2}). \tag{8}$$

The maximum density, which is equal to $1/e$, is achieved at the point $A_x = A_z = 1$. The number of particle's falling within a cell of size δ_A at the point (1,1) is $N_p = 4T_0/e$ (we assume here the same damping decrements for both directions). Defining the value of $\overline{N} = 100$, we get $T_0 \approx 70$.

Practically, the distance between the boundaries is chosen as $q = 2.5$. Under this condition, the simulation time must be $T \sim 1000$ damping times for each step. The determination of the lifetime of several hours takes usually 6–8 steps and even if the accuracy of the outflight statistics is 5% for each step, we obtain a final lifetime accuracy of 50% or better, which seems to be good enough.

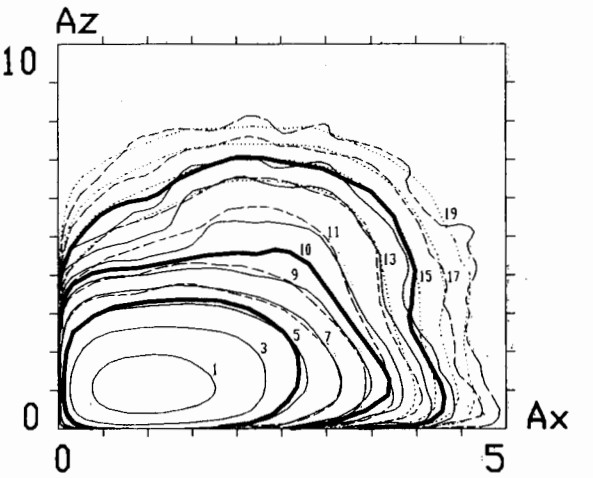


Figure 6. The level lines obtained during three sequential steps (1 — solid, 2 — dashed, 3 — dotted) are shown. Increasing of the line number by two corresponds to the equilibrium density decreasing by a factor of e. Boundaries (5, 10, 15) are shown as bold.

An important advantage of the method is the possibility of controlling the accuracy during the simulation: we can vary the simulation time T from step to step in such a way that the necessary value of $\widetilde{N}_p$ and number of outflights are achieved. Moreover, we can get the knowledge of the accuracy of the method directly from the results (see Fig. 6). Here we can see the level lines obtained from several sequential steps and three boundaries. The first step actually consists of two parts which can be called "zero" step and the first step itself. The zero step is necessary to obtain the initial distribution at small amplitudes and to draw the first boundary. During the first step we get the outflights across this boundary and improve the statistics of the distribution, so the first boundary will not exactly correspond to the final level line $Q_1 = q$. The second boundary is built after completion of the first step and goes along the level line $Q_1 = 2q$. After completion of the second step, we get the new lines (dashed, see Fig. 6) which have the statistical reliability much better than the same lines on the first step. Nevertheless, close to the first boundary they are in good agreement, which means that both sets are reliable here. When going away from the first boundary to large amplitudes, the differences between the two sets of lines grow. This is a consequence of the insufficient statistics at large amplitudes after completion of the first step. As we can see, the second boundary has been determined well enough since it is close to the level line $Q_2 = q$ obtained after completion of the second step, as well as the third boundary ($Q_2 = 2q$) which was built after the second step is close to the level line $Q_3 = q$ obtained after completion of the third step (dotted lines in Fig. 6).

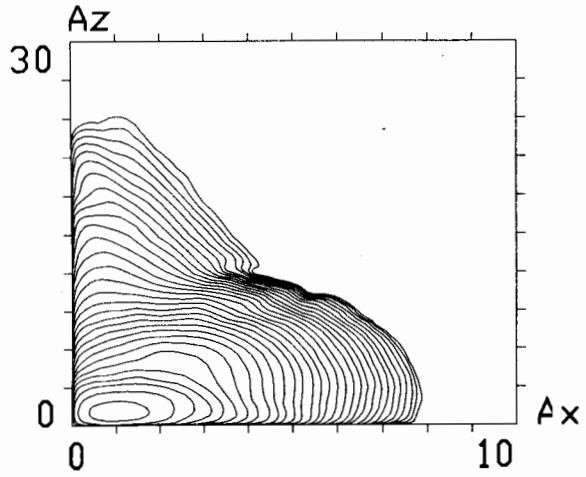


Figure. 7. The final level lines (see also Fig. 6) for the working point: $\{Q_x\} = 0.545$, $\{Q_z\} = 0.575$, $Q_s = 0.02$, $\xi_x = 0.005$, $\xi_z = 0.06$, $\sigma_x/\sigma_z = 1000$, $\sigma_l/\beta_z = 0.5$. The equilibrium density changes by a factor of e from line to line. The results of eleven sequential steps are used. The benefit in the CPU time was $\sim 10^8$.

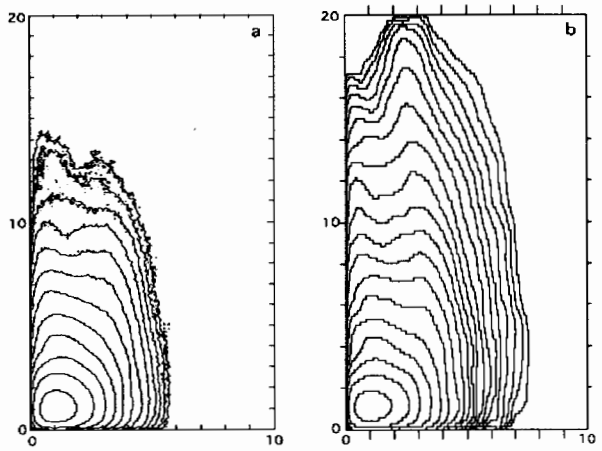


Figure. 8. The two-dimensional amplitude distribution for PEP-II B-factory working point. (a): TRS, brute force technique; (b): LIFETRAC, proposed technique.

The final level lines for this working point are shown in Fig. 7. In the core region the results of the first step are used. Between the first and the second boundaries the results of the second step are used. Between the second and the third boundaries we use the results of the third step, and so on. As is seen, the advance to large amplitudes takes place in the regions, where the equilibrium density of distribution was defined well enough during the previous step. This condition ensures good "sewing" of all the steps.

Obviously, the decisive test of the technique validity can be only get from the comparison against the brute force technique. Recently such a comparison has been carried out for three beam-beam codes[11]:

- TRS[10] is a multiparticle strong-strong code, which does brute force tracking.
- LIFETRAC[7] is a weak-strong code, which uses the described above tracking technique.
- LFM[9] is a weak-strong code, which uses tracking algorithm similar (but not identical) to LIFETRAC.

The two-dimensional amplitude distributions for PEP-II B-factory working point[11] are shown in Fig. 8. The results from TRS correspond to $5 \cdot 10^9$ particle-turns and took 818 CPU minutes to run on Cray-2S/8128. The results from LIFETRAC correspond to an effective number of $4 \cdot 10^{11}$ particle-turns and took 100 CPU minutes on VAX-6610 computer. The results from LFM are similar to the ones from LIFETRAC (see Tech. Note[11] for more information). The agreement among the codes is quite good. We hope that the next comparisons will be performed and will stimulate the progress in the tracking techniques.

In conclusion we discuss what the maximum amplitudes we can "climb" using this method are. Up to now we assumed the uniform density within a cell of size δ_A. However, at high amplitudes the level lines join together so close that this condition is violated. This means that we need the other criteria for the necessary value of $\widetilde{N}_p$ and the final lifetime accuracy (maybe, the simulation time shall increase with the increase in the step number). But we do not go deep into this problem, because it is not important for practical purposes. Indeed, the typical value of the damping time for e^+e^- colliders is about $10^3 - 10^4$ turns, which corresponds to the amplitude of noise $\delta_A \leq 1/30$. So, even for the unperturbed distribution the distance between the neighboring levels remains greater than δ_A up to the amplitudes $A \sim 30$, which is usually greater than the real aperture limit.

III. SCATTERING ON THE RESIDUAL GAS

Scattering has an essential influence on the equilibrium distribution, especially at large amplitudes. Just scattering defines the lifetime without an opposite beam. If both the beam-beam interaction and scattering occur, the interference between these two perturbations can have an effect. For example, if a strong resonance is located on large amplitudes, the scattering can essentially increase the probability of particle achieving it, providing particle's falling within the resonance directly from the core. So, including the scattering into simulation seems to be useful and important, but this is not possible directly in the new method. To clarify the problem, let us consider the elastic scattering without beam-beam effects. The scattering angle is inversely proportional to the impact parameter, so the probability of getting the amplitude jump ΔA is inversely proportional to the magnitude of this jump. Without scattering, the equilibrium density decreases as $\exp(-A^2/2)$. Hence, it can be seen that, beginning

from a certain value of the amplitude, the distribution is defined only by a single scattering from the core region. In our method this core turns out to be inside the first boundary, and scattering to large amplitudes can be considered as a particular case of the outflight. Although this process plays a main role for the distribution at high amplitudes, its probability is very small and we may get no such specific outflights in time T during the first step. This means that we lose the way of going to large amplitudes for all the next steps, as in the case shown in Fig. 4.

Nevertheless, slight modification of the technique allows us to successfully include the scattering. The idea is to simulate the scattering from the hidden region independently of the outflights statistics. We can do it correctly because we know the distribution inside this region.

Before discussing this technique, we would like to consider in detail the ordinary scattering outside the hidden region. We take into account only the elastic scattering because it has a greater influence on the equilibrium distribution (inelastic scattering is very important for lifetime definition, but actually it does not disturb the equilibrium distribution since almost all the particles lose immediately after such scattering). The cross-section for $\gamma \gg 1$ and $\theta \ll 1$ is classical:

$$d\sigma = 4Z^2 \frac{r_e^2}{\gamma^2} \cdot \frac{\mathrm{o}}{\theta^4}, \tag{9}$$

whence

$$\theta = 2Z \frac{r_e}{\gamma \rho}. \tag{10}$$

Here Z is the nucleus charge, θ is the scattering angle, ρ is the impact parameter, o is solid angle. Each act of the scattering causes the change of momenta of the electron which can be written in normalized variables as follows:

$$\Delta p_x = \frac{\beta_x}{\sigma_x} \cdot \theta \cos\varphi, \tag{11}$$

$$\Delta p_z = \frac{\beta_z}{\sigma_z} \cdot \theta \sin\varphi. \tag{12}$$

Here φ is the angle between the horizontal and scattering planes. It follows that the elastic scattering, as well as the beam-beam effects, mainly disturbs the vertical distribution (for flat beams) due to the relation $\beta_z/\sigma_z \gg \beta_x/\sigma_x$. The scattering at small angles, when repeated many times, results in small normal (Gaussian) noise which can be combined with quantum fluctuations of synchrotron radiation into certain common noise defining the beam sizes. A special approach must be applied to scattering at amplitudes comparable with δ_A or greater, on which strong perturbations of noise distribution arise (we can consider scattering as a specific noise with very long tails).

Thus, we simulate only the scattering at the angles greater than a certain angle. As a border value, we take such an angle θ_0, that $\Delta p_z = \delta_A/10$, and estimate the probability of scattering at the angle $\theta \geq \theta_0$ during a single turn. For example, we use VEPP-4 parameters: $\gamma = 10^4$, $\tau \sim 3000$ turns, perimeter P=366 m, $\langle \beta_x/\sigma_x \rangle \sim 10^4$, $\langle \beta_z/\sigma_z \rangle \sim 10^5$, $Z = 7.5$, and a pressure of the residual gas of 10^{-8} torr. As a result, we get the probability $W_s \sim 10^{-2}$. This means the following:

- Such scatterings have no contribution to the r.m.s. of noise δ_A.
- We guarantee correct reproduction of noise distribution because we take into account the tails of noise beginning from small amplitudes $\Delta p \ll \delta_A$.
- We need not to consider the multiple scattering on such angles during a single turn due to very low probability of these events.
- The increase in the CPU time due to simulation of the above scatterings is insignificant.

The simulation with account of scattering (outside the hidden region) is now as follows: first of all, the probability of scattering at the angles $\theta \geq \theta_0$ is calculated using parameters of the ring. During the simulation, a random number generator is used at each turn to decide whether the scattering occurs. If yes, the particular angle is defined according to the formula

$$\theta = \theta_0/\sqrt{R}, \qquad 0 < R < 1, \tag{13}$$

where R is the other random number. The third random number is used then to define the scattering plane inclination angle φ and the fourth random number to define the azimuth of the collider on which the scattering takes place. To calculate the jumps in the normalized momenta, we have to multiply the obtained values of θ_x and θ_z with the corresponding relations β_x/σ_x, β_z/σ_z taken at the scattering point. In practice, the mean values of these relations are used, although a real lattice and distribution of ions along the ring (it can be quite different for different places) can be readily taken into consideration.

Now we come back to the scattering from the hidden region. When a particle falls inside, it has exactly three possibilities at each turn, one of them is realized without fail:

1) The particle leaves the hidden region without scattering (ordinary outflight).

2) The particle is scattered at the angle $\theta \geq \theta_0$. As a result, it can leave the hidden region (a particular case of the outflight), and can remain inside as well.

3) The particle is not scattered and remains inside the hidden region.

The latter case is the most probable, and the essence of the above-described method is the consideration of only such events, where the particle leaves the hidden region without spending the CPU time for the third case. Now we only should take into account one more possibility of leaving the hidden region due to scatter-

ing. To reproduce this process correctly, the probability of the first case is necessary.

The algorithm of simulation is now as follows: during the first step (see Fig. 1), in time T_1, we get a number of the outflights C_1 which can be divided into two parts: the outflights with scattering (C_{1s}) and the ones without it (C_{1r}). So, we have $C_1 = C_{1s} + C_{1r}$ and only the last events are saved as positions for future restarts. Besides, the fraction of time the particle has spent in the external region $V_1 < 1$ is accounted On the second step (see Fig. 3), the probability of leaving the hidden region without scattering during a single turn is

$$W_1 = \frac{C_{1r}}{(1 - V_1) \cdot T_1 \cdot \tau}. \qquad (14)$$

Here the denominator is the number of turns the particle has spent within the internal region on the first step. The process of leaving is simulated in the following way: using a random number generator, we decide, according to the probabilities W_1 and W_s, what possibility (1 or 2) is realized at the moment. If it is the 1-st possibility, a conventional restart is produced according to the statistics of the outflights without scattering. Otherwise, the point from which the particle is scattered is chosen randomly, according to the equilibrium distribution inside the hidden region (this has been already known), then the particular angle of scattering is defined, and so on (see the scattering outside the hidden region). After all, we get new amplitudes of the particle and check whether it leaves the hidden region or not. In the last case, the whole algorithm is repeated beginning with the choice from the 1-st and 2-nd possibilities. As a result, the "process of restarting" becomes longer due to a possibility of producing a few idle scatterings inside the hidden region without leaving it. But this time has no effect on the simulation time T_2 which takes into account only the motion outside the hidden region.

During the second step, the particle makes R_2 restarts and $C_2 = C_{2s} + C_{2r}$ outflights. At the same time it spends the fraction of time $V_2 < 1$ in the external region (now it is region III). The time which is necessary to achieve the same statistics, when a conventional tracking technique is used, is called *equivalent time*. For the 2-nd step it is as follows:

$$T_{2eq} = T_1 \cdot \frac{R_2}{C_1}. \qquad (15)$$

The benefit for the CPU time due to application of the new method can be calculated as T_{2eq}/T_2. On the third step, the probability of the ordinary outflight (1-st possibility) is

$$W_2 = \frac{C_{2r}}{(1 - V_1 \cdot V_2) \cdot T_{2eq} \cdot \tau}. \qquad (16)$$

The restarts are produced like on the second step, but using W_2 instead of W_1. In this case, the equivalent time and benefit are:

$$T_{3eq} = T_{2eq} \cdot \frac{R_3}{C_2}, \qquad (17)$$

$$\frac{T_{3eq}}{T_3} = \frac{T_1 \cdot R_2 \cdot R_3}{T_3 \cdot C_1 \cdot C_2}. \qquad (18)$$

Thus, we have the recurrent formulae to define the lifetime and the probability of the outflight without scattering W_k, which allows us to simulate the restart correctly.

Here we would like to make a remark concerning the value of W_k. At the first sight it looks strange because only near the border of the hidden region the particle is able to leave it without scattering. In spite of this, W_k was defined by the full time which the particle spends within the hidden region, and the most part of this time is spent in the core, far from the border. To clarify this situation, it is necessary to remember the main condition that should be satisfied to obtain the correct distribution outside the hidden region. Namely, we must reproduce the relations between the probabilities to find the particle in a certain place of the phase space at once after it has left the hidden region. We are not interested in how and were from the particle jumps, what time correlation between such events is. We need only the relations between the probabilities and the value of W_k was defined quite correctly for this purpose.

Nevertheless, one more step must be done to successfully include the scattering into simulation. The reason is a decrease in the efficiency of the method when moving to large amplitudes. Indeed, the probability W_k falls down exponentially from step to step while the probability of scattering at the angle $\theta \geq \theta_0$, W_s, keeps the same value for all the steps. As a result, we obtain $W_s \gg W_k$ for $k \gg 1$. On the other hand, to leave the hidden region from the core, larger scattering angles are necessary with the distance of the border of the hidden region from the core. So, a lot of the CPU time will be spent for a huge number of idle scatterings within the hidden region without leaving it. To solve this problem, we use a division of the hidden region produced by sequential boundaries. It is quite easy to find the minimum scattering angles θ_{km} which can force the particle out from the region m to the region k (i.e. outside the hidden region) on the k-th step ($k > m$). Besides, we can calculate the relations between the probabilities to find the particle within these regions since we know the absolute probability for each m-th region:

$$\rho_m = V_0 \cdot V_1 \cdots V_{m-1} \cdot (1 - V_m), \qquad V_0 = 1. \qquad (19)$$

This allows us to define the probability W_{km} of scattering from the region m at the angle $\theta \geq \theta_{km}$ during a single turn for the k-th step. The whole probability of scattering at the angles greater than the limit is a

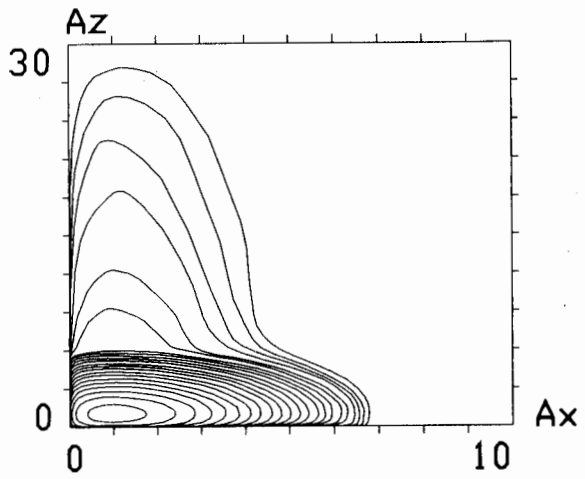


Figure. 9. Equilibrium distribution for VEPP-4 without beam-beam effects. The density of the residual gas is 10^{-8} torr.

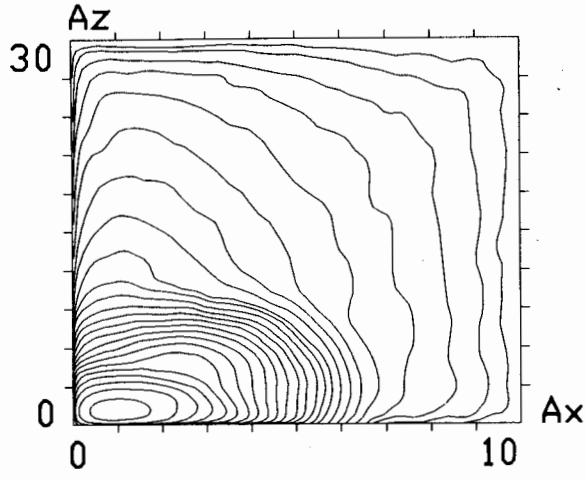


Figure. 10. The same working point as in Fig. 7 with account of the elastic scattering. The density of the residual gas is 10^{-8} torr. The roughness of level lines at large amplitudes caused from statistical errors, but anyway these are smaller than the distance between neighboring lines.

sum of W_{km}, and this value must be used instead of W_s:

$$\widetilde{W}_s = \sum W_{km}. \qquad (20)$$

Now we get $\widetilde{W}_s$ and W_k approximately of the same order of magnitude for all the steps. Now the algorithm of the restart must be changed a little. If the random number generator decides to produce the scattering, first of all we have to choose, according to probabilities W_{km}, where from (considering the region number m) this scattering must be done. Then we choose an arbitrary (according to the distribution that we have already known) point within this region and define the particular angle of scattering as

$$\theta = \theta_{km}/\sqrt{R}, \qquad 0 < R < 1, \qquad (21)$$

where R is the other random number. The inclination angle of a scattering plane and the collider azimuth are defined as usual. Finally, we obtain the new particle amplitudes. After all, we have to check whether the particle leaves the hidden region or not (the scattering on the angle $\theta \geq \theta_{km}$ does not guarantee the leaving).

For example, the equilibrium distribution without beam-beam effects is shown for VEPP-4 in Fig. 9. The lifetime was $4 \cdot 10^{10}$ turns for a vertical aperture of $30\sigma_z$ while the probability of a single scattering from the core to the aperture was $3.5 \cdot 10^{-11}$. The increase in the CPU time because of a more complicated restart algorithm was about 1%. The benefit in the CPU time due to this method was $\sim 10^5$. Fig. 10 shows the result of interference between the beam-beam interaction and the scattering (to be compared with Fig. 7, where scattering is turned off).

IV. THREE-DIMENSIONAL CASE

Up to now we considered the two-dimensional amplitude space. Evidently, all the results can be generalized for the three-dimensional case as well. This means that we have to build a distribution within the three-dimensional amplitude space and use two-dimensional boundaries (i.e., surfaces instead of lines). The only problem arises from the fact that probability to fall within a three-dimensional cell of size δ_A is much less than in the case of a two-dimensional cell. This leads to that the simulation time for each step T must be much greater in the three-dimensional case to satisfy the condition $\widetilde{N}_p \geq \overline{N}$. Moreover, the simulation time T depends now on the damping time τ. Besides, there are some technical difficulties which do not allow us to use the three-dimensional version of the method at the present time. As a compromise, we use a "three-dimensional tracking with two-dimensional distribution". This approach has a limited range of application, but anyway, even outside this range, one can get the essential information.

The algorithm we use can be presented as consisting of three independent parts: the simulation itself (outside the hidden region), building the level lines in the amplitude space, and the simulation of a particle leaving the hidden region (i.e. restarts). The first part represents the physical nature of the phenomenon under investigation and must be three-dimensional because of the important role of the longitudinal motion. Concerning the second part, we can integrate the distribution with respect to the third amplitude and build the boundary similar to that in the two-dimensional case. This means that the boundary is a cylinder within the three-dimensional amplitude space. Nevertheless, each outflight includes six values: all the amplitudes and phases (or coordinates and momenta). What is the effect of such simplification of the boundary? The finite statistics of the outflights can lead to losing some ways (see Fig. 4). For example, reproducing the probability

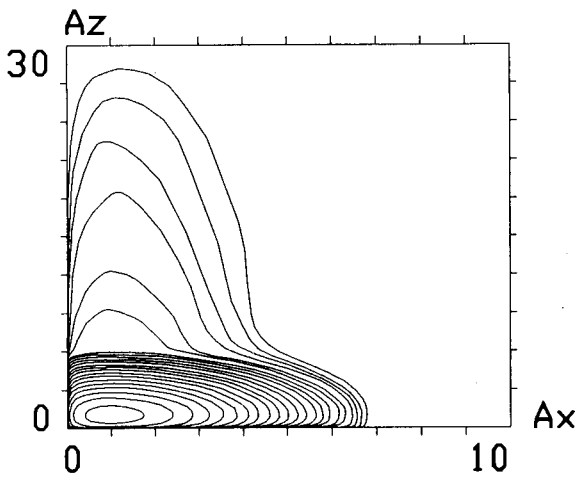


Figure. 9. Equilibrium distribution for VEPP-4 without beam-beam effects. The density of the residual gas is 10^{-8} torr.

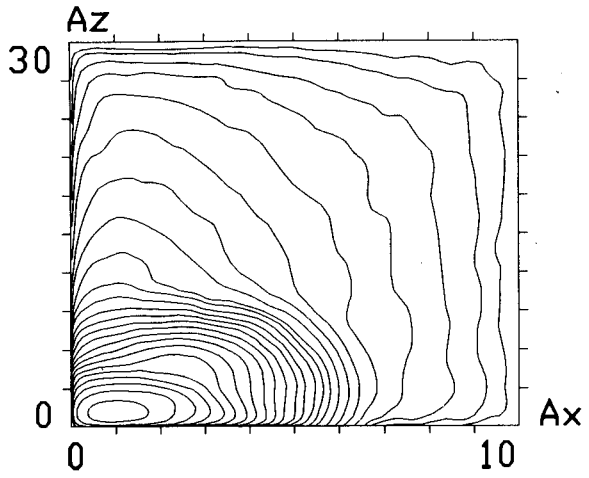


Figure. 10. The same working point as in Fig. 7 with account of the elastic scattering. The density of the residual gas is 10^{-8} torr. The roughness of level lines at large amplitudes caused from statistical errors, but anyway these are smaller than the distance between neighboring lines.

sum of W_{km}, and this value must be used instead of W_s:

$$\widetilde{W}_s = \sum W_{km}. \qquad (20)$$

Now we get $\widetilde{W}_s$ and W_k approximately of the same order of magnitude for all the steps. Now the algorithm of the restart must be changed a little. If the random number generator decides to produce the scattering, first of all we have to choose, according to probabilities W_{km}, where from (considering the region number m) this scattering must be done. Then we choose an arbitrary (according to the distribution that we have already known) point within this region and define the particular angle of scattering as

$$\theta = \theta_{km}/\sqrt{R}, \qquad 0 < R < 1, \qquad (21)$$

where R is the other random number. The inclination angle of a scattering plane and the collider azimuth are defined as usual. Finally, we obtain the new particle amplitudes. After all, we have to check whether the particle leaves the hidden region or not (the scattering on the angle $\theta \geq \theta_{km}$ does not guarantee the leaving).

For example, the equilibrium distribution without beam-beam effects is shown for VEPP-4 in Fig. 9. The lifetime was $4 \cdot 10^{10}$ turns for a vertical aperture of $30\sigma_z$ while the probability of a single scattering from the core to the aperture was $3.5 \cdot 10^{-11}$. The increase in the CPU time because of a more complicated restart algorithm was about 1%. The benefit in the CPU time due to this method was $\sim 10^5$. Fig. 10 shows the result of interference between the beam-beam interaction and the scattering (to be compared with Fig. 7, where scattering is turned off).

IV. THREE-DIMENSIONAL CASE

Up to now we considered the two-dimensional amplitude space. Evidently, all the results can be generalized for the three-dimensional case as well. This means that we have to build a distribution within the three-dimensional amplitude space and use two-dimensional boundaries (i.e., surfaces instead of lines). The only problem arises from the fact that probability to fall within a three-dimensional cell of size δ_A is much less than in the case of a two-dimensional cell. This leads to that the simulation time for each step T must be much greater in the three-dimensional case to satisfy the condition $\widetilde{N}_p \geq \overline{N}$. Moreover, the simulation time T depends now on the damping time τ. Besides, there are some technical difficulties which do not allow us to use the three-dimensional version of the method at the present time. As a compromise, we use a "three-dimensional tracking with two-dimensional distribution". This approach has a limited range of application, but anyway, even outside this range, one can get the essential information.

The algorithm we use can be presented as consisting of three independent parts: the simulation itself (outside the hidden region), building the level lines in the amplitude space, and the simulation of a particle leaving the hidden region (i.e. restarts). The first part represents the physical nature of the phenomenon under investigation and must be three-dimensional because of the important role of the longitudinal motion. Concerning the second part, we can integrate the distribution with respect to the third amplitude and build the boundary similar to that in the two-dimensional case. This means that the boundary is a cylinder within the three-dimensional amplitude space. Nevertheless, each outflight includes six values: all the amplitudes and phases (or coordinates and momenta). What is the effect of such simplification of the boundary? The finite statistics of the outflights can lead to losing some ways (see Fig. 4). For example, reproducing the probability

of being captured in the three-dimensional resonance, whose location with respect to the third axis is far from the core, can be incorrect. Besides, the lifetime can be determined by an aperture for the third dimension, but we keep low third amplitude for all the steps.

Nevertheless, there are areas of parameters where the system becomes really two-dimensional (or "almost two-dimensional"). Particularly, the distribution is exactly symmetrical with respect to arbitrary rotations in the plane (A_x, A_z) for round beams. In this case, we build the distribution in the plane (A_r, A_s), where $A_r = \sqrt{A_x^2 + A_z^2}$. Besides, the system becomes "almost two-dimensional" in the case, where the dispersion at the IP is so high, that the synchrotron transverse beam size is much greater than the betatron one (so-called *monochromatization*[3]). In this case, the horizontal displacement of the particle is mainly defined by the longitudinal motion, and we have to build the distribution in the plane (A_s, A_z). The probability of the particle going to the aperture through large amplitude A_x vanishes in this case, although the resonances are really three-dimensional.

The significance of the longitudinal motion remains essential even without dispersion at the IP due to modulation of the betatron phases. However, the betatron motion seems to be more important and the distribution must be produced in the plane (A_x, A_z). The case, where the synchrotron and betatron beam sizes at the IP becomes comparable, is most difficult. Here all three dimensions are of the same importance and the two-dimensional distribution can result in serious errors in the lifetime determination. Nevertheless even under such conditions the new method can be helpful. The thing is that all the errors caused by two-dimensional simplification of the distribution give only the increase in the lifetime. Therefore, we can use the method to quickly search for "bad" regions of the parameters (i.e. the regions, where the lifetime is short), while in "good" regions we should use a conventional tracking technique to correctly define the lifetime. The topology of such "bad" regions in the space of various parameters can be an important source of information for future investigations.

V. SOME RESULTS OF TECHNIQUE APPLICATION

The study of beam-beam effects with monochromatization for the Novosibirsk B-Factory Project has given impetus to the development of the proposed technique. As it was shown (see Gerasimov[3]), for flat beams the width of the resonance $l \cdot Q_x + m \cdot Q_z + n \cdot Q_s = k$ depends on the monochromatization parameter λ (it is defined as the ratio of synchrotron and betatron beam sizes at the IP) as follows:

$$\Delta A_z \sim \lambda^{-l/2}. \qquad (22)$$

This formula mathematically represents the fact that significance of the horizontal betatron motion decreases (i.e. the system becomes "almost two-dimensional") in case of increasing the synchrotron beam size at the IP. However, there were some doubts concerning the dispersion at the IP, since a series of strong synchro-betatron resonances arised. The simulation results obtained in 1990–1991 by using a new technique essentially clarified the situation.

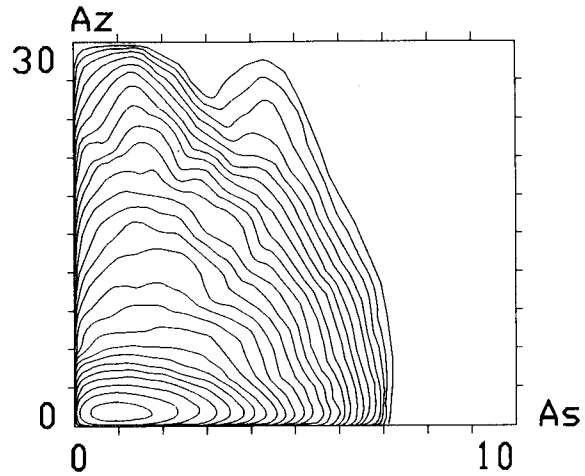


Figure. 11. Equilibrium distribution for VEPP-4M working point: $\{Q_x\} = 0.53$, $\{Q_z\} = 0.57$, $Q_s = 0.02$, $\xi_x = 0.005$, $\xi_z = 0.06$, $\sigma_x/\sigma_z = 80$, $\lambda = 2$.

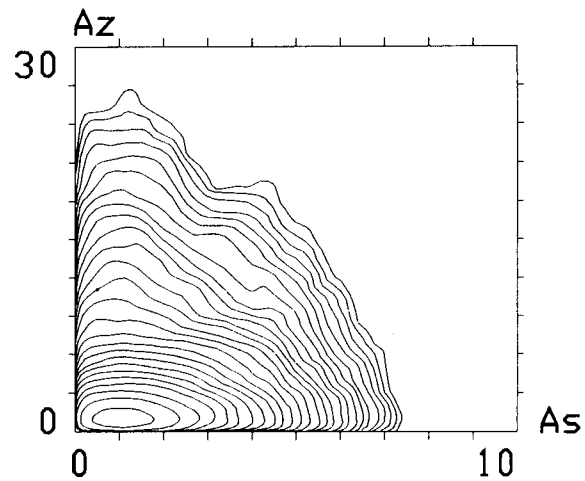


Figure. 12. The same working point as in Fig. 11, but monochromatization parameter $\lambda = 5$. The widths of resonances $l \cdot Q_x + m \cdot Q_z + n \cdot Q_s = k$ with $l \neq 0$ are decreasing here due to increasing of λ.

It is likely that VEPP-4M is the first collider with big dispersion at the IP. This dispersion arises constructively because of a magnet spectrometer for scattered electrons[4] and was considered earlier as a disadvantage. However, we expect now that the permissible tune shift parameter ξ will be sufficiently high. The simulation results for VEPP-4 are shown in Figs. 11, 12. The only distinction between these figures is the monochromatization parameter $\lambda = \sigma_{xs}/\sigma_{x\beta}$. As we can see, the widths of resonances with $l \neq 0$ really fall down with the increase in λ.

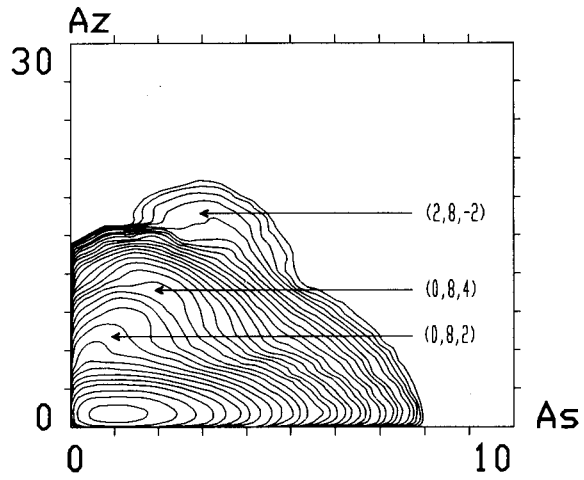


Figure. 13. The B-Factory working point without PC's: $\{Q_x\} = 0.08$, $\{Q_z\} = 0.11$, $Q_s = 0.02$, $\xi_x = 0.01$, $\xi_z = 0.05$, $\sigma_x^*/\sigma_z^* = 300$, $\lambda = \sigma_{xs}^*/\sigma x\beta^* = 10$. Here asterisk (*) denotes the values at the main IP. Resonances $l \cdot Q_x + m \cdot Q_z + n \cdot Q_s = k$ are shown as (l, m, n).

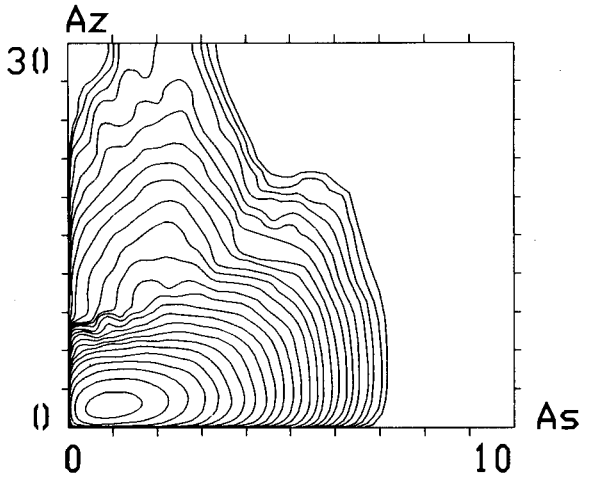


Figure. 14. The same working point as in Fig. 13 with account of two PC's (vertical separation on $50\sigma_z$). An instability arises, which results in short lifetime.

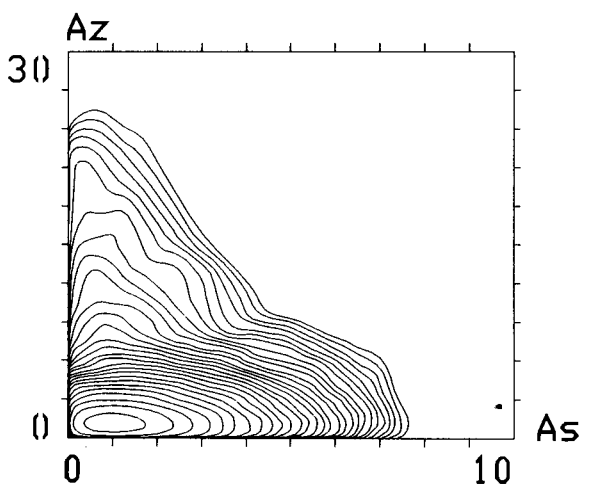


Figure. 15. The same working point, but horizontal separation on $20\sigma_x$ instead of the vertical one. Pay attention that σ_x and σ_z becomes almost equal at the PC.

A large number of bunches in the B-Factory leads to parasitic crossings (PC's). As a rule, there are two PC at a distance of about 2 meters from the main IP, all the next bunches are shielded by a vacuum chamber. In spite of considerable separation (20–40 beam sizes), the PC can essentially disturb the opposite beam due to high value of a beta-function (see Fig. 13, where there are no PC's, and compare with Figs. 14 and 15, where they are present). The direction of the separation is also very important. The technique was used to search for the minimum separation value which is allowed for both horizontal and vertical separations. The specific instability, which results in losing the particle when it achieves a certain threshold in the vertical amplitude, was discovered for the vertical separation (see Fig. 14). This threshold can be several times smaller than the separation value! In case of the horizontal separation, the PC's have much less influence (see Fig. 15). The lifetime versus the separation value is shown in Fig. 16 for both cases (the vertical aperture is $30\sigma_z$, the horizontal aperture is $10\sigma_x$, all the particles were lost at the vertical aperture).

The technique was also used in simulations for the Novosibirsk φ-Factory Project with round beams. The high intensity and low energy of the beams led to strong longitudinal beam-beam effects[5]. Particularly, strong flows to high amplitudes (both betatron and synchrotron) could arise due to these effects (see Fig. 17). In order to suppress such flows, an interesting idea of negative momentum compaction[6] was suggested by V.V. Danilov and E.A. Perevedentsev. The simulation results for the same working point as in Fig. 17 and inverse sign of the momentum compaction factor are shown in Fig. 18.

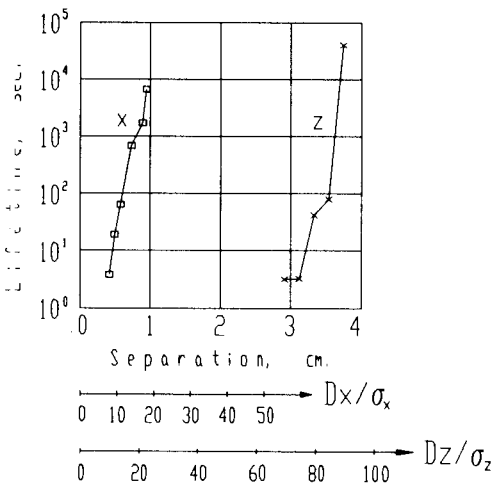


Figure. 16. Lifetime versus the separation value (horizontal or vertical) at the PC.

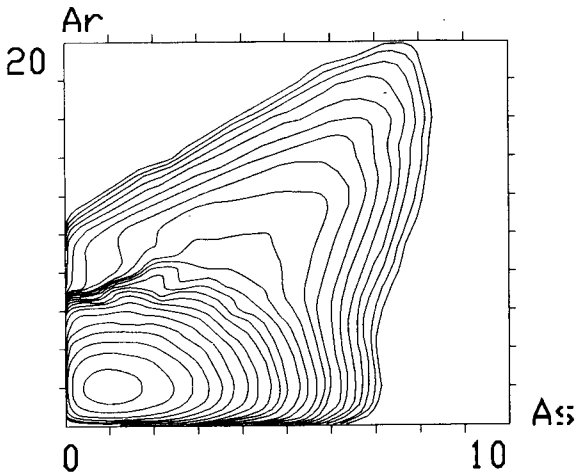


Figure. 17. Equilibrium distribution for φ-Factory with round beams. $\{Q_{x,z}\} = 0.04$, $Q_s = 0.02$, $\xi_{x,z} = 0.2$. The strong flow to large amplitudes arises due to longitudinal beam-beam effects.

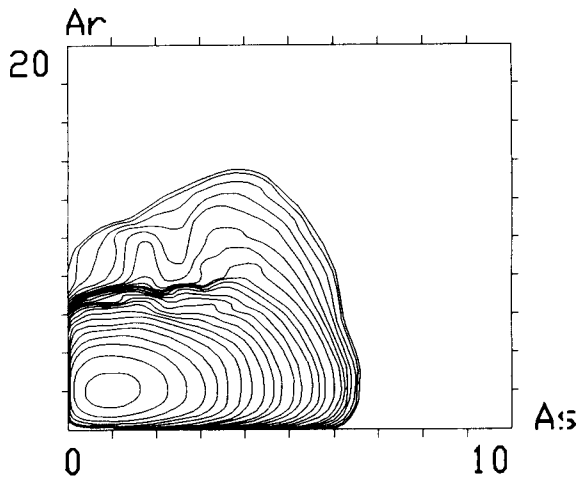


Figure. 18. The same working point as in Fig. 17, but momentum compaction factor is negative.

Moreover, some simulations results were obtained for the HERA electron beam (see Shatilov[8]). Any suggestions concerning new fields of application of the technique will be welcome.

VI. ACKNOWLEDGEMENTS

I would like to acknowledge many useful discussions with A.A. Zholents. In addition, A.L. Gerasimov made a number of valuable remarks concerning the technique.

References

[1] J. Irwin *Simulation of Tail Distributions in Electron-Positron Circular Colliders* (Third Adv. ICFA Beam Dynamics Workshop, Novosibirsk, 29 May - 3 June, 1989)

[2] J.L. Tennyson *Resonance Transport in Near Integrable Systems with Many Degrees of Freedom*, Physika D, v.5 (1982) p.123

[3] A.L. Gerasimov et al. *Beam-Beam Effects with Big Dispersion Function at the Interaction Point*, NIM **A305** (1991) 25

[4] V.M. Aulchenko et al. *Scattered Electrons Registration System of KEDR Detector for Two-Photons Process Investigation* (INP 91-49, Novosibirsk, 1991)

[5] V.V. Danilov et al. *Longitudinal Beam-Beam Effects for an Ultra-High Luminosity Regime* (IEEE Part.. Acc. Conf., San-Francisco, May 6-9, 1991)

[6] V.V. Danilov et al. *Negative Momentum Compaction in the Longitudinal Beam-Beam Effects* (Int. Conf. on High Energy Acc., Hamburg, July 20-24, 1992)

[7] D.N. Shatilov *Beam-Beam Simulations at Large Amplitudes and Lifetime Determination* (INP 92-79, Novosibirsk, 1992)

[8] D.N. Shatilov *Beam-Beam Simulations for the HERA Electron Beam* (DESY HERA 93-12, Hamburg, 1993)

[9] T. Chen et al. *Simulation of the Beam Halo from the Beam-Beam Interaction* (Phys. Rev. E, v.49, No3, p.2323, 1994)

[10] J. Tennyson *Undocumented code "TRS"*, 1989

[11] M. Furman et al. *Comparisons of Beam-Beam Code Simulations* (CBP Tech Note-59, 1995)

Comparison of Beam-Beam Simulations*

Miguel Furman and Alexander Zholents

Center for Beam Physics
Accelerator and Fusion Research Division
Lawrence Berkeley National Laboratory, MS 71-259
University of California
Berkeley, CA 94720

and

Tong Chen

Accelerator Theory and Special Projects
Stanford Linear Accelerator Center, MS 26
Stanford, CA 94309

and

Dmitry Shatilov

Budker Institute of Nuclear Physics
630030 Novosibirsk 30
Russia

August 22, 1995

Abstract

We carry out a methodical comparison among the four beam-beam codes TRS, BBTRACK3D, LIFETRAC and TAIL under a restricted set of conditions for which such a comparison is meaningful. We first study the convergence rate of five slicing algorithms as the number of kicks goes to infinity and provide a criterion for the minimum number of kicks required for acceptable accuracy in a given situation. We then focus on turn-by-turn single particle tracking in 6-dimensional phase space in weak-strong mode for a thick-lens beam-beam interaction in the absence of damping and quantum excitation effects and lattice nonlinearities. When the codes make use of the the same thick-lens slicing algorithm, the results agree within computer accuracy. We also compute the tune shift with amplitude and compare the results with those from the first-order analytic calculation. The agreement is surprisingly good except when synchrotron sidebands are prominent. We then go on to include damping and quantum excitation and compute the 2-D particle distributions out to reasonably large amplitudes. The results, which we show in the form of contour level plots, agree within the statistical accuracy of the calculations. This article summarizes Ref. [1].

*Work supported by the Director, Office of Energy Research, Office of High Energy and Nuclear Physics, High Energy Division, of the US. Department of Energy under Contracts no. DE-AC03-76SF00098 and DE-AC03-76SF00515.

1. Introduction

It is sometimes apparent that beam-beam simulations do not enjoy the same degree of respectability in today's accelerator physics community that other tools, such as single-particle tracking, do. One often hears, for example, that beam-beam simulations are better able to explain observed phenomena a posteriori rather than to predict them. Undoubtedly, the fundamental reason for this state of affairs is the complexity of the beam-beam interaction. A complete calculation would require the solution of Maxwell's and Newton's equations simultaneously for many billions of particles for millions of turns. It is clear that such a task is impossible with computers that are available today or that will be in the foreseeable future.

Nevertheless, much is known qualitatively and quantitatively about the beam-beam interaction in various regimes, and several codes have been developed that embody different approximations. Although the ultimate test of any beam-beam code is the correct and complete prediction of collider beam dynamics, it seems important for the time being to compare these codes with each other and with analytical results, and ensure that there is agreement whenever these comparisons are meaningful.

At its core, many of these codes have a common element: a thin-lens kick produced by a gaussian particle distribution. In this note we carry out a comparison among four beam-beam codes that involve this thin-lens kick. We start with the simplest case, namely the turn-by-turn tracking of a single particle colliding once per turn against an opposing gaussian bunch, and we compare the six-dimensional coordinates of the particle at every turn, in the absence of radiation damping, quantum excitation and lattice nonlinearities. We carry out the comparison for thin-lens and thick-lens beam-beam interaction, for five "slicing" algorithms, with or without synchrotron oscillations, for several initial conditions (but not in all possible combinations). When the codes do the same thing, the results indeed agree with each other within computer precision. We also compare the results for the calculated tune shift with amplitude with analytical results for the case of a thin lens. In the final step, we carry out a longer term simulation and produce the two-dimensional particle distribution in amplitude space with three of the codes. The agreement is very good, and the relatively small discrepancies are likely due to the difference in the algorithms used at this stage of the comparisons.

In all calculations presented here we use the "weak-strong" description of the beam-beam interaction. In this scheme the "strong" beam is passive and is represented by a gaussian lens (thin or thick) that is not altered by the other beam. The "weak" beam is dynamical, and we observe its behavior as a function of time as it collides repeatedly against the strong beam. In most, but not all, of the simulations carried out here, we use beam parameters that correspond closely to the PEP-II B factory [2], in which the electron beam plays the role of the strong beam and the positron that of the weak.

The four beam-beam codes we consider here are: TRS [3], LIFETRAC [4], TAIL [5] and BBTRACK3D [6]. The code TRS is a multiparticle strong-strong code that involves the soft-gaussian approximation. It is geared to assessing the luminosity performance of an e^+e^- collider. The codes LIFETRAC and TAIL are single-particle weak-strong codes geared to assessing the beam lifetime. The code BBTRACK3D is a single-particle weak-strong code geared to studying the dynamics of a single particle with specified initial conditions. Among its options, it allows different forms for the particle density of the strong beam, the gaussian being only one of them.

2. Slicing algorithms

We assume that the longitudinal distribution of the opposing bunch is described by a gaussian density

$$\hat{\rho}_\ell(z) = \frac{e^{-z^2/2\sigma_z^2}}{\sqrt{2\pi}\sigma_z} \tag{1}$$

where the caret "^" is meant to emphasize unit normalization. For the purposes of tracking simulations, we replace this density by a weighted superposition of N_s delta functions,

$$\hat{\rho}_\ell(z) \to \hat{\rho}_s(z) \equiv \sum_{k=-L}^{L} w_k \delta(z - z_k) \tag{2}$$

where $N_s \equiv 2L+1$ (we assume, as is customary, that N_s is an odd integer; if this is not the case, our calculation needs slight modifications). Each delta function gives rise to a kick at a location z_k weighted by w_k; these locations and weights must be determined according to a certain algorithm. The symmetry $\hat{\rho}_\ell(-z) = \hat{\rho}_\ell(z)$ implies that the kick locations and weights must obey the basic constraints $z_{-k} = -z_k$ and $w_{-k} = +w_k$. In addition, we require that the accumulated effects of the kicks should be the same as in the original distribution, *i.e.*, $\int dz \hat{\rho}_\ell(z) = \int dz \hat{\rho}_s(z) = 1$, which implies

$$\sum_{k=-L}^{L} w_k = 1 \tag{3}$$

For the thin-lens case ($N_s = 1$) there is a single kick at the center of the bunch with $z_0 = 0$ and $w_0 = 1$. For the thick lens case, on the other hand, there is, of course, an infinite number of possible algorithms to decide the weights and locations of the kicks consistent with the basic constraints. Here we examine only five possibilities. For the case $N_s = 5$ we list the kick locations and weights for all five algorithms in Table 1.

Algorithm #1 (equal spacing). In this case [7] the kicks are equally spaced and the weights are proportional to the gaussian density at z_k, namely

$$\frac{z_k}{\sigma_z} = \frac{2k}{N_s - 1}\left(1 + \frac{N_s - 3}{12}\right), \qquad w_k = \frac{\hat{\rho}_\ell(z_k)}{\sum_{m=-L}^{L} \hat{\rho}_\ell(z_m)} \qquad (k = 0,\ \pm 1, \cdots,\ \pm L,\ N_s \geq 3) \tag{4}$$

Algorithm #2 (equal areas). In this case the gaussian distribution (1) is divided up into N_s "slices" of equal area (implying equal charge), and the kicks are located at the center of charge of each slice. The equality of the area of the slices implies that the weights are all equal, namely $w_k = 1/N_s$. Standard formulas for the area under a gaussian curve imply that the kick locations are given by

$$\frac{z_k}{\sigma_z} = \sqrt{2}\,\mathrm{erf}^{-1}\left(\frac{2k}{N_s}\right) \qquad (k = 0,\ \pm 1, \cdots,\ \pm L,\ N_s \geq 3) \tag{5}$$

Algorithm #3. This case [8, 9] is similar to the previous one, except that the kick locations are given by

$$\frac{z_k}{\sigma_z} = N_s\left[\hat{\rho}_\ell(l_k) - \hat{\rho}_\ell(l_{k+1})\right], \qquad k = 1, \cdots,\ L \tag{6}$$

where the l_k's are the edges of the slices. By arguments similar to those in the previous case, it is easy to see that, for $k > 0$,

$$\frac{l_k}{\sigma_z} = \sqrt{2}\,\mathrm{erf}^{-1}\left(\frac{2k-1}{N_s}\right) \qquad (k = 1,\ 2, \cdots,\ L+1,\ N_s \geq 3) \tag{7}$$

For $k < 0$, the l_k's are the mirrors of those for $k > 0$ (note that there is no $k = 0$ edge, and that the $k = \pm(L+1)$ edges are at $\pm\infty$). As in all cases, the central kick is at $z_0 = 0$, and the kicks for $k < 0$ are symmetrically located with respect to those for $k > 0$. The weights are the same as in the previous case, namely $w_k = 1/N_s$.

Algorithm #4. This is a modified combination of algorithms #1 and #3 in which

$$\frac{z_k}{\sigma_z} = \frac{1}{w_k}\left[\hat{\rho}_\ell(l_k) - \hat{\rho}_\ell(l_{k+1})\right], \qquad k = 1, \cdots,\ L \tag{8}$$

where the l_k's are the same as above, and where the locations for $k < 0$ are the mirror images of those for $k > 0$. The weights are proportional to $\sqrt{\hat{\rho}_\ell(z)}$, namely

$$w_k = \frac{\sqrt{\hat{\rho}_\ell(z_k)}}{\sum_{m=-L}^{L} \sqrt{\hat{\rho}_\ell(z_m)}} \qquad (k = 0,\ \pm 1, \cdots,\ \pm L,\ N_s \geq 3) \tag{9}$$

In practice, the z_k's and w_k's are most easily found by iteration. It turns out that, of all five slicing algorithms described here, this algorithm #4 has the fastest rate of convergence as $N_s \to \infty$ (see the discussion below).

Algorithm #5. This algorithm consists of choosing the z_k's and w_k's in such a way that the area enclosed by the two functions $\int_0^z dz' \hat{\rho}_\ell(z')$ and $\int_0^z dz' \hat{\rho}_s(z')$ is minimal. This requirement leads to a set of nonlinear equations for the z_k's and w_k's which, as in algorithm #4, is most easily solved by iteration.

Table 1: Kick locations and weights for $N_s = 5$.

	Algorithm #1	Algorithm #2	Algorithm #3	Algorithm #4	Algorithm #5
	−1.166667	−1.281552	−1.399809	−1.59898	−1.44156
	−0.5833333	−0.5244005	−0.5319032	−0.67872	−0.63623
z_k's	0.0	0.0	0.0	0.0	0.0
	0.5833333	0.5244005	0.5319032	0.67872	0.63623
	1.166667	1.281552	1.399809	1.59898	1.44156
	0.1368561	0.2	0.2	0.17350	0.14943
	0.2280002	0.2	0.2	0.23222	0.22577
w_k's	0.2702873	0.2	0.2	0.26056	0.24960
	0.2280002	0.2	0.2	0.23222	0.22577
	0.1368561	0.2	0.2	0.17350	0.14943

Convergence rate of the five slicing algorithms. A reasonable requirement for any given algorithm is that the results should converge to a limit as $N_s \to \infty$. A reasonable requirement for all algorithms is that they should converge to the same answer in this limit. It remains an open problem to establish the optimal thick-lens slicing algorithm among the infinite number of possibilities. By "optimal algorithm" we mean that which yields, for a given finite number of kicks, the closest answer to the $N_s = \infty$ limit for a particular problem. This is clearly a very difficult problem: one cannot even set forth a universal criterion for such an optimization because such a criterion necessarily depends on many variables of the problem at hand, such as the working point, beam aspect ratios, etc.

In this section we try to solve a more modest problem: we study the convergence rate of the five slicing algorithms presented above as the number of kicks $N_s \to \infty$. Although this is clearly a more restricted problem than the one stated in the previous paragraph, the answer is still quite interesting because it shows clear systematics. As we show below, algorithm #4 emerges as the clear favorite among the five. Within this limited context, we also give an answer to the important practical question of how many kicks are enough for a given situation.

We proceed as follows: we first generate a weak bunch of 1,000 particles distributed gaussianly in the 6-D normalized phase space $(X_1, \ldots, X_6) \equiv (x/\sigma_{x+}, x'/\sigma_{x'+}, y/\sigma_{y+}, y'/\sigma_{y'+}, z/\sigma_{z+}, \Delta p/\sigma_{p+})$ where the subscript "+" is meant to emphasize that this is the weak (positron) beam. The coordinates are generated in an uncorrelated fashion, so that we may think of the distribution as that corresponding to a gaussian beam matched to the bare lattice at the IP. We then push this distribution once through the thick beam-beam lens produced by the strong beam for a given slicing algorithm and for a given number of kicks, and compare the resultant distribution with the one obtained by pushing the *same* initial distribution according to the "$N_s = \infty$" case which, for practical purposes, we define to be algorithm #4 with 300 kicks. Note that our criterion does not depend on any lattice parameter; it is designed to judge the beam-beam interaction by itself, as an isolated entity.

We compare the algorithms quantitatively by defining a dimensionless parameter Q for each algorithm as the sum of the rms deviations of the four transverse phase space coordinates of the final distribution from

those obtained from the $N_s = \infty$ case,

$$Q = \sum_{n=1}^{4} \sqrt{\langle (X_n - X_{n,\infty})^2 \rangle} \tag{10}$$

where $\langle \cdots \rangle$ is the average over the 1,000 particles. Obviously, the smaller is Q the better is the slicing algorithm. We present here only one case, corresponding to a flat beam with PEP-II-like parameters [2], listed in Table 2. Other cases, with qualitatively similar results, are described in Ref. [1].

Table 2: Parameters for the convergence rate tests.

β^*_{x+}/σ_{z+}, β^*_{y+}/σ_{z+}	37.5, 1.5
$\beta^*_{x-}/\beta^*_{x+}$, $\beta^*_{y-}/\beta^*_{y+}$	1.333, 1.333
σ_{x-}/σ_{x+}, σ_{y-}/σ_{y+}, σ_{z-}/σ_{z+}	1, 1, 1
σ_{x-}/σ_{y-}	25
ξ_{x+}, ξ_{y+}	0.03, 0.03

Figure 1 shows the results of plotting Q *vs.* the number of kicks N_s for the five algorithms. It is apparent that algorithm #4 has systematically the fastest convergence rate of the five. It is curious that algorithm #1 does not converge uniformly, although it becomes competitive with #4 for $\gtrsim 50$ or more kicks.

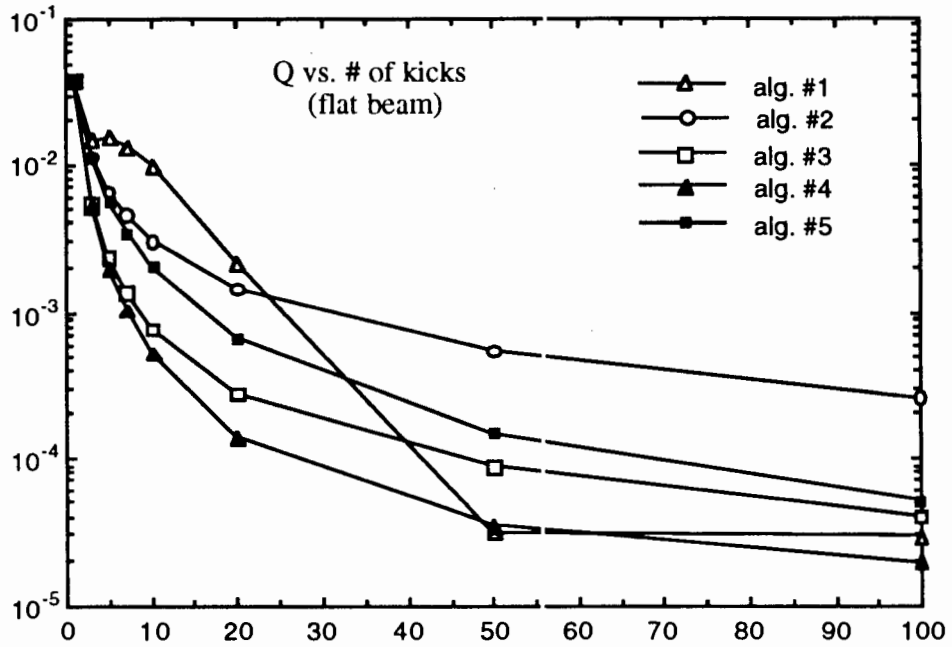


Figure 1: Convergence of the slicing algorithms: Q plotted vs. number of kicks N_s for flat beams (PEP-II-like parameters; see Table 2).

A criterion for the adequate number of kicks. It is important to decide how many kicks are enough for a given problem because, all other things being equal, the CPU time used in the calculation is proportional to N_s. We now provide a criterion for the minimum value required for N_s for issues pertaining to the beam

core (such as the beam blowup due to the beam-beam interaction, or, equivalently, the luminosity). The reasoning is as follows: due to the effects of radiation damping and quantum excitation, the rms beam size in the transverse dimension fluctuates by

$$\frac{\delta\sigma}{\sigma} \simeq \frac{1}{\sqrt{\tau}} \tag{11}$$

where τ is the damping time (in units of turn number) corresponding to the dimension considered. Because of these fluctuations, it is not justified to increase the accuracy of the beam-beam element beyond that corresponding to a value of Q given by

$$Q \simeq \frac{4}{\sqrt{\tau}} \tag{12}$$

(the factor 4 accounts for the four terms in Eq. (10)). Thus once we know the convergence rate of a given algorithm, the criterion is the following: the minimum value of N_s that gives the correct answer (within the statistical accuracy of the calculation) is that for which Q takes on the value given by Eq. (12).

For the case of PEP-II, with $\tau = 5400$, this yields $Q \simeq 0.05$. Therefore, as one can see from Fig. 1, any of the five algorithms gives the correct answer for $N_s = 3$. For other situations there are big differences in the number of slices required by each algorithm to converge to a result with a given accuracy [1]. Nevertheless, algorithm #4 has consistently the fastest convergence rate among the five possibilities shown here.

3. The thick lens beam-beam interaction

In all cases described in this article we make the following assumptions: (a) The particles are relativistic so that we can neglect their self-interactions. (b) The bunch is sufficiently short that there are no nontrivial lattice elements at the IP in a region of size comparable to the bunch length. (c) There is no dispersion in this region around the IP. (d) There is no closed orbit distortion of the strong beam, intentional or accidental. (e) There are no phasing errors and no collective oscillations, longitudinal or transverse.

As the particles in the weak beam move through the strong beam, they encounter the N_s kicks in sequence. For each kick there are four steps (listed below) that describe the algorithm for the beam-beam kick experienced by a given particle in the weak beam. These four steps are repeated for each slice and must be carried out in the *actual sequence* of kicks encountered by the particle. When the weak beam consists of many particles, which is the generic case in the code TRS, one also has to repeat all these steps for all particles.

The four steps for a single kick are the following:

Step 1: Determine the collision point. As a consequence of the assumptions listed above, the bunch centers come together at the nominal (optical) IP. Thus we assume that they move towards each other according to $s_\pm = \pm ct$, so that time $t = 0$ corresponds to the instant of the central collision. If z_+ is the longitudinal position of the positron and z_- that of the electron slice (both measured relative to their respective bunch centers), then the azimuthal coordinates of the colliding positron (s_+) and opposing electron slice (s_-) at time t are

$$\text{positron: } s_+ = ct + z_+; \quad \text{electron slice: } s_- = -ct - z_- \tag{13}$$

(we take the convention that $z > 0$ means the head of the bunch regardless of its direction of motion). The collision point between the positron and the opposing slice is determined by setting $s_+ = s_- \equiv s_c$, which implies

$$\text{collision point: } s_c = \tfrac{1}{2}(z_+ - z_-) \tag{14}$$

Step 2: Determine the transverse coordinates. In all codes considered here the longitudinal as well as the transverse coordinates of the particles are *referred to the bunch center*. Since the beam-beam kick is represented by a thick lens whose strength varies during the course of the collision (due to the s dependence of the transverse size of the opposing bunch), we have to find the actual transverse coordinates

of the colliding particle. As a consequence of the assumptions listed above, the transformation from the bunch center to the actual collision point is a simple drift:

$$x \to x + s_c x', \qquad y \to y + s_c y' \tag{15}$$

while the slopes x' and y' remain unchanged.

Step 3: Actual kick. In this step the slopes of the particle are changed according to

$$x' \to x' + \Delta x'\left(x, y, \sigma_{x-}(s_c), \sigma_{y-}(s_c)\right), \qquad y' \to y' + \Delta y'\left(x, y, \sigma_{x-}(s_c), \sigma_{y-}(s_c)\right) \tag{16}$$

while x and y remain unchanged. In computing $\Delta x'$ and $\Delta y'$ we use x and y from Step 2 and the actual beam sizes of the opposing bunch at the collision point, given by

$$\sigma_{x-}(s_c) = \sigma_{x-}(0) \times \sqrt{1 + \left(s_c/\beta^*_{x-}\right)^2}, \qquad \sigma_{y-}(s_c) = \sigma_{y-}(0) \times \sqrt{1 + \left(s_c/\beta^*_{y-}\right)^2} \tag{17}$$

In all calculations discussed here we assume that the transverse distribution of the strong bunch is gaussian. Thus a particular slice of electrons centered at the origin and having horizontal and vertical rms sizes $(\sigma_{x-}, \sigma_{y-})$ is described by the transverse particle density

$$\rho_t(x, y) = \frac{\Delta N_-}{2\pi\sigma_{x-}\sigma_{y-}} \exp\left(-\frac{x^2}{2\sigma^2_{x-}} - \frac{y^2}{2\sigma^2_{y-}}\right) \tag{18}$$

which is normalized to the number of electrons ΔN_- contained in the slice (for the k-th slice, $\Delta N_- = w_k N_-$, where N_- is the total number of electrons in the bunch).

The electromagnetic kick $(\Delta x', \Delta y')$ received by a positron from a thin-slice electron bunch is written in concise form [10, 11] in terms of the complex error function $w(z)$[1] In tracking codes it is important to compute this function as fast as possible because this is the most CPU-intensive part of any beam-beam simulation that assumes a transverse gaussian shape for the bunches. In Ref. [1] we describe four methods of computing $w(z)$. They all yield results that are accurate to better than 1 part in 10^6. However, there are major differences in the computational speed of the different methods; we shall not address this issue here.

Step 4: Restore the coordinates to the reference point. This is the inverse of Step 2, namely

$$x \to x - s_c x', \qquad y \to y - s_c y' \tag{19}$$

while the slopes x' and y' remain unchanged.

Steps 2 and 4 do not cancel each other out because the slopes have changed in Step 3; therefore, in general, the beam-beam kick alters the coordinates as well as the slopes of the particles. For this reason, Step 4 is usually referred to as "disruption." The only circumstance in which there is no disruption occurs when *both* beams have zero bunch length. If only the strong beam has zero bunch length (*e.g.*, if it is represented by a thin lens), the weak beam will still suffer disruption due to the s_c dependence in Step 3 arising from the synchrotron oscillations of its particles.

4. Short-term single-particle tracking results

Here we carry out turn-by-turn tracking for an individual particle at a time with given initial coordinates for a certain number N of turns. *For all cases in this section we completely neglect damping and quantum excitation* in order to eliminate numerical discrepancies arising from random number generators.

We assume that the lattice is decoupled and is described by a pair of 2×2 linear transport maps with given tunes. Similarly, we also assume that the longitudinal dynamics is described by a linear 2×2 map with a given synchrotron tune. We carry out a weak-strong calculation where the dynamical (or weak) beam is

[1] The function $w(z)$ is not to be confused with the weights w_k of the previous section, nor is the complex number z with the longitudinal coordinate z.

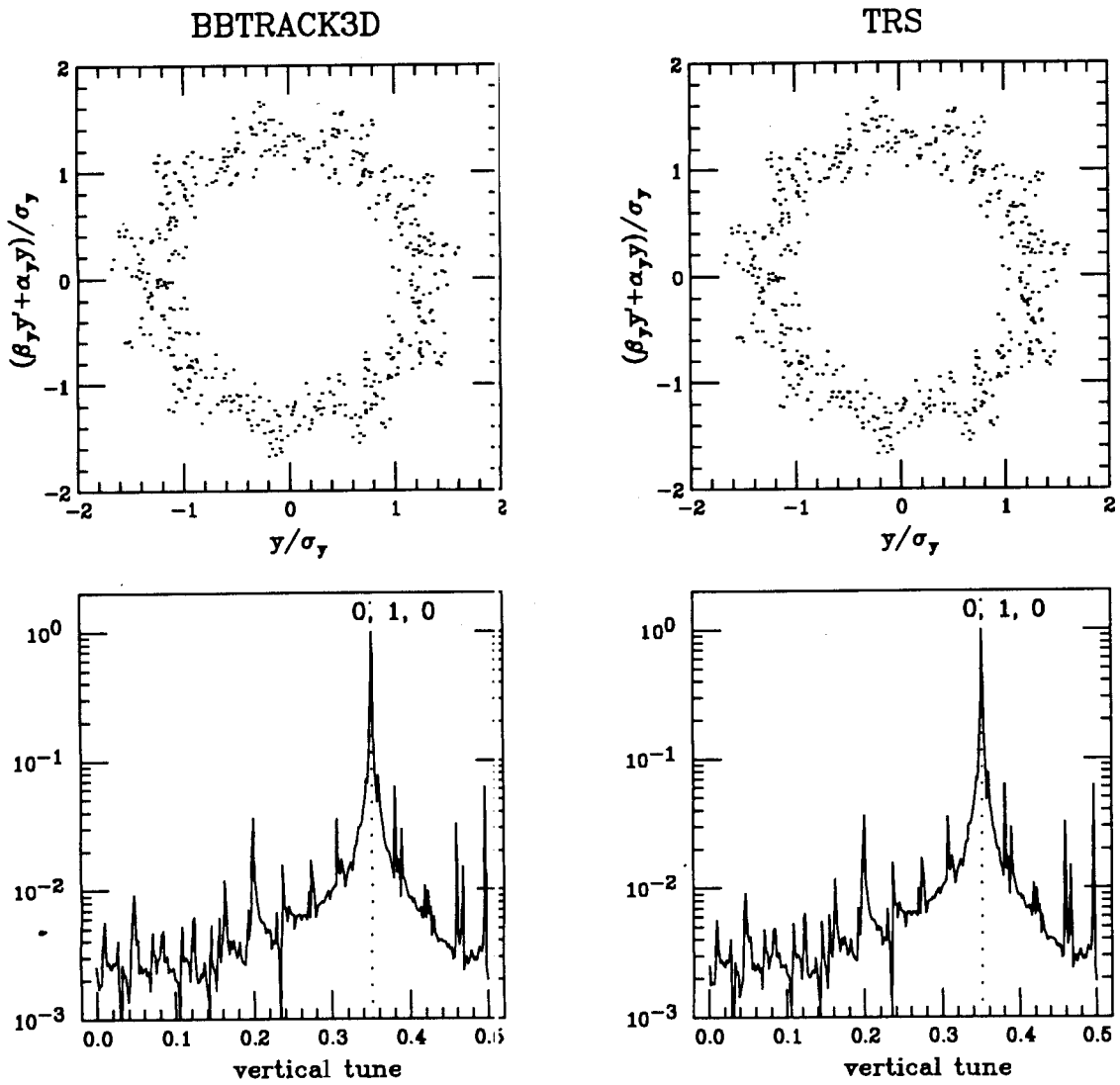


Figure 2: Single particle tracking (BBTRACK3D and TRS, $N = 512$, $N_s = 5$, slicing alg. #2).

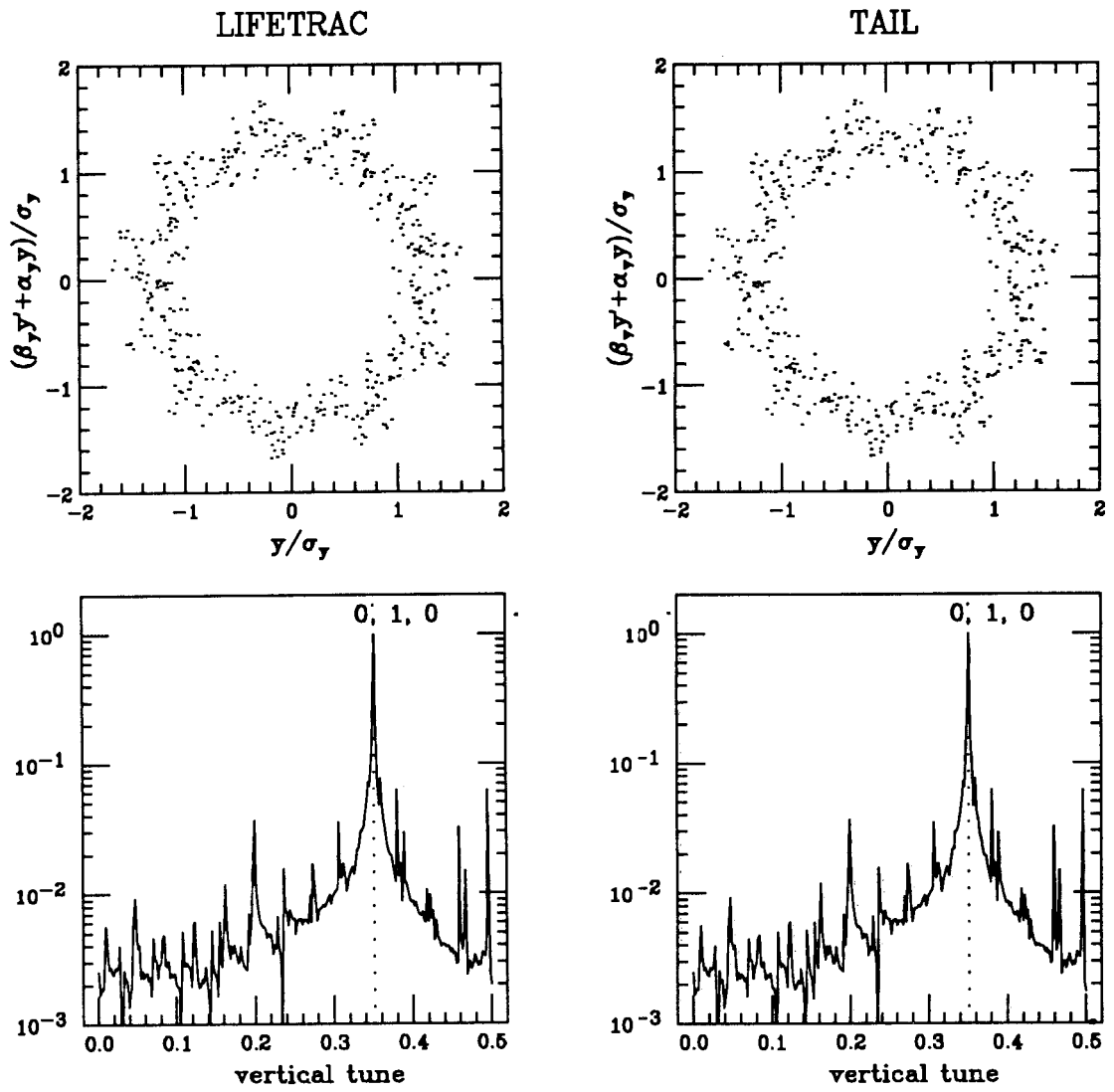


Figure 3: Single particle tracking (LIFETRAC and TAIL, $N = 512$, $N_s = 5$, slicing alg. #2).

Table 3: Parameters used in the simulations.

	weak beam (e^+)	strong beam (e^-)
E [GeV]	3.1	9.0 †
β_x^* [m]	0.375	0.500
β_y^* [m]	0.015	0.020
σ_x [μm]	151.6 †	151.6
σ_y [μm]	6.063 †	6.063
ν_{0x}	0.57	0.57 †
ν_{0y}	0.64	0.64 †
σ_z [cm]	1.0	1.0
ν_s	0.0372	0.0523 †
σ_p/p	0.809×10^{-3}	0.615×10^{-3} †
N	5.630×10^{10} †	3.878×10^{10} †
ξ_{0x}	0.03	0.03 †
ξ_{0y}	0.03	0.03 †

† These parameters do not enter the weak-strong simulation, but we list them nevertheless for the sake of completeness.

the positron beam. The particle distribution of the electron beam is assumed to remain a three-dimensional gaussian whose transverse size is modulated by the beta functions, but whose emittances remain fixed at their nominal values.

The simulation data is obtained as follows: we first assign input values to all six normalized coordinates. The particle then undergoes a linear lattice transport, then a synchrotron map, and finally the beam-beam kick. Immediately after the beam-beam kick, its six normalized coordinates x/σ_x, $x'/\sigma_{x'}$, y/σ_y, $y'/\sigma_{y'}$, z/σ_z and $\Delta p/\sigma_p$ are recorded. This process is then repeated for N turns, with one line of data per turn. The tracking data is processed with the code PORTRAIT [12], from which we obtain all three phase space plots and their corresponding Fourier spectra. Each spectrum is produced as follows: we first compute

$$\tilde{X}_k = \sum_{n=1}^{N} X_n \, e^{2\pi i (n-1)k/N}, \qquad k = 0,\, 1,\, \cdots,\, N-1 \tag{20}$$

where X_n represents here either x/σ_x or y/σ_y or z/σ_z at turn n. We then normalize the spectrum by the largest of the absolute values $|\tilde{X}_k|$'s, and plot these normalized absolute values *vs.* k/N. We only plot the spectrum for the modes $k = 0,\, 1,\, \cdots,\, N/2$ on account of the well-known reflection symmetry of $|\tilde{X}_k|$ about $k = N/2$.

In addition to the spectrum, PORTRAIT computes all three dynamical tunes ν_x, ν_y and ν_z by numerically integrating the three phases over the N turns. We then form the linear combinations $n\nu_x + m\nu_y + l\nu_z$ where n, m and l are positive or negative integers[2] up to a certain maximum absolute value, and we plot a vertical dotted line whenever $n\nu_x + m\nu_y + l\nu_z$ (aliased to the interval $[0, 0.5]$) coincides with a local peak of the spectrum that is higher than a given threshold value. In this way we can identify resonances, which are labeled by the three integers n, m and l on the plots.

The simulation parameters are listed in Table 3. The values in this table are like those considered for the PEP-II B factory [2]; for the nominal PEP-II bunch collision frequency of 238 MHz, these parameters imply a nominal luminosity of $\mathcal{L}_0 = 3 \times 10^{33}$ cm^{-2} s^{-1}.

Comparison of the four codes. We now compare the results of the four codes considered here. In all cases we track for $N = 512$ turns, use $N_s = 5$ kicks, and use slicing algorithm #2. We compute $w(z)$

[2] Except that, without any loss of generality, we choose $n \geq 0$.

by simply invoking the IMSL® library function CERFE [13] except that the code TAIL uses the Padé approximant method [14]. The initial values of the coordinates are $x_0 = 3\sigma_x$, $y_0 = 1.5\sigma_y$, $z_0 = 3\sigma_z$ and $x'_0 = y'_0 = \Delta p_0 = 0$.

In Figs. 2 and 3 we show only the vertical phase space and spectrum obtained from each of the codes. We choose the vertical spectrum because, in our experience, it is more sensitive than the horizontal (and the longitudinal) in showing differences in the results. It can be seen that the codes agree with each other almost perfectly. The tiny differences (typically in the 4th or higher digit of the values of the coordinates) can be accounted for by the differences in the accuracy of the input values and of the different computers used for the tracking (codes TRS and BBTRACK3D were run on the same computer and their results do agree to computer accuracy).

We have carried out many more simulations with different initial conditions, different number of slices and different slicing algorithms. Ref. [1] contains but a small sample of these. The excellent agreement seen in Figs. 2 and 3 is typical of the larger set.

Algorithms for the complex error function. In Ref. [1] we also present a systematic comparison of four algorithms for the computation of $w(z)$: table interpolation to 3rd and 4th order, the Padé approximant method [14], and the IMSL library function CERFE [13]. The result of this exercise is that there are only small differences in accuracy (smaller than 1 part in 10^6), but large differences in computational speed. The table interpolation to 3rd order is the fastest of the four methods.

Effects of deliberate errors. In order to get an idea of the effects of nontrivial algorithmic errors, we show in Fig. 4 the results arising from incorrect coding. The first set in this Figure corresponds to an older version of TRS in which the kick from an individual slice was incorrectly modulated by the local beta function: Step 3 of the beam-beam kick (Eq. (16)) was coded as

$$x' \to x' + (\beta_{x-}(s_c)/\beta^*_{x-})\,\Delta x', \qquad y' \to y' + (\beta_{y-}(s_c)/\beta^*_{y-})\,\Delta y' \qquad \text{(incorrect!)} \tag{21}$$

Other than this difference, all tracking conditions were identical to those used in Figs. 2 and 3. One can see clear differences: the vertical amplitudes reach out to ~ 3 in Fig. 4 rather than to ~ 1.5 in Figs. 2 and 3, and the vertical spectra are substantially different.

As discussed in Sec. 3, Step 4 ("disruption") of the algorithm for the thick lens beam-beam interaction makes the sequence of kicks experienced by the tracked particle noncommutative. The second set of results in Fig. 4 shows the results of deliberately (and incorrectly) reversing the sequence of kicks experienced by the positron for the case $N_s = 5$. As in the previous example, there was no other difference in the tracking conditions from those used in Figs. 2 and 3. The phase spaces are not substantially different, but the vertical spectra are clearly different at the low end.

5. Comparison with analytic results

In this section we compute the tune shift as a function of amplitude obtained from single-particle tracking with TRS and compare the results with first-order perturbation theory calculations. Again, we completely neglect radiation damping and quantum excitation and we use the thin-lens approximation, *i.e.* we take $N_s = 1$ slice in the beam-beam kick algorithm. Depending on the case studied, the particle may or may not perform synchrotron oscillations.

Case with no synchrotron motion. In this case the positron that is being tracked collides at the IP with a single-slice electron bunch. The rms beam sizes of the electron bunch at the IP σ_{x-} and σ_{y-} are understood to be evaluated at the IP.

The analytic calculation we use is described in Ref. [15], except for one detail which we will clarify below. The first step is to recall that the electromagnetic kick from one slice can be written as a two-dimensional vector as

$$(\Delta x', \Delta y') = -\frac{r_e N_-}{2\gamma_+}\,(\mathbf{E} + \mathbf{v}_+ \times \mathbf{B}) = -\frac{r_e N_-}{\gamma_+}\,\mathbf{E} \tag{22}$$

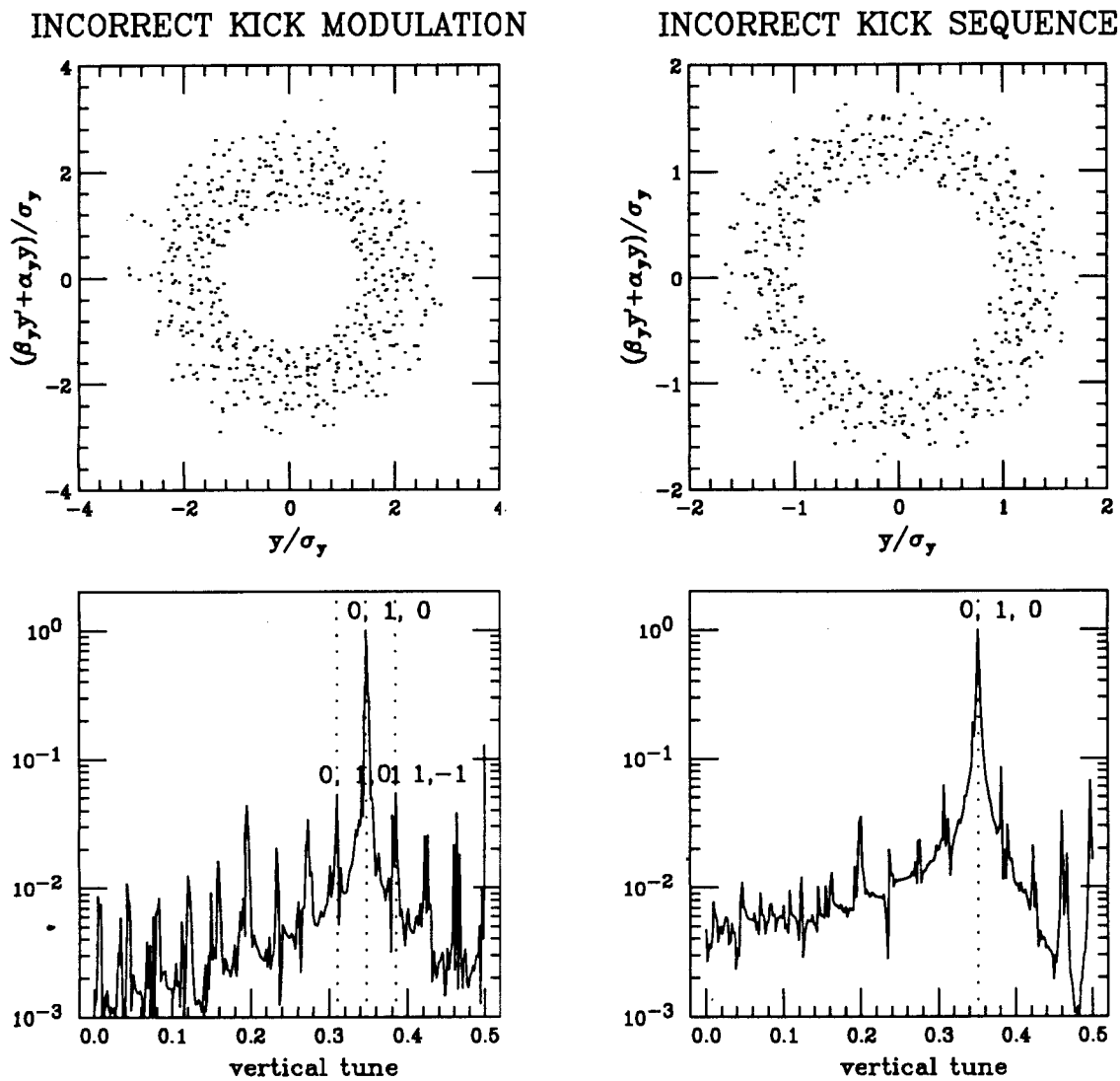


Figure 4: Single particle tracking with two deliberate errors: incorrect modulation of the kicks (Eq. (21), or inverted kick sequence (TRS, $N = 512$, $N_s = 5$, slicing alg. #2).

where the subscripts + and − refer to positrons and electrons, respectively. The electric field per unit charge produced by the electron beam, $\mathbf{E}(x, y, \sigma_{x-}, \sigma_{y-})$, is the solution of Poisson's equation, $\nabla \cdot \mathbf{E} = 4\pi\rho_t$, where $\rho_t(x, y, \sigma_{x-}, \sigma_{y-})$ is the transverse gaussian density, Eq. (18) (since the bunch is represented by a single slice, $\Delta N_- = N_-$). The fact that the magnetic and electric terms in the Lorentz force are equal is a consequence of the extreme relativistic approximation used (we also assume that the positron velocity $\mathbf{v}_+$ is antiparallel to the electron bunch velocity).

If we define the potential V as $\mathbf{E} = -\nabla V$, then the "phase averaged beam-beam parameter" (our nomenclature) of the kicked positron is given by [15]

$$\xi_i = -\frac{r_e N_-}{2\pi\gamma_+}\frac{\partial T_{00}}{\partial I_i}, \qquad i = x, y \tag{23}$$

where T_{00} is defined by

$$T_{00} = \int_0^{2\pi}\frac{d\theta_x}{2\pi}\int_0^{2\pi}\frac{d\theta_y}{2\pi}\, V\left(\sqrt{2\beta^*_{x+}I_x}\cos\theta_x, \sqrt{2\beta^*_{y+}I_y}\cos\theta_y\right) \tag{24a}$$

$$\equiv \left\langle V\left(\sqrt{2\beta^*_{x+}I_x}\cos\theta_x, \sqrt{2\beta^*_{y+}I_y}\cos\theta_y\right)\right\rangle \tag{24b}$$

Here the I's and θ's are the amplitudes and phases of the positron, respectively. The tune shifts of the positron $\Delta\nu_i$ are then obtained by solving the usual equations

$$\cos\left(2\pi(\nu_{0i} + \Delta\nu_i)\right) = \cos(2\pi\nu_{0i}) - 2\pi\xi_i\sin(2\pi\nu_{0i}), \qquad i = x, y \tag{25}$$

where the ν_{0i}'s are the "bare lattice" tunes.

In Ref. [15] the ξ's are assumed to be small enough that the approximation $\Delta\nu_i = \xi_i$ (which follows from Eq. (25) for small enough ξ) is valid. Hence in this approximation $\Delta\nu_i$ is given directly by Eq. (23). Our approach, which involves the extra step (25), can be thought of as a different perturbation expansion that reduces to the conventional one in the small-ξ limit, but that yields *the exact result when the perturbation force is linear.*[3]

It should be noted that $\sqrt{2\beta^*_{x+}I_x}$ and $\sqrt{2\beta^*_{y+}I_y}$ in Eq. (24) are nothing but the injection amplitudes x_0 and y_0 of the positron, respectively (we recall that in all our calculations the initial slopes vanish, $x'_0 = y'_0 = 0$). Therefore, by using the chain rule $\partial/\partial I_y = (\beta^*_{y+}/y_0)\partial/\partial y_0$ and $\mathbf{E} = -\nabla V$ we obtain

$$\xi_y = -\frac{r_e N_-\beta^*_{y+}}{2\pi\gamma_+ y_0}\frac{\partial}{\partial y_0}\left\langle V\left(x_0\cos\theta_x, y_0\cos\theta_y\right)\right\rangle \tag{26a}$$

$$= \left\langle 2\cos^2\theta_y\, \xi_{y\ell}\left(x_0\cos\theta_x, y_0\cos\theta_y\right)\right\rangle \tag{26b}$$

and similarly for ξ_x. We have defined the "local vertical beam-beam parameter" $\xi_{y\ell}(x, y)$ as

$$\Delta y'(x, y) \equiv -4\pi\xi_{y\ell}(x, y)\frac{y}{\beta^*_{y+}} \tag{27}$$

where $\Delta y'(x, y)$ is given by Eq. (22).

As an example, we have used the PEP-II–like parameters listed in Table 3. As before, we tracked the particle with TRS for $N = 512$ turns, used one kick ($N_s = 1$), and used the IMSL® library [13] to compute $w(z)$. Radiation damping and quantum excitation were wholly neglected. The tune was computed with PORTRAIT. The tracked particle was injected with $x_0 = z_0 = 0$, and the vertical amplitude was varied in the range $0 \le y_0 \le 10\sigma_y$. For the analytic calculation, we integrated numerically Eq. (26b). Results are shown in Fig. 5. The agreement is almost perfect.

[3] One of us (MF) is indebted to Étienne Forest for a discussion on this point.

In Ref. [1] we also carried out this exercise for a round beam. In this case the phase integrals can be carried out and the result expressed in closed form. The agreement between tracking and the analytic result is also excellent.

Case with synchrotron motion. In case when the positron is performing synchrotron oscillations, it collides against the opposing thin-slice electron bunch at a longitudinal coordinate $s_c = z/2$ (see Eq. (14)) where z is the positron's longitudinal coordinate at the time of the collision. Thus the vertical kick it receives at the collision point (x, y, s_c) is given by

$$\Delta y'(x, y, s_c) = -\frac{r_e N_-}{\gamma_+} E_y\left(x, y, \sigma_{x-}(s_c), \sigma_{y-}(s_c)\right) \tag{28}$$

and similarly for $\Delta x'$. Here E_y is computed by using the actual beam sizes $\sigma_{x-}(s_c)$ and $\sigma_{y-}(s_c)$ of the electron bunch at the collision point, given by Eq. (17). Therefore it seems clear that the generalization to the present case of the phased-averaged vertical beam-beam parameter is

$$\xi_y = \left\langle 2\cos^2\theta_y\, \xi_{y\ell}\left(x_0\cos\theta_x, y_0\cos\theta_y, (z_0/2)\cos\theta_z\right)\right\rangle \tag{29}$$

where the local vertical beam-beam parameter $\xi_{y\ell}$ is defined by

$$\Delta y'(x, y, s_c) \equiv -4\pi\xi_{y\ell}(x, y, s_c)\frac{y}{\beta_{y+}(s_c)} \tag{30}$$

with a similar expression for the horizontal counterpart. Note that the phase average $\langle\cdots\rangle$ is now three dimensional,

$$\langle\cdots\rangle = \int_0^{2\pi}\frac{d\theta_x}{2\pi}\int_0^{2\pi}\frac{d\theta_y}{2\pi}\int_0^{2\pi}\frac{d\theta_z}{2\pi}\,(\cdots) \tag{31}$$

and that the beta function in Eq. (30) has the appropriate s_c-dependence.

Case when the positron is close to the axis. Fig. 5 shows the tracking results and analytic calculation of the vertical tune plotted as a function of the longitudinal launching amplitude z_0 of the positron (z_0 is normalized to the rms bunch length of the opposing bunch). The particle is tracked with TRS for $N = 512$ turns, with $N_s = 1$, using the IMSL® library calculation of $w(z)$ [13]. The particle is launched close to the beam axis ($x_0 = 0$, $y_0 = \sigma_y/10$), with $x_0' = y_0' = \Delta p_0 = 0$, and z_0 is varied in the range $0 \le z_0/\sigma_z \le 20$.

The three cases displayed in Fig. 5 correspond to different ratios of the beta functions of the two beams (in all 3 cases, however, the beams have the same aspect ratio, $\sigma_x/\sigma_y = 25$). These are dubbed "symmetric," "nominal," and "high asymmetry." The nominal case is exactly the same as that displayed in Table 3. The number of particles per bunch in all three cases are adjusted so that the nominal beam-beam parameters remain fixed at 0.03. Table 4 lists the relevant parameters.

In the three cases the beta functions at the IP of the positron beam are held fixed, and so is the beta-function ratio for each beam, namely $\beta_x^*/\beta_y^* = 25$. Similarly, the beam aspect ratio at the IP is fixed: $\sigma_x/\sigma_y = 25$ for all cases. What changes from one case to the next is the ratio of the beta function of one beam relative to the other: the ratio β_-^*/β_+^* takes on the values 1, 1.333... and 2.666... for the symmetric, nominal and high asymmetry cases, respectively. If the positron did not perform synchrotron oscillations, it is a priori obvious that the tune shift would be the same in all three cases. However, the fact that the beta functions of the *electron beam* are different makes the modulation of the *positron* beam-beam parameter vary from case to case due to the differences in the hourglass effect [16]. In fact, for a flat beam, a simple analytic calculation for the vertical beam-beam parameter of a positron oscillating longitudinally with maximum amplitude z_0 and with $x_0 \simeq y_0 \simeq 0$ shows [16] that $\xi_{y+}(z_0)$ scales like $\xi_{y+}(z_0) \sim \beta_{y+}(z_0/2)/\sqrt{\beta_{y-}(z_0/2)}$. This scaling shows that $\xi_{y+}(z_0)$ grows linearly when $z_0 \gtrsim \beta_{y-}^*$. Also, if β_{y+}^* is kept fixed, as we do in Table 4, the tune shift is larger the larger is β_{y-}^*. Actually, if this scaling formula (properly normalized) is inserted into Eq. (25), the resultant vertical tune is in good qualitative agreement with the more accurate calculations shown in Fig. 5.

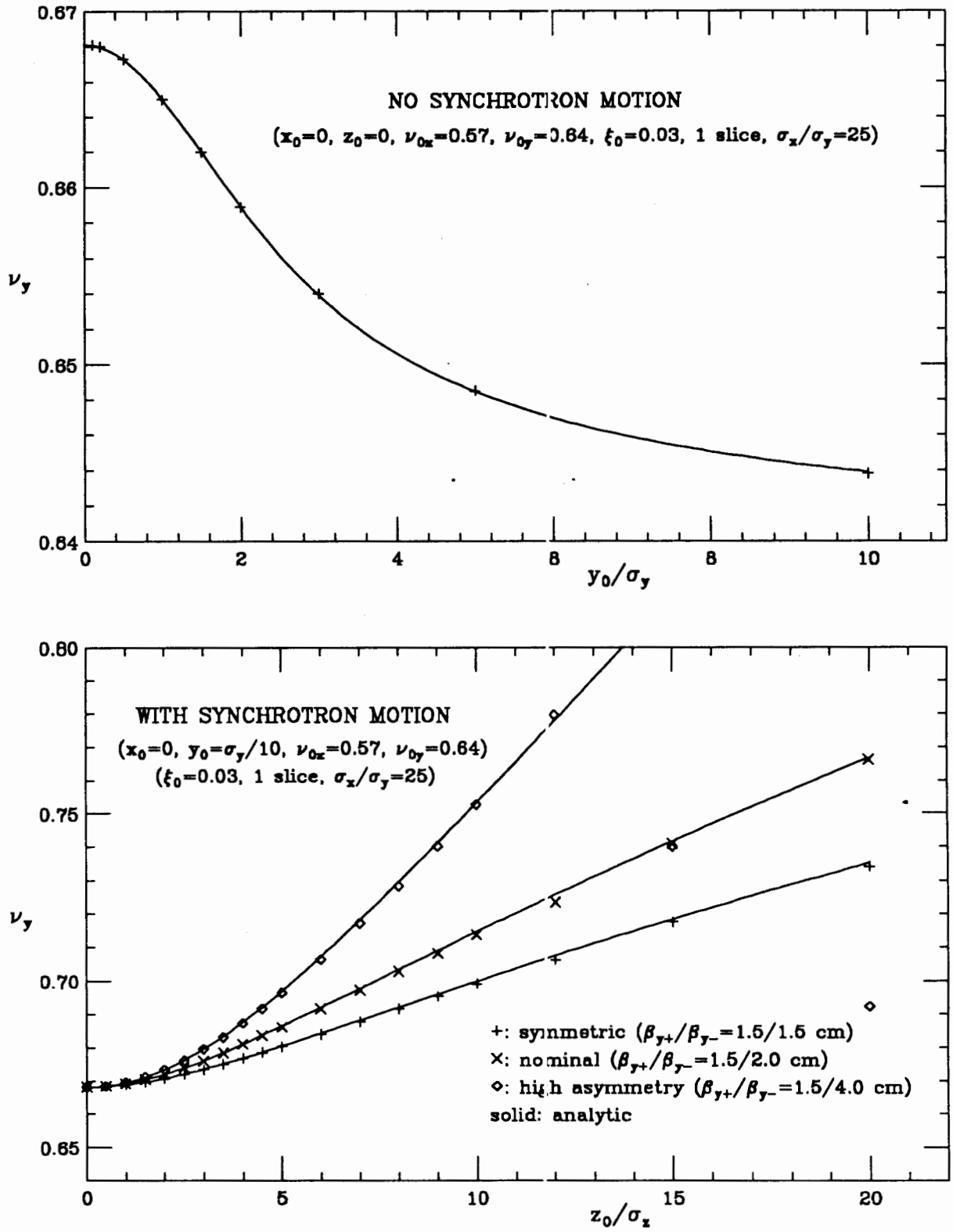


Figure 5: Top: vertical tune *vs.*vertical amplitude with no synchrotron motion; bottom: vertical tune *vs.*longitudinal amplitude for fixed (but small) vertical amplitude. Tracking results (crosses and diamonds) for a single positron colliding against a thin-lens electron beam were obtained with TRS with $N_s = 1$. In all cases the electron beam aspect ratio is $\sigma_x/\sigma_y = 25$; the differences between the three sets of data in the bottom figure are due to the hourglass effect.

Table 4: Parameters used in the three cases with synchrotron motion.

	symmetric		nominal		high asymmetry	
	e^+	e^-	e^+	e^-	e^+	e^-
E [GeV]	3.1	9.0	3.1	9.0	3.1	9.0
β_x^* [m]	0.375	0.375	0.375	0.50	0.375	1.0
β_y^* [m]	0.015	0.015	0.015	0.02	0.015	0.04
σ_x [μm]	131.3	131.3	151.6	151.6	214.4	214.4
σ_y [μm]	5.251	5.251	6.063	6.063	8.574	8.574
ν_{0x}	0.57	0.57	0.57	0.57	0.57	0.57
ν_{0y}	0.64	0.64	0.64	0.64	0.64	0.64
σ_z [cm]	1.0	1.0	1.0	1.0	1.0	1.0
ν_s	0.0372	0.0523	0.0372	0.0523	0.0372	0.0523
σ_p/p [10^{-3}]	0.809	0.615	0.809	0.615	0.809	0.615
N [10^{10}]	5.630	1.939	5.630	2.586	5.630	5.171
ξ_{0x}	0.03	0.03	0.03	0.03	0.03	0.03
ξ_{0y}	0.03	0.03	0.03	0.03	0.03	0.03

For the high asymmetry case, Fig. 5 shows that the tune turns over at $z_0/\sigma_z \gtrsim 12$. This is an artifact of the aliasing inherent in the turn-counting method used to calculate the tune. Aside from this effect, the results are in excellent agreement with the analytic calculation.

Case when the positron is away from the axis. In Ref. [1] we have also computed the tune shift when both the transverse and longitudinal amplitudes are nonzero. Space constraints do not allow us to present the results here. The result is that, when $z_0 > 0$, the tracking and the analytic results agree very well only for small values of y_0. In fact, the tracking results for the tune as a function of y_0 do not follow a smooth curve. In contrast, the analytic curves do behave smoothly. An analysis with PORTRAIT, however, shows that the synchrotron sidebands $\nu_y \pm \nu_s$ are prominent in this region of the amplitude space. It is virtually certain that these sidebands are responsible for the lack of agreement between the tracking and the analytic calculations (the analytic calculation is insensitive to these kinds of resonances, hence the smooth curves).

6. Long-term tracking: amplitude distributions

One-dimensional distributions. The one-dimensional horizontal density is defined by

$$\frac{1}{N_0}\frac{dN}{d\hat{A}_x^2}, \quad \text{with} \quad \hat{A}_x^2 \equiv \frac{x^2 + (\beta_x x' + \alpha_x x)^2}{\sigma_x^2} \tag{32}$$

with corresponding expressions for the vertical counterparts. Here N represents the number of particle-turns at normalized amplitude $\hat{A}$, N_0 is the total number of particle-turns accumulated in the tracking run, x and x' are the position and slope of the particle, α_x and β_x are the usual lattice functions of the weak beam and σ_x is its nominal rms beam size. All these quantities are referred to the observation point, which we chose to be the interaction point.

In this kind of simulation, damping and quantum excitation effects play important roles since the shape of the particle distribution is a consequence of a dynamical equilibrium between these effects and the beam-beam interaction. In Ref. [1] we present the calculation of this density for the five slicing algorithms and for different number of slices with TRS. The result of this exercise is consistent with the discussion in Sec. 2 regarding the convergence rate of the slicing algorithms, and no new information can be extracted within the accuracy of the calculation.

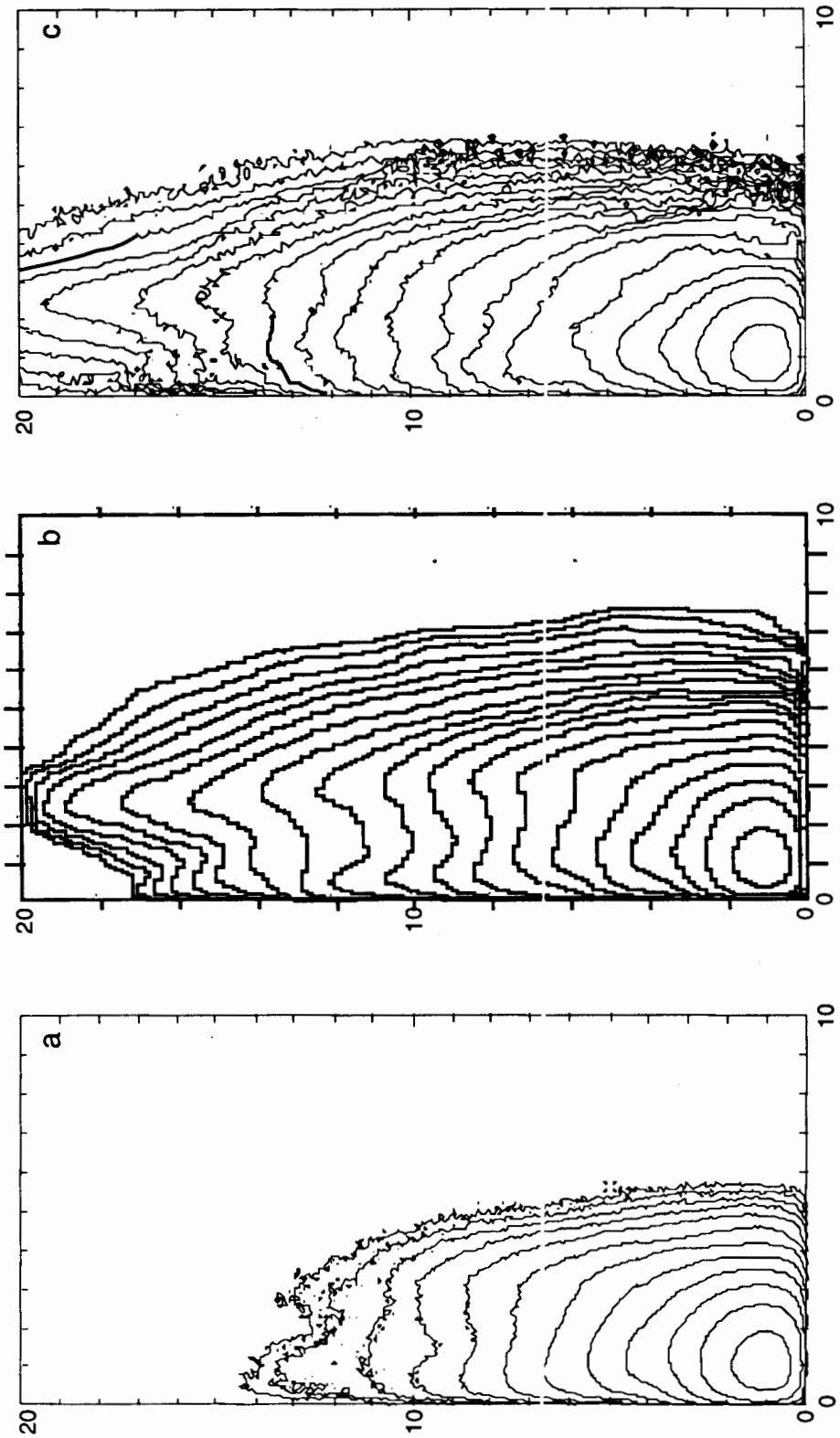


Figure 6: The 2-D amplitude distribution. (a): TRS; (b): LIFETRAC; (c): TAIL. All three cases use 5 kicks; other conditions are described in the text.

Two-dimensional distribution. We now compare the results from the codes TRS, LIFETRAC and TAIL for the 2-dimensional distribution in $(\hat{A}_x, \hat{A}_y)$ space. In this case, we follow the custom of dealing with the density

$$\frac{1}{N_0}\frac{dN}{d\hat{A}_x d\hat{A}_y} \tag{33}$$

which is normalized to unity,

$$\int_0^\infty d\hat{A}_x \int_0^\infty d\hat{A}_y \, \frac{1}{N_0}\frac{dN}{d\hat{A}_x d\hat{A}_y} = 1 \tag{34}$$

For any physical particle distribution, this density vanishes whenever $\hat{A}_x = 0$ or $\hat{A}_y = 0$ due to a zero of the volume element. For reference, the nominal gaussian distribution is

$$\frac{1}{N_0}\frac{dN}{d\hat{A}_x d\hat{A}_y} = \hat{A}_x \hat{A}_y \, e^{-(\hat{A}_x^2+\hat{A}_y^2)/2} \qquad \text{(nominal gaussian)} \tag{35}$$

For the simulation we choose a large beam-beam parameter of 0.08 in order to enhance the tails of the distribution. We achieve this value by scaling N by a factor of 8/3 relative to Table 3. The parameters that are different from Table 3, including the damping times, are displayed in Table 5.

Table 5: Parameters used in the simulations for the 2-D distributions.

	weak beam (e^+)	strong beam (e^-)
N	15.01×10^{10}	6.895×10^{10}
ξ_{0x}	0.08	0.08
ξ_{0y}	0.08	0.08
τ_x [turns]	5400	5014
τ_y [turns]	5400	5014
τ_z [turns]	2700	2507

In these 2-D simulations we use 5 kicks ($N_s = 5$) for all three codes. However, the other conditions are not exactly the same: (1) TAIL uses the Padé approximant method [14] to calculate the complex error function rather than the IMSL® library [13]; (2) TRS uses a slightly different algorithm for radiation damping and quantum excitation from the other codes; and (3) LIFETRAC uses slicing algorithm #5 as opposed to algorithm #2 used by the other two codes.

Figure 6 shows the contour plots for the resultant simulation from the three codes. The contour levels are as follows: the first level is at a height $1/\sqrt{e}$ below the peak, and successive contour levels are at a constant ratio e below each other. The agreement among the codes is quite good given the differences between them.

The code TRS does "brute force" tracking. For the particular simulation shown here, we used 1,024 particles and tracked them for 500,000 turns. Thus we accumulated a total number of particle-turns $N_0 = 0.512 \times 10^9$. The program took 818 CPU minutes to run on the Cray-2S/8128 at NERSC. On the other hand, LIFETRAC and TAIL use an "acceleration algorithm" [17] that optimizes the generation of the tails of the distribution. For the simulation shown in Fig. 6, the results from LIFETRAC correspond to an effective number $N_0 = 4 \times 10^{11}$ of particle-turns and took $\sim$ 100 CPU minutes on a VAX-6610 computer. The results from TAIL correspond to an effective number $N_0 = 6.3 \times 10^{11}$ of particle-turns and took $\sim$ 200 CPU minutes to run on an IBM RS6000/375 computer.

7. Conclusions

We have described a methodical comparison of four beam-beam codes with each other and with analytic calculations. We have carried out single-particle and multiparticle tracking calculations and have computed

the tune shifts with amplitude and the particle density distribution. In general, the agreement is almost perfect when the comparison is meaningful, and the tiny differences can be traced to round-off errors. We have studied the thin and thick lens approximations for the beam-beam interaction in weak-strong mode, different slicing algorithms, and different ways of computing the complex error function. This article is a brief summary of Ref. [1]; more details and more cases studied can be found in there. The good agreement exhibited by the cases shown here and in Ref. [1] are typical of a much larger set that space constraints do not allow us to present.

A study of the convergence rate as the number of kicks $N_s \to \infty$ of the five slicing algorithms shows that #4 is the most efficient. Based on the damping time and on the curves for the convergence rates, we have provided a criterion for the minimum number of kicks that must be used in a given situation for a given algorithm. For the case of the PEP-II nominal design, the adequate number of kicks is 3 for algorithm #4, and 15 for #1.

We found excellent agreement between the tracking results for the tune as a function of amplitude and the corresponding analytical calculations. These calculations were done for one slice, with or without synchrotron motion, for round and for flat beams. We found a discrepancy only in the case when the amplitudes of betatron and synchrotron oscillations are *both* large. In this case, however, the synchrotron sidebands of the vertical tune are prominent. Since the analytic calculation does not take these sidebands into account, the discrepancy is not meaningful.

By using the fourier spectrum of the single-particle motion as a probe, we uncovered errors in earlier versions of the code TRS. It turns out, however, that these errors lead to only minor effects in the multiparticle simulations carried out for PEP-II [2]. However, they might have been more important in other situations. One of our main motivations in carrying out the detailed single-particle comparisons was to look for these errors. It is gratifying that the spectrum of the motion provides such a useful magnifying glass through which to look at the beam-beam interaction.

The two-dimensional particle distributions in amplitude obtained from the three codes TRS, TAIL and LIFETRAC are in good agreement. In this case we do not expect the agreement to be perfect because the codes use different algorithms for slicing, radiation damping and quantum excitation.

As discussed in detail in Ref. [1], there are significant differences in computational speed (but not in accuracy) in the above-mentioned algorithms for the complex error function. In Ref. [1] we also discuss the effects from different slicing algorithms and different number of slices in the computation of the one-dimensional particle distributions; the conclusions from this particular exercise, however, are subsumed by those reached from the other calculations described here.

In summary, we have exhibited results in good agreement obtained with four different beam-beam codes. Although these codes are optimized for different purposes, it is clear that their basic "engines" are doing the same thing. Since the results also are in excellent agreement with analytical calculations, we conclude that the codes are correct to the extent that they involve the same approximations used in these calculations.

8. Acknowledgments

We are grateful to NERSC for supercomputer support.

References

[1] M. Furman, A. Zholents, T. Chen and D. Shatilov, "Comparisons of Beam-Beam Code Simulations," CBP Tech Note-59/PEP-II AP Note 95.04, July 13, 1995.

[2] "PEP-II: An Asymmetric B Factory - Conceptual Design Report," June 1993, LBL-PUB-5379/SLAC-418/CALT-68-1869/UCRL-ID-114055/ UC-IIRPA-93-01.

[3] J. L. Tennyson, undocumented code "TRS," 1989.

[4] D. Shatilov, "Beam-Beam Simulations at I arge Amplitudes and Lifetime Determination," BINP 92-79, Novosibirsk (in Russian).

[5] T. Chen, J. Irwin and R. Siemann, "Simu ation of the Beam Halo from the Beam-Beam Interaction," Phys. Rev. **E 49**, 2323 (1994); "Simulation of the Beam Halo from the Beam-Beam Interaction in LEP," SLAC-PUB-6432, Feb. 1994, to be published in the Proc. 4th annual LEP performance workshop, Chamonix, France, Jan. 1994; "Simulatio ı of the Beam-Beam Lifetime for LEP," SLAC-PUB-6561, June 1994, to be published in the Proc. 4t ı EPAC, London, England, June 27-July 1st., 1994.

[6] M. A. Furman, "The Beam-Beam code BETRACK3D" (to be documented).

[7] J. L. Tennyson, "Tune Considerations for APIARY 6.3D," ABC-28, August 1991.

[8] K. Hirata, H. Moshammer and F. Rugg ero, "A Symplectic Beam-Beam Interaction with Energy Change," Part. Accel. **40**, 205 (1993).

[9] S. Krishnagopal, "Beam-Beam Dynamics with Round Beam Profiles," Ph. D. dissertation, Cornell University, January 1991.

[10] M. Bassetti and G. A. Erskine, "Closed Exp ression for the Electric Field of a Two-Dimensional Gaussian Charge," CERN-ISR-TH/80-06.

[11] M. A. Furman, "Compact Complex Expre sions for the Electric Field of 2-D Elliptical Charge Distributions," Am. J. Phys. **62** (12), Dec. 1994, 1134–1140.

[12] M. A. Furman, "The Tracking Analysis Pr ogram PORTRAIT" (to be documented).

[13] IMSL Math/Library® Reference Manual, v. 10.0.

[14] Y. Okamoto and R. Talman, "Rational Approximation of the Complex Error Function and the Electric Field of a Two-Dimensional Charge Distrit ution," CBN 80-13, Sept. 1980.

[15] R. Siemann, "The Beam-Beam Interaction in e^+e^- Storage Rings," Proc. Joint US-CERN School on Particle Accelerators: *Frontiers of Particle Beams, Factories with* e^+e^- *Rings*, Benalmádena, Spain, October 1992, pp. 327–363 (Springer Verlag Lecture Notes in Physics no. 425, M. Dienes, M. Month, B. Strasser and S. Turner, eds.)

[16] M. A. Furman, "The Hourglass Reduction Factor for Asymmetric Colliders," ABC-21/ESG Tech Note 161, April, 1991 (rev. Aug. 1991); "Hourglass Effects for Asymmetric Colliders," LBL-30833, Proc. 1991 Particle Accelerator Conf., San Francisco, May 6–9, 1991, p. 422.

[17] J. Irwin, "Simulation of Tail Distributions in Electron-Positron Circular Colliders," Proc. Third Advanced ICFA Beam Dynamics Workshop (Beam-Beam Effects in Circular Colliders), I. Koop and G. Tumaikin, eds., Novosibirsk, May 29–June 3, 1989, p. 123.

Decoherence of a Gaussian Beam due to Beam-Beam Interaction

G.V.Stupakov [*], V.V.Parkhomchuk, V.D.Shiltsev [†]

May 15, 1995

Abstract

Using both analytical and numerical approaches, we compute the decoherence function that describes decay of the betatron oscillations of the centroid of an initially offset beam due to head-on beam-beam collisions. Based on this function, the decoherence time is estimated for the Superconducting Super Collider. We also discuss several definitions of the decoherence time arising in different beam dynamics problems.

1. Introduction

When a beam is kicked transversely, its centroid experiences decaying betatron oscillations. the decay is related to the tune spread in the beam, which – depending on a particular case – can be caused by nonlinearity of the lattice, chromaticity of the ring, or beam-beam interaction. decoherence due to the first two sources of the tune spread has been previously studied by Meller *et. al* [1]. However, for the Superconducting Super Collider (SSC) at its full energy of 20 TeV, the main source of the tune spread in the beam comes from the beam-beam interaction. For example, at 20 TeV an effective tune spread is about $\cdot 10^{-4}$ [2],$2 \cdot 10^{-5}$ due to residual chromaticity [3], and about $5 \cdot 10^{-6}$ due to the lattice nonlinearity [3]. The effect is also important in the 8 TeV Large Hadron Collider in CERN.

In this paper, we analyze the decoherence that is produced by head-on beam-beam collisions in the model of strong weak beams and give estimates of the decoherence time.

The importance of the decoherence phenomenon is associated with the fact that in the course of the damping of betatron oscillations the transverse emittance of the beam increases. Characteristic time associated with the damping determines a scale on which coherent oscillations transform to an increment of the emittance. This time is one of the key parameters required for the design of the feedback system needed to suppress emittance growth of the beam [2, 3, 4, 5]. We use two approaches to attack the problem. The first is based on an analytical consideration that reduces the problem of decoherence

[*] *SLAC, Stanford, CA, USA*
[†] *Budker INP, 630090, Novosibirsk, RUSSIA*

to calculation of a 3-dimensional integral. In addition, we performed a computer simulation in which an ensemble of particles was tracked a linear lattice subject to beam-beam interaction. Both methods gave results that agree fairly well with one another.

2. Analytical Consideration

Let us consider two colliding proton round beams with a Gaussian distribution function characterized by the rms beam width σ. due to beam-beam head-on collisions, a particle of a beam having the betatron amplitudes a_x and a_y in x and y directions, respectively, acquires a tune shift in x-direction, equal to [6]

$$\Delta\nu_x(\alpha_1,\alpha_2) = -\xi \int_0^1 du e^{-u(\alpha_1+\alpha_2)} I_0(\alpha_2 u)[I_0(\alpha_1 u) - I_1(\alpha_1 u)], \tag{1}$$

where $\alpha_1 = a_x^2/4\sigma^2$, $\alpha_2 = a_y^2/4\sigma^2$, $I_n(z)$ is the modified Bessel function of the n-th order, and ξ is the usual tune shift parameter, with $\xi = N_p r_p/4\pi\epsilon$, where N_p is the number of particles in the bunch, r_p is the classical proton radius, and ϵ is the normalized emittance. Note that $\Delta\nu_x$ is negative for collisions of particles having the same charge sign. Because of the axial symmetry of the problem, all of our equations remain valid when $x \to y$ and $y \to x$.

In terms of the variables α_1 and α_2, the distribution function of the Gaussian beam has the form

$$\rho(\alpha_1,\alpha_2) = 4e^{-2(\alpha_1+\alpha_2)}, \tag{2}$$

where $\rho(\alpha_1,\alpha_2)$ is normalized so that

$$\int_0^\infty \int_0^\infty \rho(\alpha_1,\alpha_2) d\alpha_1 d\alpha_2 = 1. \tag{3}$$

Using Eqs. (1) and (2) one can find a distribution function over the tune shift, $f(\Delta\nu_x)$, such that $f(\Delta\nu_x)d\Delta\nu_x$ gives the probability for a particle to have the tune shift $\Delta\nu_x$ within the range $d\Delta\nu_x$. The function $f(\Delta\nu_x)$ is given by the following integral:

$$f(\Delta\nu_x) = \int_0^\infty \int_0^\infty \rho(\alpha_1,\alpha_2)\delta(\Delta\nu_x - \Delta\nu_x(\alpha_1,\alpha_2))d\alpha_1 d\alpha_2. \tag{4}$$

Given $f(\Delta\nu_x)$, the average values $< \Delta\nu_x >$ and $< (\Delta\nu_x)^2 >$ are reduced to the following integrals

$$< \Delta\nu_x >= \int \Delta\nu_x f(\Delta\nu_x) d\Delta\nu_x = \int_0^\infty \int_0^\infty \rho(\alpha_1,\alpha_2)\Delta\nu_x(\alpha_1,\alpha_2) d\alpha_1 d\alpha_2, \tag{5}$$

$$< (\Delta\nu_x)^2 >= \int (\Delta\nu_x)^2 f(\Delta\nu_x) d\Delta\nu_x = \int_0^\infty \int_0^\infty \rho(\alpha_1,\alpha_2)\Delta\nu_x^2(\alpha_1,\alpha_2) d\alpha_1 d\alpha_2, \tag{6}$$

with the rms spread $\delta\nu_x$ given by

$$\delta\nu_x = \sqrt{< (\Delta\nu_x)^2 > - < \Delta\nu_x >^2}. \tag{7}$$

3. Decoherence Function

The most complete description of the decoherence process is provided by so-called decoherence function that describes evolution of the beam centroid of a kicked beam. Let $\eta = x_c/\sqrt{\beta}$, where x_c is the centroid offset and β is the beta function. The decoherence function $K(N)$ is defined in Ref. [6] as

$$K(N) = \frac{\eta(N)}{\Delta\theta\sqrt{\beta_0}}, \tag{8}$$

where n is the number of turns, $\Delta\theta$ is the initial kick angle, and β_0 refers to the location of the kick. A mathematical expression for the decoherence function that corresponds to an infinitesimally small initial kick has been derived in Ref. [7]. For our purposes it can be written as follows:

$$K(N) = \int_{-\infty}^{\infty} \sin\left(2\pi N(\nu_{x0} + \Delta\nu_x)\right) f(\Delta\nu_x) d\Delta\nu_x = Im e^{2i\pi N\nu_{x0}} \int_{-\infty}^{\infty} e^{2i\pi N\Delta\nu_x} f(\Delta\nu_x) d\Delta\nu_x, \tag{9}$$

where ν_{x0} is the unshifted tune of the beam. We restrict our attention here to considering only the modulus $\mathcal{K}(N)$ of the complex integral in Eq. (9); it has a meaning of the envelope (or amplitude) of the betatron oscillations produced by the initial kick,

$$\mathcal{K}(N) = \left| \int_{-\xi}^{0} e^{2i\pi N\Delta\nu_x} f(\Delta\nu_x) d\Delta\nu_x \right| =$$

$$= 4 \left| \int_0^{\infty}\int_0^{\infty} \exp\left(-2(\alpha_1 + \alpha_2) + 2\pi i N\Delta\nu_x(\alpha_1, \alpha_2)\right) d\alpha_1 d\alpha_2 \right|. \tag{10}$$

In Eq.(10) we explicitly took into account that the beam-beam interaction produces a tune shift in the range $-\xi < \Delta\nu_x < 0$. It is interesting to note that the tune spread $\delta\nu_x$ (see Eq. (7)) can be related to the second derivative of $\mathcal{K}(N)$ at $N = 0$,

$$\delta\nu_x = \frac{1}{2\pi}\sqrt{-\frac{d^2\mathcal{K}}{dN^2}}\bigg|_{N=0}. \tag{11}$$

4. Results of the Calculations

We computed the decoherence function $\mathcal{K}(N)$ by two methods. In the first, we numerically integrated Eqs. (1) and (10), which together constitute a 3-dimensional integral. In the second, we performed a computer simulation in which an ensemble of up to $2 \cdot 10^5$

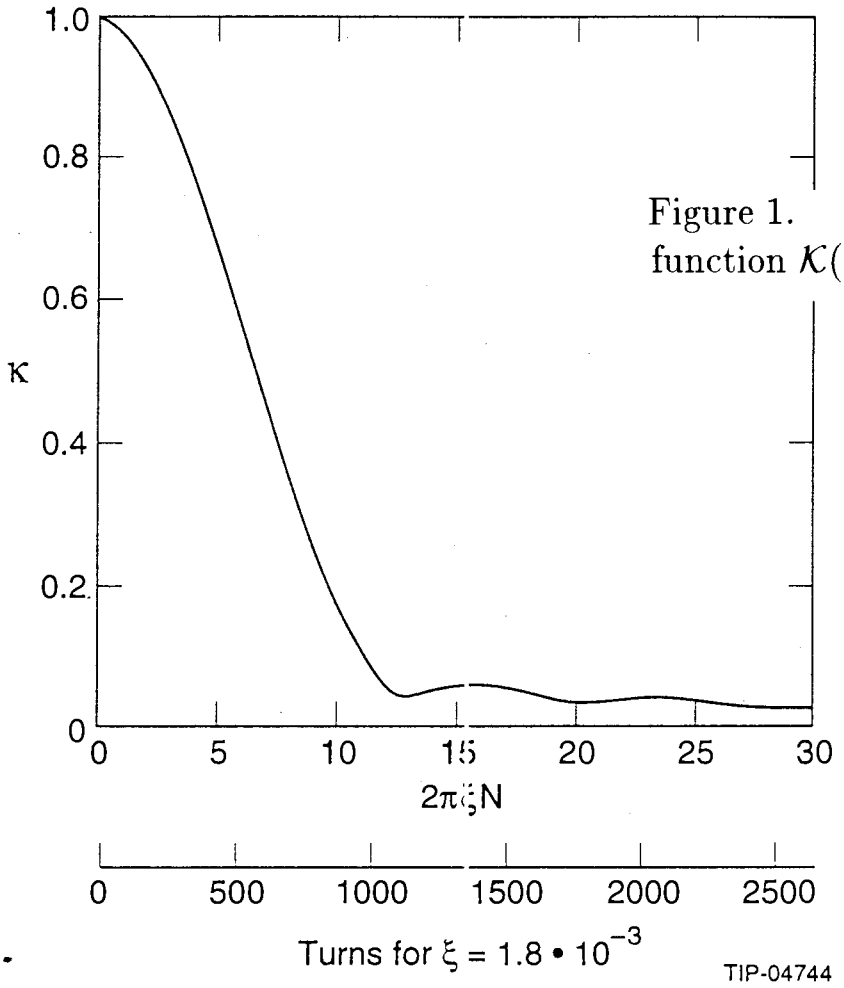


Figure 1. Decoherence function $\mathcal{K}(N)$ vs. $2\pi N\xi$.

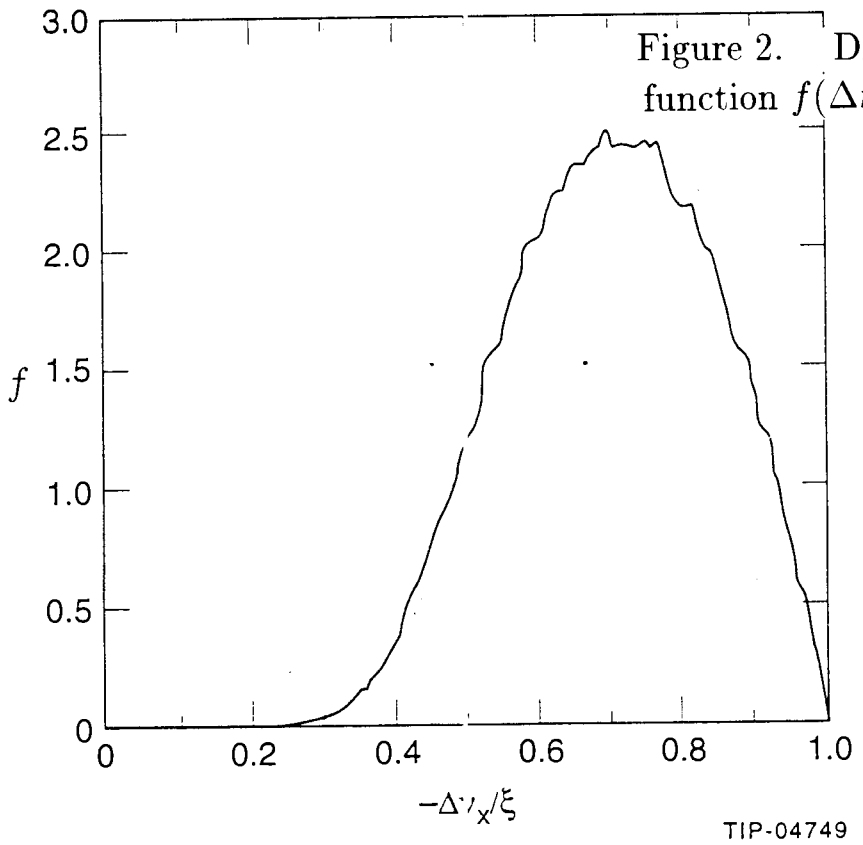


Figure 2. Distribution function $f(\Delta\nu_x)$.

particles with an initial Gaussian distribution function has been tracked several thousand turns subject to a standard linear transfer map, followed by a kick due to the beam-beam interaction. The distribution function $f(\Delta\nu_x)$ of the ensemble has been computed, and with the use of the first part of Eq. (10), $\mathcal{K}(N)$ has been calculated by means of numerical integration. Both methods agree with one another within several percent.

The function $\mathcal{K}(N)$ obtained as mentioned above is plotted in Fig.1 as a function of the variable $2\pi N\xi$. On the same plot we also show a scale with number of turns N corresponding to $\xi = 1.8 \cdot 10^{-3}$ – the nominal value of ξ for the SSC with two interaction regions.

Fig. 2 shows the distribution function $f(\Delta\nu_x)$ found from the tracking simulations. This curve is not ideally smooth (as it has to be) simply because of the limited number of particles used in the simulations. The average values characterizing this function are

$$< \Delta\nu_x >= -0.633\xi, \quad \sqrt{< (\Delta\nu_x)^2 >} = 0.655\xi, \quad \delta\nu_x = 0.167\xi. \tag{12}$$

For comparison, we have also computed decoherence curves for large amplitudes of the initial kick. These curves are plotted in Fig.3 (together with $\mathcal{K}(N)$ from Fig.1) for initial kicks equal to σ and 4σ. They demonstrate the general trend of slower decoherence for stronger kicks.

5. Decoherence Time

Having found the decoherence curve we are now in a position to estimate the decoherence time for the decay of an initial kick. Notice that there is no unique, rigorous definition of the decoherence time. In this section, we present several definitions that arise in different beam dynamics problems.

One can simply define the decoherence time (number of turns) N_{decoh}, as the time needed for the amplitude to go down to half of its initial value, $\mathcal{K}(N_{decoh} = 0.5$. From Fig.1, one finds the following estimate for N_{decoh} so defined:

$$N_{decoh} \approx \frac{1}{\xi} \tag{13}$$

For the SSC collider, where $\xi = 1.8 \cdot 10^{-3}$, this gives $N_{decoh} = 600$ turns.

For a feedback theory, a more relevant definition is associated with the behavior of $\mathcal{K}(N)$ in the region of small N. This is easy justify if one takes into account that a strong feedback systems damps the beam oscillations much more quickly before they decohere.This implies that the only an initial phase of the decoherence process is involved in the residual emittance growth of the beam [4]. Because $\mathcal{K}(N)$ has a quadratic dependence in the limit $N \to 0$, an adequate definition of N_{decoh} in this case is

$$N_{dec} = \left.\frac{1}{\sqrt{-\mathcal{K}''}}\right|_{N=0} = \frac{1}{2\pi\delta\nu_x}, \tag{14}$$

so that $\mathcal{K}(N) = 1 - 1/2(N/N_{decoh})^2$ for $N \ll N_{decoh}$. Our calculations give

$$N_{decoh} = \frac{0.95}{\xi}, \tag{15}$$

which results in $N_{decoh} = 530$ for the SSC.

Yet another N_{decoh} is related to the effect of external noise acting on the beam (without feedback). Assume that at each turn the beam experiences random, uncorrelated kicks of amplitude a_m. Its displacement after N turns is given by

$$\Delta x_c(N) = \sum_{m=1}^{N} K(N-m)a_m. \tag{16}$$

Let us find the average square of the displacement:

$$< (\Delta x_c)^2 >= \sum_{m=1}^{N} K^2(N-m) < a_m^2 >=< a^2 > \sum_{m=1}^{N} K^2(m), \tag{17}$$

where we have employed the condition of uncorrelated kicks $< a_m a_n >=< a^2 > \delta_{mn}$. Now we define the decoherence time N_{decoh} so that

$$< (\Delta x_c)^2 >= \frac{1}{2} N_{decoh} < a^2 > . \tag{18}$$

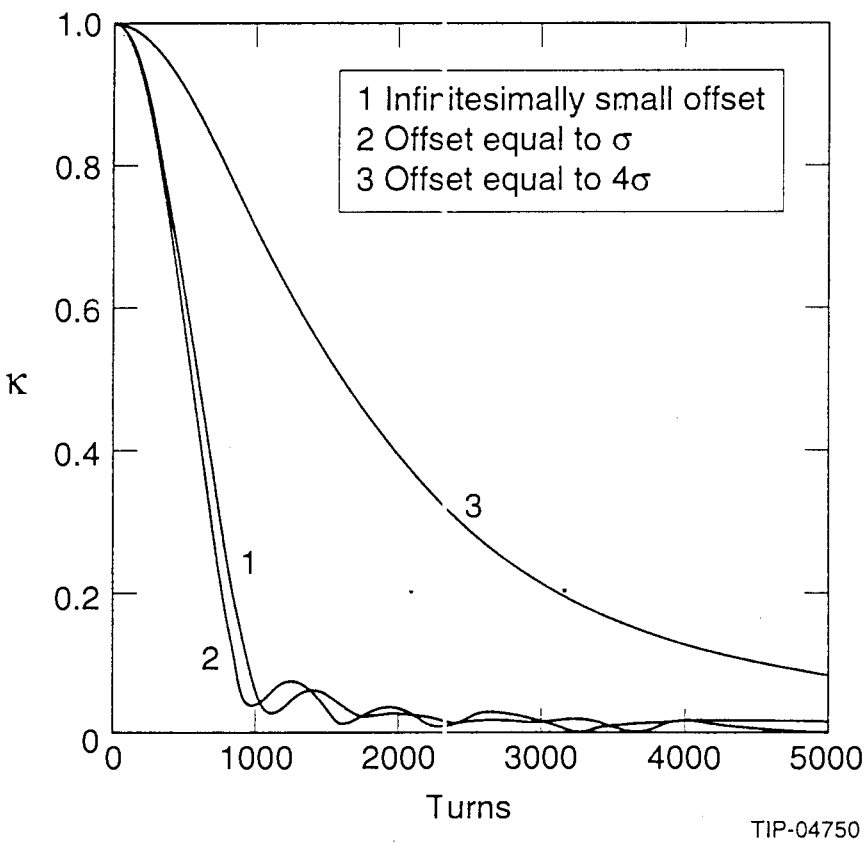


Figure 3. Decoherence curves for various initial offsets.

This gives us the relation,

$$N_{decoh} = 2\sum_{m=1}^{N} K^2(m) \approx \int_0^{\infty} \mathcal{K}^2(m)dm. \tag{19}$$

In Eq. (19) we have considered that $\mathcal{K}(m)$ is rapidly oscillating (with the betatron frequency) function, so that the average its square is equal to half of its amplitude squared. Our calculations give

$$N_{decoh} = \frac{0.81}{\xi}, \tag{20}$$

with $N_{decoh} = 450$ for the SSC. Our computer tracking confirmed Eqs. (18) and (19) within an accuracy of the statistics of the calculations.

6. Summary

In this paper, we have calculated the decoherence function for the head-on beam-beam collisions. This function gives the most complete description of the process, allowing, for example, calculation of the tune spread associated with the beam-beam interaction (see Eq.(11)). Via the Fourier transform, it is directly related to the distribution of the particles over the tune shift $\Delta\nu_x$. What is more important, this function gives us a natural characteristic time scale on which an initially driven betatron oscillation damps out. We have shown that, depending on the exact definition, the expression for N_{decoh} has a form, N_{decoh} =const/ξ, where ξ is the beam-beam tune shift and const$\approx$ 1. Our result generally agrees with the numerical study of the SSC beam decoherence [8].

7. Acknowledgment

The authors are thankful to E.Tsyganov, whose critical remarks initiated this work.

References

[1] R.E. Meller, et. al, "Decoherence of Kicked Beams" , SSC-N-360, 1987.

[2] V.A. Lebedev, V.V. Parkhomchuk, V.D. Shiltsev and A.N. Skrinsky, "Suppression of Emittance Growth Caused by Mechanical Vibrations of Magnetic Measurements in Presence of Beam-Beam Effects in the SSC", Preprint INP 91-120, Novosibirsk, 1991.

[3] W. Chou and J.O. Peterson, "The SSC Transverse Feedback System", SSCL-623, 1993.

[4] V.A. Lebedev, V.V. Parkhomchuk, V.D. Shiltsev and G.V. Stupakov, "Emittance Growth due to Noise and its Suppression with the Feedback System in Large Hadron Colliders", SSCL-Preprint-188, March 1993; and *Particle Accelerators*, vol.44, No. 3-4, pp. 147-164 (1994).

[5] V.V. Parkhomchuk and V.D. Shiltsev, "Is Transverse Feedback Necessary for the SSC Emittance Preservation? (Vibration Noise Analysis and Feedback Parameters Optimization)", SSCL-622, June 1993.

[6] G. Lopez, "Head-On and Long Range Beam-Beam Tune Shifts Spread in the SSC", SSCL-422, 1991.

[7] A. Chao and G.V. Stupakov, "Collective Effects and Beam Decoherence", SSCL-621, April 1993.

[8] E. Tsyganov et. al, "Decoherence of the SSC Beam Oscillation due to Head-On Beam-Beam Collisions", SSCL-Preprint-481, 1993.

COUPLING CORRECTION FOR THE BEAM-BEAM EFFECTS OPTIMIZATION*

D.V. Parkhomchuk

Budker Institute of Nuclear Physics, Novosibirsk, 630090, Russia

e-mail: D.V.Parkhomchuk@inp.nsk.su

1. Introduction

It is the well-known fact that beam-beam effects on the flat beams increase mainly vertical size of the beams. In the absence of beam-beam effects vertical size is generated by betatron coupling, and the horizontal size by quantum excitations. So while the horizontal beam size is defined by magnetic structure and RF acceleration parameters, we have a plenty of methods of placing skew-quadrupoles to generate the same initial vertical beam size. The question is what configuration of coupling should we choose (or avoid) to optimize beam-beam effects.

2. Simulation technique

It's clear that one cannot solve this problem analytically, so the simulation program was written. The program makes the tracking through linearized accelerator structure (VEPP-4M was taken) with variously placed skew-quadrupoles and one interaction point, where beam-beam kick was calculated by complex function Erf, assuming that the beam is short (thus kick doesn't depend on longitudinal motion). Longitudinal motion and beam profile tilt angle were taken into account. Quantum excitation is defined as a random horizontal kick for turn, that produce the calculated horizontal beam size. The excitation of the vertical beam size occurs in skew-quadrupoles.

3. Checkings

The comparison with analytical estimates [1] of vertical beam size was made, to ensure that simulation mechanism is adequate.

$$\begin{bmatrix} \dfrac{<x_\beta^2>}{\beta_x} \\ \dfrac{<x_\beta y_\beta>}{\sqrt{\beta_x\beta_y}} \\ \dfrac{<y_\beta^2>}{\beta_y} \end{bmatrix} = D \begin{bmatrix} \alpha_y \Delta\nu^2 + (\alpha_x+\alpha_y)|Q|^2 & 2\alpha_y Q_1 \Delta\nu & (\alpha_x+\alpha_y)|Q|^2 \\ \alpha_y Q_1 \Delta\nu & 2(\alpha_x+\alpha_y)Q_1^2 & -\alpha_x Q_1 \Delta\nu \\ (\alpha_x+\alpha_y)|Q|^2 & -2\alpha_x Q_1 \Delta\nu & \alpha_x \Delta\nu^2 + (\alpha_x+\alpha_y)|Q|^2 \end{bmatrix} \begin{bmatrix} H_{xx} \\ H_{xy} \\ H_{yy} \end{bmatrix}$$

$$\Delta\nu = \nu_x - \nu_y - m$$

* Work supported by the National Science Foundation under contract NKQ000 №51954

Where:

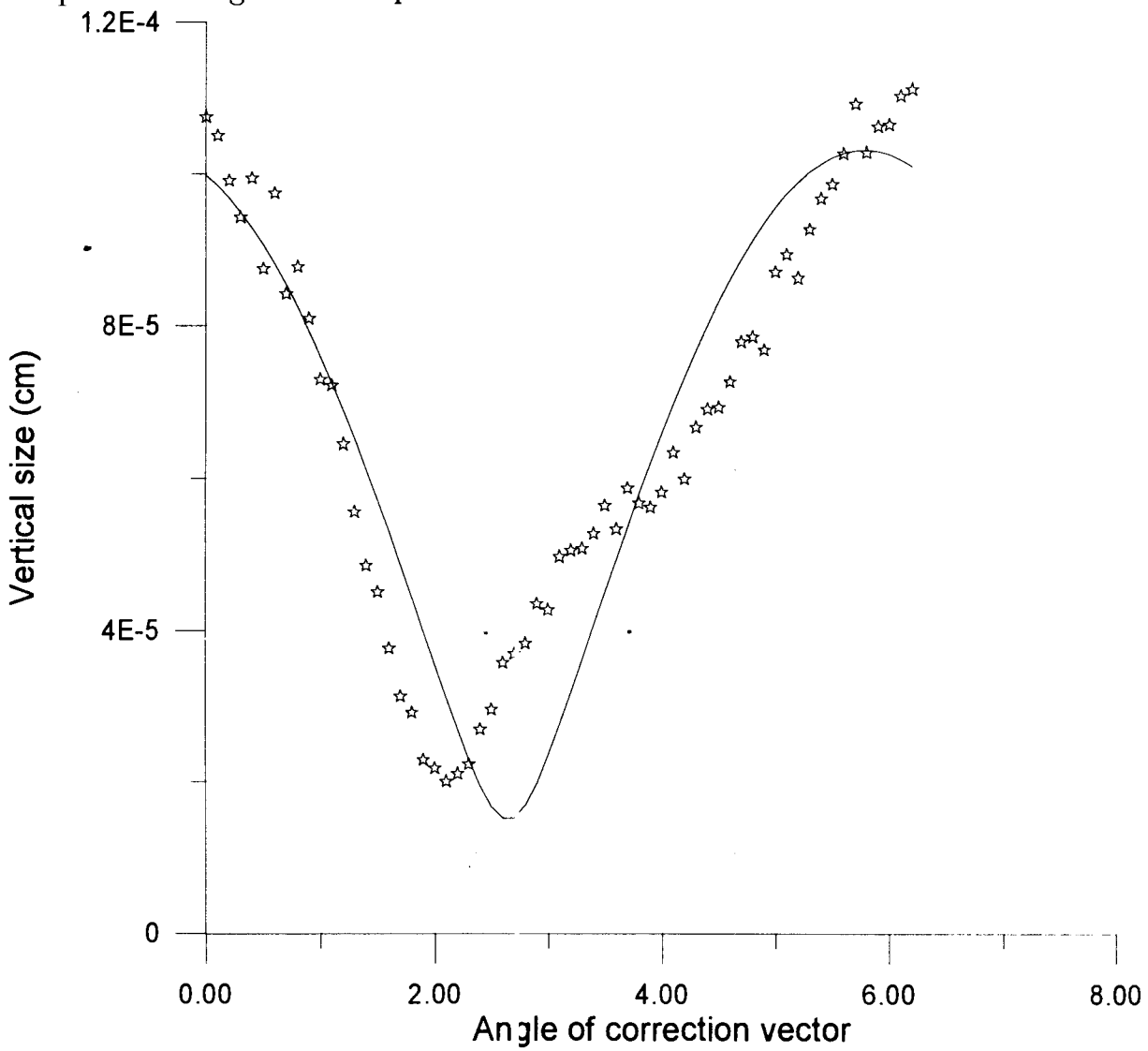
$$Q = Q_1 + iQ_2 =$$

$$= \int_{\theta_r}^{\theta_r+2\pi} d\theta \left\{ \exp\left[i \int_{\theta_r}^{\theta} d\theta \left(\frac{R}{\beta_x} - \frac{R}{\beta_y} - \Delta\nu \right) \right] \right\} \frac{\sqrt{\beta_x \beta_y}}{4\pi R} \left[S_Q - \frac{S_M R}{4} \left(\frac{\beta'_x}{\beta_x} - \frac{\beta'_y}{\beta_y} \right) - \frac{i}{2} S_M R \left(\frac{1}{\beta_x} - \frac{1}{\beta_y} \right) \right]$$

$$H_{ij} = C_L \frac{\gamma^5}{2\pi R} \oint \frac{ds}{|\rho|^3 \sqrt{\beta_i \beta_j}} \left[\eta_i \eta_j + \left(\beta \eta'_i - \frac{1}{2} \beta'_i \eta_i \right) \left(\beta_j \eta'_j - \frac{1}{2} \beta'_j \eta_j \right) \right]$$

with i,j = x,y; β_i, the betatron function; R, the average machine radius; ρ, the radius of curvative in a bending magnet; γ, the beam energy in units of rest energy; and $C_L = 55 r_e \hbar / 48\sqrt{3} m_e = 2.16 \cdot 10^{-19} m^3 / s$. $S_Q(\theta) = (\partial B_x / \partial x) R^2 / B\rho$ and $S_M(\theta) = B_z R / B\rho$, strength of skew quadrupole and solenoid fields; $B\rho$, the particle rigidity.

In this terms a skew-quadrupole generate a certain Q. So having a basis of a pair of skews we can suppress any coupling by making Q=0. The example of such compensation is given in the picture.

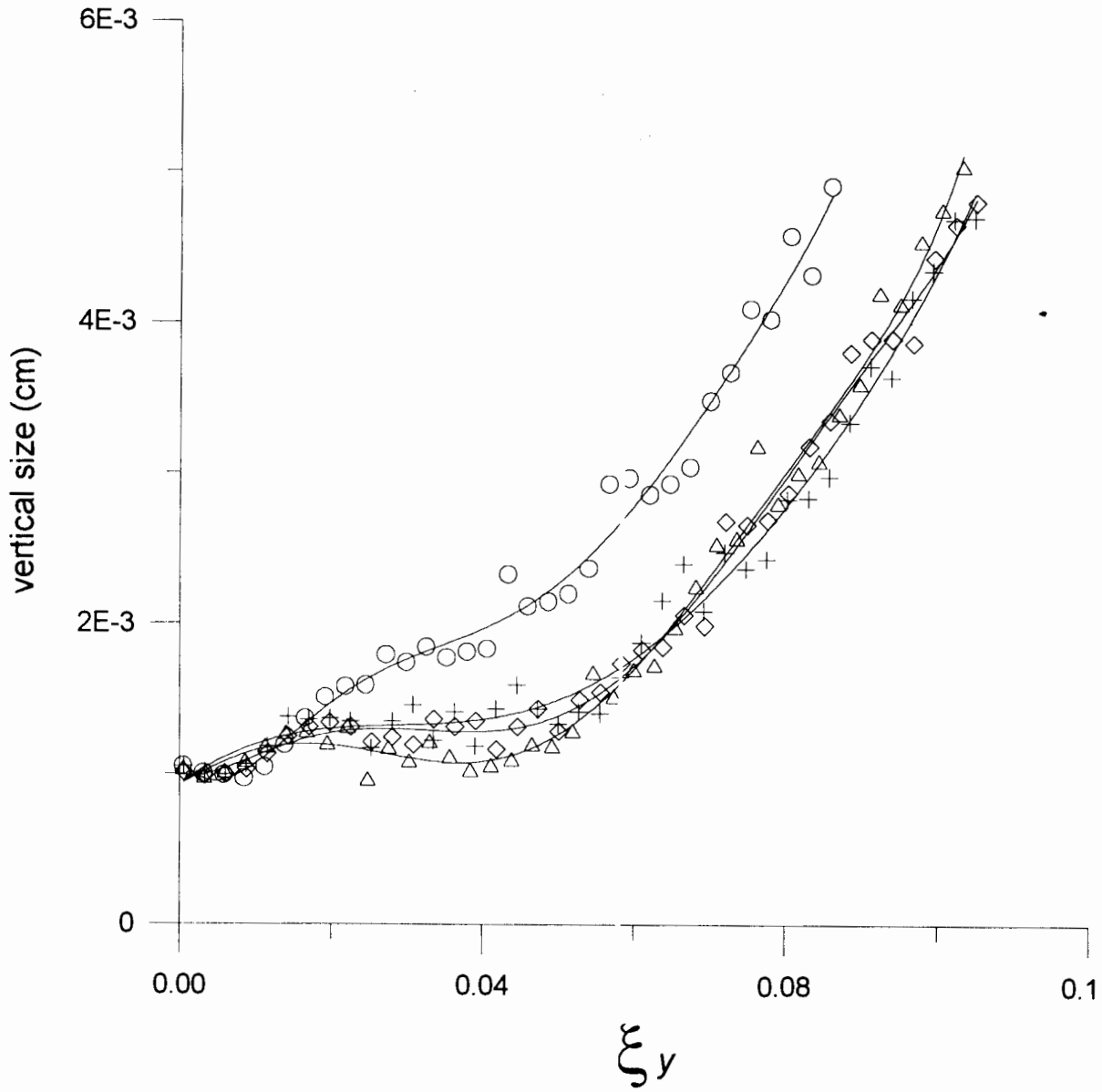


On the picture is shown the behavior of vertical beam size when there is the coupling error in the ring, and we rotate the correction vector Q with the same modules as error by the pair of skews. In one point we see the compensation, there correction vector is opposite to error vector.

So we can partly compensate the random coupling error or coupling caused by detector's solenoids by pair of skew. The picture shows rather well agreement tracking with analytical formulas for vertical size in coupled lattice without beam-beam effects.

4. Results

The different skew placement at different working point was treated to find out the "bad" and "good" type of coupling. It was not find out any preferable coupling configuration, when the coupling produced by each coupling element is less than total coupling ('no compensation' case). But when there is the compensation (the total coupling is less than the coupling of some elements) one can notice the difference. Let us look at the graphs:



Here we can see the dependence of the vertical beam size on the strength of beam-beam effects with different coupling configuration. Three of them are slightly different, but the fourth is extremely bad - the vertical size blow up at relatively low linear tune shift. As I mentioned above it is a case of 'coupling compensation'. Presently such a situation takes place on VEPP4-M, and to improve it, the localization of coupling errors is investigated now.

5. Conclusion

So one can extract the useful advice from here. It's obvious that beam-beam effects cause the shifts of coupling vectors of elements. So if one makes the compensation by elements whose coupling is more than final coupling, the shifts of them produce large shift of final coupling and compensation is destroyed.

If there are coupling errors or solenoids, coupling must be corrected by skews or solenoids which are close to the place of error and have the collinear (opposite) to the error coupling vectors, because in that case the shifts of those vectors don't produce large shift of total vector.

REFERENCES

1. A.W.Chao and M.J.Lee, "Vertical Beam Size due to Orbit and Alignment Errors," (1977).
2. Stephen Val Milton, "The Beam-Beam Interaction in Electron Storage Rings: A Study if the Weak/Strong Case," (1990).
3. M.Bassetti and G.Erskine. CERN ISR-TH/80-06 (1980).
4. M.Sands, "The Physics of Electron Storage Rings," Stanford Linear Accelerator Center Report SLAC-121 (1970).
5. G.Guignard, "The General Theory of All Sum and Difference Resonances in a Three-Dimensional Magnetic Field in a Synchrotron," CERN 76-06 (1976)
6. A.W.Chao and M.J.Lee, J. Appl Phys. 47, No. 10, 4453 (1976).

Summary of Working Group II
Multibunch Head-on Beam-Beam Effects

Coordinator **V.I. Balbekov**, IHEP, Protvino

Meetings of the Working Group covered a wide range of topics in 9 reports presented, and were attended by approximately 15 participants.

The general expression is that the most reliable and widely applied tool to treat beam-beam effects is computer tracking. Three major techniques were presented: (1) macroparticle technique, (2) the "slice" one, and (3) division of bunch into sub-regions with effective boundary conditions.

E. Simonov (BINP) has presented the straightforward approach to beam-beam effects — method of macroparticles. The scheme involved 300 × 300 macroparticles × 10^5 turns. It was applied to VEPP-2 collider in a "strong-strong" approximation. The questions studied were the transverse beam size blow-up as a function of current, and evolution of the beam-beam tune shift. The latter shows a certain maximal value around 0.1 after which it decreases with the beam current. In discussions, Dr. A. Lebedev has drawn attention to the problem of fluctuational noise of the model due to a small number of macroparticles and a relativistic compression of the electromagnetic field. A proper smoothing technique in which 300 macroparticles would represent a "grid" carrying information on the interaction, or at least a practical test of the method's convergence with N increasing should be carried out. It may well be that coherent beam-beam effects are smeared out by this very fluctuational noise.

D. Parkhomchuk (BINP) has presented computer studies of various scenarios to control the vertical beam blow-up (flat beam with ratio 17) with a family of skew quadrupoles to compensate transverse coupling imposed by lattice and beam-beam interaction. The problem of coupling compensation is by itself surely a standard one, but it is of a great practical importance for optimal tuning of the operating machine to increase its luminosity.

V. Shiltsev (BINP) has studied round Gaussian unbunched counter-rotating beams in a "weak-strong" approximation. It was shown that a nonlinear beam-beam field is a source of an incoherent betatron tune shift which is quite comparable to the one imposed by the lattice nonlinearities. The studies were performed in terms of a decoherence time of the kicked-off beam centroid. This time is an important input parameter to design a transverse feedback system to suppress the emittance growth. The feedback should provide damping time less than a typical decoherence time.

A. Gerasimov (FNAL) and K. Hirata (KEK) have drawn attention to another aspect of nonlinear beam-beam field in a "strong-strong" approximation. Coherent oscillations at large amplitudes were studied. The existence of large-amplitude steady-state solutions at π-mode is shown which, essentially, are the new orbits closed after several turns. The discussion has appreciated the methodical value of the paper. Still, a cautious feeling was expressed by Drs. P. Zenkevich and V. Shiltsev that such solutions might have no practical consequence as in this case the collider's luminosity vanishes.

D. Shatilov (BINP) and A. Zholents (LBL) have presented in details a promising approach to computation of a phase-space evolution of beams based on division of the beam portrait into sub-layers with effective boundary conditions stated in terms of "emitting absorbing walls". The approach saves a lot of CPU time and offers a reasonable estimates of beam lifetimes with many effects included: resonances, residual gas scattering, dispersion at interacting point, etc. The program was applied to PEP-2 facility. Much effort has been spent to verify the code by comparing its results with the ones available ¿from other codes.

S. Arutunian and M. Mailian (YPI) has drawn attention to the necessity of studies of the detailed microstructure of the relativistically compressed fields of colliding bunches moving along curvilinear trajectories. The effect might be important for the next generation of colliders, including the linear ones, with a large density of particles inside bunches.

V. Danilov (BINP) has proposed to make practical use of the fact that there exist integrable nonlinear systems. The idea is to add an extra nonlinear lens to the nonlinear lattice so as to build up an integrable nonlinear system which would allow one to eliminate at all, or at least control, stochastic layers and thus govern the dynamic aperture, beam blow-up due to beam-beam interaction etc. Such an approach seems to be interesting in principle, and may well imply practical use of given further detailed studies of the problem in question.

Working Group III
Multibunch Beam-Beam Manipulations

The program of the beam-beam effects study on the VEPP-4M

G.M.Tumaikin

Budker Institute of Nuclear Physics (BINP),
630090, Novosibirsk, Russia, e-mail: tumaikin@inp.nsk.su

The program of the beam-beam effects study on the collider VEPP-4M, that was put into operation after reconstruction, is discussed. There are two motives for this work: first, the increasing of the VEPP-4M luminosity and, second, getting the necessary experience for the φ-, $c-\tau$- and b-factories future projects.

INTRODUCTION

The study of the beam-beam effects in BINP was begun about 30 years ago on electron beams collider VEP-1, when for the first time the influence of nonlinear resonances on beam size and lifetime was investigated. Then experiments were continued on electron-positron colliders VEPP-2, VEPP-2M and VEPP-4 in Novosibirsk, as well as in facilities of other physical centers: ACO (ORCE), Adone (Frackati), SPEAR (Standford), DORIS (Hamburg) etc. The review of results of these experiments was submitted in series of papers[1].

Simultaneously with experimental researches for expired 30 years the large work on theoretical study of beam-beam effects is conducted. Two approaches are here allocated: analytical, based on Hamiltonian formalism, and computer simulation. In the few last years the computer simulation was more successful.

Nevertheless, the wide circle of problems for experimental and theoretical study is marked. The decision of these problems is necessary as for increasing of luminosity on existent collider generation, as for building of the future one.

The program of work on the VEPP-4M discussed below has by purpose the study of small part of unsolved problems.

1. DESCRIPTION OF THE VEPP-4M

The VEPP-4 accelerator facility includes the injection facilities and the collider VEPP-4M. The collider after stoppage in 1985 was considerably modernized[2]. First, the optics of the experimental insertion was considerably changed for the conducting of the experiments on two-photon physics, that permits now to measure energy of scattered electrons (positrons) in process $e^+e^- \to e^+e^- + X$ with high accuracy. Second, the β-function in collision point is reduced, and the multibunch mode with orbit separation in parasitic crossings (PC's) is arranged to increase the luminosity. In the interaction point (IP) the new detector KEDR is placed, enabling carry out the wide program on b-meson physics and two-photon physics.

The main parameters of the VEPP-4M are represented below.

Energy, GeV	6
Circumference, m	366
Bending radius, m	45.5
Betatron frequencies Q_x, Q_z	8.53, 7.57
Compaction factor	0.017
Horizontal emittance, mm * mrad	0.3
Vertical emittance, mm * mrad	0.001
Energy spread, %	0.1
SR loss, MV/turn	4
Synchrotron oscillation damping time, msec	2
Harmonic number	222
Bunch length, cm	4
Space charge parameters ξ_x, ξ_z	0.005, 0.05
Number of particles per bunch	$2 * 10^{11}$
Number of bunches per beam	2
Beam current, mA	50
Luminosity	$7 * 10^{31}$

The interaction point

A number of collision points	1
Vertical β-function, cm	5
Horizontal β-function, cm	70
Dispersion function, cm	80

The parasitic crossings

Type of separation - vertical electrostatic bump.

A number of crossings	3
Vertical β-function, cm	1200, 290
Horizontal β-function, cm	460, 1400
Dispersion function, cm	78,-125

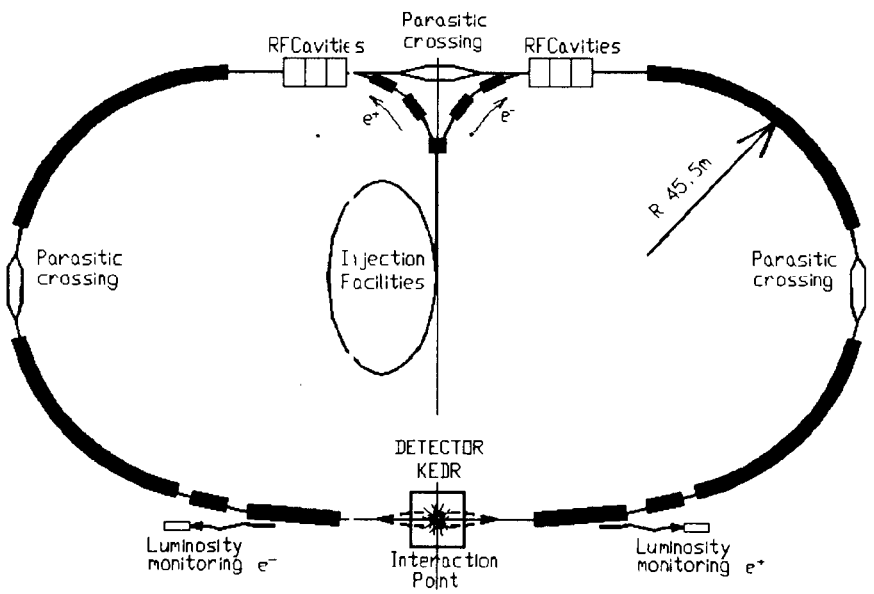


Fig.1. Interaction points on the VEPP-4M.

2. PROGRAM OF EXPERIMENTS

It is assumed to do the work in following directions which are briefly stated below.

2.1. COUPLING OPTIMIZATION FOR THE ACHIEVEMENT OF THE UTMOST SIGNIFICANCE OF SPACE CHARGE PARAMETERS ξ

Usually in electron-positron colliders in the IP's the following equations are valid:

$\sigma_x^* >> \sigma_z^*$, $\xi_z >> \xi_x$, where * denotes "in the IP".

Hence, beam-beam effects mainly increase the vertical beam size, that conducts to reduction of the luminosity and the lifetime.

It is known, that the initial vertical beam size at small currents is basically defined by the magnetic field distortion. It is possible to allocate the following main causes of excitation of initial beam size:

- quantum fluctuations of synchrotron radiation in locations with large vertical dispersion function,
- coupling resonances $n\nu_z \pm m\nu_x = k$,
- vertical dispersion in collision point,
- vertical distortion of the orbit with presence of the chromaticity.

It is expected, that the displacement of these elements concerning IP strongly influences the dynamics of counter beams even in the case of the same initial vertical beam size.

Thus, the goal is to find such a way of achieving initial vertical size at which the beam-beam effects will be minimal. To resolve this problem it is necessary to reduce the coupling, and then to find the optimum parameters of skew-quadrupoles.

2.2. INFLUENCE OF LARGE RADIAL DISPERSION

The other goal is the study of the beam-beam effects in the mode with a large dispersion function in the IP. It is important to understand which value of ξ can be obtained and how the beams will behave in the case where the betatron horizontal beam size is substantially less than the synchrotron one.

This study is necessary for the projects of the b- and $c-\tau$- factories with monochromatization of the interaction energy, where the particles are distributed by energy over the interaction region. The modern optics of VEPP-4M allows us to change the betatron-synchrotron size ratio at the IP within wide limits.

2.3. PARASITIC CROSSINGS

The third goal is the study of the PC's influence and determination of the optimal orbit separation. This task is connected with the arranging of the multibunch mode in the VEPP-4M. It is known, at present time the arranging of the multibunch mode is the main method of increasing the luminosity in existing and future colliders.

3. RESEARCH DESIGN AND METHODS

3.1. SIMULATION

The program of research work comprises three problems. They are the investigation of the beam-beam effects in the high dispersion function mode and the study of coupling and PC's influence.

All problems will be solved by numerical simulation which in the first place includes the calculation of the beam size, luminosity, and the lifetime. The simulation will be mainly performed in the weak-strong model. To fulfill this research work, we have a series of programs used earlier. We are going to use the fast tracking technique emerged from a concept proposed earlier by J.Irwin[3]. It has been developed later by D.Shatilov[4,5] for calculation of the lifetime and for beam halo determination. This technique allows us to reduce the required CPU time by several orders of magnitude against the brute-force technique.

The conditions of the problems require new programs, in particular, to study the strong-strong beam regime. The program for study of influence of various methods of vertical beam size generation on beam-beam effects in the weak-strong model is prepared. The first results show that the beam-beam effects dynamics depends on the method of generation of initial size[6]. The program for study of coherent interaction of counter bunches (strong-strong model) in view of PC's influence[7] is developing.

3.2. EXPERIMENT

The appropriate techniques and apparatus have been developed. They comprise:

a) luminosity monitoring by single and double bremsstrahlung and by the small angles scattering;
b) beam size measurement by synchrotron radiation;
c) equilibrium orbit measurement;
d) measurement of optic parameters (β-function and ψ-function);
e) automatic measurement of betatron oscillation frequency;
f) dynamic aperture measurement.

ACKNOWLEDGEMENTS

The author thanks all participants of executed program, especially D.Shatilov, E.Simonov, D.Parkhomchuk and S.Karnaev.

The author expresses a deep gratitude to Soros Fund for support of this work (Grant number NQKOOO).

REFERENCES

1. G.M.Tumaikin, A.B.Temnykh *Beam-beam Interaction and Luminosity Limit in Storage Rings* Proc. of the XIII Int. Conf. on High Energy Accelerators, Novosibirsk, 1986, v.2, p.88
2. I.Ya.Protopopov *Electron-Positron Colliding Beams in Novosibirsk. Status and Projects* Proc. of the XIII Int. Conf. on High Energy Accelerators, Novosibirsk, 1986, v.1, p. 63 (in Russian)
3. J.Irwin *Simulation of Tail Distributions in Electron-Positron Circular Colliders* Third Adv. ICFA Beam Dynamics Workshop, Novosibirsk, 29 May - 3 June, 1989
4. D.N.Shatilov *Beam-beam Simulations at Large Amplitudes and Lifetime Determination* INP 92-79, Novosibirsk, 1992
5. D.N.Shatilov, these proceedings
6. D.V.Parkhomchuk, these proceedings
7. E.A.Simonov, these proceedings

SYNCHRO-BETATRON COUPLING IN CRAB CAVITIES

Y.Alexahin

Joint Institute for Nuclear Research, Dubna 141980 Russia

1. Introduction

As proposed in Ref.[1], mutual tilt of the colliding bunches in schemes with finite crossing angle could be eliminated with the help of the so-called crab cavities, thus avoiding excitation of synchro-betatron resonances (SBR's) by the beam-beam interaction. At the same time, if the transverse kicks received by particles in the crab cavities do not exactly compensate each other they themselves can drive SBR's. In the present report the effect of chromatic and amplitude dependence of the betatron phase advance between the crab cavities is analytically estimated.

2. Hamiltonian formalism

Crab cavities located at distances $s=s_\pm$ contribute to the Hamiltonian a term

$$H_1 = \sum_{\pm} \frac{V_{cc}}{B\rho}\, x \cdot \sin\left(2\pi f_{cc}\frac{\sigma}{c}\right)\cdot\delta\left(s-s_\pm\right), \tag{1}$$

where σ is longitudinal displacement from the synchronous particle. Crab voltage V_{cc} should be chosen so as to obtain at the IP compensating tilt $x/\sigma=\alpha$ with respect to the closed orbit, where α is the crossing half-angle:

$$\frac{V_{cc}}{B\rho} = \frac{c\alpha}{2\pi f_{cc}\sqrt{\beta_x^*\beta_x^{cc}}}\,. \tag{2}$$

Assuming synchrotron amplitude being small, introducing action-angle variables I_x, ψ_x for the transverse motion, expanding (1) in the Fourier series and retaining only the resonant term one gets

$$H_1 = \frac{\alpha}{\pi\sqrt{2\beta_x^* R}}\cos\left[\phi_x(s_+) - (Q_x - n)\frac{s_+}{R}\right]\cdot\sigma\sqrt{I_x}\,\exp\left[i\left(\psi_x - n\frac{s}{R}\right)\right] + \text{c.c.}\,, \tag{3}$$

where n is the nearest integer to the betatron tune Q_x and R is the machine average radius. As can be seen from (3) the crab bump closure condition $\phi_x(s_+)=\pi(2k-1)/2$ renders H_1 negligible.

For the longitudinal motion action-angle variables may be introduced by relations

$$\sigma = \sqrt{\frac{2\alpha_M R I_s}{Q_s}}\cdot\cos\psi_s, \quad \delta_p = -\sqrt{\frac{2Q_s I_s}{\alpha_M R}}\cdot\sin\psi_s, \tag{4}$$

α_M being the momentum compaction factor and Q_s the synchrotron tune.

3. Chromatic effect

The width of SBR excited due to chromatic dependence of the betatron phase advance between the crab cavities was found in Ref.[2]. We revise this effect here in order to estimate the amount of energy being exchanged between longitudinal and transverse oscillations outside the resonance.

Without special correction the betatron phase advance from IP to the crab cavity is a function of momentum deviation δ_p:

$$\phi_x(s_+)=\frac{\pi}{2}(2k-1)+\phi'_x\cdot\delta_p,\quad \phi'_x=\int_0^{s_+}\frac{1+\frac{1}{4}\beta_x'^2}{\beta_x}ds\cdot \tag{5}$$

Let us for certainty assume Q_x to be above integer. Then employing (4) and retaining only the terms responsible for the Q_x- $2Q_s$=n resonance we obtain:

$$H_1=(-1)^k\frac{\alpha\phi'_x}{\pi\sqrt{2\beta_x^*R}}I_s\sqrt{I_x}\sin\left(\psi_x+2\psi_s-n\frac{s}{R}\right)\cdot \tag{6}$$

Performing canonical transformation to new variables

$$I_+=\frac{1}{5}(2I_s+I_x),\ I_-=\frac{1}{5}(I_s-2I_x),\ \psi_+=\psi_x+2\psi_s-n\frac{s}{R},\ \psi_-=\psi_s-2\psi_x, \tag{7}$$

with the help of generating function

$$F_2=I_+\left(\psi_x+2\psi_s-n\frac{s}{R}\right)+I_-(\psi_s-2\psi_x) \tag{8}$$

we finally arrive to the Hamiltonian

$$H=H_0+H_1=\frac{1}{R}\left\{\Delta_+I_+-C_2\sqrt{I_+-2I_-}\cdot(2I_++I_-)\sin(\psi_+-\psi_k)-(2Q_x+Q_s)I_-\right\}, \tag{9}$$

where ψ_k is some constant,

$$\Delta_+=Q_x-2Q_s-n,\ C_2=\frac{\alpha\phi'_x}{\pi\sqrt{2\beta_x^*}}.$$

Since the resonance is nonlinear, its width depends on the initial oscillation amplitudes. Let us assume that longitudinal oscillations were excited by quantum emission or the Touschek effect, so that

$$I_{+0}=\frac{2}{5}I_{s0},\quad I_-=I_{-0}=\frac{1}{5}I_{s0},\quad I_{s0}=\frac{\alpha_M R}{2Q_s}\delta_{po}^2. \tag{10}$$

Outside the resonance stop-band phase trajectories of the Hamiltonian (9) describe beating between horizontal and longitudinal oscillations, the maximum value of the horizontal action variable being

$$I_x^{max}=I_+^{max}-2I_{-0}=\left[\frac{|\Delta_+|-\sqrt{\Delta_+^2-8C_2^2I_{s0}}}{4C_2}\right]^2\approx\left(\frac{C_2I_{s0}}{\Delta_+}\right)^2. \tag{11}$$

For a particle not to be lost on the physical aperture the condition $2I_x^{max}<A_x$ should be satisfied, which according to (10,11) imposes a limitation on the synchrotron amplitude

$$\frac{\alpha|\phi'_x|\alpha_M R}{2\pi\sqrt{2\beta_x^*}Q_s|\Delta_\pm|}\delta_p^2<\sqrt{A_x}\cdot \tag{12}$$

Let us take as an illustrative example the JINR TCF design [3] parameters: $\alpha_M=1.6\cdot10^{-2}$, $R=0.6\cdot10^2$m, $Q_s=0.01$, $|\Delta_+|=0.15$, $\beta_x^*=0.5$m, $\alpha=0.012$, $\phi'_x\approx-20$. Then the maximum stable synchrotron amplitude is $\delta_p=0.012$, which may noticeably affect the beam lifetime.

4. Amplitude effect

The beam-beam interaction introduces amplitude-dependent betatron phase shift, which to the first order in the beam-beam parameter ξ_x is

$$\Delta\phi_x(s_+)=\pi\xi_x\left[1-\frac{\sin(2\pi Q_x-2\phi_x(s_+))}{\sin(2\pi Q_x)}\right]=2\pi\xi_x\cdot \tag{13}$$

From (3), (4) and (13) we obtain the $Q_x - Q_s = n$ resonance term

$$H_1 = \frac{1}{R} C_1 \sqrt{I_x I_s} \sin\left(\psi_x + \psi_s - n\frac{s}{R}\right), \quad C_1 = (-1)^{k-1} 2\alpha\xi_x \sqrt{\frac{\alpha_M R}{\beta_x^* Q_s}} \cdot \tag{14}$$

Due to synchro-betatron coupling (linear in the present case) a particle with initial synchrotron amplitude δ_{p0}, outside the resonance ($\Delta = |Q_x - Q_s - n| > 2|C_1|$) will acquire maximum horizontal amplitude corresponding to the action variable value

$$I_x = \frac{C_1^2}{\Delta^2 - C_1^2} I_{s0} = \frac{1}{2}\left(\frac{2\alpha\xi_x \alpha_M R}{\sqrt{\beta_x^* \Delta Q_s}} \delta_{p0}\right)^2 \cdot \tag{15}$$

With the given above set of the TCF parameters and $\xi_x = 0.05$ and $\delta_{p0} = 6 \cdot 10^{-4}$ one gets $2I_x = 433$ nm which should be compared with the design emittance value $\varepsilon_x = 388$ nm [3].

5. Conclusions

Chromatic and amplitude dependence of the betatron phase advance between the crab cavities can lead to an appreciable synchro-betatron coupling affecting lifetime and/or luminosity. These dependencies might be compensated with nonlinear elements installed between the crab cavities, as it is proposed in the KEK B-factory project [4] for the case of chromatic dependence. But the possibility of an octupole correction of the amplitude effect seems to be doubtful due to a large value of the beam-beam betatron phase shift.

As follows from (15) the amplitude effect may be reduced by pulling Q_x further from the integer value, as well as by:

a) decreasing ξ_x;

b) decreasing α_M;

c) increasing Q_s;

The first two remedies are inherent to schemes with monochromatistion in collision energy. The possibility of combining monochromatization and crab-crossing was considered in Ref.[5].

References

[1] K.Oide, K.Yokoya, Phys.Rev.A, 40, p.315 (1989).

[2] S.Kurokawa, D.Pestrikov, Proc. 1993 PAC, Washington, v.1, p.295.

[3] P.Beloshitsky, E.Perelstein, "Horizontal Crab-Crossing Scheme for TCF". *in* Proc. 2nd Workshop on JINR C-Tau Factory, Dubna, 1993

[4] Y.Funakoshi, "Simulations on Crab Cavity System", this Workshop.

[5] Y.Alexahin, "A Scheme of Monochromatic Tau-Charm Factory with Finite Crossing Angle", Proc. 2nd Workshop on JINR C-Tau Factory, Dubna, 1993.

Invariants for Nonlinear Accelerator Optics and Round Colliding Beams

V.V. Danilov and E.A. Perevedentsev
Institute of Nuclear Physics, 630090, Novosibirsk, Russia
E-mail: danilov@inp.nsk.su

Abstract

A model accelerator lattice composed of cells each consisting of a thin nonlinear lens and a drift space is studied. The corresponding one-dimensional nonlinear map of the "accelerator" type is proved to have an exact invariant, provided that the nonlinear kick function(s) are of a special form.

The proposed 1- and 2-cell lattices have invariants expressed as polynomials up to the sixth order in momentum. The results obtained for one-dimensional motion are partially carried over to the two-dimensional case, particularly, to the systems preserving angular momentum. Among those the round colliding beams are considered.

An example of elimination of chaotic trajectories in the motion by adding one lens is presented supporting interest in using integrable systems for improving the dynamic aperture and raising the threshold of the beam blow-up due to the beam-beam effects.

1. Introduction

Recent studies in mathematical physics show a growing interest in integrable systems. In accelerator physics, an integrable system means a one-turn map with the necessary number of commuting and independent integrals of motion. If the manifold of particle motion in the phase space is closed (the motion is finite), we can describe this motion in terms of invariant Liouville tori.

This integrable system is an analogue of a linear system, but its frequencies depend on the values of the integrals of motion. No chaotic trajectories will appear in this map.

It was shown in paper [1], that an accelerator lattice composed of cells consisting of thin nonlinear lenses and drift spaces can have a map with simple (polynomial) integrals.

This paper contains all the results of [1] re-derived by means of a new approach, and furthermore new one-dimensional integrable systems are obtained. Using this approach, we can "cure" certain nonlinear maps from chaos. In other words, we can modify certain nonlinear maps by adding one lens of the special form (which depends on the initial map), such that the stochastic trajectories disappear. The new map is still nonlinear, but integrable. As an example, the Hénon map is "cured" from chaos. This new approach gives a possibility of obtaining integrable systems even for the beam-beam effects.

The results are then extended to the two-dimensional case, and a lattice is presented which can be used as a prototype lattice for a real accelerator.

Cell Map

construct model accelerator lattices consisting of one or two cells with a nonlinear lens. In the map considered, we put $p = x'$, where x' is the slope, and take the drift length $l = 1$ to simplify formulas. The map one cell is:

$$\begin{aligned} \overline{x} &:= x + p, \\ \overline{p} &:= p + f(\overline{x}). \end{aligned} \tag{1}$$

nitial values and $\overline{x}$, $\overline{p}$ are the final values of the coordinate and momentum. nction of the nonlinear lens to be found jointly with the desired invariant. or an invariant I is:

$$I(x,p) \equiv I(x+p, p+f(x+p)) . \tag{2}$$

ss evident that it is too difficult (or impossible) to find a general solution equation, so we have to look for invariants with simple dependence on the omentum (see, for example [2, 3]).

general properties of an invariant of 1-cell map (assuming that it exists). t is convenient to use the variables $x, \overline{x} \equiv x + p$ instead of x, p ($\overline{x}$ means the end of drift space).

rkable property of an invariant of one cell is that **it is a symmetrical** l $\overline{x}$ *i.e.* it does not change when permuting x and $\overline{x}$. Let us prove this. ng of the drift space we have the coordinate x while $\overline{x}$ is the coordinate at ve start the motion from the end of the drift space in backward direction d sign of p), we have the same motion (because this transformation is rsal of time) with the initial coordinate $\overline{x}$ and the final one $x \equiv \overline{x} + (-p)$. ion starts from the beginning of the drift space (we mean that the end of he beginning of it for motion with time reversal), so this reversed motion ctory in the phase space and the same invariant (but the initial and final rmuted), hence we get:

$$I(x,\overline{x}) \equiv I(\overline{x},x) . \tag{3}$$

t this property holds only if we take the beginning (or the center) of the initial point for the map. In the linear case this property is related to the ptical functions about the center of the drift space in such a cell.

he second important property of this invariant. Directly from definitions d variables we have:

$$\begin{aligned} I(x,\overline{x}) = I(x, x+p) = I(\overline{x}, \overline{x}+\overline{p}) , \\ I(x,\overline{x}) = I(\overline{x}, x) = I(\overline{x}, \overline{x}-p) . \end{aligned} \tag{4}$$

of the first and second lines in (4) we have:

$$I(\overline{x}, \overline{x}+\overline{p}) = I(\overline{x}, \overline{x}-p) , \tag{5}$$

is the momentum after kick.

Thus, we can obtain the invariant behind the lens from the invariant before the lens by changing p to $-\overline{p}$. In other words, **transformation of the invariant on the lens** (adding its kick to the momentum) **is equivalent to sign reversal of the momentum argument** in this invariant.

These two properties are necessary and sufficient for a function I to be an invariant. It means that if we can find a function with these two properties, we have an integrable system automatically, while the kick of the nonlinear lens is no more arbitrary, its coordinate dependence is determined by the second property (5) of our invariant).

The theory just developed will now be illustrated by an example, which is significant in itself.

Note that an arbitrary function quadratic in momentum has the second property (5). Let it be $H(x,p)$:

$$H(x,p) = A(x)p^2 + B(x)p + C(x) .$$

For the new $\overline{p} = p + B(x)/A(x)$,

$$H(x,\overline{p}) = A(x)\overline{p}^2 - B(x)\overline{p} + C(x) .$$

We can see that this function expressed in the new momentum has the same form but with the opposite sign of the momentum.

Let us make a very important notice: substitution of $p + g(x)$ instead of p (where $g(x)$ is an arbitrary function of the coordinate) does not change the second property (5) of the invariant, but we have to change the kick function of the lens.

So if we have the second property (5) for p, we have the same property for the variable $\overline{x} = p + x$, and the quadratic invariant in p is also quadratic in $\overline{x}$ (it comes from the definition of $\overline{x}$). Finally we come to a very simple conclusion: every function quadratic in $\overline{x}$ and symmetrical in x and $\overline{x}$ yields an invariant.

A general form of this function is:

$$I(x,\overline{x}) = ax^2\overline{x}^2 + bx\overline{x}(x+\overline{x}) + cx\overline{x} + d(x^2+\overline{x}^2) + e(x+\overline{x}), \tag{6}$$

here a, b, c, d, e are arbitrary constants.

Let us obtain the lens kick from I. We have to change x to $\overline{x} - p$ to obtain the invariant at the end of the drift space in the form:

$$I = A(\overline{x})p^2 - B(\overline{x})p + C(\overline{x}).$$

From the second property (5) of our invariant we have:

$$I(\overline{x}, \overline{x} - p) = I(\overline{x}, \overline{x} + \overline{p}), \tag{7}$$

where $\overline{p} = p + f(\overline{x})$ is the momentum after the kick. After substituting $p = \overline{p} - f(\overline{x})$ into the invariant at the end of the drift space and using the previous equation we get:

$$A(\overline{x})(\overline{p} - f(\overline{x}))^2 - B(\overline{x})(\overline{p} - f(\overline{x})) + C(\overline{x}) = A(\overline{x})(\overline{p})^2 + B(\overline{x})\overline{p} + C(\overline{x}). \tag{8}$$

This equation yields:

$$f(\overline{x}) = -B(\overline{x})/A(\overline{x}). \tag{9}$$

So we have got the general rule: if we take the invariant after the lens, the kick of this lens is equal to the certain function whose addition to the momentum is equivalent to the sign reversal of the momentum in the invariant.

In general, the second property (5) holds for all functions of the form:

$$f_0(x) + f_1(x)(p^2 - F(x)p) + f_2(x)(p^2 - F(x)p)^2 + \ldots, \tag{10}$$

here $f_0, f_1, f_2, \ldots$ are arbitrary functions of the coordinate.

Let us introduce a notion which will often be used later: F in (10) will be called a Sign Reversal Function (SRF). We can check the second property of the invariant in (10) by substituting $p + F(x)$ instead of p.

As we noted earlier, if we put p in the form $p = p' + G(x)$, this property remains for p' too, but the new F in (10) now is:

$$F_{new}(x) = F(x) - 2G(x) .$$

For the variable $\overline{x} = p + x$ the Sign Reversal Function $F_{\overline{x}}$ is:

$$F_{\overline{x}} = F(x) + 2x . \tag{11}$$

For the invariant (6) the SRF for $\overline{x}$ is:

$$F_{\overline{x}} = -\frac{bx^2 + cx + e}{ax^2 + bx + d} .$$

So the perfect kick of the lens must be:

$$F(x) = -2x - \frac{bx^2 + cx + e}{ax^2 + bx + d} . \tag{12}$$

The same formulas were obtained in [1] in other way[1].

Now we can present one more system with a new invariant:

$$I(x, \overline{x}) = (ax\overline{x}(\overline{x} - x) + b(x + \overline{x})(\overline{x} - x) + c(\overline{x} - x))^2, \tag{13}$$

here a, b, c are arbitrary constants.

This invariant has the form (10) and it is a symmetrical function of $x, \overline{x}$. The kick of the lens for this case is:

$$F(x) = -2x + \frac{ax^2 - c}{ax + b} . \tag{14}$$

It was shown in [1], that the invariants of the third degree in momentum cannot appear in 1-cell maps. Now one can be assured that polynomial invariants with odd highest powers in momentum do not exist at all. We can note that such functions do not have the second property (5) of one cell invariant, because we can never reverse the sign of the highest odd power of momentum by adding any function of coordinate to the momentum. It proves the above statement about polynomial invariants with an odd highest power in momentum.

Moreover, after investigation of invariants of higher order in momentum, a preliminary conclusion can be drawn: it is doubtful that other invariants with finite order in momentum exist, besides (6) and (13).

[1] Recently we became aware of previous work by E.M. McMillan et al. [4], where the rational nonlinear kick (12) and the symmetric form of the invariant (6) were studied in certain particular cases. We are grateful to B.V. Chirikov for this reference and for the useful discussion.

3. Two-Cell Map

Let us take the function $J(x,\overline{x})$, which has the form (10) for x and $\overline{x}$ (or, in other words, this function has only the second property of the invariant for a 1-cell map for both variables x and $\overline{x}$, and is allowed to be non-symmetrical). The Sign Reversal Functions can be different for x and $\overline{x}$.

Let us transform this function over the two cells. Transformation over the drift space means just simply expressing the new x,p in terms of the old ones. Transformation over the lens again means expressing the new momentum $\overline{p}$ via p, and we require that this transformation be equivalent to replacing p by $-\overline{p}$ (it follows from the definition of the SRF F).

Now we have to use the indices of variables which mean the cell number for example, $\overline{x}_1$ means the coordinate at the end of the first drift space. It is evident that the coordinate at the end of the drift space is equal to the coordinate at the beginning of the next cell ($\overline{x}_0 \equiv x_1$, etc.).

Let us start from the beginning of the first cell and transform J to the beginning of the second one:

$$J(x_0,\overline{x}_0) \equiv J(\overline{x}_0 - p_0,\overline{x}_0) \equiv J(\overline{x}_0 + p_1,\overline{x}_0) \equiv J(\overline{x}_1,x_1)\ . \tag{15}$$

So the transformation of the function J over one cell is equivalent to interchanging of the variables $x,\overline{x}$. If J happens to be a symmetric function of $x,\overline{x}$ then it is an invariant for the map of the first cell alone.

Now we transform it over the second cell in the same way (as we have seen, it means just interchanging the variables):

$$J(\overline{x}_1,x_1) \equiv J(x_2,\overline{x}_2) \equiv J(x_0,\overline{x}_0)\ . \tag{16}$$

The last relation shows that J is an invariant function for the 2-cell map.

Thus, **an arbitrary function of two variables which has the form (10) in both variables generates an integrable map for the 2-cell lattice.**

This transformation over two cells was made in [1] in a direct way for quadratic polynomials in p (for them the property (10) is satisfied automatically). It was found there that the transformation of coefficients of these polynomials is the identity transformation for the 2-cell map. Now it is proved in the general way.

Let us consider an example. From the previous section we know that an arbitrary quadratic function in $\overline{x}$ has the second property of the invariant of 1-cell map. So any function, quadratic in x and $\overline{x}$, generates all the simplest integrable 2-cell maps. The general form of this invariant is:

$$I(x,\overline{x}) = ax^2\overline{x}^2 + bx\overline{x}^2 + cx^2\overline{x} + dx\overline{x} + ex^2 + f\overline{x}^2 + gx + h\overline{x}, \tag{17}$$

here a,b,c,d,e,f,g,h are arbitrary constants.

Taking here the Sign Reversal Function for $\overline{x}$ and subtracting $2x$ (see (10,11)), we obtain the kick of the first lens:

$$f_1(x) = -\frac{cx^2+dx+h}{ax^2+bx+g} - 2x\ . \tag{18}$$

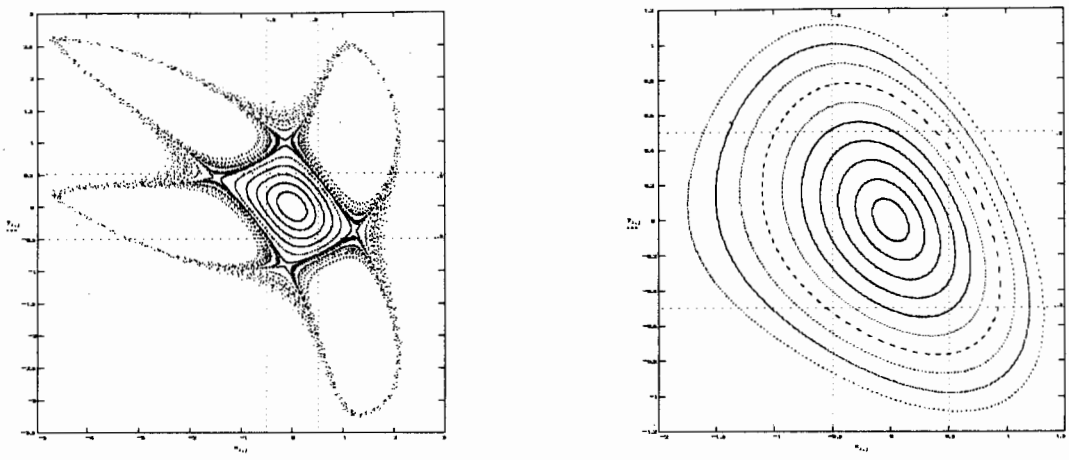


Figure 1. *left*) The Hénon map with $f_1 = -0.15x^2 - 0.6x, \quad f_2 = -0.6x$. *right*) The map corrected by (19) with the same f_1 and $f_2 = \frac{-0.3x^2-0.6x}{0.15x+1}$. For both examples $a, b, h = 0,\ e, f = 1$ in (17).

The same function for the variable x, minus $2x$, gives the second kick:

$$f_2(x) = -\frac{bx^2 + dx + g}{ax^2 + cx + e} - 2x\ . \tag{19}$$

There is an intersting combination of parameters for this case. If we set $a, b, h \equiv 0$, we have a combination of the sextupole and the quadrupole as one of the lenses (namely, the first one). If we put another lens in this 2-cell lattice as the quadrupole, we obtain a particular case of the Hénon map with two identical linear cells and a superimposed sextupole in one of them. We can "cure" this non-integrable map by changing the second lens so that it would take the form (19). In Fig. 1 one can see three phase space portaits: the Hénon map on the top and the integrable one on the bottom left as resulted from this correction. The difference of the second lens for these two cases begins from the second order in the coordinate.

Now let us assume that we have two arbitrary lenses in two cells. Can we make the corresponding map integrable by varying one of the lenses? If we know the solution to such problem, we notice that it is close to the problem of the "beam blow-up" due to the beam-beam effects: we can make the whole map, including the nonlinear kick from the opposite bunch, *integrable* (without elimination or cancellation of nonlinearities).

Some combination of parameters in the map related to the invariant (17) gives an example of elimination of overlapping resonances by means of *small correction* in one of the lenses, so as to bring it to the form (19) (see Fig. 2).

It is easy to obtain a formal series for solving the problem, mentioned above.

Let us consider the 2-cell lattice where one of the two lenses has an arbitrary kick function $f(x)$. The Sign Reversal Function F for the variable $\overline{x} = p + x$ in (10) is equal to $f + 2x$.

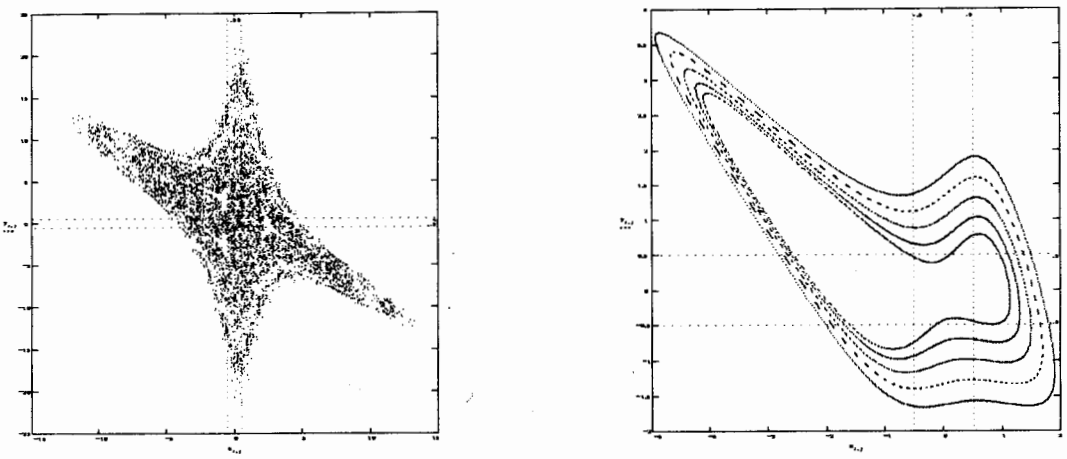


Figure 2. *left*) A globally chaotic map with $f_1 = \frac{-0.8x^3-1.2x^2+0.85x}{0.4x^2+0.77x+1}$ and $f_2 = \frac{-0.8x^3+0.141x^2+0.85x}{0.4x^2-0.34x+1}$.
right) The map corrected by (19) with with the same f_1 and $f_2 = \frac{-0.8x^3-0.09x^2+0.85x}{0.4x^2-0.34x+1}$.

So, for the reasons discussed above, our invariant must have the form (10):

$$I(x,\overline{x}) = f_0(x) + f_1(x)(\overline{x}^2 - F(x)\overline{x}) + f_2(x)(\overline{x}^2 - F(x)\overline{x})^2 + \ldots, \qquad (20)$$

here $f_0, f_1, f_2, \ldots$ are still arbitrary functions of the coordinate.

Let us choose f_i such that the invariant becomes a quadratic function in x in the coefficients of all the powers of $\overline{x}$. The coefficient of zeroth power of $\overline{x}$ is equal to $f_0(x)$, so this function must be quadratic:

$$f_0(x) = qu_0(x).$$

Then, the coefficient of $\overline{x}$ is $-f_1(x)F(x)$, so we put:

$$-f_1(x)F(x) = qu_1(x),$$

here qu_1 is an arbitrary quadratic function. Then from the next step we can find $f_2(x)$:

$$f_1(x) + f_2(x) \cdot F(x)^2 = qu_2(x)\ .$$

Now we can solve for $f_2(x)$ the above relation(s). We can perform this step-by-step operation for all powers of $\overline{x}$ so that from each relation for the i-th power we get f_i.

If this series converges, we have the second property of the invariant for x automatically, because it is constructed as a quadratic function. The analysis of convergence of this series

is not completed, it is more or less evident, that we have some freedom in choosing functions qu_i for better convergence[2].

There is an interesting case when this series takes the form of a finite sum. It gives a new integrable 2-cell system:

$$I(x,\overline{x}) = gx^2 + hx + (ex+f)((ax+b)\overline{x}^2 - (cx+d)\overline{x}) + ((ax+b)\overline{x}^2 - (cx+d)\overline{x})^2, \quad (21)$$

where a, b, c, d, e, f, g, h are arbitrary constants.

The kicks of the two lenses can be obtained from this invariant in the same way as in the case of invariant (17).

Finally, we present one more integrable 2-cell system. The corresponding integral is:

$$I(x,\overline{x}) = [((ax+b)\overline{x} - \frac{1}{2}(cx+d)) \cdot ((ax+b)\overline{x}^2 - (cx+d)\overline{x} + ex + f)]^2 , \quad (22)$$

here a, b, c, d, e, f are arbitrary constants. The squared expression is a quadratic function in x, so $I(x,\overline{x})$ has the second property for x automatically. One can check, that the Sign Reversal Function for $\overline{x}$ is:

$$F(x) = \frac{ax+b}{cx+d} .$$

So, expression (22) gives the invariant of one more family of integrable 2-cell systems.

4. Invariants Quadratic in Momentum

Previous sections dealt with the systems where the time dependence was represented by delta-functional non-linear kick functions, and the invariants were quadratic in momentum only at the kick moment. Here we construct a family of continuous time-dependent 1D Hamiltonians which have a quadratic invariant, and thus the respective motion in 1.5D is integrable. Starting from a Hamiltonian which is independent of the time variable T (with the particle mass $m = 1$):

$$H(X,P) = \frac{P^2}{2} + U(X) , \quad (23)$$

we can apply a time-dependent (canonical) transformation of the dynamic variables along with a relevant transformation of the time variable $T(t)$: $X(T), P(T) \xrightarrow{T(t)} x(t), p(t)$, so that the Hamiltonian will take the form:

$$\mathcal{H}(x,p,t) = \frac{p^2}{2} + \mathcal{U}(x,t) . \quad (24)$$

Transformation 1° is additive, use is made of any (differentiable) coordinate displacement function of time $D(t)$:

$$\begin{aligned} t &=: T , \\ x &=: X + D(t) , \\ p &=: P + \dot{D}(t) , \end{aligned} \quad (25)$$

[2]There is a great difference between the algebraic approach presented here and the algorithm by J.R. Cary et al. [5] for iterative elimination of resonance islands by introducing nonlinear corrections into a known map of one period. Convergence of this procedure is also problematic.

here 'dot' stands for the time derivative. The time-dependent Hamiltonian of the new system has the form (24):

$$\mathcal{H} = \frac{p^2}{2} + U(x - D(t)) - x \cdot \ddot{D}(t) . \tag{26}$$

Apparently, the invariant of this 1.5D system is given by the function $H(X, P)$ of Eq. (23) where X, P should be expressed in terms of the new variables x, p:

$$H = \frac{1}{2}(p - \dot{D}(t))^2 + U(x - D(t)) = const . \tag{27}$$

Transformation 2° applies an arbitrary time-dependent coordinate normalization function $A(t)$ and involves a corresponding transformation of the time variable $T \to t$:

$$\begin{aligned} dt &= A^2 dT , \\ x &= AX , \\ p &= A\dot{X} + \dot{A}X = \frac{P}{A} + \dot{A}X , \end{aligned} \tag{28}$$

where 'dot' denotes differentiation with respect to the new time t and use is made of the Hamiltonian equation $dX/dT = P$ in the last line. By its definition, $p = \dot{x}$, while the second Hamiltonian equation:

$$\dot{p} = \frac{\dot{P}}{A} - P\frac{\dot{A}}{A^2} + \dot{A}\dot{X} + \ddot{A}X = -\frac{U'}{A^3} + \ddot{A}X$$

yields the desired time-dependent Hamiltonian function:

$$\mathcal{H} = \frac{p^2}{2} + \frac{1}{A^2}U(\frac{x}{A}) - \frac{\ddot{A}}{A} \cdot \frac{x^2}{2} . \tag{29}$$

Again the invariant of this 1.5D integrable system is available from (23): using (28) we express X, P via x, p and obtain:

$$H = \frac{1}{2}(Ap - \dot{A}x)^2 + U(\frac{x}{A}) = const . \tag{30}$$

This expression is a generalization of the Courant-Snyder invariant of the linear systems[3].

Any combination of transformations 1° and 2° also provides an integrable system of the form (24), we present in Appendix an expression of the invariant combined from (27) and (30). Note that any integrable system produced with this technique involves three arbitrary functions: $U(X), D(t)$ and $A(t)$. One can prove directly that they form a complete set of freedoms for a 1.5D integrable system with the invariant quadratic in momentum, see Appendix.

Transformation 2° will be applied in the following section to the 2D systems preserving angular momentum, in particular to the problem of round colliding beams.

[3]Indeed, Hill's equation $\ddot{x} + g(t)x = 0$ implies $U = g(t)x^2/2$ in (24). Taking $U(X) = X^2/2$ in (23) we immediately obtain from (29): $\ddot{A} + g(t)A = A^{-3}$, *i.e.* the well-known equation for the betatron amplitude function, hence $A(t) = \sqrt{\beta}$, and (30) takes the usual form of the Courant-Snyder invariant. We see that x, p correspond to the conventional betatron variables, t is the machine azimuth, while X, P are the normalized betatron variables and T stands for the betatron phase advance.

5. 2D Systems with Conservation of Angular Momentum

It is generally known that two-dimensional motion in the central force has an additional integral in the form of angular momentum $M = x\,p_y - y\,p_x$, and thus is reducible to the 1D problem in the polar coordinates. The equivalent 1D Hamiltonian can be expressed in terms of $r = \sqrt{x^2+y^2}$, $p_r = \dot{r}$ with addition of the fictitious 'centrifugal' potential $U_{cf} = M^2/2r^2$:

$$\mathcal{H} = \frac{p_r^2}{2} + \mathcal{U}(r,t) + \frac{M^2}{2r^2} \tag{31}$$

Aiming at integrable two-dimensional systems of physical interest we need an invariant which exists for any value of M, *i.e.* for all particles with different angular momenta. In particular, our system must be integrable at $M = 0$.

Let us carry the results of Section 2 over 2D systems preserving angular momentum. The mapping consisting of the drift space and any kick force in the form (12) corresponds to the integrable 1D motion and fits to the case $M = 0$. However, integrable 2D systems with any $M \neq 0$ can be sought as a subset of these 1D systems, namely the two-dimensional kick (12) must be radial in order to preserve angular momentum. If we now interprete (12) as a radial component of a two-dimensional vector, then we can directly check that among all the rational forms (12), those with $b = e = 0$ correspond to integrable motion with $M \neq 0$, hence:

$$f_r = -2r - \frac{cr}{ar^2 + d}\,. \tag{32}$$

So the 1D case is partially extended to the 2D motion with axial symmetry. The obtained force (32) is interesting for the round colliding beams problem in that it corresponds to the kick from infinitely short opposing bunch in both limiting cases $r \to 0$ and $r \to \infty$.

Turning back to the continuous Hamiltonian systems, we seek possible extensions of the integrable 1D systems to the 2D systems with conservation of angular momentum. We can write an analogue of the time-dependent Hamiltonian (29) of the integrable 1D motion for these effectively one-dimensional systems in terms of r, p_r, M, ϕ:

$$\mathcal{H} = \frac{p_r^2}{2} + \frac{1}{A^2}U_{eff}\left(\frac{r}{A}\right) - \frac{\ddot{A}}{A}\cdot\frac{r^2}{2} \tag{33}$$

with $U_{eff} = U + U_{cf} = U + \dfrac{M^2}{2r^2}$.

Note the remarcable property of the centrifugal potential U_{cf}: being proportional to r^{-2}, it keeps its form irrespectively of the normalization transformation $R = r/A$ with any function A at any value of angular momentum M!

Thus we conclude that all the 1D formalism in Section 4 is immediately applicable to the 2D systems preserving angular momentum; the only modification is in addition of U_{cf} to $U(R)$, but this has no effect on the decision whether a system in question is or is not integrable, namely, whether its Hamiltonian has the form (33).

6. Round Colliding Beams

Consider the particle motion in the fields of opposing bunch[4] with the Gaussian density distribution in all the three dimensions, $\sigma_{x,y} = \sqrt{\beta_{x,y}\epsilon_{x,y}}$, σ_l are the transverse and longitudinal r.m.s. bunch sizes, respectively. The concept of Round Colliding Beams [6] envisages equal β-functions $\beta_x = \beta_y = \beta$ and equal emittances $\epsilon_x = \epsilon_y = \epsilon$ in both degrees of freedom. Let us show how the appropriate arrangement of the machine optics may bring this problem closer to integrability.

The radial force F_{rb} from the strong bunch should account for its variable cross-section (due to variable β-function) and for the relative speed of collision which is twice the speed $v \approx c$ of individual motion of the bunch and the test particle[5]:

$$F_{rb} = \frac{M^2}{r^3} - k\,\frac{1-\exp(-\frac{r^2}{2\beta\epsilon})}{\frac{r}{\sqrt{\beta}}}\cdot\frac{\exp[-\frac{(s-2ct)^2}{2\sigma_l^2}]}{\sqrt{\beta}} - g(t)r\,, \tag{34}$$

here k is proportional to the strong bunch intensity, s is the longitudinal position of the test particle in the weak bunch with respect to its centre, $g(t)$ denotes an (optional) axisymmetric focusing in the Interaction Region (IR). The time $t = 0$ corresponds to the moment when the central test particle ($s = 0$) meets the centre of the strong bunch.

On the other hand, the Hamiltonian of integrable system (33) yields the certain form of the force to be compared with (34):

$$f = \frac{M^2}{r^3} - U'(\frac{r}{A})\frac{1}{A^3} + \frac{\ddot{A}}{A}r \tag{35}$$

Using the free functions A, g we can make these two forms identical for the central particles with $s = 0$. From the radial dependence of F_{rb}, A must be proportional to the optical function in the IR: $A(t) = \sqrt{\beta(t)/\beta_1}$. Then the conventional equation for $\sqrt{\beta}$ yields the equation for A:

$$\ddot{A} + g(t)A = \frac{1}{\beta_l^2 A^3}\,. \tag{36}$$

The longitudinal modulation of F_{rb} can always be packed into the proper definition of the β-function:

$$\beta(t) = \beta_0\exp(\frac{2t^2}{\sigma_l^2})\,, \tag{37}$$

and the needed focusing $g(t)$ in the IR will result from substitution of $A(t) = \sqrt{\beta(t)/\beta_1}$ into (36). The potential function $U(R)$, $R = r/A$ can be found from:

$$U'(R) = k\,\frac{\beta_0}{\beta_1}\,\frac{1-\exp(-\frac{R^2}{2\beta_1\epsilon})}{R} + \frac{R}{\beta_1^2}\,. \tag{38}$$

[4]We treat here the head-on collision in the weak-strong model, and disregard the synchrotron motion of the test particle and the longitudinal beam-beam effects [7]

[5]To simplify the formalism, we will use scaling of lengths and time units corresponding to $c = 1$.

Thus the exact invariant for this problem is available, and the beam-beam dynamics with round colliding beams in the weak-strong model is reduced to an integrable motion for central test particles ($s = 0$) by means of the appropriate focusing in the interaction region.

The focusing function $g(t)$ is determined by the longitudinal distribution profile in the strong bunch. The longitudinal Gaussian in (34) was inessential in the above consideration[6], we may take any other reasonable longitudinal distribution and adjust to it the form of the β-function imposing the appropriate focusing $g(t)$ in the IR. Specifically, the Lorentz bell $(\tau^2 + t^2)^{-1}$ in the longitudinal profile with $\beta_1 = \beta_0 = \tau$ will result in $g(t) \equiv 0$.

Since the Gaussian longitudinal profile is the most natural, we draw some practical recommendations for this case. Apparently, the case $g(0) = 0$ is attractive, and from (37) we find a relation between the bunch length and the minimum β-value: $\sigma_l = \sqrt{2}\beta_0$. This provides for integrability of motion of the central test particles ($s = 0$). For the off-centre particles the exact invariant is not available, however for $s \leq \sigma_l$ we can expect an "almost integrable" system where the perturbative analysis is possible.

The integrable single-pass system just considered is relevant to linear collider problems. For circular colliders the opposing beam force should be transformed into a periodic function of time with the account of optics in between the repetitive passages through the IR. Although this difference may result in small deviation from integrability (the obtained exact invariant will be lost), the perturbation can always be done practically negligible and the beam-beam dynamics will be almost integrable.

7. 2D Case

It was shown in [1], that we can carry over all the results of 1D case to two dimensional motion by introducing the 2D map in complex variables:

$$\begin{aligned} z_n &= z + p^* , \\ p_n^* &= p^* + F(z_n) , \end{aligned} \tag{39}$$

here $z = x + iy$ and $p = p_x + ip_y$ are composed from the horizontal and vertical coordinates and their respective momenta. The complex kick function $F = f_x - if_y$ is combined from the components f_x, f_y of a potential force corresponding to the symplectic two-dimensional kick. Moreover, F is assumed to be an analytic function of z which corresponds to the (paraxial) Lorentz force from the fields satisfying the Maxwell equations in free space. This case of Laplacian fields is the most interesting in accelerator optics applications.

The transformation between lenses in this map (39) does not correspond to the drift space. From the first line of (39) we have:

$$\begin{aligned} x_n &= x + p_x , \\ y_n &= y - p_y . \end{aligned} \tag{40}$$

Of course, we can construct this transformation by means of linear optics.

We have to substitute z instead of x and p^* instead of p in the 1-cell invariants of 1D case and we obtain two invariants of the 2D case, namely, the real and imaginary parts of the complex invariant.

[6]Note that the Gaussian profile in the transverse distribution *was* essential.

Let us prove that the real and imaginary parts $I_1 = \mathrm{Re}I$, $I_2 = \mathrm{Im}I$ of the complex invariant $I(z, p^*)$ are functionally independent and have a vanishing commutator.

Then for the function $I(z, p^*)$ which is analytic with respect to its both complex variables the Cauchy-Riemann conditions[7]

$$\frac{\partial I_1}{\partial x} = \frac{\partial I_2}{\partial y}, \quad \frac{\partial I_1}{\partial y} = -\frac{\partial I_2}{\partial x}, \quad \frac{\partial I_1}{\partial p_x} = -\frac{\partial I_2}{\partial p_y}, \quad \frac{\partial I_1}{\partial p_y} = \frac{\partial I_2}{\partial p_x} \tag{41}$$

yield the relation between the gradients of I_1 and I_2:

$$\nabla I_1 = \left(\frac{\partial I_1}{\partial x}, \frac{\partial I_1}{\partial p_x}, \frac{\partial I_1}{\partial y}, \frac{\partial I_1}{\partial p_y}\right) = \left(\frac{\partial I_2}{\partial y} - \frac{\partial I_2}{\partial p_y}, -\frac{\partial I_2}{\partial x}, \frac{\partial I_2}{\partial p_x}\right) = \mathcal{T}\nabla I_2 . \tag{42}$$

The *real* matrix $\mathcal{T}$ in (42):

$$\mathcal{T} = \begin{pmatrix} 0 & 0 & . & 0 \\ 0 & 0 & 0 & -1 \\ -1 & 0 & 0 & 0 \\ 0 & 1 & 0 & 0 \end{pmatrix}$$

has only *imaginary* eigenvalues and eigenvectors. If we assume that the two gradient vectors are "parallel": $\nabla I_1 \propto \nabla I_2$, then from relation (42) we see that either of them should be an eigenvector of $\mathcal{T}$. But they are *real* by definition, hence the gradient vectors can never be parallel. Thus we conclude that I_1 and I_2 are independent functions.

Now let us calculate the commutator of I_1, I_2:

$$[I_1, I_2] = \frac{\partial I_1}{\partial p_x}\frac{\partial I_2}{\partial x} - \frac{\partial I_2}{\partial p_x}\frac{\partial I_1}{\partial x} + \frac{\partial I_1}{\partial p_y}\frac{\partial I_2}{\partial y} - \frac{\partial I_2}{\partial p_y}\frac{\partial I_1}{\partial y} . \tag{43}$$

Substitution of (41) into (43) yields: $[I_1, I_2] \equiv 0$, *Q.E.D.*

All maps of the form (39) have an essential fault: at small amplitudes their x- and y-frequencies are on the sum resonance. This fact results from the special form of the linear transformation of coordinate and momentum between lenses (see (40)).

One can use multi-cell lattices with larger number of lenses and with various linear transformations between them. More examples can be found in [8]. Such systems can be taken as a prototype of an "integrable accelerator".

8. Conclusion

The canonical theory can provide a general solution for a map preserving a given invariant (by means of separation of variables in the equation for the generating function of the desired transformation). However it is a problem to find the maps which correspond to the accelerator optics among all those maps.

The main result of the present paper is the construction of feasible 1D maps of the accelerator lattice type having invariants of simple form. Since these solutions can be extended to the 2D case, an implementation of the integrable lattices in practical lattice design is possible

[7] The relations between the partial derivatives w.r.t. the momenta have opposite signs because the complex invariant depends on the complex conjugate variable p^*.

in order to improve the dynamic aperture and, it is hoped, to cure resonance overlapping and global stochasticity. An integrable 2D lattice is constructed in view to give a guideline for designing an "integrable machine" optics.

An important special case of 2D systems with conservation of angular momentum is considered in detail and applied to the beam-beam problem with round colliding beams. This system is shown to be integrable with the appropriate arrangement of linear focusing in the interaction region.

Acknowledgments

We wish to thank J. Gareyte and B. Zotter for their interest in this work, we are grateful to the SL/AP Group at CERN for their hospitality and support during the part of this work.

References

[1] V.V. Danilov and E.A. Perevedentsev, "Integrable Nonlinear Map of the Accelerator Lattice Type", CERN SL/Note 94-21(AP).

[2] E.T. Whittaker, "A treatise on the Analytical Dynamics of Particles and Rigid Bodies", Cambridge, Cambridge University Press (1964).

[3] A. Lichtenberg and M. Lieberman, "Regular and Stochastic Motion", Springer-Verlag, New York (1983).

[4] E.M. McMillan, "Some Thoughts on Stability in Nonlinear Periodic Focusing Systems", Preprint UCRL-17795, Univ. of California, Lawrence Radiation Laboratory, Berkeley, California (1967).
L.J. Laslett, E.M. McMillan and J. Moser, "Long-Term Stability for Particle Orbits", Preprint NYO-1480-101, AEC Computing and Appl. Math. Center, Courant Inst. of Math. Sci., New York Univ., (1968).

[5] C.C. Chow and J.R. Cary, "Integrable Nonlinear Accelerator Lattices", Phys. Rev. Lett., **72**, p. 1196, (1994).

[6] L.M. Barkov et al., "ϕ-factory project in Novosibirsk", *in Proceedings of the 14th Int. Conf. on High Energy Accelerators*, Tsukuba, Japan, 1989, Particle Accelerators, **31**, (1990) 177.
A.N. Filippov et al. "Proposal of the round beam lattice for VEPP-2M collider", *in Proceedings of the 15th Int. Conf. on High Energy Accelerators,* Hamburg, **2** (1992) 1145.

[7] V.V.Danilov et al., "Longitudinal Beam-Beam Effects for an Ultra-High Luminosity Regime", *in Proceedings of the 1991 IEEE Part.Acc.Conf.,* San Francisco, **1** (1991) 526.
V.V.Danilov et al., "Longitudinal Effects in Beam-Beam Interaction for an Ultra-High Luminosity Regime", *in Proceedings of the Workshop on Beam-Beam and Beam-Radiation Interactions,* Los Angeles, May 13-16, 1991. World Scientific, Singapore, 1992.

[8] V.V. Danilov and E.A. Perevedentsev, "On Invariants and Integrability in Nonlinear Accelerator Optics", CERN SL/Note 94-74(AP).

Appendix: General Form of the Invariant Quadratic in Momentum

Consider a general form of invariant quadratic in momentum p, assuming that the coefficients A, B, V are arbitrary functions of time t and coordinate x:

$$I = \frac{1}{2}(Ap - B)^2 + V\,,$$

$A \neq 0$. Equating its total time derivative to zero, we account for the Hamiltonian equations of motion $\dot{x} = p$, $\dot{p} = f$, where the unknown force f depends on t, x

$$\frac{dI}{dt} = (Ap - B)\Big(A_x p^2 + (A_t - B_x)p + Af - B_t\Big) + V_x p + V_t \equiv 0\,,$$

the subscripts here denote the respective partial derivatives. The vanishing coefficients of each power of p yield a set of equations in partial derivatives for the four unknown functions: f is to be found along with A, B, V.

First of all, $A_x = 0$, and $A = A(t)$ is an arbitrary function of time. Then we take $A_t - B_x = 0$, whence:

$$B(x,t) = \dot{A}x + A^2\dot{D}\,,$$

with an arbitrary $D(t)$; dots denote the time derivatives. We choose here the special form of arbitrary additive function of time for future convenience.

The last two equations form a set of equations specifying the unknowns f and V:

$$\begin{aligned} A(Af - B_t) + V_x &= 0 \\ -B(Af - B_t) + V_t &= 0 \end{aligned}$$

The force f is thus expressed via V, B, A:

$$f = -\frac{V_x}{A^2} + \frac{B_t}{A}\,, \tag{44}$$

and V is determined by the homogeneous equation in partial derivatives of the 1st order:

$$B\,V_x + A\,V_t = 0$$

Its characteristic curve $x(t)$ is then obtained from the equation:

$$\frac{dx}{dt} = \frac{B}{A} = \frac{\dot{A}x + A^2\dot{D}}{A}\,.$$

Integration gives the lines of constant level of V:

$$X \equiv \frac{x}{A(t)} - D(t) = const\,.$$

Hence,

$$V(x,t) = U\Big(\frac{x}{A(t)} - D(t)\Big)\,,$$

where $U(X)$ is an arbitrary function.

Thus we conclude, that the general solution to our problem of integrable system in 1.5D with quadratic invariant is generated with three arbitrary functions: $A(t)$, $D(t)$, $U(X)$. The corresponding force f is then found from (44):

$$f = -\frac{1}{A^3}U' + \frac{1}{A}(\ddot{A}x + (A^2\dot{D})\dot{}) .$$

The Hamiltonian of this system can be found from the expression for f:

$$\mathcal{H}(x,p,t) = \frac{p^2}{2} + \frac{1}{A^2}U(\frac{x}{A} - D) - \frac{A\ddot{A}}{2}(\frac{x}{A})^2 - (A^2\dot{D})\dot{}\frac{x}{A} ,$$

and the final form of the desired invariant is:

$$I = \frac{1}{2}(Ap - \dot{A}x - A^2\dot{D})^2 + U(\frac{x}{A} - D) .$$

Magnetic Structure of The Novosibirsk TAU-CHARM Factory

V.Yakimenko
Budker Institute of Nuclear Physics,
630090 Novosibirsk, Russia

September 14, 1995

1. Introduction

The main purpose of the C-TAU factory project is attaining high luminosity for a beam energy ranging from 700 to 2500 MeV. To carry out this project, it is planned to construct two intersecting rings, the lengths of which should provide a sufficiently high bunch collision frequency, on the one hand, and allow us to place on a track the systems required to control the colliding beam sizes, on the other hand. Such a storage ring allows us to pass easily to the colliding beam energy monochromatization regime by introducing the vertical dispersion and creating the vertical size mainly at the expense of pulse spread with a small betatron vertical size.

To perform the experiments with the longitudinally polarized beams at the interaction point, we need special optics. Beam polarization in the storage ring at this energy using radiation polarization is inefficient because of high values of the perimeter of the storage ring and current. That is why in the polarized beam experiments we are going to inject the polarized beams from a special storage ring with short polarization time. The injected electrons and positrons will be vertically polarized. Spin rotators installed in the arcs will provide the electron and positron beams of arbitrary spiraling at the interaction point.

To obtain the maximum luminosity, the most interesting possibility is the organization of the interaction point with a small β-function by a powerful longitudinal field. The symmetrical focusing in both directions satisfies well the idea of operating with round beams and allows us to obtain the space charge parameter $\xi > 0.1$.

Energy (Gev)	2.1
Circumference (m)	773.036
Ring radius (m)	89.63
Interbunch distance (m)	8.14
Straight section lenght (m)	100
Beam radius at IP (μ m)	33
Number of rings	2
Number of bunches per beam	95
Number of particle per bunch	2×10^{11}
b-function at IP (cm)	1
Beams emittance ($\epsilon_x = \epsilon_y$) (cm/rad)	10^{-5}
RMS bunch length (cm)	0.8
Compaction factor	$0.001 \div 0.0017$
Betatron tune ν_x	29.077
Betatron tune ν_y	31.077
Vertical damping time (s)	0.11
RF voltage (kV)	1000
RF frequency (MHz)	700
Energy loss per turn (keV)	100
Energy spread	5×10^{-4}
Harmonic Number	1805
Tune shift parameter $\xi_x = \xi_y$	0.1
Design Luminosity ($cm^{-2}s^{-1}$)	10^{34}

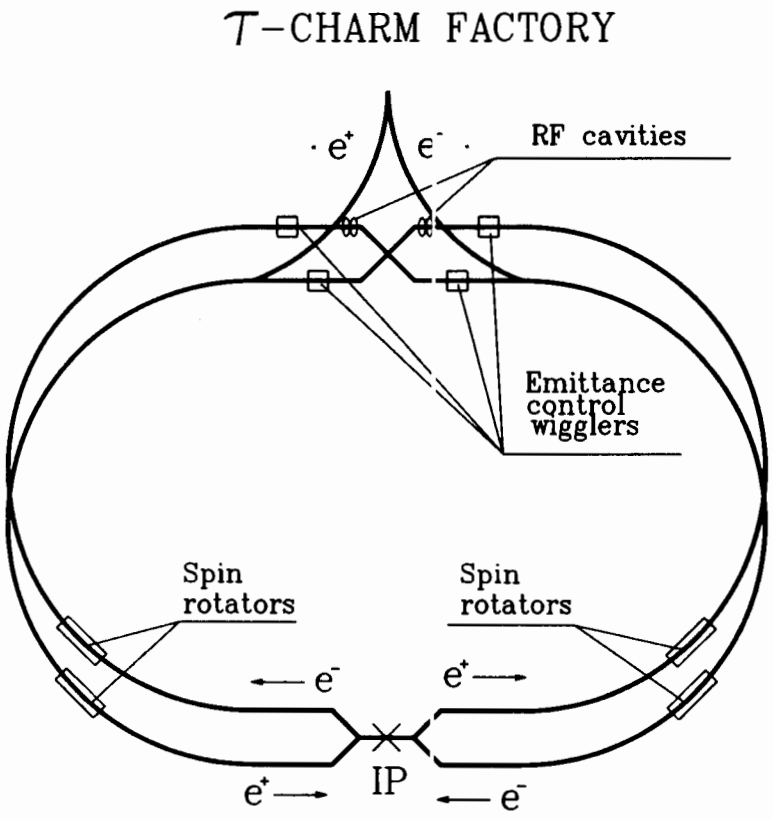
The C-TAU factory beam parameters should meet the requirement for maximum high luminosity of $1.0 \cdot 10^{34} cm^{-2}c^{-1}$. In addition to such a maximum luminosity regime, it is intended to obtain the beam parameters required for the so-called monochromatization and longitudinally polarized colliding beams. To operate in the mentioned regimes, we need the systems of beam emittance control.

In the energy monochromatization regime, the value of a vertical energy dispersion is chosen according to the energy spread. In this case, the value of monochromatization is determined by the ratio of the vertical betatron size and the vertical energy one.

It is necessary to completely reconstruct the experimental straight section to obtain the ultra monochromatic colliding beams $\sigma_M \approx 6$ keV. The strong quadrupoles and weak dipoles should be used for beam separat on and control of the vertical dispersion function at the interection point. The length of such section is estimated to be more than 30 m. The beam parameters in this case are presented in table:

Number of particles in bunch	1.510^{11}
Interbunch distance (m)	16.28
Beta-function at IP (cm) β_x/β_y	20 / 2
The value of ξ_{max}/ξ_D	0.05 / 0.01
Beam emittance ϵ_x/ϵ_y (cm)	10^{-5} / 10^{-9}
Beam current (A)	0.4
Energy resolution σ_M (keV)	6
Luminosity $(cm^{-2}s^{-1})$	5.010^{31}

2. Storage Ring Magnetic System



A magnetic system of the C-TAU factory comprises two storage rings of the same perimeter, which are placed one above another and intersecting at the interaction point. The magnetic system of each storage ring can be divided into four parts: two arcs consisting of the same periodicity elements and one spin rotator, and experimental and technical sections. Several bending magnets responsible for setting the dispersion function D_E to zero are in the experimental and technical sections.

In the experimental section, only the magnets and lenses focusing the beams at the interaction point and providing the optics matching with the arcs are placed. The beam collision is a head-on collision. After collision, the beams are separated by the electrical

field in the horizontal and the magnetic one in the vertical. The monochromatization is achieved by creating the vertical dispersion function at the interaction point (this is achieved by changing the lens gradients between the magnets separating the orbits in the vertical) and decreasing the vertical emittance. Since the D_E-function rotation by π is taken into account, the magnetic field distribution in the final focusing soleniods is made to be symmetrical with respect to the interaction point. This results in that the beam trajectory becomes S-shaped and the beams exchange the places after collision. The beam from the upper half-ring goes to the lower one and vice versa.

The inlet systems accelerating the resonators and the systems of control of the vertical and horizontal emittances are placed in the technical section, where the inverse beam transition occurs: from the upper half-ring to the lower one for one beam and vice versa for another. The emittances are controlled by the D_E-function at the sites of superconducting wiggler-magnets.

To obtain the small emittance, the rings have a very rigorous focusing ($\nu \approx 30$), giving a small value of the orbit compaction coefficient. The latter is necessary to obtain short bunches ($\approx$ 1 cm) and should be accurately controlled to provide the stability of synchrotron oscillations.

To perform the experiments with the longitudinally polarized beams of arbitrary spirality at the interaction pont, spin rotators are supposed in the arcs.

3. Experimental Section

The experimental section suggested forms the β- and D_E-functions at the interaction point for operation in two regimes:

- round beams (the same β-functions of about 1.0 cm and the zero D_E-function at the interaction point);
- monochromatization (the same β-functions of 1.0 cm and the D_E- function of $\approx$5 cm at the interaction point).

The final focusing is supposed to be made by the solenoids (2.18 m long, with a 9.6 T field, and at a 2.1 GeV energy).The focusing solenoids and a detector solenoid (1m long, with a 1.0 T field) turn the beam axis to one side exactly by π total, without introducing the coupling into the betatron oscillations at an equilibrium energy. The experimental section is symmetrical relative to the interaction point, except the separating magnets with the opposite-sign fields. This is required in the monochromatization regime to obtain the D_E-functions of different signs at the input of the focusing solenoids which turn the D_E-function by π .

The plates of electrostatic separation in the horizontal (2.0 m long, with a 100 kV/cm field) are supposed to be installed immediately after the focusing solenoids. The beam separation at the first spurious interaction point (which is immediately after the plate ending) is about 1.0 cm or has the order of 3σ . Prior to the second spurious interaction

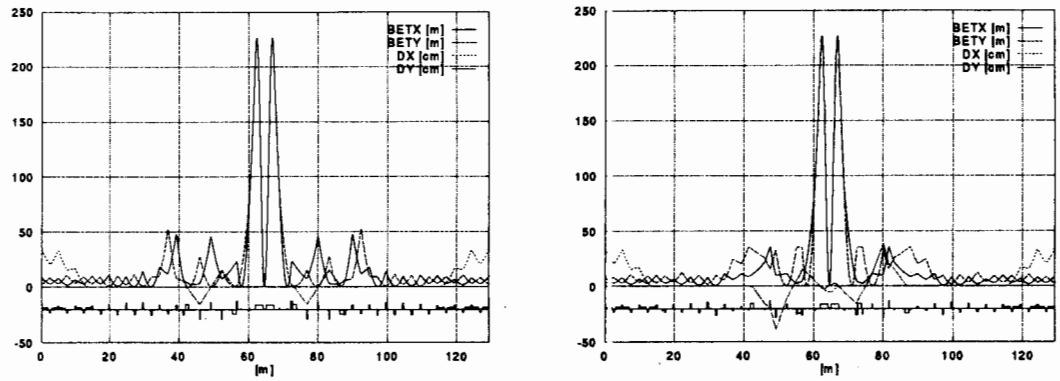


Figure 1: The experimental section with the zero D_E-function (from the left) and $D_E =$ 5 cm (from the right)

point, the beams are separated in the vertical by a septum-magnet. Since the betatron oscillation phase advance between the spurious interaction points (before and after the main interaction point) is close to π (rotation in the solenoids of final focusing and detector), their interaction is compensated. On a magnet knife, the separation is equal to ± 5 cm, allowing its thickness of 3 cm. The beam size in the magnet is about 1 mm, and the separation system has the acceptance of 10σ . The septum-magnet, the vertical magnet restoring the orbit plane, and the three lenses between them are responsible for the parallel transfer of the orbit plane by ± 0.5 m. Thus, in the regular section the orbit structures are separated by 1.0 m. In the monochromatization regime, the two additional lenses between the magnets help to obtain the required D_E-functions at the interaction point. Setting the vertical D_E-function to zero occurs in the magnet restoring the orbit plane in both regimes. The plates of the electrostatic separation can be replaced by an RF cavity, which forms a transverse electrical field of 500 kV/cm, 20 cm long. As an alternative to the variant with the solenoids of final focusing, we consider the variant at which the final focusing is made on the superconducting lenses placed inside the detector as close to the interaction point as possible. However, in this case we fail to keep the control of the D_E-function at the interaction point. From the viewpoint of optics, the field increase in the solenoids up tp 20-25 T is more attractive.

All the lenses of the experimental section have the same aperture as the lenses of the periodicity elements, except the lens splitting the D_E-functions after the focusing solenoids. A substantial change in the focusing force is achieved by changing the lens length.

4. Periodicity Element

A magnetic structure is determined by the following requirements:

- emittance minimization,
- minimization of the orbit compaction coefficient,

- compensation of high final-focusing chromaticity and β-function chromaticity at the interaction point with sextupole correctors, and
- efficiency (aperture minimization).

Based on these requirements, we chose the FODO structure with the phase advance (60°; 60°) and the gradient force reserve in order to change to one of the variants: (60°; 90°), (90°; 60°), and (90°; 90°) or the intermediate one. As shown in [2], the final focus chromaticity can be compensated by the half-ring sextupoles for the phase advance between 60° and 90° at a correct arrangement of sextupole families. This means that with the change in the phase advance, we ought to recommutate the sextupole power supply polarities or they should be supplied separately.

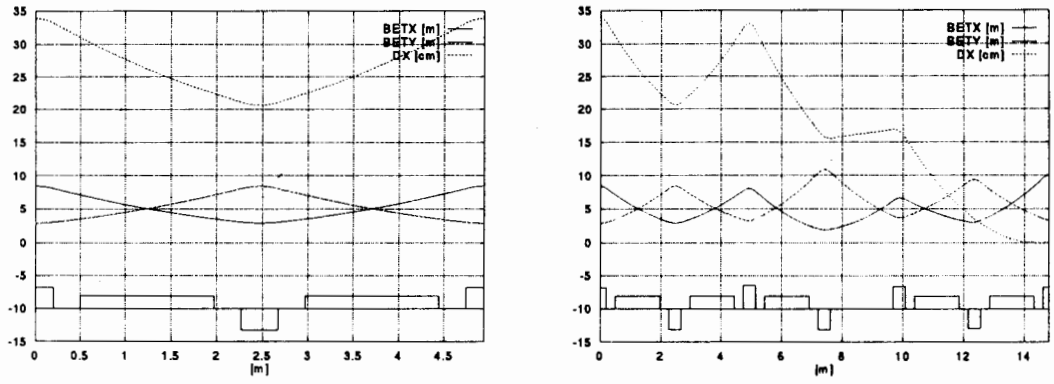


Figure 2: Periodicity element (from the left) and section of setting the D_E-function to zero (from the right)

5. Section of Setting the D_E-Function to Zero

The section of setting the D_E-function to zero consists of three periodicity elements with one "forgotten" magnet. By changing the gradients, we can provide the matching of optic functions for the phase advance on the periodicity element ranging from 60 deg. to 90 deg. without changing the ring geometry.

6. Technical Section

In the technical section, the following problems are solved:

- injection into the storage ring;
- control of horizontal emittance;
- dispersionless section with a set of the RF cavities;

- achromatic parallel orbit-plane displacement; and
- control of vertical emittance.

Injection into the storage ring is performed in the vertical. The electrons and positrons are injected by the same schemes, each of them includes the Lambertson magnet and two kicker magnets for prekick and correction. The kick is made in the vertical by the magnetic field. The front and decay duration exceeds several times the gap between the bunches in the storage rings. Therefore, both the bunch, into which a new portion of particles is injected, and several neighbouring ones are kicked during injection. The kicker-magnets with a ferrite filler and a metallized (for impedance decrease) glass or ceramic chamber are supposed to be used.

The magnetic structure is optimized to minimize the angle created by the kicker-magnet. The injection sections are at the inputs of the half-ring. The correction kicker-magnet is placed in a vacant gap of the section of setting the D_E-function to zero so that the vertical betatron phase advance from the kicker-magnet of the prekicker be exactly π. The injected bunch is carried over the orbit by the Lambertson magnet, 1 m long, with a 8 cm aperture, and the C-shaped magnet, 1.5 m long, around a preceding lens at a 30 cm distance in the horizontal. An approximate phase advance equality by $\pi/2$ between the Lambertson magnet knife and the correctors is attained automatically.

The emittance control is supposed to be made by using two analogous sections (all the elements of one section are turned by $\pi/2$), which are mirror-symmetrical relative to the superconducting wigglers installed in the middle. The field direction in the wigglers is vertical for both sections and coincides in the main pole with that in the bending magnets. This is necessary for operation with the polarized beams, makes easy the manufacture of similar wigglers, and does not produce a vertical "fan" of rigorous synchrotron radiation. The structure of each section allows us to control (in the vertical and the horizontal) the D_E-function in the wiggler from 0 to 1 m, making possible the emittance control independent of the synchrotron losses. This solution allows us to minimize the adverse increase in the emittance at the expense of a large dispersion function in the deflecting magnets, which is substantial in the monochromatization regime in the case, where the vertical emittance minimization is required.

Each structure has four FODO cells with eight magnets of the same length from each side (Fig. 3). The magnets deflect an equilibrium-orbit wave with the amplitude of no less than 5 cm:$(H, -H, -2H, 2H, 2H, -2H, -2H, 2H)$. The dispersion function is controlled by changing the gradients of the lenses (phase advance between the magnets). The magnet fields are unchanged, so the orbit distortions remain constant. The field in these magnets is due to a compromise between a desire to obtain a high value of the D_E-function and the one to minimize the contribution of the dispersion function deflecting magnets. ???

The sign alternation and setting the field integral to zero in the deflecting magnets keep the spin vertical in the wiggler, minimizing the beam polarization distortion during the vertical dispersion function deflection.

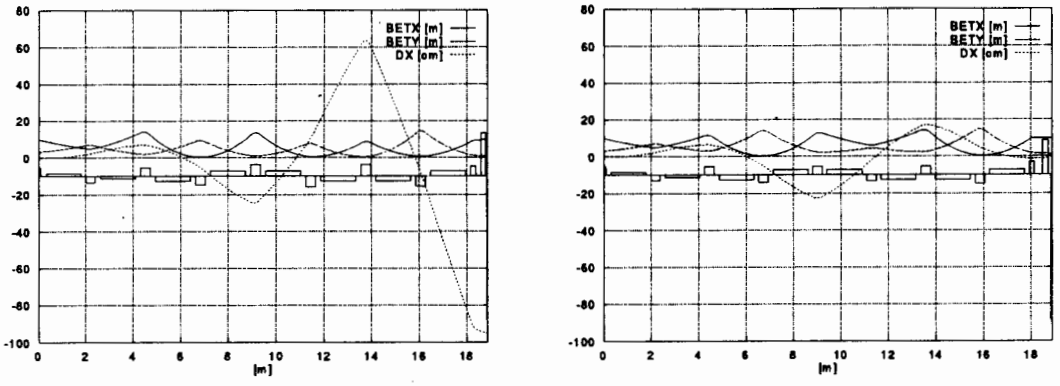


Figure 3: A half of a dispersion functior control insertion for the maximum value of D_E (from the left) and zero D_E (from the right) in the superconducting wiggler

The dipole and quadrupole magnets are as those in the periodicity elements of the arcs.

The RF cavity sections and the section of achromatic parallel orbit-plane displacement by 1 m are approximately in the middle of the technical section. The section of displacement compensates the analogous effect in the experimental section.

7. Spin Rotator

The spin rotators are optimized for minimization of orbit disturbance in the regime of operation with the nonpolarized beams The spin rotators turn the spin orientation by $\pi/2$ relative to the longitudinal axis. Their position in the arcs is chosen so that the remaining magnets turn the spin relative to the vertical axis by $\pi/2$ at the experimental energy. Thus, depending on the sign of the first turn the spin either parallel to the velocity vector or antiparallel to it at the interaction point. With a substantial change in the energy of the polarized beam experiment, the spin rotators should be rearranged.

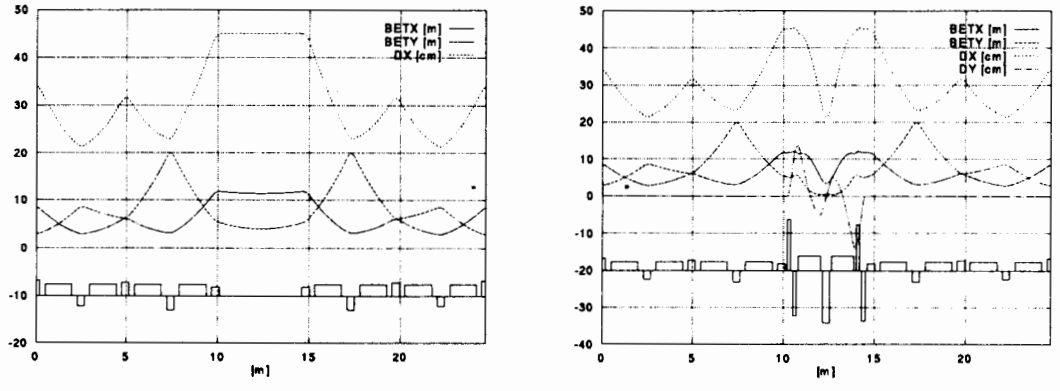


Figure 4: Optical functions for the switched-off (from the left) and switched-on (from the right) spin rotator

The spin rotator scheme is analogous to that proposed in [3], with a transport matrix of the form $\begin{pmatrix} A & 0 \\ 0 & -A \end{pmatrix}$, where $A = \begin{pmatrix} 1 & L \\ 0 & 1 \end{pmatrix}$ and L is the length occupied by the rotator. To realize this scheme, we need two lenses surrounding each solenoid and turned by $\pi/4(1 + ag)$, and a powerful (probably, superconducting) quadrupole between the solenoids.

The length L is chosen to be equal to that of the periodicity element. At the ON/OFF regime of the spin rotator, the horizontal phase does not change and the vertical one increases by 1/2 (by 1.0 on two rotators).

Two periodicity elements on each side supplied separately of the other elements of the half-ring provide the matching of the optics and geometry (the magnets additionally turn to obtain a required angle).

References

[1] Dikansky N.S., at el. *Status of the VEPP-5 Complex*, Proc. of EPAC94, London, 1994, p.482

[2] R.Brinkmann and F.Willeke, Proc. Second Advanced ICFA Dynamics Workshop on Aperture-Related Limitations of the Performance and Beam Lifetime in Storage Rings, Lugando, Switzeland,1988, CERN 88-04, (1988), 208-212.

[3] A.A. Zolents, B.N.Litvenenko, INP Preprint 81-80, Novosibirsk, (1980).

BEAMSTRAHLUNG DYNAMIC TRANSFORMATION DURING BEAM-BEAM INTERACTION

Arutunian S.G., Mailian M.R.
Yerevan Physics Institute

The beam-beam interaction process begins from the moment when the bunches' fields can be represented as fields of rectilinearly moving continuous bunches. The on-coming beam particle scattering on these fields curves the particle orbit and this results in powerful synchrotron type radiation (beamstrahlung). It is shown, that in this case the smooth part of the bunch self field also transforms. The corresponding transformations of beamstrahlung character (in fact - the hard, discrete part of self field) are investigated. The particle's scattering on the spatially separated peaks of beamstrahlung are studied.

The beam self field becomes essential at increasing the accuracy of beam dynamics analysis in accelerators, storage rings and linear colliders, at present aimed at the micron and submicron beam sizes. Thus the characteristic bunch sizes at the interaction region for next generation linear colliders are projected on the level of the order of units and tens nm in vertical direction and hundreds nm in horizontal direction [1-4]. For this field calculation one has to take into account that the beam currents in the interaction region differ from the nonrelativistic ones by two parameters: the particle energy, which is greater than the rest energy by many orders, and the curvature of the particle trajectories (the beam field of the on-coming bunch acts as an external bending field [5]).

Discrete beam model

Real beam consists of discrete charges, each generates its own microscopic Lienard-Wichert field, the collective field being the sum of these fields. The Coulomb region occupies a negligible part of the beam, therefore the spatial averaging procedure of such fields is to be considered specially. For a single particle the formal averaging of the Lienard-Wichert field by integrating (with respect to time for the non-disturbed motion of the test particle or by smearing the point charge along the trajectory for the fixed instant of observation), leads to the results of continuous one-dimensional beam model. The question is when such or similar procedure is correct for the real beam. In papers

[6-8] the Lienard-Wichert field of the relativistic point charge is analysed by means of retardation equation solution. A notable structure of field is found out:

$$\vec{E}=\frac{e}{R^2}\,\frac{2\mu^2}{[\,(\mu^2-\mathrm{sign}(\rho-1)/2)^2+1/2(\rho-1)\gamma^2\,]^2}\left[-\frac{\mu\vec{e}_1(\Psi)}{|\rho-1|^{5/2}}\right. \tag{1}$$

$$\left.+\frac{(\mu^2-\mathrm{sign}(\rho-1)/2)\vec{e}_2(\Psi)}{(\rho-1)^2}\right],\quad \vec{H}=-\vec{e}_3(\vec{E}\vec{e}_1(\Psi)),$$

where R is the curvature radius, ρR and Ψ are the observation point radial and tangent deviations (corresponding unit vectors are noted $\vec{e}_1(\Psi)$ and $\vec{e}_2(\Psi)$, $\vec{e}_3=[\vec{e}_1(\Psi)\times\vec{e}_2(\Psi)]$), μ is the root of the equation

$$\mu^4-3\mu^2-3\mu\Psi/|\rho-1|^{3/2}-3/4=0. \tag{2}$$

A region of small angular deviations $\Psi/|\rho-1|^{3/2}\approx 1$, is separated out. The difference in behaviour of the field along the radius is determined by the term $\mathrm{sign}(\rho-1)$. Indeed, at $\rho<1$ the field is of the form

$$\vec{E}\approx\frac{e}{R^2}\,\frac{2\mu^2}{(\mu^2+1/2)^2}\left[-\frac{\mu\vec{e}_1(\Psi)}{(\rho-1)^2}+\frac{(\mu^2-1/2)\vec{e}_2(\Psi)}{(\rho-1)^2}\right],\quad \vec{H}=-\vec{e}_3(\vec{E}\vec{e}_1(\Psi)), \tag{3}$$

while for $\rho>1$ a γ-dependent region of the field (γ-region) separates out, corresponding to the condition $\mu^2\approx 1/2$ ($3\Psi\approx -(2(\rho-1))^{3/2}$). Here

$$E\approx H\approx\frac{2^{3/2}e\gamma^4}{R^2(\rho-1)^{1/2}}. \tag{4}$$

This region is the spatial localization of the hard part of synchrotron radiation field. The behaviour of the field within the γ-region is analysed in [9] in details.

The transverse size of the γ-region in the orbit plane is of the order of $R\gamma^{-3}$, as it is seen from formulae (1,2), while the vertical transverse size $\approx 2R(\rho-1)^{1/2}\gamma^{-1}$.

We define the synchrotron radiation packing density k_{SY} as the ratio of the γ-regions volume to the beam volume [10] :

$$k_{SY}=N(\sigma_x R^3)^{1/2}/(\gamma^4\sigma_y\sigma_z), \tag{5}$$

where σ_x, σ_y, σ_z are the bunch transverse and longitudinal

sizes, N is number of particles. Here we also present Chen's criteria of continuity for rectilinearly moving particles [11]

$$k_{CHEN} \approx N(\sigma_x \sigma_y)^{1/2} / \gamma \sigma_z . \qquad (6)$$

It is defined as the ratio of the sum of volumes of all particles relativistic fields to the volume of the bunch. The values $k_{SY} \gg 1$ determine the correctness of using beam continuous model when studying the influence of the beam self field on its individual charge dynamics.

The estimations show that the beam field consists of the smooth mean field and the stochastic component of the synchrotron radiation (beamstrahlung). The results of continuous beam model are valid for field smooth component calculations. The stochastic component is of purely quantum nature (in the space volume with characteristic length of field variation there is no enough energy for photon of the same wavelength [12]).

Scattering on the beamstrahlung hard component

In discrete bunches one can separate out the scattering of particles of on-coming bunch on the spatially localized peaks of synchrotron radiation for cyclic accelerators. The scattering on this component leads to the dynamic processes similar to the quantum fluctuation of the particle trajectories caused by its own synchrotron radiation [13] .

Below it is shown that similar by their physical nature processes can also take place in linear colliders. In this case the electromagnetic field of on-coming bunch serves as an external field causing the trajectories bending near the interaction region.

The average radius of the particle trajectory curvature for continuous rectilinearly moving on-coming bunch one can set $\bar{r} \approx \gamma \sigma_x \sigma_z / r_0 N$ [5] . In table 1 the characteristic values of bunch parameters in the interaction region for some typical projects of next generation linear colliders are presented. One can see that the values of $\bar{r}$ are extremely small. Here we also present parameters k_{SY} and k_{CHEN}.

The estimates of scattering on isolated peaks of the beamstrahlung we perform on the basis of calculation of classical radiation friction force and its subsequent quantum refinement.

Beam field discreteness allows to separate out a single act of scattering. The component of radiation friction force contributing in its integral over the particle trajectory, acting on the particles in the beam is written as [14] :

$$\vec{f} = -\frac{2e^4}{3m^2c^4}\vec{\beta}\gamma^2((\vec{E} + [\vec{\beta}\times\vec{H}])^2 - (\vec{\beta}\vec{E})^2), \qquad (7)$$

the collision energies are set the same, $\vec{\beta}c$ is the particle velocity. In view of field formula (7) we obtain the friction force in γ-region

$$f_{CLASS} \approx 64\gamma^{10} mc^2 r_0^3/3(\bar{r})^3\sigma_x \qquad (8)$$

The energy losses of the particle we estimate as the work of the friction force through the distances of the order of $\bar{r}\gamma^{-3}$ - the width of γ-region. The ratio of these losses to the particle energy is written as:

$$D_{CLASS} = E_{LOSSES}/mc^2\gamma \approx 64\pi\gamma^6 r_0^3/3(\bar{r})^2\sigma_x \qquad (9)$$

The corresponding values are > 1 for some colliders projects (see Table 1). This physically incorrect result is connected to the fact that for given parameters the scattering process is exclusively quantum phenomenon. However, the field in γ-region can be calculated using classical formula, because the energy of the hard photon is less than that of the radiating particle. The corresponding values of $Y = \hbar\omega/mc^2\gamma$ are presented in Table 1.

In this case let's use the approach developed in [14] to determine the quantum refinement of the radiation friction force. The friction force can be written as $\vec{f} = \sigma W'\vec{n}$ ($\vec{n}$ - is the unit vector in the electromagnetic wave propagation direction) where σ is the cross-section of process, W' - the electromagnetic energy mean density in the frame where the particle rests. In this system the radiation friction force is written by means of the general expression for Compton cross-section of scattering in the general case. For low energetic photons it leads to the Thompson cross-section $8\pi r_0^2/3$ and the classical result is restored. In the ultrarelativistic case $\sigma \approx 2\pi r_0^2(\ln\varepsilon + 1/2)/\varepsilon$, where $\varepsilon = 2\omega'\hbar/mc^2$ (ω' - the photon frequency in the frame where the electron rests). I.e., the friction force $\vec{f}'$ in the frame of scattering particle is written as:

$$\vec{f}' \approx \vec{n}\, r_0^2(\ln\varepsilon + 1/2)E^2\gamma^2(1 + \beta)^2/2\varepsilon \qquad (10)$$

To calculate the friction force in the laboratory system let's take the corresponding Lorentz transformation of the 4-force $(0,\vec{f}'/c)$, formed on the basis of three-dimensional friction force. After the transformation for the friction force in laboratory frame we have $\vec{f} = \vec{f}'$. In view of (10) we have:

$$\vec{f} = s\vec{f}_{CLASS}. \qquad (11)$$

Here the factor of smallness $s = 3(\ln 4\gamma^2\Upsilon + 1/2)/16\gamma^2\Upsilon$ is separated out in comparision with the classical expression. Importance of Compton cross-section suppression for high energy particles for given problem is pointed out by V.Tel'nov [15].

The corresponding energy losses with respect to the particle energy

$$D_{QUANT} = sD_{CLASS} = 7\pi\gamma^4 r_0^3(\ln 4\gamma^2\Upsilon + 1/2)/8(\bar{r})^2\sigma_x\Upsilon \qquad (12)$$

are presented in Table 1. It is seen from the table that these values << 1. Let's take into account, however, that the particle is scattered practically on all the γ-regions of charges of on-coming bunch. In spite of the fact that during a single act of scattering a small part of the particle energy is scattered, the total energy losses at the intersection of the whole beam becomes comparable with its energy (the corresponding values presented in Table 1 become $\approx$ 1). This results in essential changes in the content of beamstrahlung and distortion of the beam particle dynamics.

Table 1.

Linear coll.	Energy (GeV)	γ	N	σ_x (nm)	σ_z (nm)	σ_s (mm)	$\bar{r}$(cm)
SLC	50	9.78×10^{4}	7.2×10^{10}	2070	1650	1.0	99.83
DLC-300	150	2.94×10^{5}	2.1×10^{10}	914	37	0.5	226.68
DLC-500	250	4.89×10^{5}	2.1×10^{10}	400	32	0.5	165.34
DLC-1000	500	9.78×10^{5}	2.8×10^{10}	447	16	0.5	277.16
NLC-500	250	4.89×10^{5}	6.5×10^{9}	300	3	0.1	80.13
NLC-1000	500	9.78×10^{5}	1.3×10^{10}	425	2	0.1	113.52
JLC-500	500	4.89×10^{5}	1.2×10^{10}	335	4.5	0.1	54.77

k_{SY}	k_{CHEN}	D_{CLASS}	Υ	s	D_{QUANT}	ND_{QUANT}
6.8×10^{-4}	1360	3.5×10^{-6}	3.7×10^{-3}	1.0×10^{-7}	3.6×10^{-13}	0.026
5.0×10^{-4}	26.3	1.1×10^{-3}	1.5×10^{-2}	3.4×10^{-9}	3.6×10^{-12}	0.076
3.1×10^{-5}	9.7	9.8×10^{-2}	1.6×10^{-2}	3.5×10^{-10}	3.5×10^{-11}	0.725
1.2×10^{-5}	4.8	2.0	1.3×10^{-1}	4.0×10^{-11}	8.1×10^{-11}	2.277
1.5×10^{-4}	4.0	5.3×10^{-1}	1.2×10^{-1}	1.7×10^{-10}	9.3×10^{-11}	0.604
5.6×10^{-5}	3.9	12.2	3.3×10^{-1}	1.7×10^{-11}	2.1×10^{-10}	2.714
9.7×10^{-5}	8.4	1.0	1.7×10^{-1}	1.2×10^{-10}	1.3×10^{-10}	1.523

The above-presented analysis has of course a preliminary character. The parameter of trajectory curvature ρ needs an essential refinement. At its calculation the head and the tail of the bunch are to be separated and the rectilinear approximation of the field (it plays a role of the external field and defines the radius of curvature) can be used for particles near the head and for the first moment of the overlapping only. The effects of the beam disruption and some other are also to be taken into account.

The authors are grateful to G.A.Nagorsky, whose ideas stimulated them in their activities in this area for many years. They are also thankful to R.Brinkman, K.Flötman, J.Rossbach, P.Chen, K.Oide, K.Yokoya, V.Tel'nov, A.Ioannissian for helpful discussions.

References

1. Seeman J. SLC. - Proc. of ECFA Workshop on e^+e^- Linear Coll. (July, Aug. 1992, Garmish-Partenkirchen), v.1, p. 93.
2. Weiland T. DLC. - Ibid, v.1, p. 121.
3. Ruth R. NLC. - Ibid, v.1, p. 155.
4. Takata K. JLC. - Ibid, v.1, p. 207.
5. Amaldi U. Introduction to the next generation of linear colliders. - In Lectures Notes in Physics (Spr.-Ver.,1988).
6. Arutunian S.G.An equal-time picture of a field near the moving in a circle ultrarelativistic charged particle. - Rep. EPI-387(45)-79, Yerevan, 1979.
7. Arutunian S.G.,Nagorsky G.A.Coherent superposition of fields of relativistic charged particles moving along curved trajectories.- Zh.Tekh.Fiz., 55, 1494 (1985).
8. Jackson J. Classical electrodynamics. - (Wiley, New York, 1975).
9. Arutunian S.G.,Mailian M.R.,High electric field generation by synchrotron radiation fields interference amplification. - Zh. Tekh.Fiz, 61, 8, 175 (1991).
10. Arutunian S.G.,Nagorsky G.A.Accelerator and storage ring intensity effects connected with Lienard-Wichert particle field. - Rep. EPI-452(60)-80, Yerevan, 1980.
11. Chen P.The nature of beamstrahlung. - Rep. SLAC-PUB-4293,1987.
12. Berestetskii C.B., Lifshits E.M., Pitaevskii L.P. - Quantum electrodynamics (Pergamon, Oxford, 1982).
13. Arutunian S.G. The particle scattering on the hard part of synchrotron radiation:the influence on the beam dynamics. - Proc. 1 Europ. Part. Accel. Conf. (1988, Rome), v.1, p.629.
14. Landau L.D., Lifshits E.M. Field theory. - (Moscow, 1973).
15. Tel'nov V. Private communucation.

List of participants

H. Burkhardt, CERN	hbu@cernvm.cern.ch
A. Piwinski, DESY	h01pwn@dsyibm.desy.de
J. Le Duff, LAL	leduff@lalcls.in2p3.fr
J. Welch, CESR	welch@cesr10.lns.cornell.edu
T. Chen, SLAC	tchen@slac.stanford.edu
A. Zholents, LBL	zholents@csa1.lbl.gov
A. Gerasimov, FNAL	andrei@calvin.fnal.gov
Y. Funakoshi, KEK	funakosi@kekvax.kek.jp
K. Hirata, KEK	hirata@kekvax.kek.jp
L. Palumbo, IFNF	lpalumbo@frascati.infn.it
Y. Shatunov, BINP	shatunov@inp.nsk.su
D. Pestrikov, BINP	pestrikov@inp.nsk.su
D. Shatilov, BINP	shatilov@inp.nsk.su
E. Simonov, BINP	simonov@inp.nsk.su
D. Parkhomchuk, BINP	parkhomd@inp.nsk.su
V. Shiltsev, BINP	shiltsev@inp.nsk.su
V. Parkhomchuk, BINP	parhomcuk@inp.nsk.su
V. Yakimenko, BINP	yakimenko@inp.nsk.su
Y. Eidelman, BINP	eidelur@inp.nsk.su
G. Tumaikin, BINP	
V. Danilov, BINP	danilov@inp.nsk.su
V. Balbekov, IHEP	balbekov@balbekov.ihep.su
S. Ivanov, IHEP	ivanov_s@mx.ihep.su
V. Mokhov, IHEP	mokhov_v@mx.ihep.su
P. Zenkevich, ITEP	zenkevich@vitep3.itep.ru
A. Lebedev, Physical Institute	anlebede@npad.fian.msk.su
V. Aleksandrov, JINR	aleks@nusun.jinr.dubna.su
Y. Alexahin, JINR	alexahin@sunse.jinr.dubna.su
P. Beloshitsky, JINR	beloshitsky@main1.jinr.dubna.su
V. Zhabitsky, JINR	main@jinr.dubna.su
I. Meshkov, JINR	meshkov@nusun.jinr.dubna.su
V. Mikhailov, JINR	mikhail@lhe36.jinr.dubna.su
V. Kazacha, JINR	kazacha@main1.jinr.dubna.su
N. Kazarinov, JINR	kazarinov@main1.jinr.dubna.su
E. Perelstein, JINR	perel@nusun.jinr.dubna.su
A. Sissakian, JINR	sisakian@jinr.dubna.su
S. Arutunian, Yerevan Physical Institute	femto@uniphi.yerphi.am

Proceedings of VII ICFA Beam Dynamics Workshop on
Beam-Beam Issues for Multibunch,
High Luminosity Circular Colliders

Труды VII Рабочего совещания секции ICFA динамики пучков
«По эффектам встречи в кольцевых коллайдерах»

E9-96-21

Ответственный за подготовку сборника к печати П.Ф.Белошицкий

Редактор Э.В.Ивашкевич. Макет Р.Д.Фоминой

Рукопись сборника поступила 24.01.96. Подписано в печать 09.04.96
Формат 60 × 84/8. Офсетная печать. Уч.-изд. листов 19,0
Тираж 200. Заказ 49026. Цена 13300 р.

Издательский отдел Объединенного института ядерных исследований
Дубна Московской области